UNIVERSIDAD D CÓRDOBA

Doctorado en Biociencias y Ciencias Agroalimentarias

# *Control of cytosolic pH homeostasis in the fungal plant pathogen Fusarium oxysporum*

# *Control de la homeostasis del pH citosólico en el fitopatógeno Fusarium oxysporum*


***Melani Mariscal Gómez***


Tesis doctoral d*irigida por:*

Prof. Dr. *Antonio Di Pietro*

Dra. *Tânia Alicia Ribeiro Fernandes*

Córdoba, Febrero 2023

TITULO: *Control of cytosolic pH homeostasis in the fungal plant pathogen Fusarium oxysporum*

AUTOR: *Melani Mariscal Gómez*


Campus de Rabanales
Ctra. Nacional IV, Km. 396 A
14071 Córdoba

https://www.uco.es/ucopress/index.php/es/
ucopress@uco.es

**TÍTULO DE LA TESIS:** Control of cytosolic pH homeostasis in the fungal plant pathogens *Fusarium oxysporum*

**DOCTORANDO/A: Melani Mariscal Gómez**

## INFORME RAZONADO DEL/DE LOS DIRECTOR/ES DE LA TESIS

(se hará mención a la evolución y desarrollo de la tesis, así como a trabajos y publicaciones derivados de la misma).

La Tesis Doctoral de Dña. Melani Mariscal Gómez se ha llevado a cabo en el Departamento de Genética de la Universidad de Córdoba, en el seno del Grupo "Genética molecular de la patogénesis fúngica" (BIO-138). Su desarrollo ha permitido a la doctoranda adquirir una sólida formación en Genética y Biología Molecular. Durante la realización de la Tesis, Dña. Melani ha mostrado tener una gran capacidad de trabajo y aptitud para la investigación científica. En el trabajo se ha llevado a cabo, por primera vez, una caracterización detallada de distintos reguladores del pH citosólico en un hongo fitopatógeno, *Fusarium oxysporum*. Además, se han investigado los mecanismos que conectan el pH citosólico con las rutas de señalización MAP quinasas, que son factores en la patogénesis fúngica. Los resultados obtenidos se han comunicado en varios congresos nacionales e internacionales y se ha recogido en dos artículos y un capítulo de libro publicados revistas y editoriales internacionales.

Por todo ello, se autoriza la presentación de la tesis doctoral.

Córdoba, 8 de Febrero de 2023

Firma de los directores

DI PIETRO ANTONIO COSTANTE - X1583221Q

Digitally signed by DI PIETRO ANTONIO COSTANTE - X1583221Q
Date: 2023.02.08 12:44:41 +01'00'

Fdo.: Antonio Di Pietro

Signed by : **TÂNIA ALÍCIA RIBEIRO FERNANDES**
Identification number: 13781412
Date: 2023.02.08 14:07:08 +0000

Fdo.: Tania Fernandes

This work has been conducted in the Department of Genetics of the University of Córdoba and financially supported by the fellowship *Formación Personal Investigador* (FPI) from the Spanish Ministry of Science and Innovation (BES-2017-082775).

“A scientist in his laboratory is not a mere technician: he is also a child confronting natural phenomena that impress him as though they were fairy tales.”

*Marie Curie*

# Index

## List of figures

## List of tables

## Abbreviations

**aa** amino acid

**AA** acetic acid

**BCECF-AM** (2',7'-Bis-(2-Carboxyethyl)-5-(and-6)-Carboxyfluorescein, Acetoxymethyl Ester

**bp** base pair

**BSA** Bovine Serum Albumin

**cAMP** cyclic Adenosine Monophosphate

**CFW** Calcofluor White

**CR** Congo Red

**cryo-EM** Cryogenic electron microscopy

**CWI** Cell Wall Integrity

**DES** Diethylstilbestrol

**dhSph** dihydrosphingosine

**dNTP** deoxynucleotide Triphosphate

**DPSS** Diode-Pumped-Solid-State

**ER** Endoplasmic Reticulum

**ESCRT** Endosomal Sorting Complexes Required for Transport

**Fo-RALF** *Fusarium* RALF

**f. sp.** *Forma specialis*

**ff. spp.** *Formae speciales*

**FungiDB** The Fungal and Oomyte Genomics Resource

**GpdA** Glyceraldehyde phosphate dehydrogenase promoter

**HCl** Hydrochloric acid

**HOG** High Osmolarity Glycerol

**Hyg$^{R}$** Hygromycin resistance

**IG** Invasive growth

**Kb** Kilobase

**KDa** KiloDalton

**L** liter

**LA** Luria-Bertoni with agar

**LB** Luria-Bertoni

**LCB** Long Chain Base

**LS** Lineage-Specific

**M** Molar

**MAPK** Mitogen-Activated Protein Kinase

**MAPKK** MAPK Kinase

**MAPKKK** MAPK Kinase Kinase

**mg** milligram

**ml** milliliter

**mM** millimolar

**MM** Minimal Medium

**MCP** Membrane Compartment of Pma1

**NAD** Nicotinamide Adenine Dinucleotide

**NaOH** Sodium Hydroxide

**Neo$^{R}$** Neomycin resistance

**nm** nanometer

**O.N.** Overnight

**OD** Optical Density

**ORF** Open Reading Frame

**PCR** Polymerase Chain Reaction

**PDA** Potato Dextrose Agar

**PDB** Potato Dextrose Broth

**Pheo$^{R}$** Phleomycin resistance

**$pH_c$** cytosolic pH

**$pH_v$** vacuolar pH

**PI** Phosphatidylinositol

**PM** Plasma membrane

**Pma1** Plasma membrane $H^+$-ATPase 1

**PS** Phosphatidylserine

**RALF** Rapid Alkalinization Factor

**ROS** Reactive Oxygen Species

**rpm** revolutions per minute

**RT** Room Temperature

**SGD** *Saccharomyces* Genome Database

**Tm** Temperature of melting

**TOR** Target of Rapamycin

**TrpC** Anthranilate synthase terminator

**V-ATPase** Vacuolar $H^+$-ATPase

**v/v** volumen-volumen

**YPD** Yeast Extract Peptone Dextrose

**YPDA** YPD Agar

**µ** micro

**µg** microgram

**µl** microliter

**µm** micrometer

**µM** micromolar

## Abstract

pH is one of the most important environmental factors affecting development and virulence in fungi. In the soilborne vascular wilt fungus *Fusarium oxysporum*, pH acts as a master regulator of the conserved Fmk1 MAPK cascade, which is essential for invasive growth and pathogenicity on tomato plants. In addition, pH also modulates the activity of the cell wall integrity MAPK Mpk1 and the high-osmolarity response MAPK Hog1. Recent studies have demonstrated that ambient pH modulates MAPK signaling via fluctuations on cytosolic pH ($pH_c$) suggesting that pH-driven signaling responses are largely regulated by $pH_c$. The essential $H^+$-ATPase Pma1 is the most abundant protein in the plasma membrane and acts as the main regulator of $pH_c$ homeostasis in fungi. Here, we found that loss of casein kinase 1 (Ck1), a negative regulator of Pma1, resulted in increased Pma1 activity, reduced alkalinization of the surrounding medium as well as decreased hyphal growth. Importantly, the *ck1*Δ mutants were impaired in hyphal chemotropism towards plant roots and in pathogenicity on tomato plants. On the other hand, a *F. oxysporum* mutant carrying a temperature-sensitive *pma1* allele (*pma1*$^{ts}$) showed a significant decrease in Pma1 activity after a shift from the permissive to the restrictive temperature. Interestingly, live-cell imaging of fluorescently labelled Pma1 in *F. oxysporum* and the human pathogen *Candida albicans* revealed that this plasma membrane-localized $H^+$-ATPase is excluded from the hyphal tip, suggesting a possible role in regulating polarized growth. Our studies revealed that fungal germ tubes can re-direct growth towards acidic pH in a Mpk1-dependent manner. Overall, these results shed light on the regulation of $pH_c$ by Pma1 and its role in development and virulence of fungal pathogens.

## Resumen

El pH es uno de los factores ambientales más importantes que afecta el proceso de desarrollo y virulencia en hongos. En el patógeno del suelo *Fusarium oxysporum*, causante de la marchitez vascular, el pH actúa como regulador maestro de Fmk1, una MAPK altamente conservada, esencial para el crecimiento invasivo y patogenicidad en plantas de tomate. Además, el pH también modula la actividad de las cascadas de señalización MAPK de respuesta a la integridad de la pared celular Mpk1 y de alta osmolaridad Hog1. Estudios recientes han demostrado que el pH ambiental modula la señalización de MAPK a través de fluctuaciones en el pH citosólico ($pH_c$), lo que sugiere que las respuestas de señalización impulsadas por pH están ampliamente reguladas por $pH_c$. La esencial $H^+$-ATPasa Pma1 es la proteína más abundante en la membrana plasmática y actúa como principal regulador de la homeostasis $pH_c$ en hongos. Aquí nosotros encontramos que la pérdida de la caseína kinase 1 (Ck1), un regulador negativo de Pma1, caseína quinasa 1, resulta en una mayor actividad de Pma1 que conduce a una reducida alcalinización del medio circundante, así como un menor crecimiento de la hifa. Es importante destacar que los mutantes de *ck1*Δ exhiben defectos en el quimiotropismo de la hifa hacia las raíces de las plantas y en la patogenicidad en las plantas de tomate. Por otro lado, un mutante de *F. oxysporum* que presenta un alelo *pma1* sensible a la temperatura (*pma1*$^{ts}$) mostró una disminución significativa en la actividad de Pma1 tras un cambio de temperatura permisiva a restrictiva. Las imágenes de células vivas de Pma1 marcadas fluorescentemente en *F. oxysporum* y el patógeno humano *Candida albicans* revelaron que esta H+-ATPasa localizada en la membrana plasmática está excluida del extremo de la hifa, lo que sugiere un posible papel en la regulación del crecimiento polarizado. Nuestros estudios determinan que las germínulas pueden redirigir el crecimiento hacia el pH ácido de una manera dependiente de Mpk1. En general, estos resultados ayudan a comprender la regulación del $pH_c$ a través de Pma1 y su papel en el desarrollo y virulencia de patógenos fúngicos.

# Introduction

# Introduction

## 1. Fungal pathogens

The fungal kingdom encompasses a great diversity of taxa with various habitats, lifestyles, morphologies, and nutrient requirements. Part of the evolutionary success of fungi lies in their ability to grow indefinitely as a multinucleated columnar structure called hypha. Armed with an extremely high metabolic diversity, fungi have colonized numerous ecological niches and have shaped a whole world of interactions with other organisms. Many fungal species are cosmopolitan and generalists, but others are specialists adapt to restricted substrates or habitats where the extreme conditions would be expected to prevent the development of life, such as the cold niches of the Antarctic dry valleys and high Arctic glaciers or hypersaline niches such as salt flats and hypersaline microbial mats or even plant trichomes (Cantrell *et al.*, 2011; Naranjo-Ortiz & Gabaldón, 2019).

Some fungal species are pathogens that can thrive on living organisms. Pathogens face unfavorable conditions during host colonization and thus need to be resilient to its immune responses and able to obtain nutrients under these conditions.

Fungal plant pathogens are the most devastating infectious agents on crops, causing severe economic impact on world agriculture. Plant pathogens use different infection strategies, allowing to categorize them into biotrophs, necrotrophs and hemibiotrophs. Biotrophs manipulate plant defenses to obtain the nutrients from living plants cells by specialized structures called haustoria, formed within the host cell, while necrotrophs obtain the nutrients needed from dead or dying cells, which have been killed through the release of toxins and enzymes secreted by the pathogen. Hemibiotrophic pathogens initially invade live cells prior to transitioning to a necrotrophic lifestyle to obtain nutrients by killing the host cells (Rajarammohan, 2021).

Human fungal pathogens are hidden killers a with high impact on global health. They cause invasive infections taking the lives of one and a half million people every year. It should be noted that for most human fungal pathogens such as *Aspergillus* and *Cryptococcus*, the human host is not the primary niche, and that they only cause serious diseases such as lung pulmonary aspergillosis and the brain cryptococcal meningoencephalitis, respectively, in individuals with a weakened immune system.

Similarly, *Candida* spp., which are commonly found in the fungal mycobiome of healthy people, only cause systemic infections when the host immune system becomes compromised or when there is a physical breach in the barriers of the gastrointestinal tract (Kim, 2016; Sun *et al.*, 2020).

## 2. Fusarium oxysporum

*Fusarium* is an ascomycete genus with high genetic diversity and a worldwide distribution. Many members of the of the genus are plant pathogens that infect crops, causing huge economic losses. In addition, these pathogens have serious impacts on human and animal health by producing multiple mycotoxins such as trichothecenes, which contaminate grains and processed products posing a serious risk to human and animal health (Qu *et al.*, 2022). Besides being plant pathogens, some *Fusarium* spp. are able opportunistic pathogens of humans where they cause fusariosis (Pérez-Nadales *et al.*, 2021).

The *F. oxysporum* species complex (Sordariomycetes, Hypocreales, Nectriaceae) includes more than 150 different *formae speciales* (ff. spp.) which have been classified according to their specificity for a given host plant. Among these are field crops of great economic interest such as tomato (f. sp. *lycopersici*), cotton (f. sp. *vasinfectum*) or banana (f. sp. *cubense*) (Edel-Hermann & Lecomte, 2019). *Formae speciales* have originate from different clades (polyphyletic) and can be further sub-divided into pathogenic races classified according to differential virulence on different host cultivars (Rana *et al.*, 2017). Since there is no known sexual stage in the life cycle of *F. oxysporum*, the phenomenon of gene duplication (GD) and horizontal gene transfer (HGT) appears to be responsible for their continuous diversification, for example by acquisition of virulence genes through HGT or further diversification due to GD and gene loss (Jaramillo *et al.*, 2015; Steindorff AS *et al.*, 2015). Complete genome sequence analysis of the *F. oxysporum* f. sp. *lycopersici* strain *Fol4287* demonstrated the existence of lineage-specific (LS) genomic regions, including four entire chromosomes, that are absent from another *Fusarium* spp. such as *F. graminearum* and *F. verticillioides* (Ma *et al.*, 2010). On the other hand, *F. oxysporum* f. sp. *lycopersici* presents three different races (1, 2 and 3) defined by virulence/avirulence phenotypes that have successively evolved as a result of mutations in virulence-associated effector genes encoded on LS chromosome. However, the origin of the ancestral race remains unknown (Biju *et al.*, 2017).

*F. oxysporum* displays a variable morphology and color depending on the environmental conditions. The culture conditions also affect growth rate, shape, size and abundance of conidia as well as number of septa and pigmentation. The species produces three types of asexual spores: microconidia (single-cell dispersal structures), macroconidia (3 to 5 cells commonly found on the surface dead plants) and chlamydospores. The chlamydospore is the main structure for long-time survival during unfavorable periods in the soil and play an important role as primary inoculum for plant root infection (Couteaudier & Alabouvette, 1990; Ma *et al.*, 2013; Srinivas *et al.*, 2019). When the appropriate conditions for infection occur, spores in the soil germinate and hyphae are attracted towards the plant by peroxidase signals released by roots (Turra & Di Pietro, 2015). Moreover, germlings adhere to the plant roots and penetrate them directly without requirement of specialized structures such as appressoria, which are formed in other fungal plant pathogens. Root penetration occurs mainly through natural openings or wounds in the roots (Pérez-Nadales & Di Pietro, 2011).

The initial root colonization happens through a biotrophic phase, with hyphae growing mainly intercellularly in the root cortex (Redkar *et al.*, 2022b). Molecular events during biotrophy of *F. oxysporum* remain largely unknown, including how the fungus obtains nutrients while evading host recognition. During later stages of infection, fungal hyphae cross the root endodermis until reaching the highly protected and nutrient poor xylem vessels, which they use as avenues to colonize the entire plant. This step requires a battery of effectors known as 'Secreted In Xylem' (SIX) proteins, that were shown to be *forma specialis*-specific. Some SIX proteins are recognized by the plant as race-specific avirulence (AVR) factors (van Dam *et al.*, 2016). Specifically, *F. oxysporum* f. sp. *lycopersici*, SIX4 is AVR1, while SIX3 is AVR2 and SIX 1 is AVR3, the three avirulence factors that interact with the resistance genes of tomato I-1, I-2 and I-3, respectively. Thus, the proteins SIX1 and SIX3 are recognized by the tomato receptor-like kinases I-3 and I-2 in the nucleus and function as resistance proteins to induce plant defenses (Rep, 2005; Rep *et al.*, 2005).

Within the xylem, the fungus produces hyphae and microconidia, which germinate and colonize the upper vascular vessels, leading to disease symptoms such as progressive wilting, defoliation and plant death (Dean *et al.*, 2012; Pérez-Nadales & Di Pietro, 2011; Yadeta & BP, 2013). In the later stages of infection, the

fungus propagates through parenchymatous tissue and begins to sporulate abundantly on the macerating host tissue, enhancing its propagation though soil, transplants, etc. (Jangir *et al.*, 2021) [Figure 1]. Besides plant infection, *F. oxysporum* can survive in the soil for long time periods, either as chlamydospores or by growing as a saprophyte on decaying organic matter.

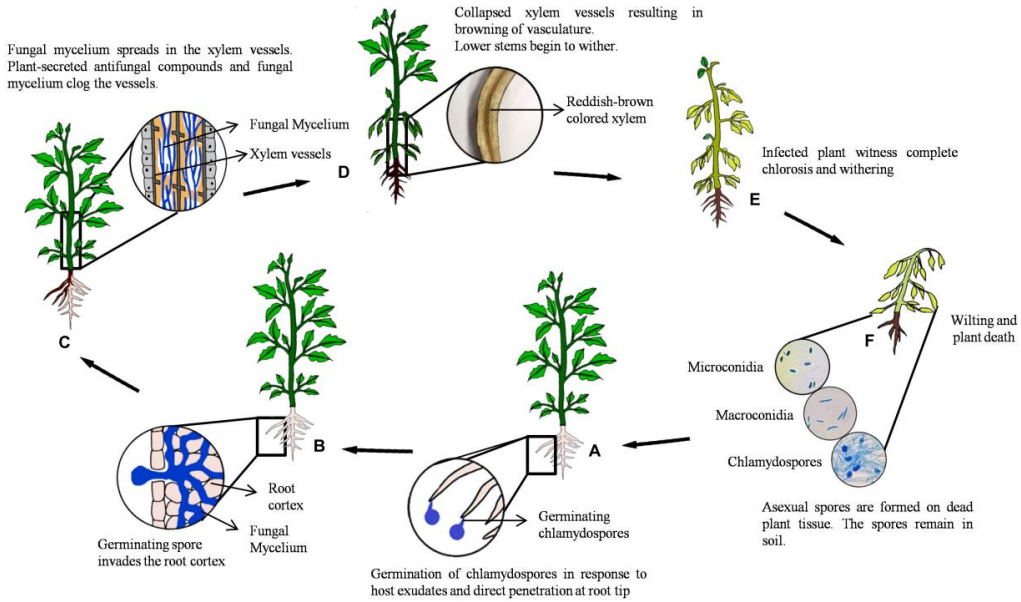


**Figure 1. Life cycle of *F. oxysporum*.** (**A**) Secretion of root exudates by host plant triggers spore germination and the development of infection hyphae performing penetration of the root epidermis at the tip. (**B**) The hypha progresses intercellularly via the root cortical cells until it enters the xylem tissue, parenchymal cells, and vessels, through xylem pits. (**C**) The pathogen colonizes vascular vessels causing blockage and browning as a result of excessive mycelial growth. (**D**) The initial stage of infection shows symptoms at the stem base and slowly advancing upward, triggering withering of young leaves. (**E**) Marginal yellowing or complete chlorosis in mature leaves is observed. (**F**) Disease progression results in wilting and death of the host plant. Fungal spores (microconidia, macroconidia, and chlamydospores) are formed on dead plant tissue and remain dispersed in soil (Jangir *et al.*, 2021).

## 3. Ambient pH controls fungal pathogenicity

The ability of fungal pathogens to sense and adapt to changes in ambient pH is crucial for their survival, particularly within the host (Fernandes *et al.*, 2017; Vylkova, 2017). More recently, pH has emerged as a key factor in virulence. Moreover, fungal pathogens can modulate the pH of the host tissue to increase their infectious potential (Alkan *et al.*, 2013; Mariscal *et al.*, 2022; Masachis *et al.*, 2016). Although the

mechanism of pH sensing and response is well studied in fungi, how pH contributes to virulence is not fully understood.

### 3.1. pH sensing and adaptation in fungi: the Pal/Rim pathway

In order to survive, grow and reproduce, fungi must be able to sense and respond to change in the ambient pH. The most important signal transduction mechanism related to ambient pH responses in fungi is the Pal/Rim pathway (Peñalva *et al.*, 2008). Studies conducted primarily in the model organisms *Saccharomyces cerevisiae* and *Aspergillus nidulans* have cemented our understanding of how fungi sense and respond to pH (Peñalva *et al.*, 2014).

Fungi detect alkaline pH through the concerted action of two cell surface proteins, PalH/Rim21 and PalI/Rim9, which carry seven and four-transmembrane domains, respectively (Calcagno-Pizarelli *et al.*, 2007; Lucena-Agell *et al.*, 2016). Studies in *S. cerevisiae* suggest that the C-terminal cytosolic domain of PalH/Rim21 detects altered lipid asymmetry in the plasma membrane (PM) as a result of alkaline-induced depolarization (Nishino *et al.*, 2015). This leads to dissociation of PalH/Rim21 from the PM and to ubiquitination and phosphorylation of its associated α-arrestin PalF/Rim8 (Herranz *et al.*, 2005; Obara & Kamura, 2021). Further transduction of the pH signal includes endocytosis of the PalF-PalH complex and recruitment of the Endosomal Sorting Complexes Required for Transport (ESCRT) scaffold to PM associated (Peñalva *et al.*, 2014). The ESCRT complex components Vps20 and Snf7 then recruit the interacting proteins PalA/Rim20 and the capain-like protease PalB/Rim13 to the endomembrane (Henne *et al.*, 2012; Ost *et al.*, 2015). PalA binds to the C-terminal inhibitory domain of the inactive full-length version of the zinc finger transcription factor PacC/Rim101 and contributes to its proteolytic cleavage and activation by the protease PalB. The processed PacC protein functions both as an activator of alkaline-expressed genes and as a repressor of acidic-expressed genes, thereby orchestrating the cellular response to alkaline pH (Peñalva *et al.*, 2008) [Figure 2].

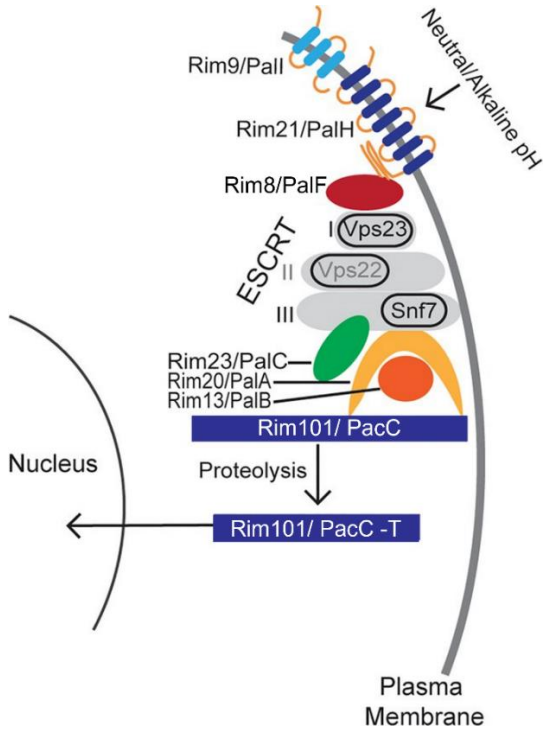


**Figure 2. A model of the Pal/Rim pathway signaling in fungi.** The PalH at the PM senses a shift to alkaline pH and mediates PalF activation. PalH-PalF complex is relocated to the endosomes and activates PalB, that leads to processing and activation of the transcription factor PacC. Activated PacC enters the nucleus and directs the transcription of alkaline-expressed genes. Adapted from (Ost et al., 2015).

Besides its role in fungal adaptation to alkaline pH, PacC/Rim101 is also involved in other relevant processes such as sporulation, toxic secondary metabolite production, and virulence (Fernandes *et al.*, 2017; Merhej *et al.*, 2011; Wasserstrom & Wendland, 2021). Loss of PacC/Rim101 leads to reduced virulence in most fungal pathogens tested so far, including the human pathogens *Candida albicans* and *Aspergillus fumigatus (Bertuzzi et al., 2014; Davis, 2009)* or the plant pathogens *Magnaporthe oryzae*, *Botrytis cinerea, Penicillium expansum* or *Trichothecium roseum* (Chen *et al.*, 2018; Landraud *et al.*, 2013; Rascle *et al.*, 2018; Wang *et al.*, 2022), but is dispensable for virulence in others such as the soilborne vascular wilt fungus *F. oxysporum* and the biotroph *Ustilago maydis* (Cervantes-Chávez *et al.*, 2010; Fernandes *et al.*, 2022a).

In contrast to alkaline pH, only few studies have addressed the mechanisms underlying acidic pH sensing in fungal pathogens. Genome-wide expression analysis

was used to explore how gene expression in *S. cerevisiae* is remodeled in response to changes of ambient pH to acidic or alkaline conditions. Some genes showed inversed responses to acid and alkali that might be indicative of pH-responsive genes. Among these, Pdr12 encoding an ABC transporter important for weak acid resistance, is induced under acid and repressed under alkaline conditions, and Trk2 encoding a potassium transporter responsible for a $K^+$ current at low pH, showed a similar pattern of expression (Causton *et al.*, 2001). By contrast, the Pho89 sodium phosphatase symporter, which catalyzes sodium-dependent phosphate uptake active at alkaline pH (Serra-Cardona *et al.*, 2014), was upregulated at alkaline pH and repressed upon a shift to low pH (Causton *et al.*, 2001). This control was shown to involve activation of the calcineurin-dependent transcription factor Crz1p and is under the control of several repressors coordinately regulated by the Snf1 protein kinase and the Rim101 transcription factor (Serra-Cardona *et al.*, 2014).

Multiple genomic studies have been conducted for sensitivity to different weak acids, mainly motivated by their commercial importance and their prominent role as fungal growth inhibitors (Mollapour *et al.*, 2004). Weak acids are usually uncharged at low extracellular pH and can cross the membrane and dissociate in the higher pH of the cytosol. This causes stress to the fungal cell, as dissociation of the acid leads to cytosolic acidification through proton accumulation (Stratford *et al.*, 2013). Genomic studies addressing mechanisms of adaptation to different weak acids showed both general and specific responses, correlated with the structure and hydrophobicity of the anion (Mira *et al.*, 2010b). The transcription factors Msn2 and Msn4 mediate a general environmental stress response, including upregulation of chaperones and proteins involved in energy metabolism and ergosterol biosynthesis (Gasch *et al.*, 2000; Schüller *et al.*, 2004). By contrast, the transcription factor War1 responds specifically to sorbic acid, triggering upregulation of Pdr12, which encodes a plasma membrane ABC transporter involved in sorbic acid efflux (Schüller *et al.*, 2004). Overall, these findings suggest that fungi detect and respond to changes in ambient pH, either through alkalinization or acidification. However, the exact mechanism by which fungi sense acidification of the environment remains to be elucidated.

### 3.2. Active modulation of ambient pH and its role in plant pathogenicity

Besides developing efficient mechanisms for adapting to ambient pH changes, fungal pathogens are able to efficiently modulate the pH of the host tissue by secreting acids or alkali. Fungi can naturally produce a number of weak organic acids, such us gluconic, oxalic or citric acid, which act as virulence factors to damage the host tissue in necrotrophic pathogens (Jiao *et al.*, 2022; Park *et al.*, 2017). Necrotrophic pathogens such as *Sclerotinia sclerotiorum* or *Botrytis* spp. decrease the host pH by secreting significant amounts of oxalic acid (Manteau *et al.*, 2003; Rollins & Dickman, 2001), whereas others release gluconic acid, either alone such as *Phomopsis mangiferae* (Davidzon *et al.*, 2010) or together with citric acid as *Valsa mali* (Zhang *et al.*, 2022). The combination of gluconic and citric acid has been described to decrease the environmental pH in the pathogens *Penicillium* and *Aspergillus* spp. (Prusky *et al.*, 2004; Ruijter *et al.*, 1999).

While acidification has been mostly reported in necrotrophic pathogens, alkalinization has been described mainly in hemibiotrophic pathogens during the early biotrophic stages of infection (Alkan *et al.*, 2013). Alkalinization of the host environment is mainly achieved through the release of ammonia and promotes fungal pathogenicty (Miyara *et al.*, 2012). For instance, in *Colletotrichum gloeosporioides*, release of ammonia leads to the activation of pathogenicity factors associated with differentiation of appressoria for host penetration, as well as the production of cell wall degrading enzymes such as pectate lyase (Shnaiderman *et al.*, 2013). Similarly, in *M. oryzae*, alkalinization induces the differentiation of asexual spores and secretion of lytic enzymes (Landraud *et al.*, 2013), while in *Cryptococcus neoformans* it induces melanin formation and capsule production (Vecchiarelli *et al.*, 2013) and in *C. albicans* it promotes filamentation, adhesion and invasion (Nobile *et al.*, 2008; Sun *et al.*, 2015). Although the exact mechanism that leads to extracellular accumulation of ammonia remains to be elucidated, ammonia production by fungal pathogens appears to require the regulated uptake of amino acids via amino acid permeases or their mobilization from vacuolar stores, followed by catabolism through different routes involving steps of deamination (Bi *et al.*, 2016; Miyara *et al.*, 2012; Shnaiderman *et al.*, 2013; Vylkova *et al.*, 2011). To protect the cell from the toxic effects resulting from accumulation of ammonia, the compound is released either through passive diffusion

or by action of transporters such as the members of the Ato protein family (Danhof & Lorenz, 2015; Vylkova *et al.*, 2011).

In many fungi, the capability to acidify or alkalinize surrounding tissues is largely dictated by the availability of the carbon source. An excess of carbon is metabolized by glucose oxidase to gluconic acid, whereas catalysed deamination of non-preferred carbon sources, such as the amino acid glutamate, results in the accumulation of ammonia (Bi *et al.*, 2016; Vylkova *et al.*, 2011). These findings are of biological relevance, because pathogens are likely to encounter different levels of carbon availability, depending on the host niche or the stage of infection (biotrophic versus necrotrophic). Thus, carbon availability might ultimately dictate whether pathogens follow an acidic or an alkaline colonization strategy.

Host plant alkalinization can also be triggered by secretion of a functional homologue of the plant Rapid Alkalinizing Factor (RALF) during early stages of infection in the hemibiotrophic soilborne pathogen *F. oxysporum* (Masachis *et al.*, 2016). Plant RALFs are secreted peptides that were first identified for their ability to trigger a rapid increase in ambient pH when added to crops (Pearce *et al.*, 2001). Interestingly, was recently sghown that *F. oxysporum* secretes F-RALF, a functional homologue of plant RALFs (, that triggers rapid alkalinization of the apoplast. Isogenic *F. oxysporum* mutant lacking functional F-RALF failed to induce root alkalinization and showed markedly reduced virulence towards tomato plants (Masachis *et al.*, 2016). F-RALF appears to target the plant receptor-like kinase FERONIA, which also mediates responses to endogenous plant RALF peptides. RALF-FERONIA signaling leads to inactivation of the plant PM $H^+$-ATPase AHA2 and to extracellular alkalinization (Haruta *et al.*, 2014). This process regulates a series of developmental and physiological responses including a complex immune response in plants (Blackburn *et al.*, 2020; Zhang *et al.*, 2020). An Arabidopsis mutant defective in FERONIA failed to respond to F-RALF and displayed enhanced resistance against *F. oxysporum* (Masachis *et al.*, 2016). By contrast, in the flower-infecting wheat pathogen *F. graminearum,* RALF is not relevant for virulence, and transient silencing of two FERONIA homologs did not alter the outcome of the fungal-host interaction (Wood *et al.*, 2020).

## 4. pH regulates fungal pathogenicity through MAPK signaling

Fungus-induced pH modifications trigger important cellular changes such as alterations in the cell wall, often accompanied by larger morphological transitions that promote host colonization. In the human fungal pathogen *C. albicans*, pH-directed cellular responses include the ability to transition between yeast-like and invasive hyphal growth forms (Davis, 2009; Garnaud *et al.*, 2018; Selvig & Alspaugh, 2011). In the necrotrophic fungus *C. gloeosporioides,* alkalinization by ammonia is required for appressorium formation as well as for the transition from quiescent-biotrophic to active-necrotrophic interactions that determine the extent of host colonization (Miyara *et al.*, 2010). These morphogenetic switches, which are critical for the virulence of all fungal pathogens, are mediated by the invasive growth (IG) mitogen-activated protein kinase (MAPK) cascade (Davis, 2009; Lengeler *et al.*, 2000; Xu & Hamer, 1996; Zhao *et al.*, 2005).

### 4.1. Role of MAPKs in fungal pathogenicity

MAPK cascades are widely conserved eukaryotic signaling pathways, which transduce external cues into appropriate cellular responses, regulating a wide variety of processes in fungi such as cell growth, differentiation, survival and pathogenicity (Turrà *et al.*, 2015; Turrà *et al.*, 2014). MAPK cascades are evolutionarily conserved three–tiered protein kinase modules composed of a MAPK kinase kinase (MAPKKK) that phosphorylates the downstream MAPK kinase (MAPKK), which in turn activates the MAPK for downstream transmission of cellular signals (Turrà *et al.*, 2014). This module is activated mostly after sensing of external signals by receptors at the PM, and their activation results in a number of substrates phosphorylation including transcription factors that trigger the regulated expression of genes relevant for cell response to the stimuli (Rispail *et al.*, 2009). Current understanding of MAPK pathway is largely based on the model organism *S. cerevisiae*, in which five different MAPKs signaling pathways have been reported (Chen & Thorner, 2007). By contrast, most ascomycete fungi only have three conserved MAPK pathways (Turrà *et al.*, 2014). The ortholog of the yeast Fus3/Kss1 MAPKs was shown to be crucial for fungal invasive growth and appressorium formation in several plant pathogens including the rice blast fungus *Magnaporthe* oryzae (Lev *et al.*, 1999; Ruiz-Roldán *et al.*, 2001; Takano *et al.*, 2000; Xu & Hamer, 1996; Zhao *et al.*, 2005). In the soil-borne

ascomycete *F. oxysporum*, the Fus3/Kss1 homologue Fmk1 was found to be crucial for infection-related functions such as IG, vegetative hyphal fusion, root adhesion and virulence towards the tomato plant (Prados Rosales & Di Pietro, 2008; Turrà *et al.*, 2015). In addition, orthologs of the yeast cell wall integrity (CWI) MAPK Mpk1/Slt2, are involved in the infection process in several fungal pathogens such as citrus postharvest *Penicillium digitatum* and *M. oryzae*, mutants lacking *mps1* showed restricted infection at the penetration point (Gandía *et al.*, 2019; Zhang *et al.*, 2017). In the soil-borne pathogen *F. oxysporum*, the *mpk1*Δ mutant strains have defects in chemotropic sensing of tomato roots, penetration and colonization, leading to decreased pathogenicity (Nordzieke *et al.*, 2019; Segorbe *et al.*, 2017; Turrà *et al.*, 2014). Finally, the orthologs of the yeast high osmolarity glycerol (Hog1) MAPK, required for the response to hyperosmotic stress, have also been shown to contribute to virulence in some fungal pathogens. However, the exact role during infection remains unknown (Day *et al.*, 2017; Day *et al.*, 2018; Igbaria *et al.*, 2008; Turrà *et al.*, 2014).

### 4.2. Regulation of MAPK signaling by pH

Although pH and MAPK signaling have both been known as master regulators of fungal pathogenicity, their interplay in controlling fungal pathogenicity was not considered until recently (Fernandes *et al.*, 2017; Mariscal *et al.*, 2023). A previous study in *F. oxysporum* revealed that ambient pH regulates fungal pathogenicity by modulating the phosphorylation status of the IG Fmk1 MAPK [Figure 3A]. It was found that extracellular alkalinization promotes rapid phosphorylation of Fmk1, leading to enhanced invasive growth and virulence on tomato plants, while extracellular acidification prevents invasive growth and other infeccion-related processes such as tomato root penetration (Masachis *et al.*, 2016). Interestingly, the other two MAPKs Mpk1 and Hog1 are regulated in an opposite way by ambient pH, since their phosphorylation is promoted by extracellular acidification [Figure 3B] (Fernandes *et al.*, 2022a).

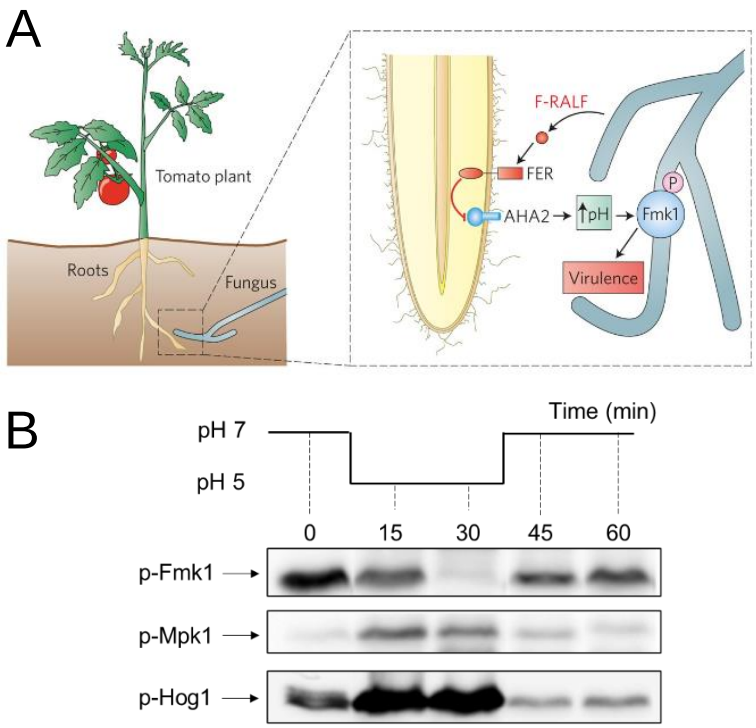


**Figure 3. Fungus-triggered alkalinization modulates MAPK signaling.** (**A**) Schematic illustration of the effect of secreted *F. oxysporum* F-RALF peptide. F-RALF induced alkalinization triggers IG Fmk1 MAPK phosphorylation promoting virulence on tomato plants (from (Kamoun & Zipfel, 2016)). (**B**) Ambient pH effect on MAPK phosphorylation status. Fmk1 MAPK is activated at pH 7 and inactivated at pH 5. By contract, Mpk1 and Hog1 MAPKs show an increase in phosphorylation upon extracellular acidification (pH5) and a decrease upon alkalinization (pH 7) (from (Segorbe, 2014)).

## 5. Cytosolic pH acts as a master switch of virulence

In contrast to ambient pH, cytosolic pH ($pH_c$) tends to be constant and tightly regulated in all organisms (Kane, 2016; Zhou *et al.*, 2021). However, rapid changes in $pH_c$ can occur in response to different stimuli (Orij *et al.*, 2011). For instance, changes in ambient pH have been shown to affect $pH_c$ dynamics in filamentous fungi (Bagar *et al.*, 2009; Fernandes *et al.*, 2022a). Furthermore, recent data have shown that rapid and transitory fluctuations in $pH_c$ can trigger activation of pathogenicity-related signaling pathways (Fernandes *et al.*, 2022a).

### 5.1. *Regulation of cytosolic pH homeostasis in fungi*

Two conserved plasma membrane (PM) and vacuolar proton-pumping ATPases are key players in fungal pH homeostasis (Kane, 2016; Palmgren &

Morsomme, 2019). In particular, the PM $H^+$-ATPase Pma1 is the major determinant of $pH_c$, the most abundant PM protein and essential for survival. Pma1 mediates ATP-dependent proton extrusion from the cell establishing an electrochemical gradient across the PM, which drives the active uptake of nutrients and inorganic ions via secondary transporters (Kane, 2016; Palmgren & Morsomme, 2019). The membrane Compartment containing Pma1 (MPC) is strictly localized to the sphingolipid-rich PM microdomain (Bianchi *et al.*, 2018; van 't Klooster *et al.*, 2020). Structurally, Pma1 is a 100 kDa polypeptide consisting of ten membrane-embedded α helices (M domain), and 3 cytosolic domains: A (actuator), N (nucleotide-binding) an P (phosphorylation) [Figure 4A] (Ambesi *et al.*, 2000). Pma1 carries regions at both its N- and C-terminus, which have been implicated in regulation and autoinhibition (Eraso & Portillo, 1994; Kühlbrandt *et al.*, 2002; Zhao *et al.*, 2021). The N-terminal domain is responsible for binding the A-domain but its function is still elusive (Zhao *et al.*, 2021) while the C-terminal autoinhibitory regulatory domain (R domain) forms an α helix that folds against the P domain (Heit *et al.*, 2021). Pma1 is assembled into a hexamer in the PM [Figure 4B] (Kühlbrandt *et al.*, 2002; Rhee *et al.*, 2002).

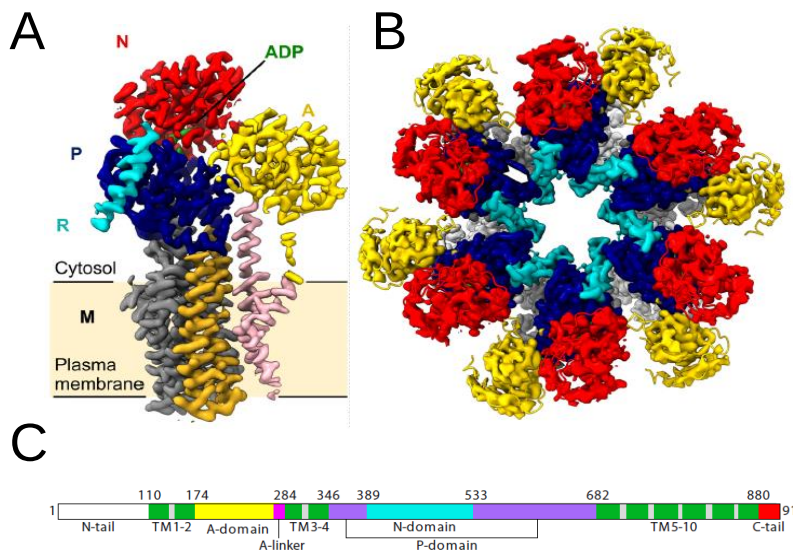


**Figure 4. The structure of the Pma1 monomer and hexamer.** (**A**) Cryo-EM map of the Pma1 monomer subunit. Nucleotide binding (N) domain in red, actuator (A) domain in yellow, phosphorylation (P) domain in blue, regulatory (R) domain in cyan, and adenosine diphosphate (ADP) in green. The 10 helices of the M domain are colored in pink (M1-M2), gold (M3-M4), and gray (M5-M10). In the bottom panel, ADP is shown as sticks and a potassium ion as a purple sphere; unmodeled loops are indicated by dashed lines. (**B**) Cryo-EM map of the Pma1 hexamer subunit. The M domains of individual monomers are shown in alternating shades of

gray, and cytosolic domains and ADP are colored as in (A). White arrows indicate contact sites between monomers (adapted from (Heit *et al.*, 2021)) (**C**) The Pma1 *S. cerevisiae* domain map (adapted from (Zhao *et al.*, 2021)).

The vacuolar $H^+$-ATPase (V-ATPase) is also highly relevant for $pH_c$ homeostasis regulation in fungal cells by pumping protons out of the cytosol, keeping the vacuole more acidic than the surrounding cytosol (Martínez-Muñoz & Kane, 2017). In contrast to the single-subunit Pma1, V-ATPase consists of fourteen subunits arranged in two subcomplexes. The peripheral subcomplex V1 harbors the site for ATP hydrolysis, while the V0 subcomplex is embedded in the organellar membrane and contains the proton pore. Like Pma1, V-ATPase is regulated by glucose via a process of reversible disassembly of peripheral V1 subunits from the membrane-bound V0 sector under glucose-depleted conditions (Kane, 2016).

The activity of both Pma1 and V-ATPase is also regulated by changes in ambient pH through a mechanism independent of glucose availability. While Pma1 activity is positively regulated by extracellular acidification (Carmelo et al., 1997; Orij et al., 2012; Zhao et al., 2021), V-ATPase assembly and activity is promoted by alkaline pH (Diakov & Kane, 2010). Moreover, the structure of Pma1 can also be affected by fluctuations in $pH_c$. In *S. cerevisiae,* the R-domain binds to the P-domain of two neighboring Pma1 subunits at alkaline pH locking the hexamer in an autoinhibited state, while the R-domain becomes disordered at low pH thus leading to activation of the Pma1 hexamer (Zhao et al., 2021). The activation process is accompanied by a 6.7Å downward shift and a 40° rotation of transmembrane helices 1 and 2 that line the H+ translocation path [Figure 5].

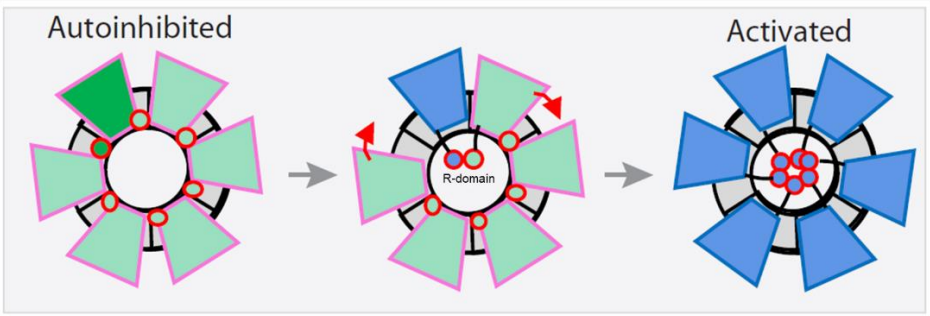


**Figure 5. A proposed cooperative activation model of the Pma1 hexamer.** When one $H^+$ in the PM Pma1 hexamer is activated, this protomer induces the activation of the next protomer by releasing its R-domain from the neighboring P-domain. Sequential release of the R-domain around the hexamer leads to the activation of all six protomers (adapted from(Zhao *et al.*, 2021)).

In contrast, V-ATPase assembly is negatively regulated by a decrease in $pH_c$ (Dechant *et al.*, 2010). An alkaline $pH_c$ leads to an enhanced V- ATPase activity as a result of higher levels of V1 subunits, suggesting that V-ATPase activation in response to pH also occurs at the level of V1-V0 assembly (Diakov & Kane, 2010). As a general rule, activation of $H^+$ pumping ATPases leads to a $pH_c$ increase by increasing $H^+$ export, whereas their inhibition triggers cytosolic acidification.

### 5.2. $pH_c$ control of signaling and cell growth

Tight regulation of $pH_c$ is of utmost importance for all processes in eukaryotic cells. For instance, changes in $pH_c$ can interfere with protein folding and enzyme activity, vesicle trafficking or even impact the function and integrity of organelles. In fungi, $pH_c$ homeostasis regulates fundamental processes including growth, development, ageing or virulence (Deprez *et al.*, 2018; Dolz-Edo *et al.*, 2019). In general, cytosolic acidification is correlated with slow growth whereas an alkaline cytosolic pH is associated with fast growth. Young *et al*. (2010) reported a new mechanism of regulation membrane biosynthesis by $pH_c$. They found that a decrease in $pH_c$ triggers the release of Opi1, a transcriptional repressor, from its binding to phosphatidic acid in the ER membrane, leading to its translocation into the nucleus. Nuclear Opi1 is then able to inhibit transcription of multiple phospholipid biosynthetic genes, limiting membrane biosynthesis and growth (Young et al., 2010). These results provided new insights into the role of $pH_c$ as a signaling mechanism coordinating the synthesis of membrane precursors with nutrient availability and growth rate.

Similarly, Dechant *et al*. (2010) found that growth rate and cell size are regulated by $pH_c$ in response to glucose availability. Glucose limitation induces a depletion of the $H^+$-ATPase Pma1 and as consequence, a decrease in $pH_c$, thereby triggering cell cycle arrest in early G1. Importantly this G1 arrest cand be reversed by increasing ambient pH, suggesting that it is caused by cytosolic acidification. Moreover, a decrease of $pH_c$ caused inactivation of the Ras signaling pathway, consistent with $pH_c$ acting as a signal for nutrient status (Dechant *et al.*, 2010). Furthermore, the V-ATPase plays a central role in $pH_c$ signaling in response to nutrient status. The mechanism proposed is that glucose levels are sensed through maintenance of neutral or slightly alkaline $pH_c$, and that the assembled V-ATPase is required to transmit the pH signal to downstream effectors such as protein kinase A

(PKA), Ras or TORC1 (Dechant *et al.*, 2010; Dechant *et al.*, 2014; Diakov & Kane, 2010). The small GTPase Arf1 was shown to interact with Stv1-containing the Golgi/endosome form of the yeast V-ATPase, thereby activating the upstream Ras pathway. Similarly, TORC1 pathway activation requires interactions between the Vph1-containing V-ATPase at the vacuole and the small GTPase Gtr1/2 at the vacuole [Figure 6] (Dechant *et al.*, 2010; Dechant *et al.*, 2014). TORC1 activation results in phosphorylation of the Sch9 kinase (Novarina *et al.*, 2021) and triggers disassembly of the vacuolar V-ATPase in a negative feedback mechanism (Wilms *et al.*, 2017). Therefore, Sch9 along with the V-ATPase appears to be required for a proper control of both $pH_c$ and vacuolar pH ($pH_v$) (Deprez *et al.*, 2018; Wilms *et al.*, 2017). Overall, Sch9 appears to play an integratory role through the assembly of V-ATPase in nutrient sensing and $pH_c$ that allows for coordination and fine-tuning of diverse signaling cascades. However, more studies are required to fully understand the molecular mechanisms underlying cell growth control by $pH_c$.

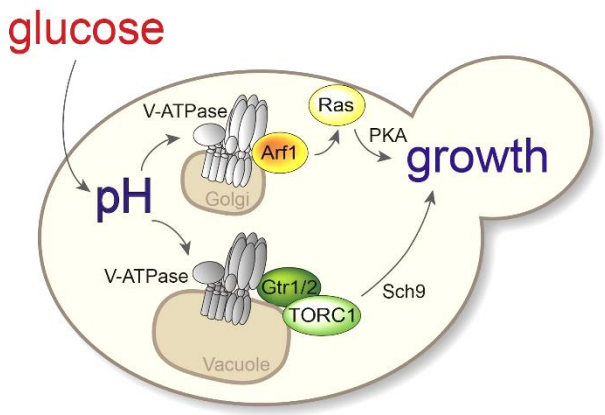


**Figure 6. $pH_c$ acts as a signal to activate Ras/PKA and TORC1 in response to glucose availability.** The glucose levels are translated through maintenance of neutral/alkaline $pH_c$, to keep V-ATPase in its assembled conformation. V-ATPase interacts with two distinct GTPases, Arf1 and Gtr1, which are required for Ras and TORC1 activation, respectively (from (Dechant et al., 2014)).

### 5.3. $pH_c$ as a regulator of fungal pathogenicity

Recently, a link between $H^+$-ATPase activity and virulence has begun to emerge. In the dimorphic fungi *Histoplasma capsulatum*, *C. neoformans* and *Candida* sp., mutants defective in V-ATPase were blocked in the yeast-hypha transition and showed attenuated virulence in a murine infection model (Hilty *et al.*, 2008; Hu *et al.*,

2021; Kim *et al.*, 2019; Minematsu *et al.*, 2019). In *M. oryzae*, the lack of a subunit of the V-ATPase complex produced a reduction of vacuolar acidification and the formation of small non-functional appressoria. Importantly, the mutant failed to cause disease even when inoculated through wounds, suggesting that V-ATPase is not only necessary for infection-related morphogenesis, but also for additional pathogenicity functions (Chen *et al.*, 2013). Given the critical role of the $H^+$-ATPase Pma1 in fungal growth by maintaining $pH_c$ homeostasis and regulation ion and nutrients uptake, one could anticipate a role virulence. In mycorrhizal fungi, Pma1 facilitates proton pumping activity and energizes nutrient uptake during fungal invasion of plant roots (Wang *et al.*, 2014). The biological function of Pma1 and its potential as a key antifungal target have been studied in different fungi. In *S. cerevisiae*, Pma1 has been characterized through the study of partial loss-of-function mutants (Ambesi *et al.*, 2000; Mason *et al.*, 2014). However, previous work reported that truncations at different regions of Pma1 produce different phenotypes (Mason *et al.*, 2014; Rane *et al.*, 2019).

Pharmacological inhibition of Pma1 $H^+$-ATPase activity with the specific inhibitor diethylstilbestrol (DES) (Kahm *et al.*, 2012; Moskvina *et al.*, 1999) has been key for discerning the role of Pma1 in virulence. In presence of DES, Pma1 activity is totally inhibited, producing a rapid and sustained decrease of $pH_c$ in the fungal plant pathogen *F. oxysporum* (Fernandes *et al.*, 2022a). The cytosolic acidification produced by the addition of DES controls the regulation of MAPKs in a manner similar to extracellular acidification (i.e. inhibition of Fmk1 and activation of Mpk1 and Hog1). Besides, ambient pH shifts are translated into MAPK reprogramming through a rapid and transitory change in $pH_c$ [Figure 7A] (Fernandes *et al.*, 2022a). Collectively, these results nsuggest that $pH_c$ acts as a second messenger controlling fungal pathogenicity, which could have significant implications in the development of target approaches for mitigation of crop diseases [Figure 7B].

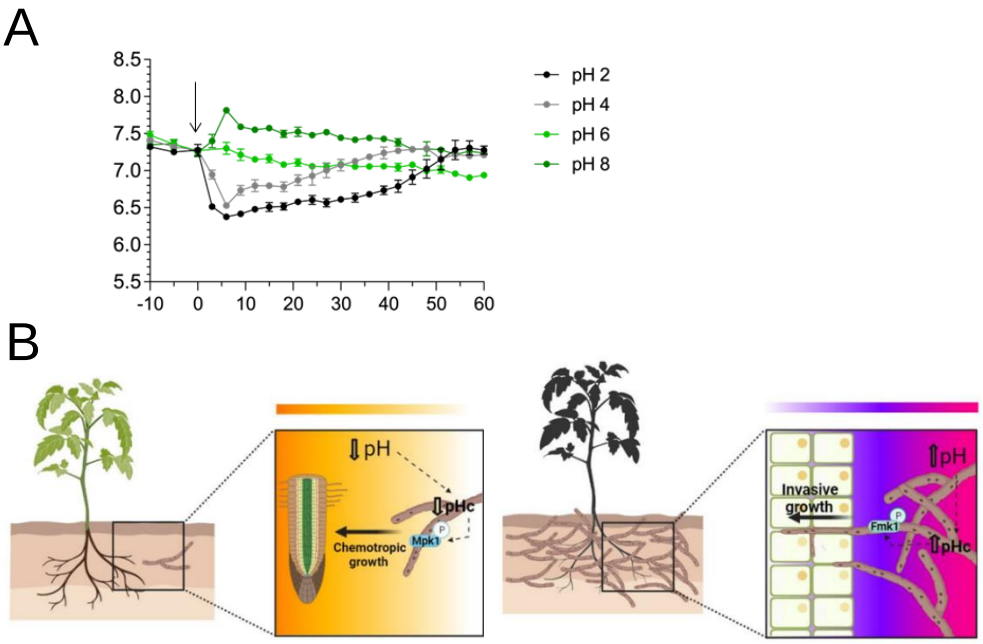


**Figure 7. $pH_c$-mediated MAPK regulation acts as a master switch in the control of fungal pathogenicity on plants.** (**A**) The $pH_c$ is affected by changes in ambient pH. Acidification or alkalinization of the external medium triggered a marked down- or upshift, respectively, of external pH tested in F. oxysporum (from (Fernandes *et al.*, 2022a)). (**B**) Early stages of infection: Signal molecules released by plant roots trigger chemotropic attraction of root-colonizing fungi. Chemotropic growth of F. oxysporum towards tomato root exudates was previously shown to require the MAPK Mpk1. Late stages of infection: Fungal phytopathogens such as F. oxysporum induce alkalinization of the surrounding host tissue to increase virulence. The effect of ambient pH on virulence-related functions is largely mediated by changes in $pH_c$ (from (Mariscal et al., 2023)).

# Aims of the study

## Objetivos del estudio

## Aims of the study

The main goal of the present study was to clarify the role of $pH_c$ homeostasis on regulation of MAPK signaling and pathogenicity of the fungal pathogen *Fusarium oxysporum*. To achieve this goal, we set out to:

1. Evaluate the role of pH in hyphal chemotropism of *Fusarium oxysporum.*
2. Understand the role of the long chain sphingolipid dihydrosphingosine as a signal for pH response and regulation of the CWI MAPK signaling.
3. Uncover the role of the plasma membrane $H^+$-ATPases Pma1 and Pma2 on $pH_c$ homeostasis and pathogenicity.
4. Characterize different regulators of Pma1 and their involvement on $pH_c$ homeostasis, MAPK signaling and virulence of *F. oxysporum.*
5. Perform a combination of genetic and biochemical approaches to manipulate Pma1 expression and activity.
6. Study the Pma1 localization in the plasma membrane of the fungal pathogens *F. oxysporum* and *Candida albicans*.

## Objetivos del estudio

El objetivo principal del presente estudio ha sido entender el papel de la homeostasis $pH_c$ en la regulación de la señalización de las cascadas MAPKs y virulencia en el patógeno fúngico *Fusarium oxysporum*. Para lograr este objetivo, nos propusimos a:

1. Evaluar el papel del pH en el quimiotropismo de la hifa en *Fusarium oxysporum.*
2. Estudiar el papel del esfingolípido de cadena larga dihidroesfingosina como señal para la respuesta del pH y regulación en la señalización de la MAPK Mpk1.
3. Descubrir la función de las $H^+$-ATPasas plasmáticas Pma1 y Pma2 en la homeostasis de $pH_c$ y patogenicidad.
4. Caracterizar los diversos reguladores de Pma1 y su papel en la homeostasis $pH_c$, señalización de las MAPKs y virulencia en *F. oxysporum*.
5. Realizar una combinación de enfoques genéticos y bioquímicos para manipular la expresión y actividad de Pma1.
6. Estudiar la localización de Pma1 en la membrana plasmática de los patógenos fúngicos *F. oxysporum* y *Candida albicans.*

# Materials and methods

# Materials and methods

## 1. Fungal strains and plant materials.

### 1.1 Fungal strains

#### 1.1.1 *Fusarium oxysporum* strains

The *F. oxysporum* strains used in this study are described in [Table 1]. All are derived from the *F. oxysporum* f. sp. *lycopersici* wild type strain 4287.

**Table 1. *F. oxysporum* strains used in this study.**

| Strain | Genotype | Reference |
|---|---|---|
| 4287 (FGS 9935) | Wild type; Race 2 | FGS[1] |
| Δ*pmp1* | *pmp1*::HYG | This study |
| Δ*pma2* | *pma2*::HYG | This study |
| Δ*ck1* | *ck1*::HYG | (Mariscal *et al.*, 2022) |
| Δ*ptk2* | *ptk2*::NEO | (Fernandes, unpublished) |
| *pHluorin* expressing strain | *pHlourin;*HYG | (Fernandes *et al.*, 2022b) |
| Δ*ck1* expressing pHluorin | *ck1*::PHLEO; *pHlourin;*HYG | This study |
| Δ*ptk2* expressing pHluorin | *ptk2*::PHLEO; *pHlourin;*HYG | This study |
| *pma1*$^{ts}$ | Homologous insertion of the *pma1*$^{A168G,\ V200I}$ allele;HYG | This study |
| pma1- OE | Extra insert of *Pma1*; HYG | This study |
| T-pma1 | Extra insert of *pma1* under the strong elongation factor 1-alpha (*tef1*) promotor from *F. oxysporum* | This study |
| Pma1::clover | Labelled version of *pma1* with*Clover in the carboxy terminus*; HYG | This study |
| *ypk1*$^{ts}$ | Homologous insertion of the *ypk1*$^{I428T,\ Y480C}$ allele;HYG | This study |

[1] Fusarium Genetics Stock Center

### 1.1.2 *Candida albicans* strains

The *C. albicans* strains used in this study are described in [Table 2]. All are derived from the *C*. albicans wild type strain BWP17.

**Table 2. *C. albicans* strains used in this study.**

| Strain | Genotype | Reference |
|---|---|---|
| BWP17 | *ura3Δ::λimm434/ura3Δ::λimm434 his1Δ::hisG/his1Δ::his arg4::hisG/arg4Δ::hisG* | (Wilson *et al.*, 1999) |
| PMA1/PMA1.mScarlet | Same as BWP17 with PMA1.mScarlet::HIS1/PMA1 | This study |
| PHL2 | Same as BWP17 with PKE1-PHL2 | This study |
| PHL2 PMA1/PMA1.mScarlet | Same as BWP17 with PMA1.mScarlet::HIS1/PMA1 PKE1-PHL2 | This study |

## 1.2. Plant material

The tomato cultivar used in this study is described in [Table 3].

**Table 3. Tomato variety used in this study.**

| Strain | Cultivar | Specifications | Source |
|---|---|---|---|
| *Solanum lycopersicum* | Monika (seeds) | Susceptible to *F.oxysporum f. sp. lycopersici* Race 2 | Syngenta, Almería (Spain) |

## 1. Plasmids

The plasmids used in this study are listed in [Table 4]. They include plasmids used for amplification of resistance cassettes to transform *F. oxysporum* and *C. albicans.*

**Table 4. Plasmids used in this study.**

| Plasmid | Features | Reference |
|---|---|---|
| pGem®-T | Derived from plasmid pGEM®-5Zf(+), linearized with EcoRV and with a T added in both 3' ends | Promega |
| pAN7-1 | Derived from pUC18; *A.nidulans* gpdA promoter; phosphotransferase hygromicin B (hph) gene; *A. nidulans TrpC* terminator | (Punt *et al.*, 1987) |
| pAN-8.1 | Derived from pUC18; *A.nidulans gpdA* promoter; phleomycin resistance gene; *A. nidulans trpC* terminator | (Mattern *et al.*, 1988) |
| PGEMT-*hph*BB | Derived from pAN7-1 plasmid with shorter version of *GpdA* promoter and *TrpC* terminator | Our group |
| PGEMT- *Neo* | Derived from pAN7-1; *GpdA* promoter; neomycin resistance gene; *TrpC terminator* | Our group |
| P_pHluorin | Derived from pGEMT*; A. nidulans gpdA* promoter*; pHluorin* gene; *S. cerevisiae ADH5* terminator | (Fernandes *et al.,* 2022b) |
| PUC57-3xFOmclover | Derived from PUC57; *A. nidulans* gpdA promoter; 3xFo-mClover3:3xFLAG | (Redkar *et al.*, 2022a) |

| | | |
|---|---|---|
| PFa-mScarlet.CdHIS1 (CP035) | The nucleotide sequences for the monomeric red fluorescent protein CamScarlet were optimized for *C. albicans* and commercially synthesized. The CdHis1 marker was obtained from pFA-GFP-CdHIS1 plasmid | (Puerner, unpublished) |
| pKE4-PHL2 | Derived from PKE1; *C. albicans tef1* promotor; optimized coding sequence of PHL2; *C. albicans adh1* terminator | (Tournu H *et al.,* 2017) |

## 2. Media and buffer solutions

All media were prepared with RO deionized water and sterilized by autoclaving at 1.2 atm and 120 °C for 20 minutes. Buffer solutions were prepared with RO ultrapure water and sterilized by filtration (0.22 µm pore size, Millipore). RO deionized and RO ultrapure water were obtained through the Direct-Q® 8 UV remote water purification system (Merck Millipore). [Table 5] lists the media and buffer solutions used in this study for fungal growth and maintenance. For each protocol of molecular biology, the buffer solutions prepared will be described in the respective section.

**Table 5. Media and buffer solutions used for bacterial and fungal growth.**

| | |
|---|---|
| **Media for *E. coli* (w/v)** | |
| LB | 1% tryptone, 0.5% yeast extract, 1% sodium chloride |
| LA | 1% tryptone, 0.5% yeast extract, 1% sodium chloride and 2% agar |
| **Media for *F. oxysporum* (w/v)** | |
| PDB | Boil 200 g of peeled potatoes in 0.6 L of deionized water for 60 minutes. Stir and add 20 g of glucose and deionized water up to 1 L |
| PDA | 3.9% potato dextrose agar |
| YP | 2% glucose and 2% tryptone |
| YPG | 2% glucose, 2% tryptone and 1% yeast extract |
| YPGA | 2% glucose, 2% tryptone, 1% yeast extract and 1.5% agar |
| Puhalla's MM | 0.05% $MgSO_4 \cdot 7H_2O$, 0.05% KCl, 0.1% $KH_2PO_4$, 0.22% $NaNO_3$, 3% sucrose and 1.5% oxoid agar |
| Regeneration MM | 0.05% $MgSO_4 \cdot 7H_2O$, 0.05% KCl, 0.1% $KH_2PO_4$, 0.2% $NaNO_3$, 2% glucose, 20% sucrose and oxoid agar (1.5% for Petri dishes and 0.5% for top agar) |
| **Media for *C. albicans* (w/v)** | |
| YPD + Uri | 2% glucose, 2.2% tryptone, 1.1% yeast extract, 0.1% uridine |
| LM2 | 8 g/L yeast nitrogen base without amino acids, 55 mg/l adenine, 55 mg/l tyrosine |

| | |
|---|---|
| FCS | 50% (v/v) YPD + Uri (1% glucose, 1.1% tryptone, 0.55% yeast extract, 0.05% uridine) + 50% (v/v) FCS |
| **Selective minimal media (w/v)** | |
| -URA | LM2, 2% glucose, 1/100 volume of -Ura drop out mix |
| -HIS | LM2, 2% glucose, 1/100 volume –His drop out mix |
| -URA -HIS | LM2, 2% glucose, 80 mg/L uridine, 1/100 volume –His dropout mix |
| **Buffer solutions** | |
| HEPES | 1 M HEPES, adjust the pH to 7.4 with NaOH 10N |
| KSU | 50 mM $K_2HPO_4$, 50 mM sodium succinate and 25 mM Urea. Adjust the pH according to the experiment. |

LB - Luria-Bertoni; LA - Luria-Bertoni con Agar; YPD -Yeast Extract Peptone Dextrose; YPDA - Yeast Extract Peptone Dextrose Agar; SC - Synthetic Complete medium; PDB - Potato Dextrose Broth; PDA - Potato Dextrose Agar; MM - Minimal Medium; FCS - Fetal Calf Serum.

## 4. Growth conditions

### 4.1. Bacteria

The *Escherichia coli* strains were grown overnight (O.N.) at 37 °C in LA medium. Grown colonies on plate were picked and grown in LB medium O.N. at 37 °C with orbital shaking at 250 rpm. LB medium was supplemented with the appropriated antibiotic.

Bacterial cells were preserved at -80 °C in 30% (v/v) glycerol.

### 4.2. *Fusarium oxysporum*

*F. oxysporum* strains were cultured in PDB medium at 28 °C with orbital shaking at 170 rpm. When needed, the following antibiotics were added to the culture medium: hygromicin B at 20 µg/ml, phleomycin at 4 µg/ml and geneticin at 10 µg/ml. After 3 to 5 days of culture in liquid medium, microconidia were collected by filtration through a nylon filter (Monodur; mesh size 10 µm) and then by centrifugation at 8000 rpm for 10 minutes. Depending on the experimental condition and design, microconidia were either germinated in rich medium or plated on solid media for phenotypical assays. For transformants selection on solid medium, antibiotics were added at the following concentrations: 55 µg/ml of hygromicin B, 11 µg/ml of phleomycin or 27.5 µg/ml of geneticin.

For long-term storage of the different strains, microconidia collected from 3 to 5 days-old cultures were resuspended in 33% (v/v) glycerol and stored at -80 °C.

These suspensions were used for later inoculation to obtain fresh microconidia.

### 4.3. *Candida albicans*

*C. albicans* strains were grown in YPD+Uri medium at 30 °C with orbital shaking at 170 rpm for budding growth. Hyphal formation was induced by incubating at 37 °C in 50% (v/v) FCS and 50% (v/v) YEPD+Uri.

### 4.4. Tomato plant culture

Tomato seeds were surface sterilized in 20% (v/v) bleach for 30 minutes. Then, seeds were washed 3 times for 10 minutes with sterilized Milli-Q water. Seeds were sown in wet vermiculite and incubated for 14 days (until the first pair of true leaves appeared) in a growth chamber with defined conditions (28 ºC, relative humidity of 40-70% and a photoperiod of 14 hours of 36 W white fluorescent light and 10 hours of darkness).

## 5. Molecular methodology

Macromolecules were isolated from bacterial and fungal cultures for subsequent downstream processes, analytical or preparative purposes. The protocols employed in this study will be described in detail in the sections below.

### 5.1. Nucleic acid extraction and quantification

#### 5.1.1 Plasmid DNA extraction from *Escherichia coli*

For plasmid DNA extraction from bacteria, the CTAB method was used as previously described (Murray & Thompson, 1980). Briefly, a single colony of bacteria grown O.N. on a LA plate at 37 °C was peaked to liquid LB medium (containing antibiotic if required) and grown O.N. at 37 °C with orbital shaking of 250 rpm. The day after, cells were collected by centrifugation 2 minutes at 13400 rpm and resuspended in 200 µl of STET[2] solution, supplemented with 4 µl of lysozyme (50 mg/ml; Sigma Aldrich) and 4 µl of RNase (10 mg/ml; Roche Life Science), and incubated 10 minutes at RT. Then, cells were boiled for 45 seconds and centrifuged 10 minutes at 13400 rpm. The obtained pellet was removed using a sterile wood stick

[2] STET: 8% (w/v) sucrose, 0.1% (v/v) Triton X-100, 50 mM EDTA pH 8.0, 50 mM Tris-HCl pH 8.0.

and 10 µl of 5% CTAB extraction buffer[3] were added to precipitate the plasmid DNA. After 10 minutes of incubation at RT, samples were centrifuged 10 minutes at 13400 rpm. Each pellet was resuspended in 350 µl of 1.2 M NaCl and 750 µl of 100% ice-cold ethanol and centrifuged again for 10 minutes at 13400 rpm. Precipitated plasmid DNA was then washed for two times more with 1 ml of ethanol 70%, dried and resuspended in sterile Milli-Q water.

### 5.1.2. Nucleic acids extraction from *Fusarium oxysporum*

#### *5.1.2.1. DNA extraction*

Genomic DNA extraction was mostly performed from *F. oxysporum* mycelium grown for 3-4 days and by using the CTAB method (Torres *et al.*, 1993), with some modifications. Briefly, frozen mycelium was lyophilized using a freeze-drying system (Labconco) and then pulverized using the homogenizer Fast prep® (Bio 101 Systems, Qbiogene, Madrid, España) with 1-5 mm diameter glass beads (Sigma). Each sample was resuspended in 1 ml of CTAB extraction buffer, 4 µl of β-mercaptoethanol and 24:1 (v/v) chloroform:octanol to make up a final volume of 2 ml. This mix was homogenized by inversion and incubated at 65 ºC for 30 minutes. After incubating at RT for 15 minutes, samples were centrifuged for 10 minutes at 13400 rpm. The upper aqueous phase was transferred to a new Eppendorf tube, precipitated by adding 1 ml of 100% ice-cold ethanol and incubated at -20 ºC for at least 1 hour (O.N. preferred). Precipitated DNA was then centrifuged for 10 minutes at 13400 rpm and washed two times with 1 ml of 70% (v/v) ethanol. DNA pellet was dried and resuspended in 50 µl of sterile Milli-Q water with 5 µl of RNase (10 mg/ml; Roche Life Science) and incubated at 37 ºC for 45 minutes. The DNA obtained was stored at -20 ºC.

For DNA extraction from fungal colonies (colony PCR), the Phire Plant Direct PCR Master Mix kit (Thermo Scientific™) was used. Shortly, a *F. oxysporum* colony was picked (in the most external part) with a sterile wood stick and put into a 1,5 ml Eppendorf tube with 20 µl of sterile Milli-Q water. The mycelium was crushed against the Eppendorf tube for 5-6 times and 1 µl of this suspension was added to 4 µl of

[3] CTAB extraction buffer: 12.1 g/l Trizma base, 7.44 g/l EDTA, 81.8 g/l NaCl and 20 g/l Cetyltrimethylammonium bromide. Heat to 60 ºC to dissolve and adjust to pH 8.0 with NaOH 10 N. Store to 37 ºC to avoid precipitation.

dilution buffer provided in the kit. The sample was incubated for 2 hours at RT and 0.5 µl of this mix was used to directly perform a PCR analysis.

#### *5.1.2.2. RNA extraction*

For RNA extraction from *F. oxysporum*, frozen mycelium was lyophilized and pulverized, as previously described. Each sample was then resuspended in 1 ml of Tripure Isolation Reagent (Roche) and centrifuged at 4 ºC for 10 minutes at 13000 rpm. The supernatant was transferred to a new Eppendorf tube and incubated for 5 minutes on ice to allow dissociation of nucleoprotein complexes. Then, 200 µl of chloroform were added and mix was vortexed for 15 seconds prior incubation on ice for 5 minutes. After that, samples were centrifuged at 4 ºC for 15 minutes at 13000 rpm, resulting in the visualization of three phases. The upper clear phase was transferred to a new Eppendorf tube containing 500 µl of isopropanol. The Eppendorf tube was mixed by inversion and incubated for 10 minutes on ice. Subsequently, the samples were centrifuged at 4 ºC for 10 minutes at 13000 rpm. The RNA pellet was washed with 1 ml of 70% (v/v) ice-cold ethanol and centrifuged at 4 °C for 5 minutes and 8000 rpm. Finally, the pellet was dried, resuspended in 50 µl of sterile Milli-Q water (RNase free) and incubated for 15 minutes at 60 ºC. The RNA obtained was stored at -80 ºC.

#### *5.1.2.3. Nucleic acid quantification*

DNA/RNA quantification and purity was assessed either by electrophoresis by using a 0.7 % (w/v) agarose gel or through a Nanodrop® ND-1000 spectrophotometer, where the ration of 260/280 nm and 260/230 nm allow to determine the quality of the DNA and RNA extracted.

### 5.1.3. Nucleic acids extraction from *Candida albicans*

For genomic DNA extraction from *C. albicans*, a 5 µl cell suspension grown O.N. at 30 °C in YPD was diluted (1:2) in the same medium and centrifuged at 13000 rpm for 2 minutes. Pellet cells were resuspended in 100 µl of LitAct-SDS lysis solution[4]. Prior to incubation at 70 ºC for 5 minutes for cell lysis, two successive washing steps (with 300 µl of ethanol 96% and 500 µl of ethanol 70%, respectively)

[4] LitAct-SDS lysis solution: Lithium acetate 200mM, 1%SDS.

were performed. Then, cells were centrifuged at 13000 rpm for 3 minutes and pellets were dried at 50 ºC for 20-30 minutes. Finally, DNA was resuspended in 50 µl of TE1X[5].

### 5.2. DNA amplification reactions

After extraction and quantification, plasmid and genomic DNA were used to amplify fragments of interest. Standard and Fusion PCR reactions were employed using synthetic oligonucleotides that were designed according to the experimental purpose.

#### 5.2.1. Standard PCR

PCR amplification reactions were performed in a thermocycler using different thermostable Taq DNA polymerases depending on the objective of the experiment and the fragment size. For reactions where high fidelity in amplification was required, the enzyme *Expand High Fidelity PCR System* (Roche) or the enzyme *Phusion® High-Fidelity DNA Polymerase* (New England Biolabs) were used, following the manufacturer´s instructions. For knockout mutant confirmation and Southern blot probes, the thermostable *BioTaq™ DNA Polymerase* (Bioline) was used. Each PCR reaction contained 300 nM of each primer, 2.5 mM $MgCl_2$, 0.8 mM of dNTPs mix and 0.05 U/µl of polymerase. Genomic DNA was added at 5-10 ng/µl and plasmid DNA at 1-5 ng/µl final concentration. The amplification conditions are detailed in [Table 6].

**Table 6. Standard PCR conditions.**

| Polymerase | Step | Temperature; Time | Cycles |
|---|---|---|---|
| Expand High Fidelity PCR System | Initial denaturation | 94 °C; 5 minutes | 1x |
| | Denaturation | 94 °C; 35 seconds | 35x |
| | Annealing | Tm [6]; 35 seconds | |
| | Elongation | 72 / 68 °C [7]; 1 minute /Kb | |
| | Final elongation | 72 / 68 °C; 10 minutes | 1x |
| | Hold | 4°C; unlimited time | - |
| | Initial denaturation | 98°C; 30 seconds | 1x |

[5] TE1X (Tris-EDTA): 10mM Tris HCl pH8.0, 1mM EDTA pH8.0.
[6] Tm is the binding temperature of the primers to the template.
[7] For PCR products larger than 3 kb, elongation temperature should be 68 °C.

| | | | |
|---|---|---|---|
| Phusion ® High-Fidelity DNA Polymerase | Denaturation | 98°C; 10 seconds | 35x |
| | Annealing | Tm ;30 seconds | |
| | Elongation | 72 °C; 30 sec/Kb | |
| | Final elongation | 72 °C; 10 minutes | 1x |
| | Hold | 4°C; unlimited time | - |
| Bio Taq™ DNA Polymerase | Initial denaturation | 94 °C; 5 minutes | 1x |
| | Denaturation | 94 °C; 35 seconds | 35x |
| | Annealing | Tm ;35 seconds | |
| | Elongation | 72 °C; 1 minute /Kb | |
| | Final elongation | 72 °C;10 minutes | 1x |
| | Hold | 4°C; unlimited time | - |

### 5.2.2. Colony PCR

Colony PCR was performed using the Phire Plant Direct PCR Master Mix kit (Thermo Scientific™) from isolated DNA (as described in section 3.5.1.2.). Each PCR reaction contained 525 nM of each primer, 1X Phire Plant Direct PCR Master Mix, and 0.5 µl of DNA. The amplification conditions are detailed in [Table 7].

**Table 7. Colony PCR conditions.**

| Step | Temperature, Time | Cycles |
|---|---|---|
| Initial denaturation | 98°C; 5 minutes | 1x |
| Denaturation | 98°C; 5 seconds | 35x |
| Annealing | Tm; 5 seconds | |
| Elongation | 72°C; 20 seconds/kb | |
| Final elongation | 72°C; 1 minute | 1x |
| Hold | 4°C; unlimited time | - |

### 5.2.3. Fusion PCR for generation of *Fusarium oxysporum* knockout mutants

The generation of knockout mutants in *F. oxysporum* was carried out by targeted gene deletion using the Split-marker technique consisting of the replacement of the wild type allele of the gene with a resistance cassette (Catlett *et al.*, 2003). Gene deletion was performed by fusion PCR or overlap extension, a method used to fuse two or more PCR products (Yang *et al.*, 2004), as schematically represented in [Figure 8A]. Complementary oligonucleotides and PCR are used to generate two DNA fragments with overlapping ends. In this PCR reaction (PCR I), an approximately 2

Kb fragment upstream (promoter) and downstream (terminator) of the Open Reading Frame (ORF) of the target gene are amplified with oligonucleotides containing a tail homologous to the selectable marker cassette (named '*Resistance gene*' in Figure 8). The amplified fragments are then combined in a fusion reaction (PCR II) without oligonucleotides in which the overlapping ends anneal. In this reaction, the 3' overlap of each strand serves as a primer for the extension of the complementary strand and the promoter and terminator regions are fused with the selectable marker cassette (PCR II). The resulting fusion products are used as template for further amplification reactions (PCR III) using the primers of interest (P7/P8 to fuse the selectable marker with promotor region and P9/P10 with terminator region). Thus, two fragments carrying approximately 75% of the resistance gene are obtained, including an overlapping region, and 1.5 Kb of the promoter or terminator region of the target gene. Both overlapping fragments are then used for protoplasts transformation and for replacement of the target gene with the resistance cassette, which 36 occurs by a double homologous recombination event, as illustrated [Figure 8B].

For transformation, PCR products were precipitated, and equimolar quantities of the purified products were used for protoplasts transformation.

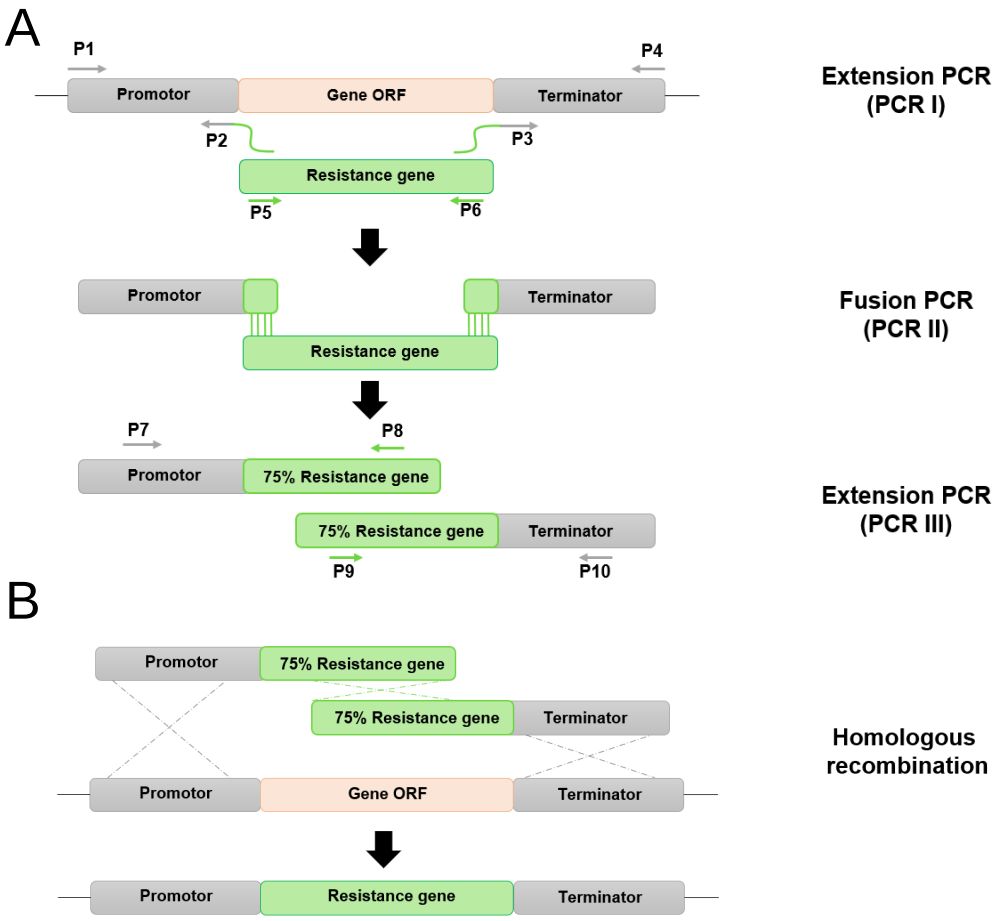


**Figure 8. Schematic representation of the split-marker deletion strategy for knockout mutants generation in *F. oxysporum.*** (**A**) PCR reactions involving: (i) amplification of the Promoter upstream (P1/P2) and Terminator downstream (P3/P4) regions of the target gene with primers containing tails homologous to the Resistance gene, which is also amplified (P5/P6; PCR I); (ii) fusion of DNA fragments in a reaction without primers (PCR II) in which the overlapping ends anneal; (iii) amplification of fused fragments using primers in the internal part of the resistance gene (P8/P9) and in the flanking regions of the target gene (P7/P10). (**B**) Homologous recombination of the two PCR fragments generated in PCR III, and replacement of the target gene ORF with the Resistance gene, during fungal protoplasts transformation.

### 5.2.4. Synthetic oligonucleotides

The oligonucleotides used in this study are listed in [Table 8] and were designed with the Primer Analysis Software Oligo version 7,0 (Molecular Biology Insights, Inc. – Colorado, USA). Internal stability, duplex and hairpin formation and different physicochemical parameters, such as temperature of melting (Tm; calculated through the [2(A+T)°+4(G+C)°] method) were determined in each case.

Oligonucleotides were synthesized by Isogen Life Science, Netherlands.

**Table 8. List of primers used in this study. Lowercase nucleotides do not belong to the original sequence and were introduced to generate overlapping ends for fusion PCR reactions.**

| Gene/ Vector | Name | [Tm]_Sequence 5'→3' |
|---|---|---|
| *hyg* | HygG | [62]_CGTTGCAAGACCTGCCTGAA |
| | HygY | [62]_GGATGCCTCCGCTCGAAGTA |
| *phleo* | Leo | [62]_GCCACGAAGTGCACGCAGTT |
| | Phe-5 | [62]_CGGAGCGGTCGAGTTCTGG |
| *neo* | NeoG | [62]_TGCCCTGAATGAACTGCAAGA |
| | NeoY | [62]_CCAAGTTCTTCAGCAATATCAC |
| Casete *hyg/phleo* | gpdA15B | [62]_GGATCCCGAGACCTAATACAGCCCCT |
| | gpdA16B | [62]_AGGGGCTGTATTAGGTCTCG |
| | trpC8B | [62]_GGATCCAAACAAGTGTACCTGTGCATTC |
| | trpC4B | [62]_CCTGGGTTCGCAAAGATAATT |
| | M13F | [62]_CGCCAGGGTTTTCCCAGTCACGAC |
| | M13R | [62]_AGCGGATAACAATTTCACACAGGA |
| *Actin* | Pact-2P | [62]_GGCTGCAGCATTAGAAAGTTC |
| | Pact-3 | [62]_GGCTGTGGATTACGGTGTGT |
| *tef1* promotor | Ptef1_for | [64]_TCCACAGTGGCTGGACATGAT |
| | Ptef1_for2 | [64]_AACACACAGGCGCAAGACCAA |
| | Ptef1_rv | [64]_TGTGAGTACTCTCCTCGACA |
| *ypk1$^{ts}$* | Ypk1_fwd | [62]_GTCTCGCTTCTCCTTCTCATT |
| | Ypk1_fwd_nested | [62]_ACCCCAACCATCAAATACCTC |
| | Ypk1_rv | [62]_CATCAAGGTTGGCTGACTGG |
| | Ypk1_rv_nested | [62]_CAATCTCTCCGATCTCAGCC |
| | Ypk1 I484T fwd | [62]_AGGCCATACTGCTCTTTGCG |
| | Ypk1 Y536C rv | [62]_CAACATCTCGCACAGCAAAAC |
| | Ypk1_SEC1 | [62]_CTACTCAAGGTCGTCGGCAA |
| | Ypk1_SEC2 | [62]_ AATGTGAGAGACTGGGAAAAGA |
| *pmp1* | Pmp1_P_Fwd | [62]_GAAGCCCCAAATATCTATCAAC |
| | Pmp1_P_Nested | [62]_AGGCGTTGGGCAGGGAAATA |
| | Pmp1_P_Rv | [62]_tttacccagaatgcacaggtacacttgtttAGGCCGACGTT AAGGAGAGT |
| | Pmp1_T_Fwd | [62]_tggtcgttgtaggggctgtattaggtctcgTGTGTCTGGAGT GGAGAGATT |

| | | |
|---|---|---|
| | Pmp1_T_Nested | [62]_ATGGGTTGCGTCGATTTAGATA |
| | Pmp1_T_Rv | [62]_TGGGCTTGCTGTGATGGATG |
| *pma2* | Pma2_P_Fwd | [62]_CACTTGCCGTCAGATAGGTTT |
| | Pma2_P_Nested | [62]_GCTCCATCAACTCAAGACCAT |
| | Pma2_P_Rv | [62]_tttacccagaatgcacaggtacacttgtttTATCGTTCAAGCAGATTATGATG |
| | Pma2_T_Fwd | [62]_tggtcgttgtaggggctgtattaggtctcgCTGCTGTGTTGTGGTGATGA |
| | Pma2_T_Nested | [62]_GGTCGCCATGCAGTGTCCA |
| | Pma2_T_Rv | [62]_TGGGAGGACTTCAGCACGG |
| | Pma2.qPCR.Fwd | [62]_GAGGCAGGTCATCTTGGAGT |
| | Pma2.qPCR.Rv | [62]_CCGTGTACTTATGCTCTGGG |
| *pma1* | Pma1_1 | [62]_TCGCCGTAGGACCCGTTTG |
| | Pma1_1N | [62]_TACAGCCGCACTCTACACAC |
| | Pma1_ATG | [62]_ATGGCTGAAGAGAAGGCGGC |
| | Pma1_6 | [62]_AGACCAGGAGCAAGGAAAACA |
| | Pma1_6N | [62]_GGGTCAGAGCAAGGCATAATT |
| | Pma1_Fwd_ts | [62]_TCTGCTGGAGTTTAATTCTTGG |
| | Pma1_nested_nested | [62]_AGACCGACAGGGACACCGA |
| | Pma1_Prom_Fwd | [64]_CACTCTCTGTCTCTAGTTTCCA |
| | Nested_ORF | [62]_CCCTTTGATCCCGTCTCCAA |
| | Pma1_nested | [62]_GTTTGTGGCCTTTCTCGGTG |
| | Linker2_Clover_Fwd | [62]_GGCTCTACTTCTGGCAGCAT |
| | Pma1_ORF_Rv_Linker2Clov | [62]_atgctgccagaagtagagccCTGAGACTTCTCGTGCTGAGT |
| | Pma1_Term_Fwd_cola3xFLAG | [62]_gacgatgacgataagctttaaATATACCCGGACCACCATCGA |
| | 3xFLAG_Rv | [62]_TTAAAGCTTATCGTCATCGTCC |
| | Pma1_Rv | [62]_CACAGAGAGAGCGAAAGTAGA |
| | Pma1_Term1_Rv | [62]_GAAGCGGCAAATGTGAGCAGT |
| | Pma1_Ter3_nested | [62]_GGACAGCGACTCTCTGGTAG |
| | Pma1_Term1_nested | [62]_GGCAACACAAATAAGGTCCGA |
| | Pma1.ATG-Tef1 | [64]_tgtgagtactctcctcgacaATGGCTGAAGAGAAGGCGGC |

| | | |
|---|---|---|
| | Pma1.qPCR.Fwd | [62]_CGAAGATGAGGAGCCCGAC |
| | Pma1.qPCR.Rv | [62]_CCCCATTTGCGTCGTCGGT |
| *pma1$^{ts}$* | Pma1_2 | [62]_ACTTACCCTTGGAACTCTTGG |
| | Pma1_3 | [62]_AGAGTTCCAAGGGTAAGTTTATT |
| | Pma1_4 | [62]_ATATCACCGGGAATGACCTC |
| | Pma1_5 | [62]_GAGGTCATTCCCGGTGATAT |
| *ck1* | Ck1-1 | [62]_gaggtaggattgggtgcgac |
| | Ck1-2 | [62]_CACGGGAAGGGTTGAGAGAG |
| | Ck1-3 | [62]_tttacccagaatgcacaggtacacttgttATTTAGGCGGCG AAGGCGGT |
| | Ck1-4 | [62]_tggtcgttgtaggggctgtattaggtctcgTCATTGCTGCG GCGTTGTGC |
| | Ck1-5 | [62]_TCATCGTGTCGTTTCTCAGCG |
| | Ck1-6 | [62]_TCTGTTTCACCCCTTCGTCCA |
| | Ck1-Fwd | [62]_GGCAAGAAGATTGGAGAGGG |
| | Ck1-Rv | [62]_CTCGCCATCCTCAACCTCG |
| *ptk2* | Ptk2-1f | [62]_AGTATCTCGGGCTGTCCATC |
| | Ptk2-1n | [62]_AGTTTTTGGCGTTGTGTATCTG |
| | Ptk2-1r | [62]_AAGTCGGGTGCTGAGAAATAG |
| | Ptk2-2f | [62]_GTCCTACAAACACTAAACAACC |
| | Ptk2-2n | [62]_CACGCCCTTCTCTCATTCAC |
| | Ptk2-2r | [62]_AATCAGCCCTCCTACCTCTC |
| PFa-mScarlet.CdHIS1 (CP035) | CaPma1pXFP_S1 | [79]_CGGTAGAAAACCACAACAACACACTGACAAG AGATCCTTGGAAGATTTCCTTGTGTCCATGCAAAG AGTATCTACTCAACACGAAAAATCTACTggtgctggcg caggtgcttc |
| | CaPma1pXFP_S2 | [74]_CAATGACAAAAACAAACATGCAAAATTAGTAA TAACAATTGTCGATTAATATTAATCTCCAATTATTC ACATCAACAACGATATCATCAAATtctgatatcatcgatga attcgag |
| | CamScarletm108 | [55]_CCGACATAGTCTTTCACTGC |
| *CaPma1* | CaPma1p2512 | [55]_GGTCTTTCFFTFTCTTCTGT |
| PHL2 | LUXINTDETF | [55]_CTGACCTTTAGTCTTTCCTGC |
| | LUXINTDETR | [55]_CAGTAGTACTTGTTGTTGTATCG |

### 5.2.5. Precipitation of DNA and Southern blot probes

Precipitation of DNA was routinely performed by using ammonium acetate. Briefly, 1/10 volume of 3 M sodium acetate was added to DNA and carefully mixed. Two volumes of 100% cold-ethanol were added, and samples were incubated at -20 ºC for, at least, one hour. Precipitated DNA was then centrifuged at 13400 rpm for 30 minutes at RT. Pellet DNA was washed with 70% ethanol, dried and finally resuspended with sterile Milli-Q water.

DNA probes for Southern blot were precipitated with lithium chloride (LiCl). For this protocol, 25 µl of PCR product were mixed with 2,5 µl of LiCl 8 M, carefully mixed, and 75 µl of 100% (v/v) ice cold-ethanol was added. DNA was precipitated by incubating the samples for 30 minutes at -20 ºC. Precipitated DNA was then centrifuged at 13400 rpm for 30 minutes at 4ºC. Pellet DNA was washed with 70% (v/v) ethanol, dried and finally resuspended in 10 µl of sterile Milli-Q water.

## 5.3. RNA reactions: Reverse transcriptase PCR

Prior complementary DNA (cDNA) synthesis, isolated RNA was treated for 30 minutes at 37 ºC with DNase I Recombinant kit (Roche) to remove DNA debris. Thus, 1 µg of total RNA was mixed with 0.2 µl RNAse, 1µl of 10x Incubation buffer and sterile Milli-Q water to a final volume of 9.5 µl. To stop the reaction, the mix was incubated at 75 ºC for 10 minutes, adding EDTA at a final concentration of 2.5 mM to prevent hydrolysis of RNA during heating.

The resulting treated RNA was treated with the Transcriptor Universal cDNA Master Kit (Roche) to synthesize the cDNA. For this purpose, to the 10 µl of RNA previously treated with DNase, 4 µl of buffer, 1 µl of reverse transcriptase and 5 µl of sterile Milli-Q water were added. The reverse transcription conditions are detailed in [Table 9].

**Table 9. Reverse transcription conditions.**

| Step | Temperature, time |
|---|---|
| Annealing | 25 °C, 5 minutes |
| Reverse transcription | 55 °C, 10 minutes |
| Denaturation | 85 °C, 5 minutes |
| Hold | 4 °C, unlimited time |

### 5.3.1. Quantitative Real-time PCR

Quantitative Real-time PCR (RT-qPCR) were performed in a CFX Connect TM Real-Time PCR System (Bio-Rad).

For assessment of gene expression, a quantitative reverse transcription PCR (RT-qPCR) was carried out using 5 µl of cDNA (diluted 1:1), 7.5 µl of FastStart Essential DNA Green Master (Roche), 300 nM of each primer and sterile Milli-Q water was added to a final volume of 15 µl. The amplification conditions are detailed in [Table 10]. For each sample, three simultaneous technical replicates were performed.

**Table 10. Real-time PCR conditions.**

| Step | Temperature, time | Cycles |
|---|---|---|
| Initial denaturation | 95 °C, 10 minutes | 1x |
| Denaturation | 95 °C, 10 seconds | 40x |
| Annealing | Tm, 10 seconds | |
| Elongation | 72 °C, 20 seconds [9] | |
| Fluorescence measurement | 80 °C, 5 seconds | 1x |

[9] Elongation time for 200 bp amplicons.

To analyze the products obtained in the PCR, denaturation curves (Melting Curves) were performed. For this purpose, increments of 0.5 ºC were programmed every 5 seconds, starting at 65 ºC until reaching 95 ºC, determining the fluorescence after each increase in temperature.

Once Ct values were obtained (Ct are the number of cycles required for the fluorescent signal to cross the threshold), comparison of multiple samples was performed using relative quantification by the $2^{-\Delta\Delta Ct}$ method (Livak & Schmittgen, 2001; Pfaffl, 2001), normalizing the data against the actin gene as an endogenous reference.

$$RE = 2^{-\Delta\Delta Ct}$$

$$\Delta\Delta Ct = (Ct_t - Ct_c)\, T_{to} - (Ct_t - Ct_c)\, _{Ref}$$

**RE:** Relative expression of the target gene with respect to the control gene
**t:** Target gene
**c:** Control gene
**Tto:** Treatment conditions
**Ref:** Reference conditions

## 6. Genetic transformation

### 6.1. Generation of *Fusarium oxysporum* transformants

#### 6.1.1. Generation de protoplasts of *Fusarium oxysporum*

Protoplasts were obtained following a protocol described before (Powell & Kistler, 1990), with minor modifications. Briefly, $5x10^8$ microconidia were inoculated in 200 ml of PDB for 14 hours at 28 ºC and orbital shaking at 170 rpm. Germlings were harvested by filtration with a Monodur and carefully washed with OM[8] solution. Germlings were then transferred to a sterile 50 ml Falcon tube, containing 5% (w/v) of Extralyse® enzyme preparation (Laffort) dissolved in OM solution. Digestion was performed for at approximately 1 hour at 30 ºC with shaking at 60 rpm. Protoplasts generation was monitored every 15 minutes, 45 minutes after starting the incubation, in a microscope. When a high number of protoplasts was achieved, the digestion was stopped by adding ice-cold STC[9] solution up to 50 ml. Protoplasts were filtered through a double layer of Monodur filters and washed with 200 ml of ice-cold STC solution. The flow-through containing the protoplasts was collected in pre-chilled Corex (Pyrex) centrifuge tubes. Samples were centrifuged at 3000 rpm for 15 minutes at 4 ºC. Pelleted protoplasts were then carefully resuspended in 1 ml STC and the concentration of protoplasts/ml determined. The protoplast suspension was adjusted to a final concentration of $3x10^8$ protoplasts/ml and stored as 100 µl aliquots in Eppendorf tubes to be used for transformation. For long-term storage at -80ºC, 10% of (v/v) PEG[10] and 1% (v/v) DMSO were added.

#### 6.1.2. Transformation of *Fusarium oxysporum* protoplasts

Transformation was performed as described (Malardier *et al.*, 1989) with minor modifications. First, the transforming DNA (approximately 2 µg), aurintricarboxylic acid (ATA; 10 µl of a 0.1M stock previously centrifuged 3 minutes at 13400 rpm) were mixed in an Eppendorf tube with TEC[11] solution to a final volume of 60 µl. Simultaneously, a transformation control tube without DNA, and containing sterile Milli-Q water, was prepared. The mixtures were incubated for 20 minutes on ice, and

[8] OM: 1.2 M $MgSO_4$, 10 mM $Na_2HPO_4$, pH 5.8 adjusted with orthophosphoric acid.
[9] STC: 0.8 M sorbitol, 50 mM $CaCl_2$ and 50 mM Tris-HCl pH 7.5.
[10] PEG: 60% (w/v) polyethylene glycol 4000 in 0.6 M MOPS.
[11] TEC: Tris-HCl 10 mM at pH 7.5; EDTA 1 mM and $CaCl_2$ 40 mM.

after this time, they were carefully mixed with 100 µl of protoplasts ($3x10^7$) and incubated on ice for 20 minutes more. Then, 160 µl of PEG solution was added, carefully mixed, and incubated for 15 minutes at RT. Then, 1 ml of STC was added and the samples were centrifuged for 5 minutes at 3000 rpm to pellet the protoplasts that were finally resuspended in 200 µl of STC. In the case of the protoplasts incubated with the transforming DNA, 4 aliquots of 50 µl were mixed with 3 ml of Top agar (prewarmed to 45 ºC) and spread on plates with regeneration MM. On the control condition (without DNA), $10^{-3}$ and $10^{-4}$ dilutions were made in STC, adding 100 µl of each dilution to 3 ml of Top agar and spread on plates with the same medium, to obtain different protoplast concentrations and determine the percentage of regeneration and its viability. In addition, a $10^{-4}$ dilution of the control condition was performed using sterile Milli-Q water (instead of STC solution) to cause protoplasts rupture and evaluate thereby the percentage of spores (or intact cells) on the mixture. A final control was carried out by mixing 190 µl of the control solution with 3 ml of Top agar, to certify the absence of growth in selective medium containing the same antibiotic as for the transformants. Plates were incubated at 28 ºC for 90 minutes, 3 hours or 14 hours before adding the 3 ml of Top agar containing phleomycin (400 µg), 44 nourseothricin (1.625 mg) or hygromycin B (2 mg), respectively. Any antibiotic was added to the regeneration and spore control situations. Plates were finally incubated at 28 ºC for an additional 4-5 days until the appearance of transformant colonies that were transferred to selective medium and subjected to two consecutive rounds of single monoconidial purification.

### 6.1.3. Gene deletion mutant confirmation

For the confirmation of correct insertion of the deletion alleles constructed into the genome, genomic DNA of each transformant was extracted and analyzed by PCR and Southern blot. PCR was performed using pairs of primers located inside the selective marker and upstream or downstream of the insert. Southern blot analysis with gene-specific probes was performed as described (Di Pietro & Roncero, 1998) using the non-isotopic digoxigenin labelling kit for DNA labeling and detection (Roche Life Sciences).

## 6.2. Generation of *Candida albicans* transformant

### 6.2.1. Transformation of *Candida albicans* by electroporation

Genetic manipulations in *C. albicans* were performed using electroporation as a standard protocol. For this, the O.N. cultures were ten times in 10 ml of YEPD+Uri medium, and cells were incubated at 30 °C for 4-5 hours with shaking at 200 rpm. To prepare cells for electroporation, cultures were then centrifuged and resuspended in 8 mL of sterile Milli-Q water and added 1ml of 1 M lithium acetate and 1ml of TE 10X[12], incubated at 30°C for 45 minutes. 25 mM dithiothreitol (DTT) was then added, and cells were incubated for an additional period of 15 minutes. After incubation, cells were washed twice with ice-cold ultrapure water (40 ml then 25 ml) and once with cold 1 M sorbitol (5 ml). Cells were then resuspended in 40 µl of cold 1 M sorbitol per electroporation and kept on ice. For the electroporation, 40 µl of prepared cells were placed in electroporation cuvettes (Cell Projects, 0.2 mm electrode gap) with 5 µg of DNA (5-10 µl of DNA resuspended in ultrapure water). DNA used for electroporation was prepared by isopropanol precipitation for PCR product cassettes and by column purification for digested plasmid cassettes. Cells were electroporated at 18 kV to achieve a time constant between 5 and 6 milliseconds (Eppendorf electroporator 2510). After electroporation, cells were removed from cuvettes by suspending them in 1 ml of 1 M sorbitol. Cells were pelleted by centrifugation and the supernatant was removed. The cells were resuspended in LM2 media and then plated on selective medium plates.

### 6.2.2. Confirmation of *Candida albicans* mutants

For the confirmation of correct insertion of the alleles constructed into the genome, genomic DNA of each transformant was extracted and analyzed by PCR and checked by fluorescence in a spinning disk laser microscope system (Revolution XD; Ardor Technology) comprised of a fully motorized inverted microscope (model IX-81; Olympus) or wide-field confocal microscope (LSM510META; CarlZeiss) with Zeiss software version 3.2.

[12] TE10X: 100mMTris-HCL, 10mM EDTA, pH7.5.

## 7. Western blot

### 7.1. Protein extraction and quantification in *Fusarium oxysporum*

For western blot analysis in *F. oxysporum*, $2.5x10^6$ spores/ml were germinated in YD medium at pH 8.0 supplemented with 20 mM of HEPES pH 7.4, for 15 hours. Germinated microconidia were then washed, transferred to KSU buffer at pH 6,0 and incubated for one hour at 28 ºC, 170 rpm. At the indicated time-points, samples of 10 ml ($2.5x10^7$ germlings) were quickly harvested by filtration through a Monodur in a vacuum filter system, and immediately chilled in liquid nitrogen. Frozen mycelia were thawed on ice and combined with 1 ml of fresh prepared lysis buffer[13]. Simultaneously to alkaline lysis, cellular disruption was achieved by mechanical homogenization using a T10 Ultra-Turrax (IKA). TCA (75 µl) was added to each sample to precipitate proteins, and samples were thoroughly mixed with the micropipette. Extracts were incubated for 10 minutes on ice, and precipitated proteins harvested by centrifugation at 13400 rpm for 5 minutes at 4 °C. The supernatant was removed, and the pellet resuspended in 100 µl of Tris-base 1 M and 200 µl 2X loading buffer[14]. Samples were boiled at 95 °C for 5 minutes and 10 µl of each sample was loaded into a Coomassie gel for determination of protein amounts.

### 7.2. Western blot analysis

For western blot analysis, the volume to load was determined by Coomassie gel. The proteins were separated in 10% Bis-Tris acrylamide[15] gels at 80 mV during the initial 40 minutes and 180 mV for one hour more, using Tris-HCl/glycine/SDS as running buffer[16]. The proteins in the gel were transferred to a nitrocellulose membrane (Bio-Rad) using the Trans-Blot® Turbo™ Transfer System RTA Transfer Kit (Bio-Rad) according to the instructions of the manufacturer. Membranes were blocked for 45 minutes in TBS-T[17] supplemented with 5% (w/v) skim milk. Then, membranes were

[13] Lysis buffer: 200 µM NaOH 10 N and 0.2% (v/v) β-mercaptoethanol.
[14] Loading buffer: 20 mM Tris-HCl pH 6.8, 8% (v/v) glycerol, 1.6% (w/v) SDS, 4% (v/v) β-mercaptoethanol and 0.1 % (w/v) bromophenol blue.
[15] 10% Bis-Tris acrylamide 1.0 mm gel (1 gel): Resolving gel is prepared by mixing: 4.25 ml deionized water, 2 ml LGB (1.5 M Trizma base and 0,4% SDS, dissolved in water and pH adjusted to 8.8), 1.75 ml acrylamide (40%; 37.5:1), 10 µl tetramethylethylenediamine (TEMED) and 40 µl ammonium persulfate (APS) 10%. Stacking gel contains 3.25 ml deionized water, 1,25 ml UGB (0.5 M Trizma base and 0,4% SDS, dissolved in water and adjusted the pH to 6.8), 0.5 ml acrylamide (40%; 37.5:1), 10 µl TEMED and 30 µl APS 10%.
[16] Running buffer: 250 mM Trizma base, 1.92 M glycine and 1% (w/v) SDS.
[17] TBS-T: 202 mM Trizma base, 137 mM NaCl and 0.1% (v/v) Tween 20. Adjust the pH to 7.6.

incubated O.N. at 4 ºC with the respective primary antibody. Membranes were washed three times with TBS-T for 10 minutes and incubated with the secondary antibody for 1 hour at RT. Membranes were washed three times more with TBS-T for 10 minutes. Proteins of interest were detected by chemiluminescence in a Fujifilm LAS 3000, after membrane staining with the ECL Select™ Western blotting Detection reagent (GE Healthcare, Amersham™). Primary and secondary antibodies were prepared in TBS-T conjugated with 1% (w/v) BSA or 5% (w/v) skim milk, respectively. The primary and secondary antibodies used in this work as well as the concentration of antibodies and manufacturers are shown in [Table 11].

**Table 11. List of antibodies and respective concentrations used in this study.**

| Antibody | Isotype | Dilution | Manufacture |
|---|---|---|---|
| Anti-phospho-p44/42 (Thr202/Tyr204) | Rabbit IgG | 1:3000 | Cell signaling (#4370) |
| Anti-α-tubulin | Mouse IgG | 1:5000 | Sigma Aldrich (T9026) |

### 7.3. Western blot band intensity analysis

Densitometric quantification of western blot signals was performed using the ImageJ software (Schindelin *et al.*, 2012). Briefly, bands of each time course were selected, and a profile plot was obtained for each individual band (peak). To minimize the background noise, each peak floating above the baseline of the corresponding profile plot was manually closed off using the straight-line tool. Finally, the closed peak intensity was measured using the wand tool. The phospho-MAPK signal was determined and normalized to the loading control, α-tubulin for each individual blot.

## 8. *In vivo* determination of cytosolic pH through the genetically encoded pH sensor pHluorin

For analysis of cytosolic pH ($pH_c$) in *F. oxysporum*, the untransformed wild type strain and the wild type strain expressing the pH sensor pHluorin (Fernandes *et al.,* 2022a) were used for background subtraction and pHc determination, respectively. $2.5x10^6$ spores/ml were germinated in YD medium at pH 8.0, supplemented with 20 mM HEPES pH 7.4, for 15 hours. Cultures were incubated at 28 ºC, with orbital shaking at 170 rpm. Germinated microconidia were washed and resuspended in KSU

buffer at pH 3.0 or 6,0 according to the experiment, resulting in a concentration of germlings/ml of approximately five times.

### 8.1. Measurement of cytosolic pH in a fungal cell population

The determination of cytosolic pH ($pH_c$) of fungal cell population was performed spectrophluorometrically in microtiter wells as described (Fernandes *et al.*, 2022a). Briefly, a calibration curve was obtained by incubating cells in different calibration buffers[18] ranging from 5,0 to 8,5, supplemented with freshly prepared nigericin (37 mg/ml; Sigma Aldrich) to permeabilize cells. For that, a 96-well Microtiter™ Microplate was prepared by dispensing 80 µl of each calibration buffer and 80 µl of KSU buffer for the wells predetermined for pHc determination, in triplicate. To each well, 20 µl of germlings of the untransformed wild type or the wild type expressing pHluorin were added in triplicate for each calibration buffer or experimental condition, according to the scheme in [Figure 9]. Cell concentration in the wells by determined by absorbance (640 nm) and approximately 0.5-0.7.

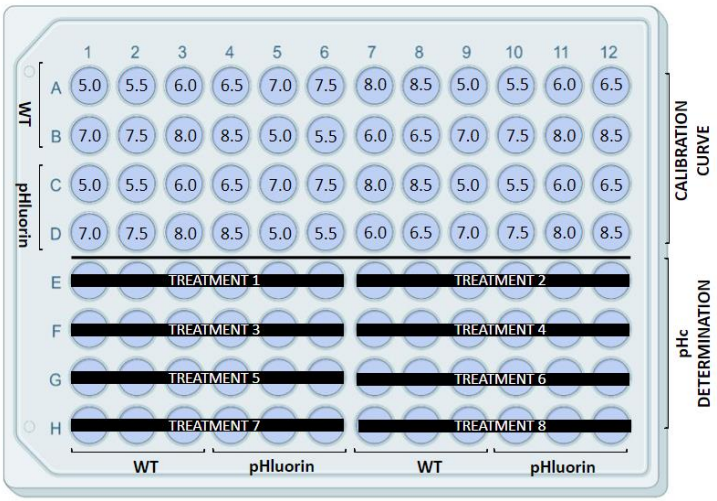


**Figure 9. Scheme of the cells distribution in a 96-well microtiter microplate for pHc determination** (adapted from (Fernandes et al., 2022b)).

[18] Calibration buffer: 50 mM HEPES, 50 mM MES, 50 mM KCl, 50 mM NaCl, 0.2M C2H7NO2, 10 mM $NaN_3$. Adjust the pH from 5,0 to 8,5, with 0.5 pH units steps.

The plate was incubated for 30 minutes to allow nigericin to equilibrate the intra- and extracellular pH for the calibration curve and cells to adapt to the KSU buffer for analysis of pHc. Fluorescence intensities after excitation at 395 and 475 nm on a spectrofluorometer (Infinite M200 PRO, TECAN Life Sciences, Switzerland) were recorded every 5 minutes for 30 minutes. After this period, cells were treated with different compounds and fluorescence were monitored for at least one hour more.
For all pHc measurements, the reported pHc values correspond to the mean and standard deviation of at least two independent experiments with three technical replicates each one. Cells were treated with the reagents and its solvent as control [Table 12]. The external pH was changed by applying different concentrations of HCl or NaOH.

**Table 12. Treatments tested in manipulation of cytosolic pH.**

| Reagent | Stock solution [Solvent] | Final concentration |
|---|---|---|
| Diethylstilbestrol (Sigma) | 200 mM [Methanol] | 0.5 mM |
| Acetic acid (VWR) | 0,4 M [ultrapure water] | 40 mM |
| Concanamycin (Santa Cruz) | 100 µM [DMSO] | 25 µM |

### 8.2 Single-cell measurement of cytosolic pH

The determination of cytosolic pH (pHc) of single-cell was performed in a fluorescence microscope, set the excitation wavelength as describe (Fernandes *et al.,* 2022b) in wt::pHluorin from *F. oxysporum* and *C. albicans* (PHL2 strain). Briefly, a calibration curve was obtained by incubating cells during 30 minutes in different pH calibration buffers ranging from 5,0 to 8,5, supplemented with freshly prepared nigericin (37 mg/ml; Sigma Aldrich) to permeabilize cells. The pHc analysis was performed using a Spinning-disk confocal microscope equipped with Diode (405 nm) and Argon (488 nm) lasers and a UMPL APO 40x dry objective. For each single-cell a line delimiting the shape of the hypha was drawn and fluorescence intensity within the line was measured at 405 and 488 nm wavelength. For each pH analyzed, three independent batches of cells (n = 10 cells per batch) were scored.

### 8.3 Determination of cytosolic pH

The ratios (395/475 nm) were calculated in a fungal cell population by first subtracting the background (wild type strain not expressing pHluorin) from each

fluorescence value obtained in the wild type strain expressing pHluorin, as described in the following equation:

$$R_i\ (395/475) = (F_{395\ i} - F_{395\ background})/(F_{475\ i} - F_{475\ background})$$

$R_i$ is the emission ratio at a given pH, $F_{395nm}$ and F475nm are the fluorescence intensities for a given pH, and F405nm background and F475nm background are average background fluorescence intensities for a given pH.

For single-cell determination, the images were set to 8 bits and subtract the background using the lookup table HiLo (ImageJ/Fiji) and adjusting the contrast. We subtracted the same background value for all images of an experiment, and the ratio 405/488 nm were calculated.

The ratio of fluorescence intensities was converted to $pH_c$ values by fitting the following equation to the calibration curve:

$$pH_c = pK_a - \log_{10}\left[(R_i - R_{min})/(R_{max} - R_i)\right]$$

$R_{max}$ and $R_{min}$ are the limiting values for the ratio at the extreme acid (pH 5,0) and alkaline (pH 8,5) pH values, respectively, and $pK_a$ the apparent $pK_a$ value of the pHluorin fluorophore.

## 9. Cell staining with fluorescent dyes and fluorescence microscopy

For vacuolar pH determination in *F. oxysporum*, a similar protocol to the pHc determination was established using the vacuole-specific dye BCECF-AM (2',7'- Bis-(2-Carboxyethyl)-5-(and-6)-Carboxyfluorescein - Acetoxymethyl Esther; SC Biotech). Briefly, microconidia were germinated for 15 hours and stained with 5 µM BCECF-AM (stock prepared at 1 mg/ml in DMSO) for 15 minutes in the dark with orbital shaking (170 rpm) at 28 ºC. Unstained cells were also incubated and used as control. Cells were then washed and resuspended in KSU buffer at pH 6 to remove the excess of dye and incubated for one more hour at 28 ºC. A calibration curve was obtained by incubating cells in different pH calibration buffers ranging from 5,0 to 8,5, supplemented with freshly prepared nigericin to permeabilize cells, as described in section 8.3 for $pH_c$ determination. Vacuolar pH was determined by measuring fluorescence intensity after excitation at 440 and 490 nm (535 nm emission) in a spectrofluorometer and calculating the ratio of intensities at 490/440 nm. Ratios

(490/440 nm) were calculated by first subtracting the background (unstained cells) from each fluorescence value obtained in stained cells with BCECF-AM and then by fitting the values to the standard curve to determine the vacuolar pH values, as described for the $pH_c$.

### 9.1 Wide-field fluorescence microscopy

Wide-field fluorescence imaging was performed using a Zeiss Axio Imager M2 microscope equipped with a Photometrics Evolve EMCCD camera. To display the location of the fluorescence protein Pma1 in the labeling of the strain *F. oxysporum* with Clover (variant GFP).

### 9.2 Spinning disk confocal microscope

Time lapses and fluorescent images were obtained using a spinning disk confocal microscope (inverted IX81 Olympus microscope with a 100X objective and a numerical aperture 1,45) and an EMCCD camera (Andor technology, UK). Z-stacks (images of 0,4-micron sections) were acquired every 15 minutes. Maximum or sum intensity projections were generated from 21 z-sections with ImageJ software. Laser illuminations of Diode (405 nm), Argon (488 nm) and DPSS (561 nm) were used.

## 10. Extracellular pH measurements

### 10.1. Determination of extracellular pH on fungal colonies

Determination of the pH surrounding the fungal colony was performed as described (Shaw *et al.*, 2022), with minor modifications. Briefly, a drop of $5x10^4$ fresh microconidia was inoculated on the center of minimal medium (MM) agar plates and incubated at 28 °C for 7 days. Samples of 4 $mm^2$ of diameter from each colony were collected with a sterile spatula and homogenized in 50 µl of sterile Milli-Q water [Figure 10]. The pH was monitored 3, 4, 5, 6 and 7 days after inoculation using a pH microelectrode (9618S-10D MicroToupH electrode, Horiba). This assay was performed at three times.

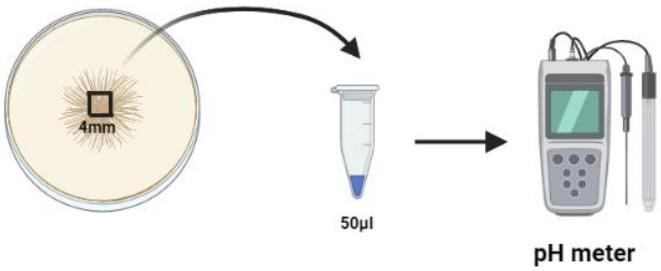


**Figure 10. Schematic diagram of the colony pH measurement.** Aliquots of $5x10^4$ fresh microconidia were spot-inoculated on MM plates and incubated for 7 days. Samples of 4 $mm^2$ were collected from each colony and homogenized in 50 µl of ultrapure water. The pH was measured by using a pH meter.

## 11. Determination of Pma1 ATPase activity

### 11.1. Isolation of fungal membranes

For determination of the activity of the PM $H^+$-ATPase Pma1 in *F. oxysporum*, PM fractions were obtained as previously described (Mahmoud *et al.*, 2017) with minor modifications. Briefly, samples of $1,25x10^8$ germlings per time point were rapidly harvested by filtration through a monodur (mesh size 10 µm) and flash-frozen in liquid nitrogen. For crude membrane purification, mycelia were resuspended in 3 mL extraction buffer [19] supplemented with 40 µL protease inhibitor cocktail (Roche Life Sciences). Then, pre-cooled 0,5 mm glass beads (5 mL per sample) were added, and samples were vortexed for 3 consecutive cycles of 90 seconds interrupted by 30 seconds on ice. Cell lysates were centrifuged for 5 minutes at 3000rpm, and the supernatant was further centrifuged for 20 minutes at 14300 rpm. Pellets were resuspended in a mixture of 100 µL glycerol buffer [20] and 900 µL of cold ultrapure water and centrifuged 30 minutes at 13000 rpm to remove inorganic phosphate and other contaminants. Finally, the membrane fraction was resuspended in 100 µL glycerol buffer.

[19] Extraction buffer: 0.3 M Tris-HCl pH 8.0, 0.3 M KCl, 30 mM EDTA, 5.3 mM dithiothreitol.
[20] Glycerol buffer: 20% (v/v) glycerol, 10 mM Tris-HCl pH 7.6, 1 mM EDTA, 1 mM dithiothreitol.

### 11.2. Quantification of protein concentration by Bradford

The Bradford protein assay was used to measure the concentration of total protein per membrane extract. First, we prepared 9 dilutions of the Bovine serum albumin (BSA) stock protein (5 mg/ml) in the range of 0-1.4 mg/ml and we prepared a 1/20 dilution of the previously isolated membranes. For this test we used the DC™ Protein Assay Reagents Package Kit (Biorad) and we prepare solution A' [21]. The reaction is carried out in a 96-well microtiter plate, in which we add 5 µL of each BSA dilution or 1/20 dilution of membranes and 25 µL of solution A'. Finally, we added 200 µL of reagent B and mixed gently with the pipette. The absorbance after 15 minutes at 750 nm on a spectrofluorometer (Infinite M200 PRO, TECAN Life Sciences, Switzerland) were recorded. Through the known solutions of BSA and the absorbance of each one we make a calibration line that allows us to precisely determine the amount of protein for each isolated membrane sample.

### 11.3. Determination of ATPase activity

The diethylstilbestrol (DES)-sensitive ATPase activity was measured as described (Kahm *et al.*, 2012), with minor changes. Briefly, samples with 6 µg membrane extracts were assayed for ATPase activity in a 96-well microtiter plate in the presence of 0.2 mM of the Pma1-specific inhibitor DES or methanol (solvent control). The plate was incubated for 30 minutes at RT to allow irreversible inhibition of Pma1 activity by DES. Then, reaction buffer [22] was added, and samples were incubated for 40 minutes at 30 ºC. The reaction was stopped by adding detection buffer [23] and incubated for 20 minutes before reading absorbance at 750 nm in a spectrofluorometer (Infinite M200 PRO, TECAN Life Sciences, Switzerland). Specific Pma1 $H^+$-ATPase activity was calculated by subtracting the residual activity value obtained in the presence of DES from the total activity (methanol), expressed in mmol/min/g protein assayed and normalized to time point zero for each time-course. For all ATPase Pma1 activity tests, the reported values correspond to the mean and

[21] Solution A': For each mL of reagent A add 20 µL of reagent S.
[22] Reaction buffer: 50 mM MES-Tris pH 5.7, 5 mM $MgSO_4$, 50 mM $KNO_3$, 5 mM sodium azide, 0.3 mM ammonium molybdate, 2 mM ATP.
[23] Detection buffer: 2% (v/v) sulfuric acid, 0.5% (w/v) ammonium molybdate, 0.5% (w/v) SDS and 0.1% (w/v) ascorbic acid.

standard deviation of at least two independent experiments with three technical replicates each one.

## 12. Fungal vegetative growth and cell survival

### 12.1. Determination of fungal growth rate

To analyze the growth capacity of the generated strains in comparation with the wild type strain, $5x10^4$ spores of each strain were allowed to grow on PDA and MM plates. Plates were incubated at 28 °C and fungal growth was imaged 3 days after inoculation using a Perfection V500 scanner (Epson). To compare the growth capacity of the wild-type and mutant strains in different media, the area of the fungal colony was measured with MultiGauge software.

For analysis of fungal growth in liquid medium, $5x10^6$ conidia/ml of each *F. oxysporum* strain was inoculated in YD medium buffered at pH 7.4 with 20 mM HEPES. 200 µl of were added in triplicate for each strain to wells in a 96-well Microtiter TM Microplate and incubated at 28 °C with shaking at 170 rpm for 3 days. Fungal growth was evaluated by measuring absorbance at 600 nm in a spectrofluorometer (Infinite M200 PRO, TECAN Life Sciences, Switzerland). To compare fungal growth throughout the time, values of absorbance were normalized to the time-point zero for each strain. The statistical analysis was performed on the last point analyzed using the t-test for unequal variances, also known as the Welch's test.

### 12.2. Evaluation of conidiation and germination rate

To evaluate the conidiation and germination rate, $5x10^6$ microconidia/ml were inoculated on PDB medium and incubated at 28 °C with shaking at 170 rpm. After 15 hours, the numbers of germinated and ungerminated conidia were counted using a Leica DMR microscope. At least 300 conidia were examined for each experimental condition, and each experiment was performed at least 3 times. Conidial germination was expressed as the percentage of germinated conidia over the total number of counted conidia. To determine the conidiation capacity, the strains were incubated for 48 hours and the concentration of microconidia of each strain was determined by counting a $10^{-3}$ dilution in a Thoma cell counting chamber under a Leica DMR microscope. Statistical analysis was conducted using the t-test for unequal variances,

also referred to as Welch's test. All experiments were performed at least three times with similar results.

### 12.3. Phenotypic analysis under different stresses

For phenotypic analysis of colony growth, drops of 2 µl from serial dilutions containing $10^5$, $10^4$ and $10^3$ fresh microconidia were spot-inoculated on YPGA plates supplemented plates with different chemical agents [Table 13]. Furthermore, YPGA medium was also adjusted to different pH values with different buffers. Briefly, the medium was buffered to pH 4.0 with 30.7 mM citric acid and 38.6 mM dibasic sodium phosphate; to pH 6,0 with 17.9 mM citric acid and 64.2 mM dibasic sodium phosphate and to pH 8,0 with 6 mM monobasic dihydrogen phosphate and 94 mM dibasic monohydrogen phosphate. Plates were incubated at 28 °C for 2 or 3 days and then imaged. Three independent plates were prepared per treatment.

**Table 13. Chemical compounds added to YPGA medium plates for phenotypical characterization.**

| Compound | Final concentration |
|---|---|
| Congo Red (CR)* | 100 µg/ml |
| Calcofluor White (CFW)* | 50 µg/ml |
| Sodium dodecyl sulfate (SDS) | 7.5 /12,5 mg/ml |
| Menadione | 20 µg/ml |
| NaCl | 1,2 M |
| Sorbitol | 1,25 M |
| KCl | 1,2 M |
| Manganese | 50 /100 mM |
| Acetic acid | 15 mM |
| Propionic acid | 10 mM |
| Aminobenzoic acid | 10 mM |
| H2O2 | 2 mM |

* YPDA plates buffered to pH 6.5 with 1% (w/v) MES.

### 12.4. Determination of fungal survival in response to acid conditions

To determine the ability of *F. oxysporum* strains to survive in the presence of cell death inducing concentrations of acetic and hydrochloric acids, $5x10^6$ microconidia/ml were inoculated on PDB medium and incubated at 28 °C with shaking at 170 rpm for fifteen hours. A time-point zero sample was then collected and acetic

acid[24]/ HCl were added for a final concentration of 30 or 40mM/60mM Samples of around 250 germinated microconidia were plated in PDA plates for each time-point and incubated 48 hours at 28 °C. After that, the number of colonies was quantified and normalized to time point zero for each time-course. Statistical analysis was conducted using the two-way ANOVA and Tukey's multiple comparisons test. Data presented are the mean from three independent biological experiments. All experiments were performed at least three times with similar results.

## 13. Evaluation of fungal pathogenicity

### 13.1. Assessment of fungal chemotropic growth

Chemotropic growth was measured using a quantitative plate assay as previously described (Turrà *et al.*, 2015), with minor modifications. Briefly, $10^6$ microconidia were embedded in 0.5% (w/v) water agar, incubated 8 hours at 28 °C in the presence of a chemoattractant gradient, and the direction of germ tubes relative to a central scoring line was determined in an Olympus binocular microscope at 9200X magnification [Figure 11]. For each sample, five independent batches of cells (n=100 cells per batch) were scored. Calculation of the chemotropic index was done as described (Turrà *et al.*, 2015). Experiments were performed at least three times with similar results. For pH chemotropism, a gradient competition assay was performed between two wells at both sides of the scoring line containing as chemoattractants 25 mM HCl or 25 mM NaOH, respectively.

[24] Prior to the acetic acid treatment, the medium was adjusted to pH 3 to allow acetic acid gets into the cells by diffusion. Those flasks were pre-incubated for 1 hour at 28ºC before acetic acid treatments.

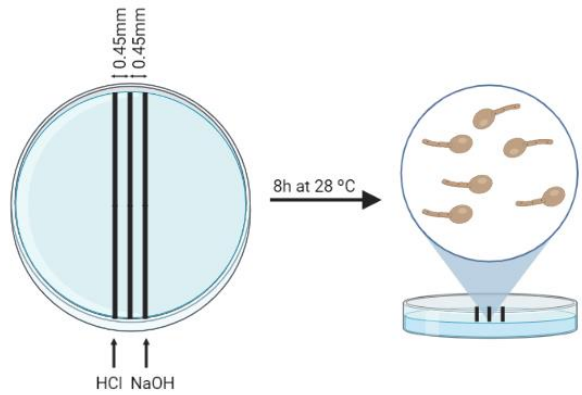


**Figure 11. Schematic diagram of the chemotropic assay.** Eight-hours germinated microconidia in water-agar plate at 28 °C in presence of a gradient competition between HCl and NaOH at both sides of the central scoring line. At the microscope, the number of hyphal tips growing towards each chemoattractant was quantified.

### 13.2. Determination of fungal invasive growth

A cellophane membrane assay was performed to determine the invasive growth capacity of the generated strains as previously described (López-Berges *et al.*, 2010). Briefly, unbuffered MM and MM buffered with 0.1 M MES (2-(N-morpholino) ethanesulfonic acid) to pH 5 or pH 7 were covered with a cellophane membrane and $5x10^4$ microconidia were spot-inoculated on the top and at the center of the plate. After 3 days of incubation at 28°C, the cellophane membrane with the fungal colony was carefully removed and plates were incubated for 1 additional day at 28°C. Plates were scanned before and after cellophane removal. Triplicates were performed for each strain and condition, and three independent experiments were performed with similar results.

### 13.3. Evaluation of pathogenicity through a tomato plant infection assay

Tomato root infection assays were performed in a growth chamber as described (Di Pietro & Roncero, 1998), using the susceptible *Lycopersicon esculentum* cultivar Monika. Briefly, two-week-old tomato seedlings (see section 3.4.4) were inoculated with *F. oxysporum* strains by immersing the roots in a microconidia suspension of $5x10^6$ spores/ml for 30 minutes. A water-control without spores was also included. Then, plants were transplanted into seed sockets with new

vermiculite and grown in a growth chamber with the conditions previously described (see section 3.4.4). Ten days after inoculation, the severity of disease symptoms and percentage survival were recorded daily for 30-40 days as previously described (López-Berges *et al.*, 2010). Ten plants were used for each treatment. Survival was estimated by the Kaplan-Meier method and compared among groups using the log-rank test.

## 14. Bioinformatic analysis

### 14.1. Gene search and sequence retrieval

*In silico* gene search of both *F. oxysporum* and related fungal species was performed using the BLAST algorithm (Altschul et al., 1990) from the National Center for Biotechnology Information (NCBI; http://www.ncbi.nlm.nih.gov), Fungal and Oomycete genome database (FungiDB; https://fungidb.org/fungidb/app) and Saccharomyces Genome Database (SGD; https://www.yeastgenome.org).

### 14.2. Sequencing and protein alignment

Prior to the analysis by sequencing, a standard PCR was performed using the thermostable DNA polymerase Expand High Fidelity (Roche Life Sciences) (see section 3.5.2.1) PCR products obtained were sequenced by STAB VIDA company, Portugal. Proteins alignment was made using the ClustalOmega software (http://www.ebi.ac.uk).

## 15. Software and online tools

Data management and processing was performed using the following software products listed in [Table 14].

**Table 14. Softwares and websites used in this study.**

| Software | Application |
|---|---|
| Adobe Ilustrator CS5 | Figure design |
| AxioVision 4.7 | Microscope imaging and analysis |
| CFX Maestro 1.1 (Bio-Rad) | qPCR data acquisition and analysis |
| GraphPad Prism v8.0 | Graph creating and statistical analysis |
| Image Reader LAS-3000 | Capture, editing and analysis of images obtained after revealed by chemiluminescent detection |
| ImageJ | Image editing / Image quantification and measurement |

| | |
|---|---|
| Kodak ID Image Analysis | Capturing photographic images of agarose gels |
| MultiGauge v3.0 | Image editing / Image quantification and measurement |
| Oligo 7 | Design and analysis of oligonucleotides |
| Snapgene | Editing and analysis of nucleotide and protein sequences |
| **Website** | **Application** |
| National Center for Biotechnology Information (NCBI) https://www.ncbi.nlm.nih.gov | BLAST: Sequence alignment Genome database: Retrieval of gene and protein sequences |
| FungiDB https://fungidb.org/fungidb/app | BLAST: Sequence alignment Genome database: Retrieval of gene and protein sequences |
| Saccharomyces Genome Database (SGD) https://www.yeastgenome.org | BLAST: Sequence alignment Genome database: Retrieval of gene and protein sequence |
| Clustal Omega | Multiple Sequence alignment |

# Chapter I

**The results of this chapter have been accepted for publication in mBio (Fernandes *et al.*, 2022a)**

# Chapter I: pH and sphingolipids regulate chemotropic growth and virulence in *Fusarium oxysporum*

## Overview

Ambient pH acts as an important environmental factor regulating development, growth and virulence in fungi by modulating several molecular and biochemical mechanisms (Mariscal *et al.*, 2022). In *F. oxysporum*, extracellular alkalinization increases virulence through phosphorylation of the conserved invasive growth (IG) mitogen-activated protein kinase (MAPK) Fmk1 (Di Pietro *et al.*, 2001; Masachis *et al.*, 2016). On the other hand, recent studies indicated that extracellular pH also modulates the activity of the two other MAPKs, the cell wall integrity (CWI) MAPK Mpk1 and the high osmolarity response MAPK Hog1, in an opposite way to Fmk1 (Fernandes *et al.*, 2022a). Moreover, it was demonstrated that extracellular pH controls MAPK signaling in fungi by affecting cytosolic pH ($pH_c$), which acts as a second messenger determining MAPK phosphorylation status (Fernandes *et al.*, 2022a). Besides its essential role in the maintenance and remodeling of the cell wall in response to several stresses, activation of the CWI MAPK Mpk1 was also demonstrated to be crucial for cell cycle progression, development and pathogenicity, especially at early stages of fungal-host interactions (Nordzieke *et al.*, 2019; Selvig & Alspaugh, 2011; Turrà *et al.*, 2015).

The recent findings that the Mpk1 MAPK cascade is activated in response to either extracellular or cytosolic acidification prompted the study of the molecular mechanisms operating upstream of Mpk1 activation in response to pH decrease. Firstly, we studied the role of the highly conserved cell surface sensors Wsc1, Mid2 and Mtl1, which have been implicated in responses to stress affecting the cell wall. However, the results showed that Mpk1 MAPK activation in response to $pH_c$ acidification is independent of these components (Fernandes *et al.*, 2022a). Previous studies identified the AGC kinase Ypk1/2 as a key upstream branch for activation of Mpk1 in *S. cerevisiae* (deHart *et al.*, 2002), but its role in filamentous fungi has not be clarified so far [Figure 12]. In yeast, activation of the Ypk1/2 is a complex multi-step process which is triggered by sphingolipid depletion at the PM. This leads to re-localization of Ypk1/2 and their consequent phosphorylation and activation by the target of rapamycin complex 2 (TORC2) at two different residues located in the C-terminal regulatory domain (Luo *et al.*, 2008; Niles *et al.*, 2012; Niles & Powers, 2012).

Moreover, the protein kinases Pkh1/2 phosphorylate Ypk1/2 on the activation loop of the kinase domain to become fully activated (deHart *et al.*, 2002; Niles *et al.*, 2012). Finally, activation of the Pkh1/2-Ypk1/2 complex induces sphingolipid synthesis in a feedback-loop mechanism (García-Marqués *et al.*, 2016; Roelants *et al.*, 2011).

Previous results of our group demonstrated that extracellular and cytosolic acidification changes sphingolipid homeostasis by significantly increasing the content of the long chain base (LCB) sphingolipid dihydrosphingosine (dhSph). Importantly, it was also demonstrated that this increase is similar in the wild type and *mpk1*Δ mutant strains (Fernandes *et al.*, 2022a), suggesting that dhSph synthesis occurs upstream of Mpk1 activation in this process.

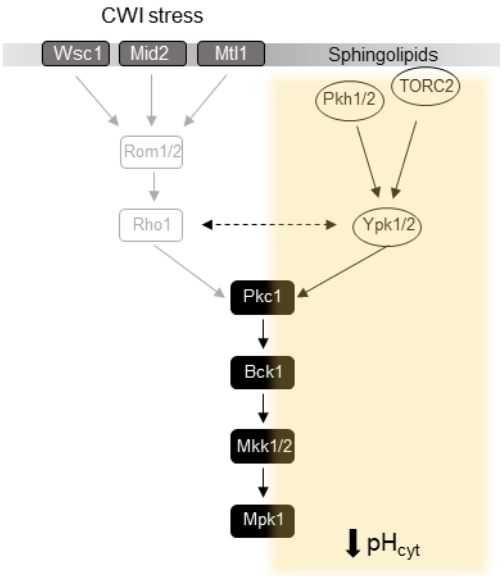


**Figure 12. Schematic illustration of the CWI MAPK cascade activation in response to cytosolic acidification**. Mpk1 MAPK activation by the Ypk1/2 proteins, which was triggered by the protein kinases Pkh1/2 and the TORC2 complex (from (Fernandes *et al.*, 2022a).

In this chapter, we proposed to investigate for the first time the possible role of extracellular pH in *F. oxysporum* chemotropism. On the other hand, we examined the possible role of Ypk1/2 in MAPK Mpk1 signaling, as well as the possible role of sphingolipid dhSph in the fungal chemotropism.

## Results

### 1. Mpk1 controls hyphal chemotropism towards acid pH

A fundamental step during infection is the capacity of fungi to grow toward host roots in the soil, a phenomenon known as chemotropism (Turra & Di Pietro, 2015). Recently, it was shown that the plant chemoattractant signal peroxidase can trigger Mpk1 phosphorylation (Nordzieke *et al.*, 2019). Since our previous data demonstrated that pH regulates the Mpk1 MAPK cascade, we decided to examine the role of pH in the chemotropic hyphal growth of this fungal pathogen. For this purpose, a chemotropic assay was performed in the presence of competing alkaline and acidic pH gradients. We found that *F. oxysporum* hypha grew towards the acidic pH. Interestingly, the *mpk1*Δ mutant strain exhibited the opposite tropism, growing towards the alkaline pH, while the complemented strain restored the acid tropism [Figure 13]. We also tested the behavior or the other two MAPK mutants, both of which showed chemotropic growth towards acid pH as the wild type strain. However, the *hog1*Δ mutant showed a reduced chemotropic response compared to the wild type.

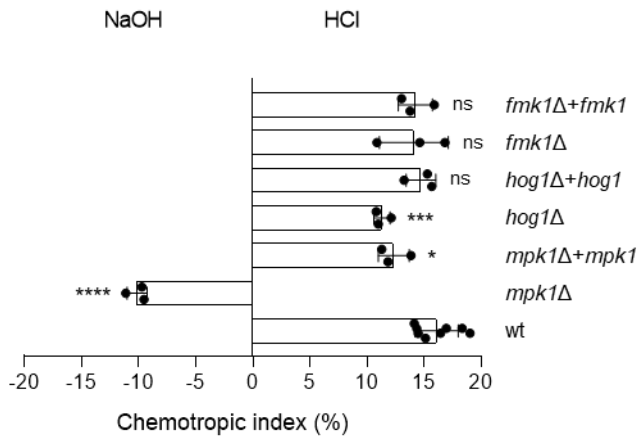


**Figure 13. Mpk1 is required for chemotropic growth of *F. oxysporum* towards acid pH.** Directed growth of germ tubes of the *F. oxysporum* wild type (wt) and the indicated MAPK mutants and complemented strains was determined after eight hours exposure to opposing gradients of 25 mM HCl and NaOH. (****) $p$ <0.0001, (***) $p$ <0.001, (*) $p$ <0.05 and ns (non-significant) *versus* wt according to Welch's t-test. Data show the mean ± s.d. from three independent experiments with three replicates (n=500 germ tubes per experiment) each.

## 2. Generation of a strain carrying a temperature-sensitive *ypk1* allele

Previous results of our group had demonstrated that the Pkh1/2-Ypk1/2 branch of the Mpk1 MAPK cascade plays a key role in regulation Mpk1 activation in response to cytosolic acidification in *S. cerevisiae* (Fernandes *et al.*, 2022a). To validate this result in *F. oxysporum*, we firstly tried to obtain an *ypk1*Δ mutant. This approach was unsuccessful, suggesting that this gene is essential for *F. oxysporum* survival. Following an approach previously described in *S. cerevisiae* (Casamayor *et al.*, 1999), we next tried to generate a temperature-sensitive *ypk1* mutant allele (*ypk1*$^{ts}$) to uncover the role of this kinase in Mpk1 activation in response to acidification.

We first performed an amino acid sequence alignment between the Ypk1 proteins from *S. cerevisiae* (YKL136W) and *F. oxysporum* (FOXG_07521). This revealed that the position of the I428 and Y480 amino acid residues mutated in the yeast *ypk1*$^{ts}$ mutant is conserved among the two fungal species [Figure 14A]. To generate the mutations, fragments were amplified from *F. oxysporum* genomic DNA using primers carrying the mutations (ypk1_fwd/ypk1-Y480C-rv; ypk1-I428T-fwd/ypk1_rv) [Figure 14B]. The two amplified fragments were then fused through a PCR reaction without primers, and further amplified by using the primers ypk1_fwd_nested/ypk1_rv_nested. The resulting DNA fragment and the hygromycin resistance cassette, previously amplified with primers GpdA15B/TrpC8B, were used to co-transform freshly prepared *F. oxysporum* protoplasts [Figure 14B]. Hygromycin-resistant transformants that showed reduced growth at 33 °C, but wild type growth at 28 °C were selected for further analysis (data not shown). To verify homologous insertion of the *ypk1*$^{ts}$ allele, genomic DNA was extracted from each transformant and PCR products of amplification using the primers Ypk1_Fwd_nested/ Ypk1_rv_nested, were subsequently sequenced with the primers ypk1_ts_SEC1 and ypk1_ts_SEC2. The alignment of the nucleotide sequences obtained with the *ypk1* ORF of *F. oxysporum* and the mutated sequence *ypk1*$^{ts}$ shows that the transformant *ypk1*$^{ts}$ #34 presented the targeted I428T and Y480C mutations [Figure 14C].

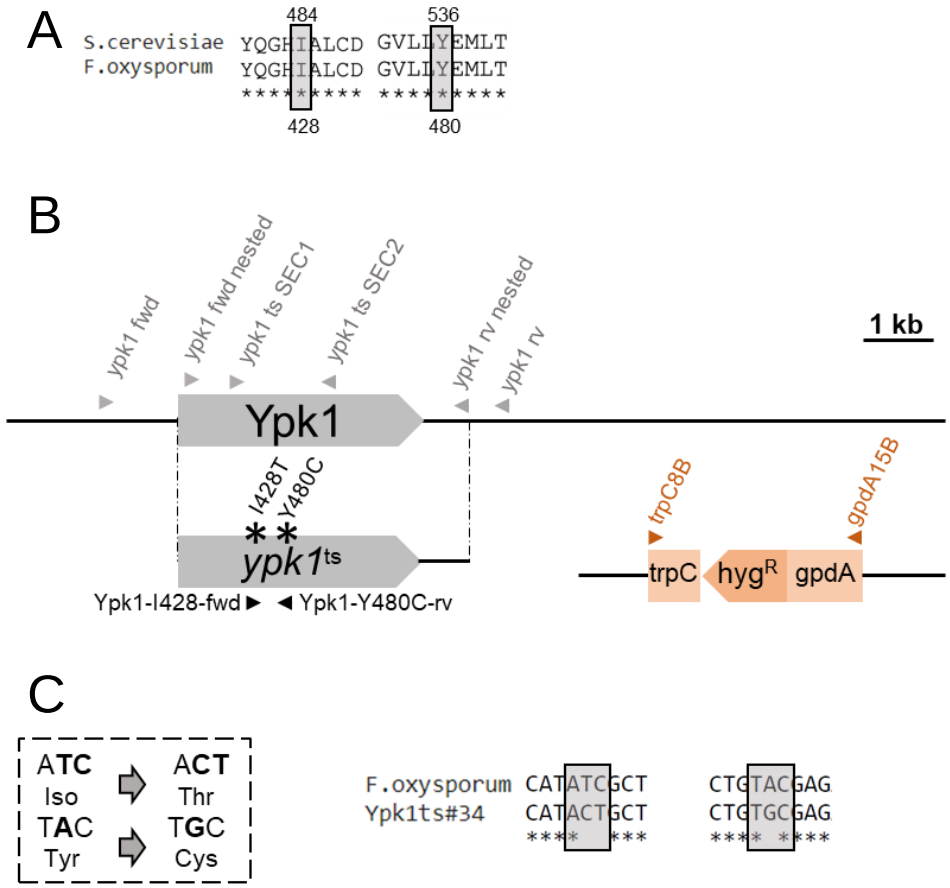


**Figure 14. Targeted mutation of the *F. oxysporum ypk1* gene to generate an *ypk1$^{ts}$* mutant strain.** (**A**) Alignment of the *S. cerevisiae* residues I484 and Y536 (grey box) responsible for the temperature-sensitive phenotype in *ypk1$^{ts}$* yeast mutant, which shows that these residues are conserved in *F. oxysporum* Ypk1. (**B**) Schematic representation of the strategy used for the replacement of the ypk1 coding region with *ypk1$^{ts}$* allele by co-transformation with the *Hyg*$^{R}$ cassette as selective marker. The relative position of the gray primers (*ypk1*), black primers (carrying the mutations) and orange primers (*Hyg*$^{R}$ cassette) are indicated by arrowheads. Scale bar, 1kb. (**C**) Sequencing result from the relevant region of the ypk1$^{ts}$ #34 transformant using the primers Ypk1_ts_SEC1 (forward) and Ypk1_ts_SEC2 (reverse).

## 3. Temperature sensitivity of the *ypk1$^{ts}$* strain

To determine temperature sensitivity of the mutant, the wild type and *ypk1$^{ts}$* #34 strains were grown in PDA medium at different temperatures ranging from 22 ºC to 34 ºC. We observed that the colony growth of the *ypk1$^{ts}$* #34 mutant strain was not significantly affected at the lowest temperature tested (22 ºC), but was slightly reduced at higher temperatures (28 and 34 ºC) compared to the wild type strain, although

growth of the latter was also affected at 34 ºC [Figure 15A]. We also tested the effect of temperature (24, 28, 30 and 37 ºC) on fungal growth in liquid medium and detected no significant differences between the *ypk1$^{ts}$* #34 mutant and the wild type strains in 24 hours of growth [Figure 15B-C].

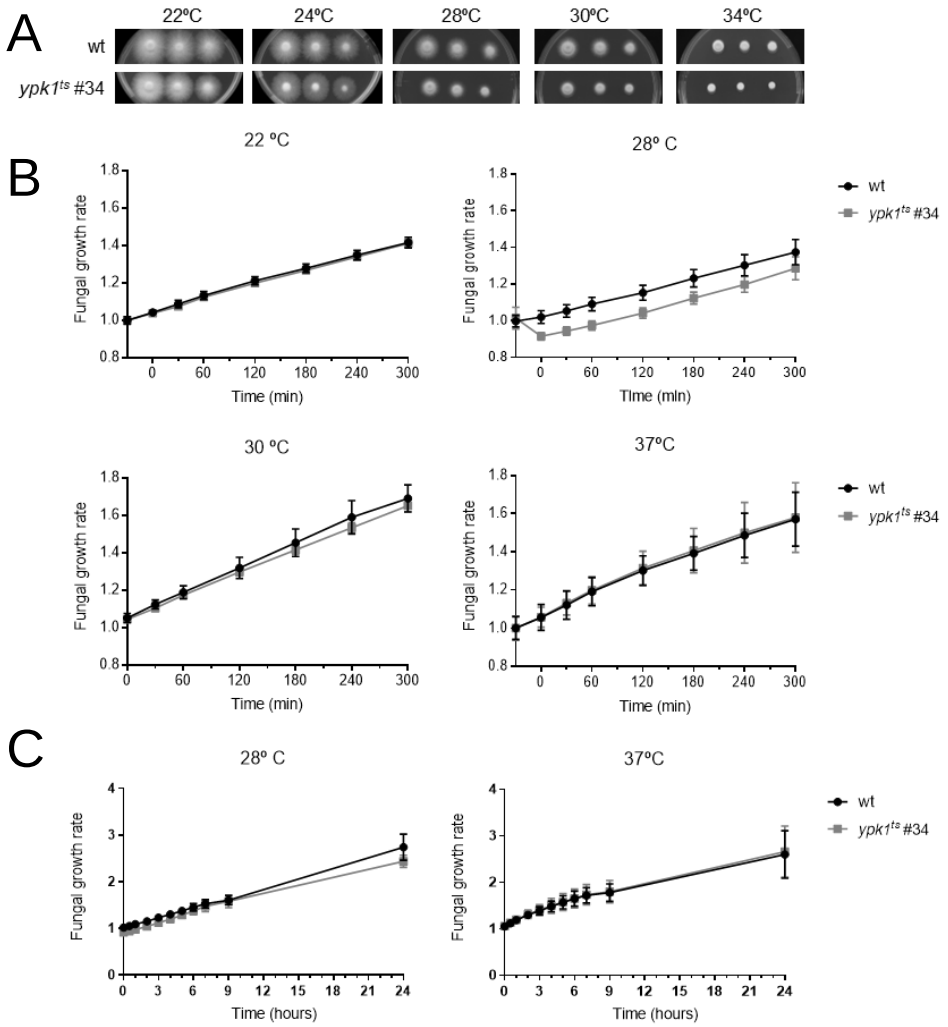


**Figure 15. Effect of the *ypk1$^{ts}$* allele of temperature sensitivity of *F. oxysporum.*** (**A**) Aliquots of $10^5$, $10^4$ and $10^3$ fresh microconidia of the wild type (wt) and *ypk1$^{ts}$* mutant strains were spot-inoculated on PDA plates, incubated at indicated temperature and scanned after 3 days. Plates shown are representative of three independent replicates for each strain and growth condition. (**B, C**) Microconidia ($2.5x10^4$) of the wild type (wt) and *ypk1$^{ts}$* #34 strains were germinated in 200 µL YPD (pH 8.0) with 20 mM HEPES (pH 7.4) in 96 Microtiter™ plate wells for 15 hours at 22 ºC and 170 rpm. At time 0, the temperature was changed from 22 ºC to 28 ºC, 30 ºC or 37 ºC, or kept at 22 ºC as a control. Absorbance at 600 nm was measured before (time -30 min) and at the indicated times after the temperature change for 5 (B) hours or 24 hours (C) Values were normalized to time-point 0'. Graphs show the mean ± s.d. from six independent replicate microwells from one representative experiment. Experiments were performed twice with similar results.

Overall, these results suggest that, in contrast to S. cerevisiae, the ypk1ts allele does not confer a strong temperature sensitivity phenotype in F. oxysporum, invalidating its usefulness for studying the role of Ypk1 in regulation of Mpk1 signaling.

## 4. Dihydrosphingosine acts as a signal regulating the CWI MAPK

Previous results from our group showed that extracellular and cytosolic acidification triggers an increase in the levels of the LCB sphingolipid dhSph, in a mechanism functioning upstream of Mpk1 (Fernandes *et al.*, 2022a). Here we found that external application of 10 µM dhSph induces a rapid (10 minutes) and marked increase in phosphorylation levels of Mpk1, which returned to basal levels after 30 minutes [Figure 16A]. Interestingly, dhSph did not affect the phosphorylation level of the MAPK Fmk1 [Figure 16A]. Importantly, addition of dhSph had no significant effect on $pH_c$ [Figure 16B], suggesting that dhSph acts downstream of cytosolic acidification to trigger the Mpk1 activation.

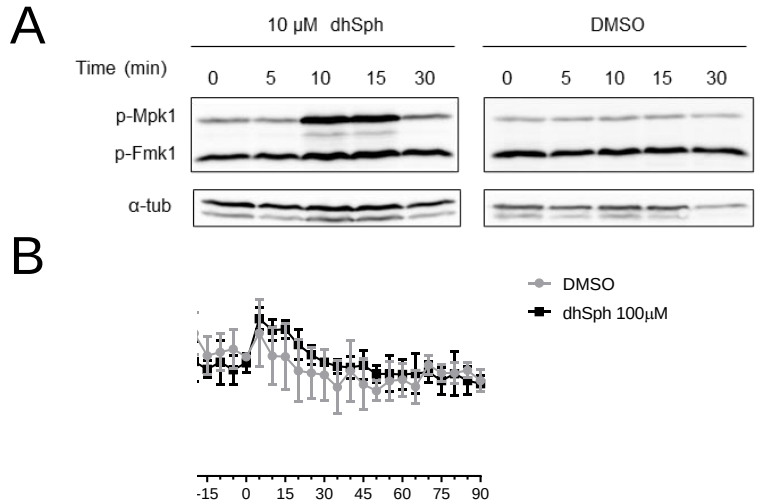


**Figure 16. The LBC sphingolipid dhSph activates the CWI MAPK downstream of $pH_c$ acidification.** (**A**) Western blot analysis of MAPK phosphorylation of *F. oxysporum* in response to addition of 10 µM dhSph (left panel) or the solvent DMSO (right panel). Total protein extracts collected at the indicated times were subjected to immunoblot analysis with anti-phospho-p44/42 MAPK to detect phosphorylated p-Mpk1 and p-Fmk1. Anti-α-tubulin (α-tub) was used as loading control. (**B**) Fifteen-hour germinated microconidia of *F. oxysporum* wild type strain were washed and resuspended in KSU buffered at pH 6,0 and incubated for one hour at 28ºC. At time 0, 100 µM of the dhSph or DMSO (solvent control) were added to the KSU buffer. The $pH_c$ was monitored every 5 minutes for 90 minutes. Graph show the mean ± s.d of six replicate microwells from one representative experiment. Experiments were performed twice with similar results.

## 5. Dihydrosphingosine acts as a chemoattractant for *Fusarium oxysporum*

We previously showed that the CWI MAPK Mpk1 controls hyphal chemotropism towards acidic pH [Figure 13]. Since dhSph triggers activation of Mpk1, we explored whether this LCB sphingolipid also functions as a chemoattractant for *F. oxysporum* hyphae. Indeed, we found that dhSph triggered a chemotropic response in a dose-dependent manner [Figure 17A]. interestingly, the *mpk1*Δ and the *fmk1*Δ mutants had lost the ability to grow towards dhSph, suggesting that these two MAPKs are required for the chemosensing process. By contrast, the high osmolarity response MAPK Hog1 was dispensable for this response [Figure 17B].

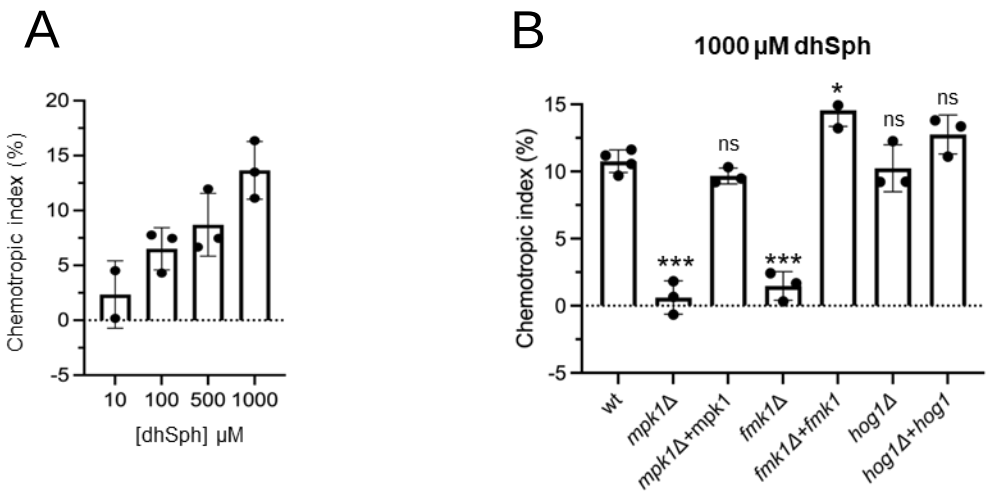


**Figure 17. Dihydrosphingosine (dhSph) acts as chemoattractant for *F. oxysporum*.** (**A**) Directed growth of germ tubes of the *F. oxysporum* wild type (wt) was determined after eight hours exposure to the indicated concentrations of dhSph. (**B**) Directed growth of germ tubes of the wt and the indicated mutant and complemented strains was determined after eight hours exposure to 100 µM dhSph. (*) $p$ <0.05, (***) $p$ <0.001 and ns (non-significant) *versus* wt, according to Welch's t-test. Data show mean ± s.d. from at least three independent experiments with three replicates (n=500 germ tubes per experiment) each.

# Chapter II

# Chapter II: Role of the $H^+$-ATPase Pma2 in *Fusarium oxysporum*

## Overview

The essential PM $H^+$-ATPase Pma1 functions as the main regulator of $pH_c$ homeostasis in fungi by pumping protons out of the cell through hydrolysis of ATP (Morsomme *et al.*, 2000; Palmgren & Morsomme, 2019; Serrano, 1993). Under basal conditions, Pma1 consumes up to 20% of cellular ATP (Morsomme & Boutry, 2000). Given the importance of this master $H^+$-ATPase, it is not surprising that mutations which drastically reduce its activity are lethal (Serrano, 1993). Interestingly, some fungi have a second PM $H^+$-ATPase, Pma2, which exhibits a low level expression level and apparently is not essential (Supply *et al.*, 1993a). Pma2 exhibits some key differences with its paralog Pma1 including the lack of conserved phosphorylation sites at the C-terminal, which are fundamental for regulation of Pma1 activity (Supply *et al.*, 1993a). Some studies have demonstrated that Pma2 can partially relieve the lethality of *pma1* deletion if overexpressed under control of the Pma1 promoter, but even under these conditions, only a low fraction of Pma2 was found to reach the PM (Supply *et al.*, 1993b).

While Pma2 is absent in some hemibiotrophic plant pathogens such as *Uromyces fabae* (Struck *et al.*, 1998) or *Blumeria graminis* (Both *et al.*, 2005), it has been identified in others such as *Magnaphorte oryzae* and *Colletotrichum higginsianum* when performing genetic screens for pathogenicity genes (Franck *et al.*, 2013; Korn *et al.*, 2015). In contrast to *pma1*, which is constitutively expressed, *pma2* was up-regulated in these phytopathogens specifically during appressoria formation and infection (Franck *et al.*, 2013; Korn *et al.*, 2015). A *pma2* deletion mutant of *C. higginsianum* failed to penetrate the host plant, consistent with a crucial role of this $H^+$-ATPase in fungal virulence (Franck *et al.*, 2013). In *M. oryzae*, *pma2* gene expression was up-regulated by ammonia (Zhang *et al.*, 2011), suggesting that *pma2* might be activated during infection by pathogen-induced alkalinization. Thus, the presence of a second PM $H^+$-ATPase, in addition to Pma1, appears to be relevant during infection in ascomycete pathogens. In the soil-borne pathogen *F. oxysporum*, where pH has been shown to play a crucial role in virulence, there is little information on the role of Pma2. Therefore, we decided explored the role of Pma2 in pH homeostasis and fungal invasive growth.

## Results

### 1. *In silico* identification of a *pma2* ortholog in *Fusarium oxysporum*

A BLASTp search of the *F. oxysporum* genome sequence with the amino acid sequence of *S. cerevisiae* Pma2 (YPL036W) identified a single Pma2 orthologue in *F. oxysporum* (FOXG_03480). This gene is located on chromosome 8 and encodes a predicted protein of 1021 amino acids that exhibits 34% identity with Pma2 of *S. cerevisiae* and more than 60% identity with Pma2 of phytopathogens fungi such as *M. oryzae* (MGG_04994; 65%), *C. higginsianum* (CH63R_02929; 64%), *Botrytis cinerea* (BCIN_12g06020; 68%) and *Aspergillus nidulans* (GAQ45986.1; 69%).

### 2. Expression level of the $H^+$-ATPase genes *pma1* and *pma2* in *Fusarium oxysporum*

To measure the expression levels of the *pma1* and *pma2* genes in *F. oxysporum*, a RT-qPCR analysis with gene-specific primers was performed using cDNA from the wild type strain, obtained after fifteen hours of germination in PDB medium. As previous described in yeast, the transcript level of the *pma2* gene was very low, being at least 25000 orders of magnitude lower than that of the *pma1* [Figure 18].

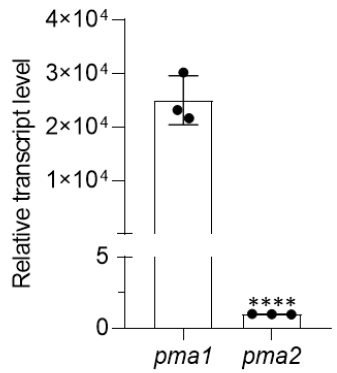


**Figure 18. Relative transcript level of *pma1* and *pma2* genes in *F. oxysporum.*** Microconidia were germinated fifteen hours in PDB and total RNA was isolated and reverse transcribed to cDNA. RT-qPCR was performed with specific primers of *pma1* (Pma1.qPCR.Fwd/ Pma1.qPCR.Rv) and *pma2* (Pma2.qPCR.Fwd/ Pma2.qPCR.Rv). Transcript levels were calculated relative to those of the actin gene and were normalized to that of the pma2 gene. (****) $p$ <0.0001 *versus* Pma1, according to Welch's t-test. Data show means ± s.d. from three technical replicates.

## 3. Targeted deletion of *pma2* in *Fusarium oxysporum*

To investigate the role of Pma2 in *F. oxysporum*, we performed targeted deletion of the *pma2* gene in this pathogen. We generated a *pma2*Δ allele by replacing the complete ORF with the *Hyg*$^{R}$ cassette by using the "split-marker" approach [Figure 19A]. The two constructs obtained, , each containing a flanking region of the gene and about 75% of the *Hyg*$^{R}$ cassette, were used each containing a flanking region of the gene and overlapping parts of the *Hyg*$^{R}$ cassette, were used to transform protoplasts of the *F. oxysporum* wild type strain. Transformants carrying a homologous insertion at the *pma2* locus were initially identified by PCR analyses using two pairs of primer pairs that bind outside of the constructs used for transformation and inside of the resistance cassette [Figure 19B]. Candidate knockout mutants were further analyzed by Southern blot to confirm the homologous insertion of a single copy of the construct into the genome. The genomic DNAs of the wild type strain and putative knockouts in *pma2* were treated with the restriction enzyme *Hind* III and hybridized with a probe located in the promotor region of the *pma2* gene, confirming the replacement of the 3,7 Kb hybridizing band of the wild type *pma2* allele by a 7,4 Kb band in the *pma2*Δ transformants #10, #11, #16, #20, #22, #25, #29, and #30, indicative of a single homologous replacement event [Figure 19C].

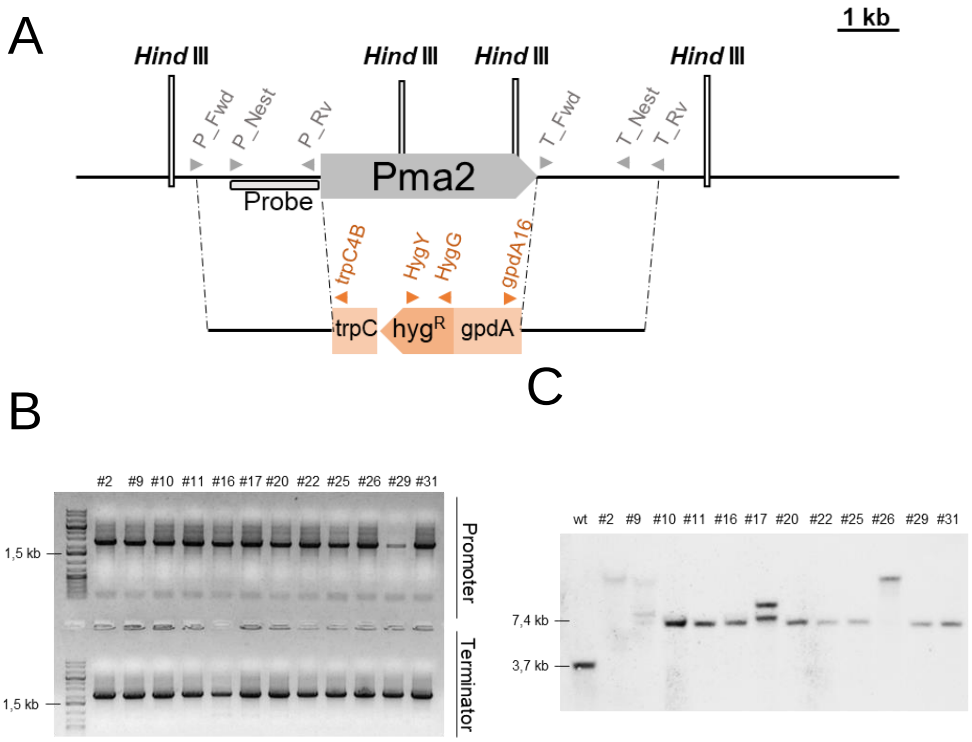


**Figure 19. Targeted deletion of the *F. oxysporum pma2* gene.** (**A**) Physical maps of the *pma2* locus and strategy for the replacement of the coding region with the split-marker method using the *Hyg*$^R$ cassette as selective marker (*pma2*Δ allele). Positions of *Hind* III restriction sites are shown. Gray (*pma2*) and orange (*Hyg*$^R$) arrowheads indicate the relative positions of the primers used for generation of the gene disruption constructs and PCR analyses of the transformants; the probe used for Southern blot analysis is indicated as gray bar. Scale bar, 1kb. (**B**) PCR analysis to confirm homologous recombination of the construct into the genome of the transformants using the pairs of primers: P_Fwd /trpC4B (promotor region) and T_Rv /gpda16 (terminator region). (**C**) Southern blot hybridization analysis of the wild type strain and the different *pma2*Δ transformants. Genomic DNA was treated with *Hind* III, separated in an agarose gel, transferred to a nylon membrane and hybridized with the probe indicated in (A).

## 4. Expression and ATPase activity of Pma1 is slightly increase in the *pma2*Δ deletion mutants

Considering that Pma1 and Pma2 could have complementary functions, we decided to analyze the effect of *pma2* deletion on both *pma1* expression level and Pma1 ATPase activity. To measure the expression levels of the *pma1* gene, RT-qPCR analysis with gene-specific primers was performed using cDNA from the wild type, *pma2*Δ #10 and *pma2*Δ #11 strains obtained after fifteen hours of germination in PDB

medium. We found that the *pma2*Δ mutants showed a slight increase in *pma1* transcript levels compared to the wild type [Figure 20A]. Furthermore, the Pma1 ATPase activity in membrane fractions of the *pma2*Δ mutants was also slightly increased [Figure 20B].

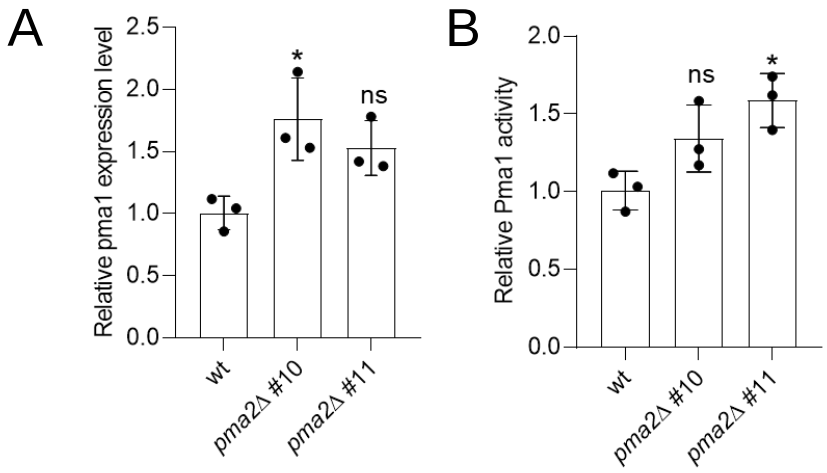


**Figure 20. Relative transcript level and ATPase activity of Pma1 in the wild type and *pma2*Δ mutant strains.** (**A**) Microconidia of the wild type (wt) and *pma2*Δ mutant strains were germinated 15 hours in PDB and total RNA was isolated, and reverse transcribed to cDNA. RT-qPCR was performed with specific primers of the *pma1* gene (Pma1.qPCR.Fwd/ Pma1.qPCR.Rv). Transcript levels were calculated relative to those of the actin gene and normalized to those of the wt strain. (*) $p$ <0.05, ns (not significant) *versus* wt, according to Welch's t-test. Data show means ± s.d. from three technical replicates. (**B**) Analysis of Pma1 ATPase activity was assayed in total membranes isolated from mycelia obtained as indicated in (A). Activity was normalized to that of the wt strain. (*) $p$ <0.05, ns (non-significant) *versus* wt according to Welch's t-test. Data shown are the mean ±s.d. from three independent technical replicates each.

## 5. Pma2 is not important for vegetative growth in *Fusarium oxysporum*

To evaluate the role of the $H^+$-ATPase Pma2 on vegetative growth, the wild type, *pma2*Δ #10 and *pma2*Δ #11 mutants strains were grown on PDA or minimal medium (MM) plated for 9 days [Figure **21. Effect of *pma2* deletion on colony growth.** (**A**) Aliquots of 5x104 fresh microconidia of the wild type (wt), and *pma2Δ* mutants were spot-inoculated on potato dextrose agar (PDA) or minimal medium (MM) plates and incubated at 28°C for 9 days. Colonies were imaged after 3, 6 and 9 days. Plates shown are representative of three independent replicates for each strain and growth condition. (**B**) Colony area of the indicated strains on PDA and MM after 9 days was measured and normalized to that of the wild-type strain (100%). (*) p <0.05, ns (non-

significant) versus wt according to Welch's t-test. Data show means ± s.d from three independent plates per strain and condition. 21A]. The *pma2*Δ mutants showed a slight increase in colony growth on PDA compared to the wild type strain, although the difference was only statistically significant for *pma2*Δ #11 [Figure 21B]. On the opposite, no significant difference in growth were observed between the wild type strain and the *pma2*Δ mutants strains on MM [Figure 21A, B].

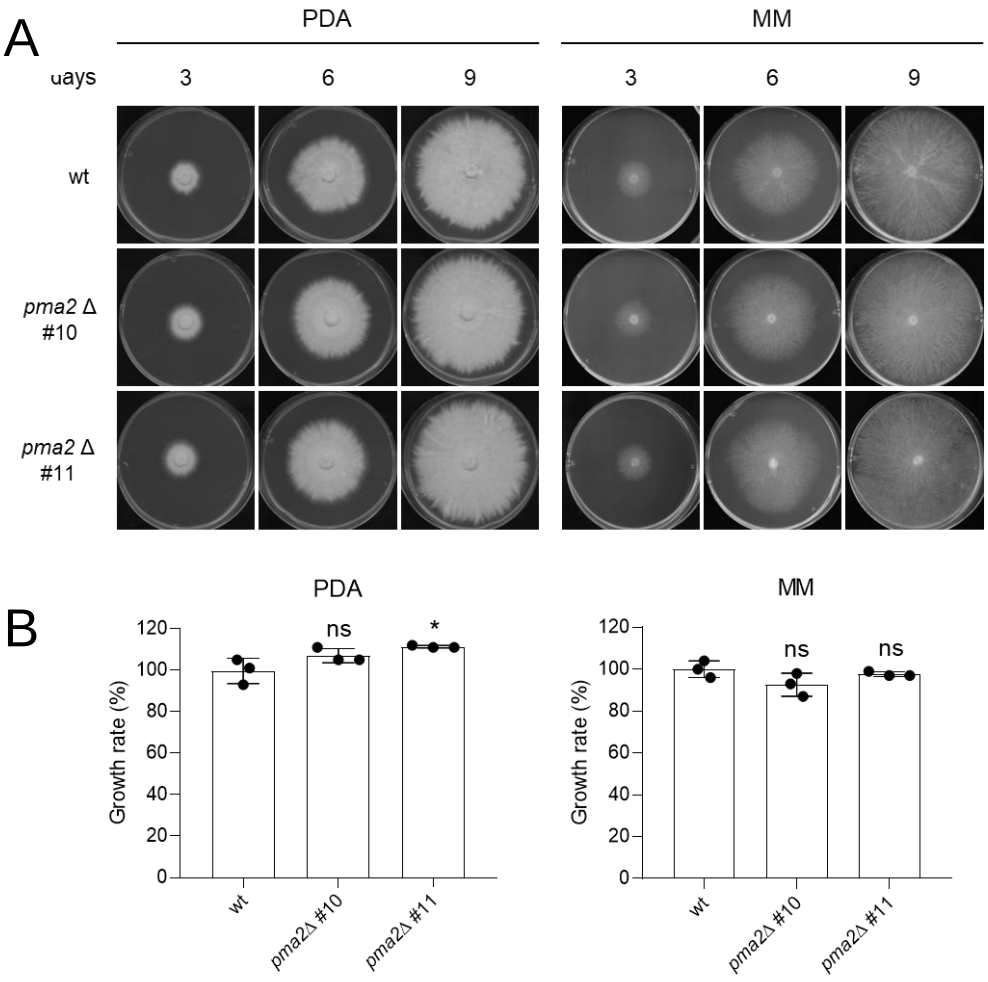


**Figure 21. Effect of *pma2* deletion on colony growth.** (**A**) Aliquots of 5x10$^4$ fresh microconidia of the wild type (wt), and *pma2*Δ mutants were spot-inoculated on potato dextrose agar (PDA) or minimal medium (MM) plates and incubated at 28°C for 9 days. Colonies were imaged after 3, 6 and 9 days. Plates shown are representative of three independent replicates for each strain and growth condition. (**B**) Colony area of the indicated strains on PDA and MM after 9 days was measured and normalized to that of the wild-type strain (100%). (*) $p$ <0.05, ns (non-significant) *versus* wt according to Welch's t-test. Data show means ± s.d from three independent plates per strain and condition.

## 6. Deletion of *pma2* promotes growth at acid pH and affects adaptation to cell wall and heavy metal stress

To test the potential role of Pma2 in pH adaptation, we analyzed the growth of the *pma2*Δ mutants on YPD medium buffered to pH 4, 6 or 8. At pH 4, the wild type strain formed compact colonies that almost lacked any filamentous growth, while the *pma2*Δ mutants presented an increased colony size with filamentation [Figure 22]. Interestingly, the differences in colony morphology between pH 4 and 6 were more accentuated in the wild type than in the *pma2*Δ mutants. At pH 8, the wild type strain and the *pma2*Δ mutants showed a similar phenotype with increased filamentous growth that was more pronounced in the *pma2*Δ mutants.

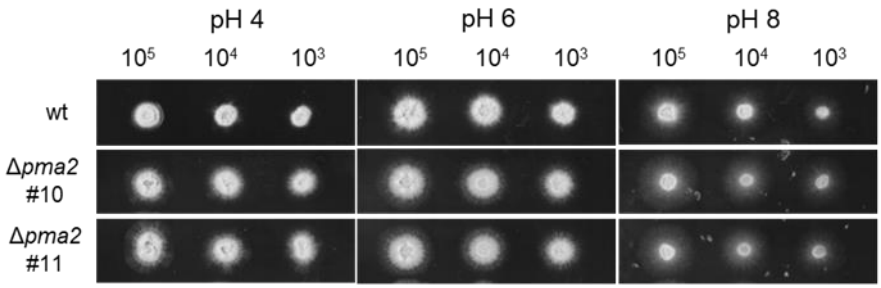


**Figure 22. Deletion of *pma2* promotes filamentous colony growth at low pH.** Aliquots of $10^5$, $10^4$ and $10^3$ fresh microconidia of the indicated strains were spot-inoculated on YPDA plates buffered at pH 4, 6 or 8. The plates were incubated at 28°C for 3 days and scanned. Plates shown are representative of three independent replicates for each strain and growth condition.

We next examined the role of Pma2 in cell wall and osmotic stress response by growing the wild type and *pma2*Δ mutant strains in the presence of congo red (CR) or calcofluor white (CFW) (cell wall stress), as well as sodium chloride (NaCl) or sorbitol (hyperosmotic stress). The *pma2*Δ mutants exhibited a higher sensitivity to CFW compared to the wild type strain. Nevertheless, in the presence of CR, another cell wall stress inducer, the mutants showed a similar growth to the wild type strain [Figure 23]. The *pma2*Δ mutants did not show increased sensitivity to osmotic stress induced by NaCl or sorbitol suggesting that Pma2 is not relevant for this response [Figure 23].

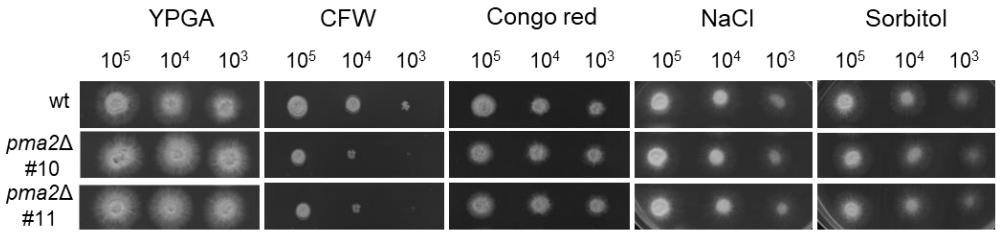


**Figure 23. Pma2 contributes to cell wall stress response in *F. oxysporum*.** Aliquots of $10^5$, $10^4$ and $10^3$ fresh microconidia of the indicated strains were spot-inoculated on YPDA plates supplemented with Calcofluor White (50 µg/mL), Congo Red (100 µg/mL), NaCl (1,2 M) or Sorbitol (1,25 M). Control plates without any compound were also included. The plates were incubated at 28 °C for 3 days and scanned. Plates shown are representative of three independent replicates for each strain and growth condition.

In *S. cerevisiae*, it was demonstrated that Pma2 is important for adaptation to toxic concentrations of manganese. Further, transcriptome analysis of cells adapted to this heavy metal revealed an upregulation of the *pma2* gene (Andreeva *et al.*, 2017). Therefore, we examined the growth of the wild type strain and the *pma2*Δ mutants in the presence of 50- or 100-mM manganese. In line with the previous report in yeast, the *pma2*Δ mutants exhibited increased sensitivity to manganese compared to the wild type strain with a 63.4% reduction in the colony area, and their filamentous growth was dramatically compromised [Figure 24 A,B].

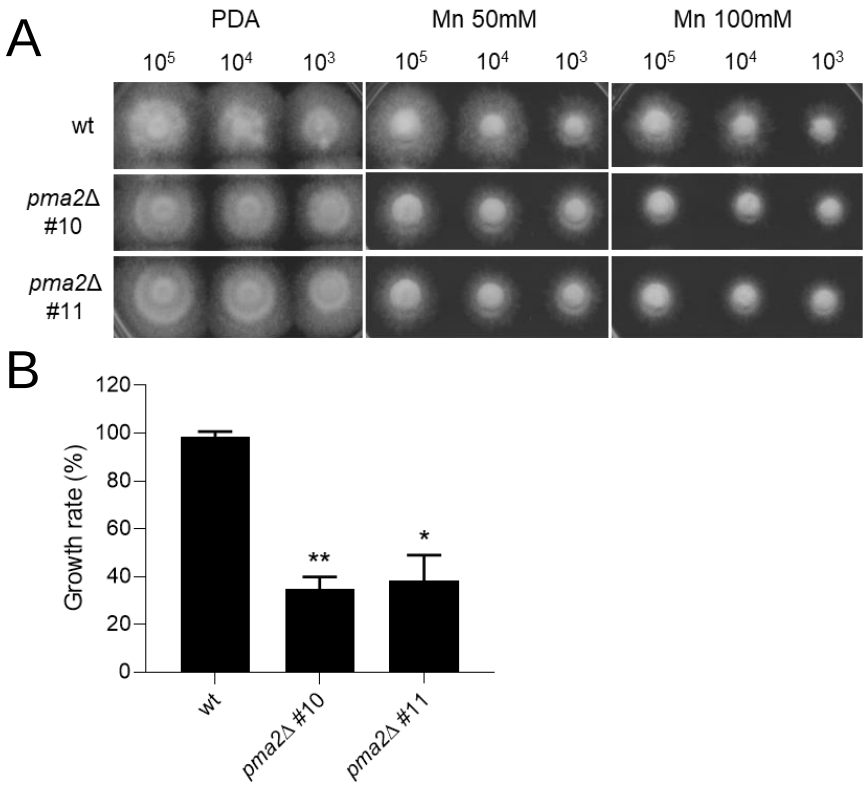


**Figure 24. Pma2 is important for adaptation to manganese.** (**A**) Aliquots of $10^5$, $10^4$ and $10^3$ fresh microconidia of the indicated strains were spot-inoculated on PDA plates supplemented with 50 mM or 100 mM manganese. Control plates without any compound were also included. The plates were incubated at 28 °C for 3 days and scanned. (**B**) Determination of colony area of the different strains on PDA plates supplemented with 100 mM of manganese at $10^4$ microconidia concentration. Data was normalized to that of the wild type (wt) strain (100%). (*) $p$ <0.05, (**) $p$ <0.01 *versus* wt, according to Welch's t-test. Data show representative means ± s.d, from two independent plates per strain.

## 7. Loss of Pma2 promotes invasive growth at acidic pH

Previous results of our group showed that pH plays a central role in infection mechanisms, including invasive growth, chemotropism and infection (Fernandes *et al.*, 2022a; Masachis *et al.*, 2016). A cellophane penetration assay was performed to analyze the capacity of the fungus to penetrate through a cellulose layer, as process that requires a combination of physical pressure and secretion of lytic enzymes (Prados Rosales & Di Pietro, 2008). The assay was carried out on MM plates, either unbuffered or buffered at pH 5 or 7. As previously described (Masachis *et al.*, 2016),

the wild type strain was able to penetrate the cellophane membrane on unbuffered and buffered medium at pH 7, but not at pH 5 [Figure 25A]. By contrast, the *pma2*Δ mutants strains were able to penetrate both at pH 7 and 5.

To further understand the role of Pma2 in infection-related processes, a tomato root infection assay was performed by dip-inoculating the roots with fresh microconidia of the wild type or *pma2*Δ mutant strains. No significant differences in plant survival were observed between the strains [Figure 25B]. Overall, these results suggest that Pma2 is not relevant for the infection process itself, although it appears to play a role on invasive growth under acidic conditions, which could be indicative of its relevance for the first stages of infection previous to fungus-induced alkalinization of the surrounding environment.

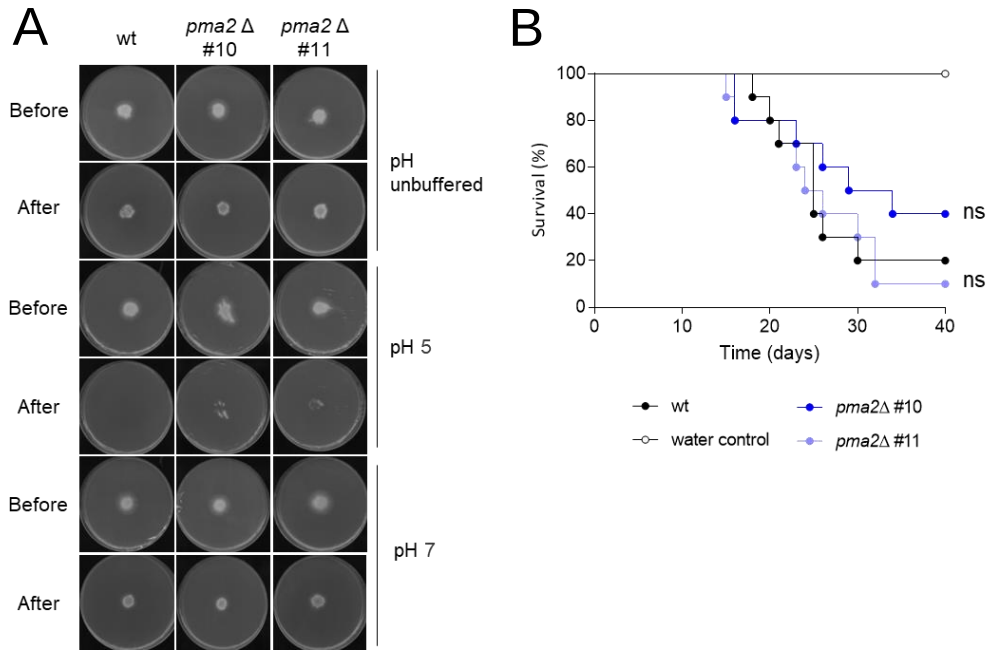


**Figure 25. Loss of Pma2 promotes invasive growth at acidic pH.** (**A**) Invasive growth of the *F. oxysporum* wild type (wt), *pma2*Δ #10 and *pma2*Δ #11 mutant strains was determined by growing fungal colonies on top of cellophane membranes placed on MM plates either unbuffered or buffered at pH 7,0 or 5,0 with 100 mM MES. After 3 days at 28 ºC, plates were imaged (before), the cellophane with the fungal colony was removed and plates were incubated for an additional day to visualize the presence of mycelium, indicating penetration through the cellophane (after). Images shown are representative of two independent experiments, each with three plates per treatment. (**B**) Kaplan–Meier plots showing survival of tomato plants (cv. Monica) inoculated by dipping roots into a suspension of $5x10^6$ microconidia/mL of the indicated fungal strains. Percentage survival of tomato plants was plotted for 40 days. Data shown are from one representative experiment. ns (non-significant) *versus* wt according to log-rank test.

# Chapter III

Subchapter I. Casein kinase 1, a negative regulator of the plasma membrane $H^+$-ATPase Pma1, is required for development and pathogenicity of *Fusarium oxysporum*

Subchapter II. Role of the small Pma1-associated peptide Pmp1 in *Fusarium oxysporum*

**The results of the *subchapter I* have been published in the Journal of Fungi (Mariscal *et al.*, 2022)**

# Chapter III: Regulation of Pma1 activity and its relevance for pH homeostasis, fungal growth and pathogenicity

## Overview

The $H^+$-ATPase Pma1 is the most abundant PM protein and the major regulator of $pH_c$ homeostasis in fungal cells. Pma1 pumps protons out of the cell keeping the PM potential ($\Delta\psi$) and $pH_c$ constant, which is fundamental for cell function and survival (Kane, 2016; Palmgren & Morsomme, 2019).

Due to the high abundance of Pma1 in the PM and its relatively long half-life, the activity is mainly regulated by changes at the post-translational level, which can be triggered by different stimuli. Glucose is by far the best-studied activator of Pma1 activity by triggering phosphorylation of the residues Ser-899, Ser-911 and T912 which are localized in the R domain and highly conserved among fungi (Lecchi *et al.*, 2007; Portillo, 2000). Furthermore, truncation of the C-terminal domain of Pma1 leads to a drastic cytosolic acidification which affects fungal growth and filamentation (Rane *et al.*, 2019). Pma1 post-translational regulation is also controlled by two protein kinases that respond to glucose metabolism, Protein Kinase 2 (Ptk2) and Hrk1. In response to glucose, Ptk2 phosphorylates Pma1 at Ser-899, leading to a 5 to 10-fold increase in $H^+$-ATPase activity and an acidification of ambient pH (Eraso *et al.*, 2006; Goossens *et al.*, 2000). Ptk2 involvement in the increase of $H^+$-ATPase affinity for ATP was subsequently confirmed (Pereira *et al.*, 2015). The first biological role attributed to the Ser/Thr Kinase Hrk1 was a subtle activation of Pma1 in response to glucose (Goossens *et al.*, 2000). However, Hrk1 was later shown to play an essential role in the response and tolerance to acetic acid stress in *S. cerevisiae* (Mira *et al.*, 2010a), suggesting that this kinase could have a relevant role in Pma1 activity regulation by acid conditions. Other studies also suggested a role for calcium-dependent signaling in glucose-mediated Pma1 activation, although the underlying mechanism is still unknown (Bouillet *et al.*, 2012; Pereira *et al.*, 2008; Trópia *et al.*, 2006). By contrast, the Ser/Thr kinase Casein Kinase 1 (Ck1) has been described as a negative regulator of Pma1. Ck1-mediated phosphorylation of Pma1 at Ser-507 inhibits Pma1 activity in *S. cerevisiae* (Estrada *et al.,* 1996). Some recent reports have shown that activity of Ck1 can be controlled by important signaling pathways, such the Rapamycin Complex 1 (TORC1), Protein Kinase A (PKA) or, even in response to oxidative stress, demonstrating the relevance of pH homeostasis for controlling

cellular responses (Baron *et al.*, 2015; Devare *et al.*, 2020; Kang *et al.*, 2015). Besides a role on Pma1 activity, new findings have indicated that the yeast Ck1 might also have a role in controlling the alkaline pH Pal/Rim pathway, through phosphorylation of the α-arrestin Rim8 (Herrador *et al.*, 2015).

Other proteins have been also described to have a role on Pma1 regulation. The Pmp1, a small PM proteolipid, was copurified with the Pma1 protein, suggesting to be a regulatory subunit of this $H^+$-ATPase (Navarre *et al.*, 1994; Navarre *et al.*, 1992). More recent studies have demonstrated that this protein forms a unique helix and exhibits a positively charged cytoplasmic domain that is able to specifically interacts with phosphatidylserine lipids (Beswick *et al.*, 2011; Coic *et al.*, 2005). A marked groove formed at the helix surface is thought to play a major role in the related lipid-protein interaction network (Mousson *et al.*, 2002). Pma1 is a major component of the glycosphingolipid- and cholesterol-enriched microdomains in the PM, called lipid rafts (Bagnat *et al.*, 2000). Interestingly, Pma1 is missorted in mutants which lose the ability to flip phosphatidylserine, or which lose this lipid from the cytosolic leaflet (Hankins *et al.*, 2015). However, how this peptide regulates and interacts with the membrane protein Pma1 remains to be discovered. Here we propose to study the role of these proteins described as regulators of $H^+$-ATPase Pma1 and its possible involvement in pH homeostasis.

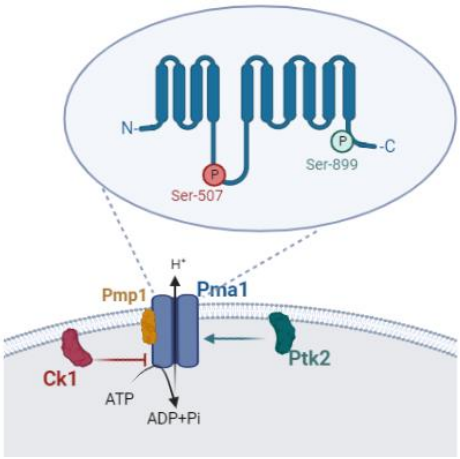


**Figure 26. Key regulators $H^+$-ATPase Pma1 activity.** The $H^+$-ATPase Pma1 pumps protons out of the cell by hydrolyzing ATP and is critical for $pH_c$ homeostasis in fungi. Pma1 activity is tightly controlled through different regulatory proteins and stimuli. Ptk2 positively regulates Pma1 activity through phosphorylation of the residue Ser-899 in the C-terminal domain, while Ck1 negatively regulates Pma1 through phosphorylation of the residue Ser-507 (ATP-binding site). Pmp1 has been shown to be associated with Pma1, but its role in Pma1 activity remains to be clarified.

# Subchapter I. Casein kinase 1, a negative regulator of the plasma membrane $H^+$-ATPase Pma1, is required for development and pathogenicity of *Fusarium oxysporum*

## Results

### 1. *In silico* identification of the *ck1* ortholog in *Fusarium oxysporum*

In order to study the role of Ck1 in *F. oxysporum* we started by making a BLASTp search using *S. cerevisiae* Yck1 (YHR135C) and Yck2 (YNL154C) as a bait. A single Ck1 orthologue in *F. oxysporum* (FOXG_05428) was identified. The FOXG_05428 gene is located on chromosome 7 and encodes a predicted protein of 453 amino acids that exhibits around 70% identity with either Yck1 or Yck2 of *S. cerevisiae* and around 85% identity with filamentous fungi such as *M. oryzae* (*MGG_08097;82%)*, *C. neoformans (CNA05390; 82%*) and *Verticillium dahliae (VDAG_08537; 88%).*

### 2. Targeted deletion of the *ck1* gene in *Fusarium oxysporum*

To investigate the role of Ck1 in *F. oxysporum*, we generated a *ck1*Δ allele by replacing the complete ORF with the *Hyg*$^R$ resistance cassette using the "split-marker" technique [Figure 27A]. The two constructs obtained, each containing a flanking region of the gene and about 75% of the *Hyg*$^R$ cassette, were used to transform protoplasts of the *F. oxysporum* wild type strain. PCR analysis identified six hygromycin resistant transformants producing amplification patterns indicative of homologous replacement of the *ck1* gene that were further tested by Southern blot analysis, which confirmed the replacement of a 6,1 kb *Pst* I fragment corresponding to the wild type *ck1* allele by a 3,4 kb fragment in the *ck1*Δ transformants #10 and #22, indicating that a single homologous replacement event had occurred [Figure 27B]. Next, we complemented the *ck1*Δ #10 mutant strain by co-transforming *ck1*Δ #10 protoplasts with the *Phleo*$^R$ cassette together with a 4,3 kb DNA fragment encompassing the *ck1* wild type gene PCR analysis with gene-specific primers identified eleven independent transformants showing a PCR amplification product identical to that obtained from the wild type strain, which was absent in the *ck1*Δ knockout mutant, indicating that these *ck1*Δ+*ck1* transformants had integrated the wild type *ck1* allele [Figure 27C].

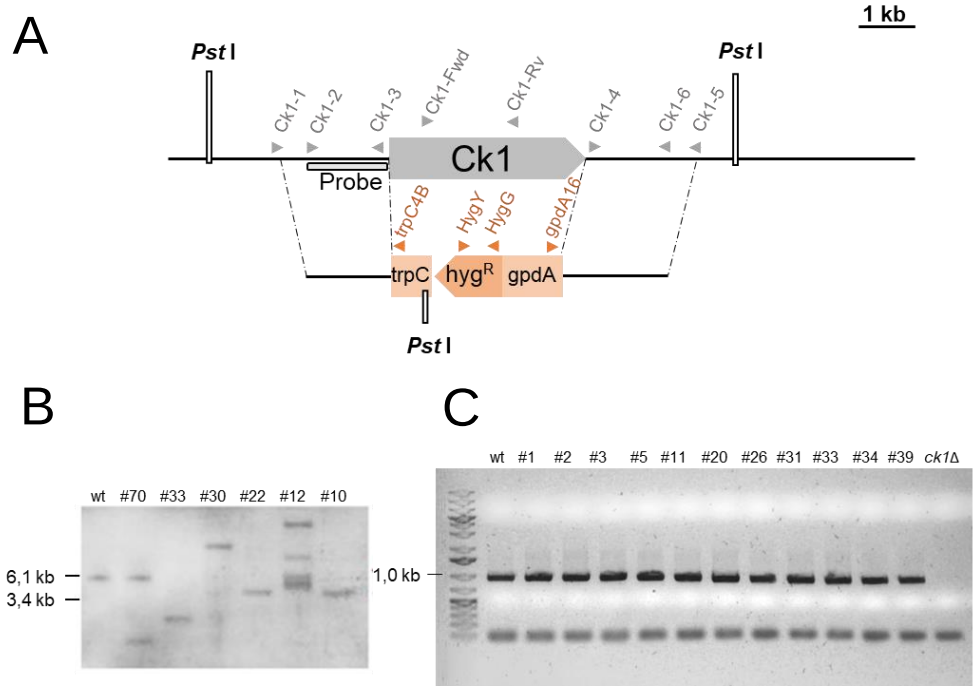


**Figure 27. Targeted deletion of the *F. oxysporum ck1* gene.** (**A***) Physical maps of the *ck1* locus and strategy for the replacement of the coding region with the split-marker method using the *Hyg*$^{R}$ cassette as selective marker (*ck1*Δ allele). Positions of *Pst* I restriction sites are shown. Gray (*ck1*) and orange (*Hyg*$^{R}$) arrowheads indicate the relative positions of the primers used for generation of the gene disruption constructs and PCR analysis of the complemented transformants; the probe used for Southern blot analysis is indicated as gray bar. Scale bar, 1kb. (**B***) Southern blot hybridization analysis of the wild type strain (wt) and six independent *ck1*Δ transformants. Genomic DNA was treated with *Pst* I, separated in an agarose gel, transferred to a nylon membrane, and hybridized with the probe indicated in (A). (**C**) PCR amplification of genomic DNA of the wild type (wt) and eleven independent complemented strains, using primers Ck1-Fwd and Ck1-Rv indicated in (A). *****Experiments conducted by Dr. Cristina de Miguel Rojas.

## 3. Ck1 negatively regulates Pma1 activity in *Fusarium oxysporum*

In *S. cerevisiae*, Ck1 negatively regulates the $H^+$-ATPase activity of Pma1 by phosphorylating the Ser-507 residue (Estrada *et al.*, 1996). Inspection of an amino acid sequence alignment between Pma1 proteins from different fungal species revealed that this region is highly conserved among filamentous fungi where a conserved Thr residue is at an analogous position to the yeast Ser-507 [Figure 28A]. This suggests that regulation of Pma1 by Ck1 may be functionally conserved between *F. oxysporum* and other fungal species. To validate the role of Ck1 in this fungal plant pathogen, we measured Pma1 activity in the *ck1*Δ mutant. Pma1 activity was approximately 3-fold higher in the *ck1*Δ mutant than in the wild type and the complemented strain, suggesting that Ck1 acts as a negative regulator of Pma1 also *F. oxysporum* [Figure 28B].

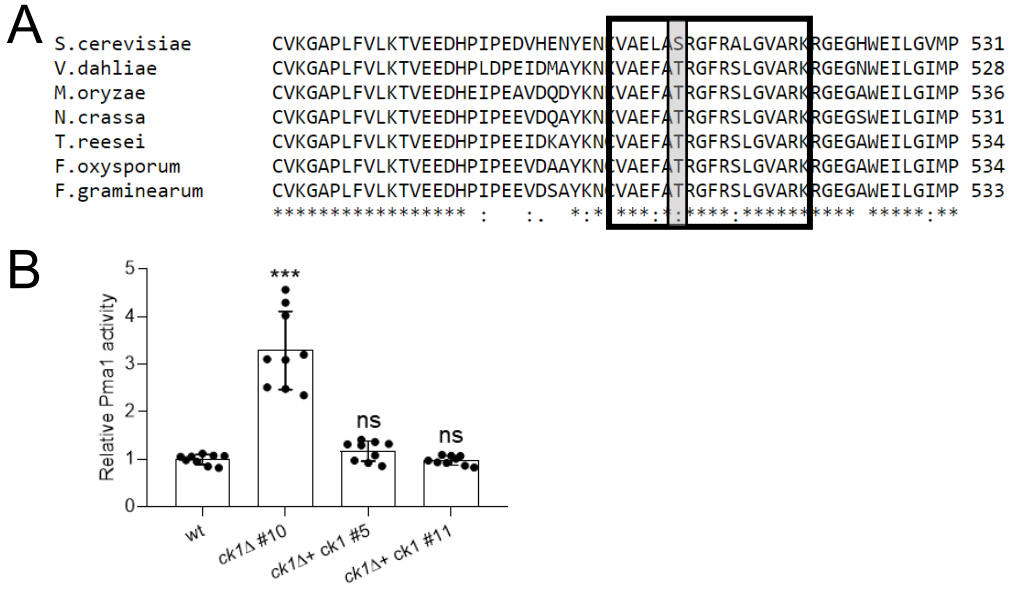


**Figure 28. The casein kinase Ck1 negatively regulates Pma1 activity in *F. oxysporum.*** (**A**) Amino acid sequence alignment of Pma1 proteins from *Saccharomyces cerevisiae* (YGL008C), *Verticilliium dahliae* (XP_009652327), *Magnaporthe oryzae* (MGG_07200), *Neurospora crassa* (NCU01680), *Trichoderma reesei* (TRIREDRAFT_78757), *Fusarium oxysporum* (FOXG_11289) and *Fusarium graminearum* (FGRAMPH1_01G03505). Boxed in gray is the Ser-507 in *S. cerevisiae* Pma1 and the corresponding Thr residue conserved among filamentous fungi. Boxed in black is the consensus phosphorylation motif for Ck1. (**B**) Analysis of Pma1 ATPase activity was assayed in total membranes isolated from fifteen-hours germinated microconidia in PDB medium of the *F. oxysporum* wild type (wt), *ck1*Δ and complemented strains. Activity was normalized to that of the wt strain. (***) $p$ <0.001 and ns (non-significant) *versus* wt according to Welch's test. Data shown are the mean ± s.d. from three independent biological replicates, with three technical replicates each.

## 4. Ck1 controls vegetative growth and conidiation in *Fusarium oxysporum*

To evaluate the role of Ck1 in vegetative growth, the wild type, *ck1*Δ mutant and *ck1*Δ+ck1 complemented strains were grown for three days on solid complete medium (YPGA) and minimal medium (MM) plates [Figure 29A]. The *ck1*Δ mutant strains exhibited a strong (around 80%) reduction in colony diameter when compared to the wild type and the complemented strains, both on YPGA and MM media [Figure 29B].

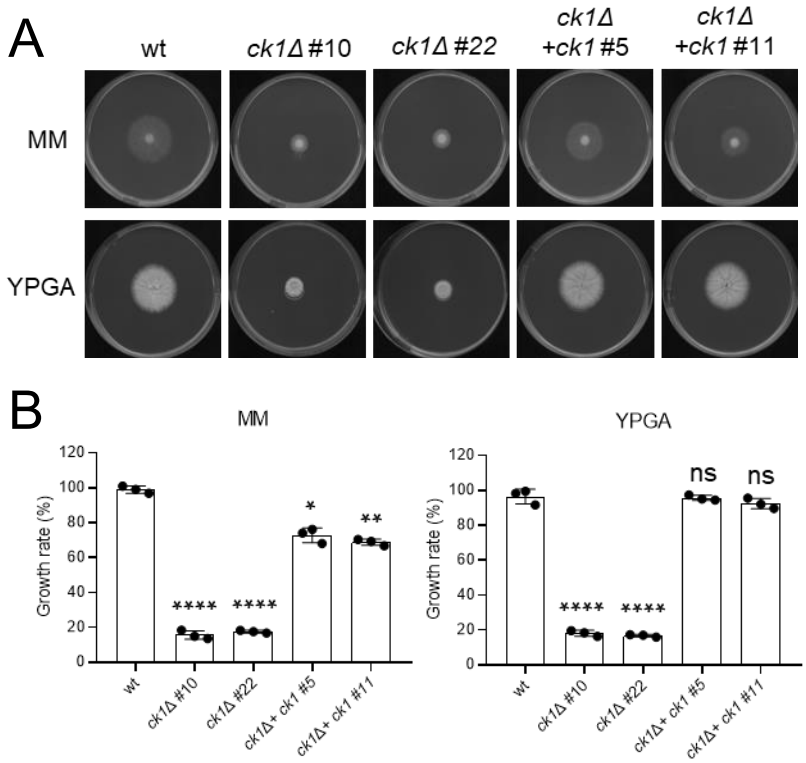


**Figure 29. Loss of ck1 strongly impacts *F. oxysporum* vegetative growth.** (**A**) Aliquots of 5x10$^4$ fresh microconidia of the wild type (wt), *ck1*Δ mutants and complemented strains were spot-inoculated on complete medium (YPDA) and minimal medium (MM) plates and incubated at 28°C for 3 days. Plates shown are representative of three independent replicates for each strain and growth condition. (**B**) Colony area of the indicated strains on YPGA and MM after 3 days was measured and normalized to that of the wt strain (100%). (*) $p$ <0.05, (**) $p$ <0.01, (****) $p$ <0.0001 and ns (non-significant) *versus* wt, according to Welch's t-test. Data show means ± s.d. from three independent plates per strain and condition.

We next examined the role of Ck1 in growth in liquid medium by measuring absorbance at 600nm. Our results demonstrated that the growth rate of the *ck1*Δ

mutant was also significant reduced in liquid YD (yeast extract-dextrose) medium when evaluated for 54 hours. However, differences among the *ck1*Δ knockout mutant and the wild type or complemented strains were less marked than in solid medium [Figure 30A]. Furthermore, we evaluated the role of Ck1 on fungal germination and found that it is apparently not relevant for this process [Figure 30B]. Conversely, conidiation rate in the *ck1*Δ mutant was strongly affected, presenting a reduction of about 60% compared with the wild type and complemented strain [Figure 30C].

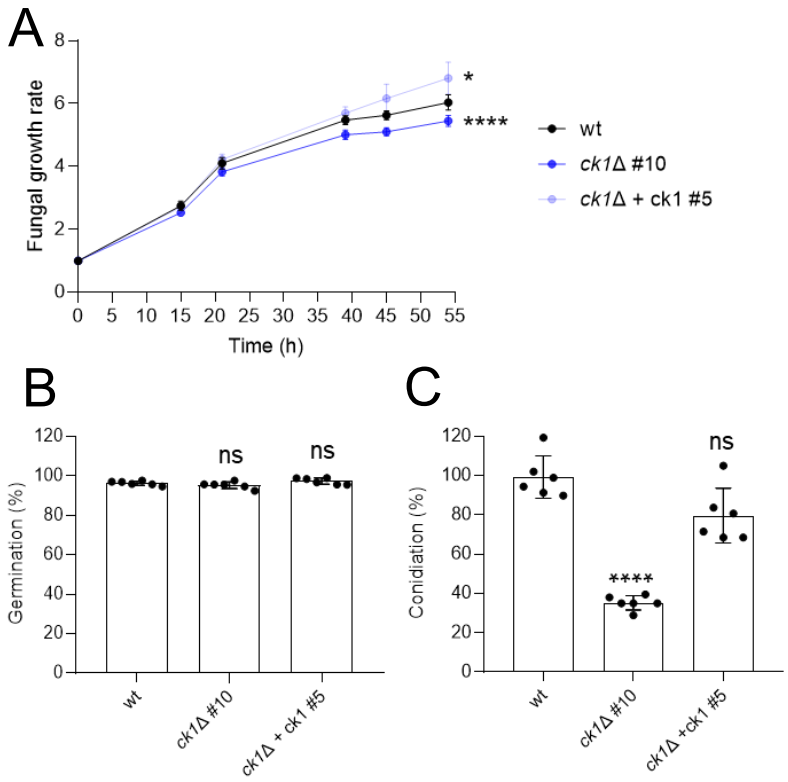


**Figure 30. Deletion of *ck1* severely affects fungal growth in liquid medium and conidiation rate in *F. oxysporum*.** (**A**) Determination of fungal growth in YD medium buffered at pH 7.4 with 20 mM HEPES at 28°C was monitored in 96 Microtiter™ by measuring absorbance at 600 nm for each indicated strain. Values were normalized to time-point 0'. Data show the mean ± s.d. of three independent replicates microwells from one representative experiment. (**) $p$ <0.01 and (****) $p$ <0.0001 *versus* wt, according to Welch's t-test. Experiments were performed twice with similar results. (**B**) Germination rate was determined after fifteen-hours of microconidia incubation in PDB medium. ns (non-significant) *versus* wt, according to Welch's t-test. Data shown are the mean ± s.d. of two biological replicates with three technical replicates each one. (**C**) Conidiation rate was determined 48 h after grow in PDB medium in the indicated strains. Data was normalized to the wt strain (100%). (****) $p$ <0.0001 and ns (non-significant) *versus* wt, according to Welch's t-test. Data show means ± s.d. of two biological replicates with three technical replicates each.

## 5. Relevance of Ck1 for pH, hyperosmotic and cell wall stress responses

To test whether the reduced growth capacity of the *ck1*Δ mutants could be pH-dependent, we performed a phenotypic growth assay of wild type, *ck1*Δ mutants and complemented strain in YPGA plates, either unbuffered or at pH 4, 6, or 8. The *ck1*Δ #10 and *ck1*Δ #22 mutants exhibited a severe growth reduction at acidic pH and a slight reduction at pH 6 and 8 as well as on the unbuffered medium plates [Figure 31].

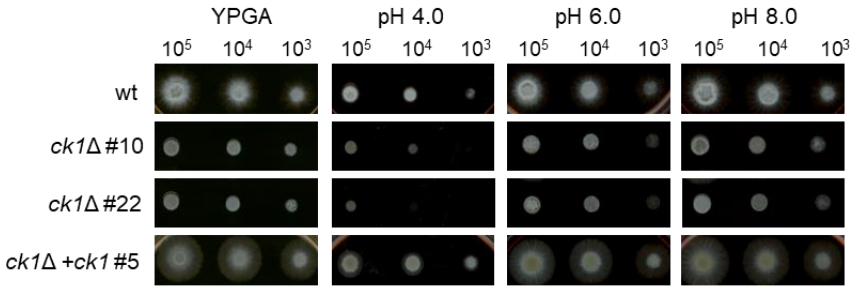


**Figure 31. Ck1 has a minor role in adaptation to acidic pH. (A)** Aliquots of $10^5$, $10^4$ and $10^3$ fresh microconidia of the indicated strains were spot-inoculated on YPGA plates adjusted to the indicated pH values. Control plates without adjustment were also included. The plates were incubated at 28 °C for 2 days and scanned. Plates shown are representative of three independent replicates for each strain and growth condition.

We next tested the sensitivity of the *ck1*Δ mutant strains to different compounds triggering cell wall and hyperosmotic stress. We found that the *ck1*Δ mutants were more sensitive to membrane and osmotic stress caused by sodium dodecyl sulfate (SDS) or by high concentrations of sodium chloride (NaCl) or potassium chloride (KCl) [Figure 32]. By contrast, sensitivity of the *ck1*Δ mutants to the cell wall perturbing agents calcofluor white (CFW) and congo red (CR) was not altered [Figure 32].

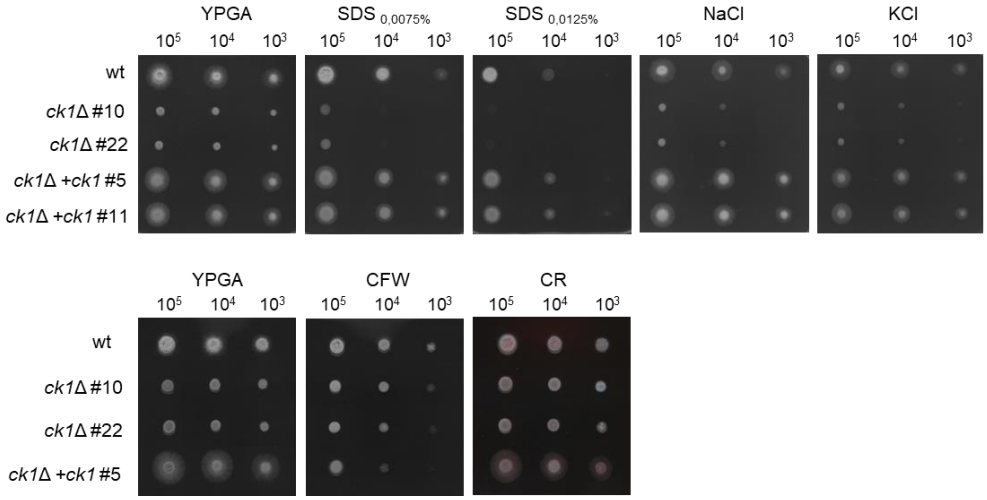


**Figure32. Ck1 regulates the osmotic and membrane stress responses.** Aliquots of $10^5$, $10^4$ and $10^3$ fresh microconidia of the indicated strains were spot-inoculated on YPGA plates supplemented with SDS (7,5 mg/ml and 12,5 mg/ml), NaCl (1,2 M), KCl (1,2 M), CFW (50µg/ml) and CR (100µg/ml). Control plates without any compound were also included. The plates were incubated at 28 °C for 2 days and scanned. Plates shown are representative of three independent replicates for each strain and growth condition.

## 6. The deficient growth of *ck1*Δ mutant strains is independent of glucose

The activity of Pma1 has been shown to be positively regulated by glucose, which induces phosphorylation of conserved C-terminal residues (Eraso *et al.*, 2006; Lecchi *et al.*, 2007). Therefore, we examined whether growth of *ck1*Δ mutants was affected by increasing concentrations of glucose. However, we found no differences on fungal growth under the different glucose concentrations tested in this study [Figure 33].

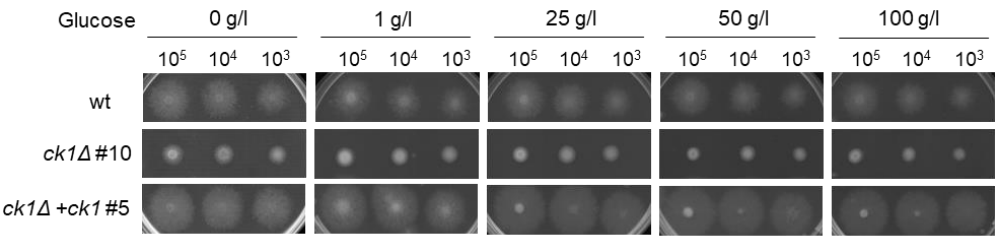


**Figure 33. The defective growth of *ck1*Δ mutant is not dependent of glucose.** Aliquots of $10^5$, $10^4$ and $10^3$ fresh microconidia of the indicated strains were spot-inoculated on minimal medium (MM) plates supplemented with increasing concentrations of glucose. The plates were incubated at 28 °C for 2 days and scanned. Plates shown are representative of three independent replicates for each strain and growth condition.

## 7. Ck1 regulates extracellular pH homeostasis

We previously observed that the absence of *ck1* leads to increased Pma1 $H^+$-ATPase activity. To test whether this increase is related with extracellular accumulation of protons and concomitant acidification, we measured the pH at the center and the margins of fungal colonies grown on minimal medium, as previously described (Shaw *et al.*, 2022). No difference was detected in the pH at the center and the margin of the colony (data not shown). However, while the pH in the wild type colonies increased steadily from around 6,0 at day 3 to 6,7 at day 7, the pH in the *ck1*Δ mutant colonies was significantly lower (5,7) and remained stable throughout the monitored time period [Figure 34]. The complemented strain showed an intermediate extracellular pH phenotype.

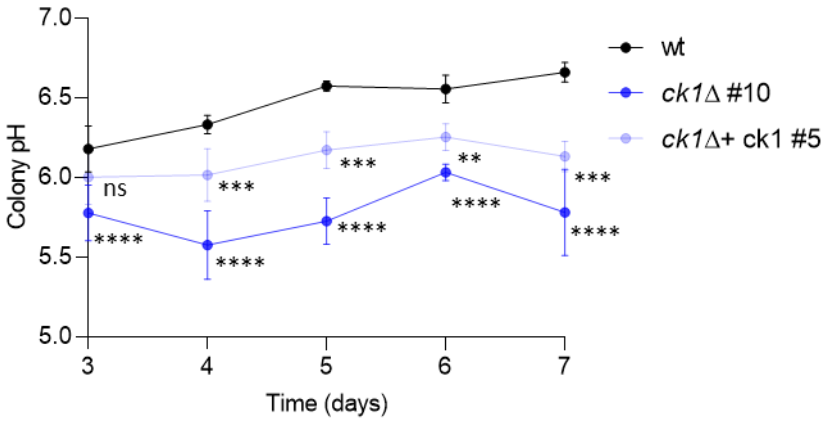


**Figure 34. The casein kinase Ck1 controls alkalinization of media in *F. oxysporum.*** Aliquots of $5x10^4$ fresh microconidia of the wild type (wt), ck1Δ and complemented strain were spot-inoculated on minimal medium (MM) plates and incubated for 7 days. Samples of 4 $mm^2$ were collected from each colony at indicated time points and homogenized in 50µl of ultrapure water. The pH was measured by pH meter. (**) $p$ <0.01, (***) $p$ <0.001, (****) $p$ < 0.0001 and ns (non-significant) *versus* wt according to two-way ANOVA and Turkey Test. Data presented are the mean ± s.d. from three independent biological experiments.

## 8. Increased Pma1-activity in *ck1*Δ improves resistance to acid-induced cell death

Acetic acid (AA) is a weak acid that displays antimicrobial action. At low pH, AA is in its undissociated form and can enter the cell by rapid diffusion through the PM. Once inside the cytosol, AA dissociates into anions and protons which, being charged, are lipid insoluble and accumulate inside the cell (Stratford *et al.*, 2009). In *S.*

*cerevisiae*, AA induces concentration-dependent cell-death in exponentially growing cells at pH 3,0 (Guaragnella *et al.*, 2011). When *F. oxysporum* germlings expressing the ratiometric pH probe pHluorin were treated with 30 mM or 40 mM AA, a rapid and sustained acidification of the cytosol was observed, as previous reported for yeast cells (Arneborg *et al.*, 2000). Both 30- and 40-mM AA triggered a drop on $pH_c$ from 6,8±0.2 to 5,9±0.03 in about 5 minutes [Figure 35]. Importantly, no recovery of $pH_c$ homeostasis was observed throughout the 90 minutes duration of the experiment.

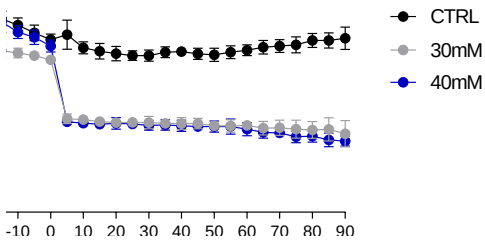


**Figure 35. Acetic acid induces a drop of cytosolic pH in *F. oxysporum.*** Fifteen-hour germinated microconidia in PDB medium of the *F. oxysporum* strains expressing pHluorin were washed and resuspended in KSU buffer at pH 3.0 and transferred to microwells and pre-incubated one hour at 28 °C. The $pH_c$ was monitored spectrophluorometrically every 5 minutes starting 20 minutes before adding acetic acid 30- or 40- mM of acetic acid. The ratio between the emission intensities at 510 nm after excitation at 395 nm and 475 nm was calculated and normalized to the standard curve. Data show the mean ± s.d of three independent replicates microwells from one representative experiment. Experiments were performed twice with similar results.

Recent work has shown that the overexpression of Pma1 can enhance tolerance to acids (Lee *et al.*, 2017). To investigate whether overactivation of Pma1 in the *ck1*Δ mutants (see Figure 28B) enhances AA-tolerance, we performed an AA survival assay with same concentration used for monitoring $pH_c$. We found that 15 min after treatment with 40 mM AA, only 33,2% of the wild type cells survived while survival in the *ck1*Δ mutant strain was approximately double at this time point [Figure 36A]. Even after 60 min of AA treatment, more than half (54.8%) of the *ck1*Δ cells survived compared to only 6,8% and 11,2% in the wt and the complemented strain, respectively.

Considering that the differential AA-response could be related with the Pma1 activity in these strains, we decided to study the role of the protein kinase Ptk2, a Pma1 activator, in this process. Ptk2 is located at the PM and induces activation of

Pma1 in response to glucose through phosphorylation of residue S899 in yeast (Eraso *et al.*, 2006). We reasoned that reduced Pma1 activity in the *ptk2*Δ mutant could result in a decreased export of protons which might lead to enhanced sensitivity to cytosolic acidification triggered by AA. To explore this hypothesis, we analyzed the survival after AA-treatment in a *ptk2*Δ mutant of *F. oxysporum* (FOXG_06362), that was previously generated in our group (Fernandes, 2017). We found that 15 min after treatment with 30 mM AA, 50,4% of the wt cells survived in comparison to 39,2% and 28,6% in the *ptk2*Δ #1 and #3 mutants, respectively [Figure 36B]. Thus, the *ck1*Δ mutant is more resistant while Ptk2 appears to have a less marked effect in this process.

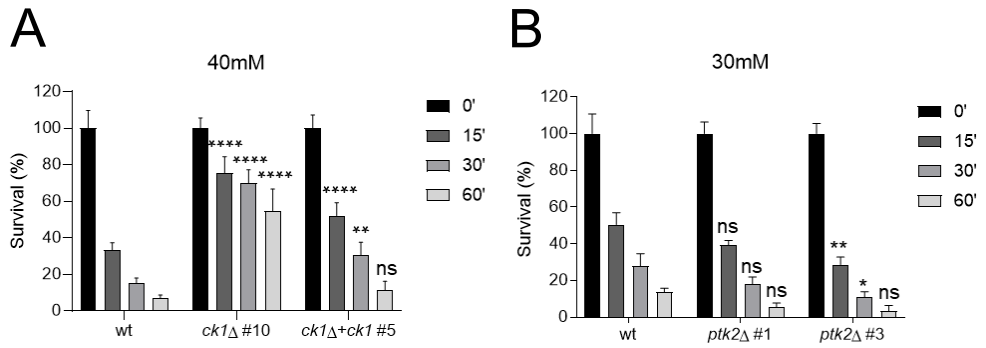


**Figure 36. *ck1*Δ displays increased resistance to acetic acid-induced cell death.** Fifteen-hours germinated microconidia in PDB medium were adjusted pH 3,0 with HCl and pre-incubated one hour at 28°C. (**A**) At time 0', 40 mM AA was added to medium of wild type (wt), *ck1*Δ mutants and complemented strains. (**B**) At time 0', 30 mM was added to medium of wt and two *ptk2*Δ mutant strains. Germlings collected before (time 0') and 15, 30, 60 minutes after AA-treatment were diluted 1:100 and plated on PDA plates. After two days of incubation at 28 °C, the number of colonies was counted to determine the effect of acetic acid on cell survival. (*) $p$ <0.05, (**) $p$ <0.01, (****) $p$ <0.0001 and ns (non-significant) *versus* wt according to two-way ANOVA Bonferroni Test. Bars show mean ± s.d from at least two independent biological experiments with three technical replicates each.

We next asked whether the increased Pma1 activity in the *ck1*Δ mutant strains could also increase resistance to strong acids such as HCl. Previous results of the group had demonstrated that external HCl causes a drop in $pH_c$ (Fernandes *et al.*, 2022a). We observed that 30 minutes after treatment with 60 mM HCl, 58,6 and 52,9% of the *ck1*Δ #10 and #22 cells survived respectively, while only 30,2% of the wild type cells had survived. However, after 60 min HCl-treatment, the *ck1*Δ mutants showed a survival rate similar to the wt strain [Figure 37]. These results demonstrate that *ck1*Δ mutants are more resistant at the initial stages of HCl-treatment.

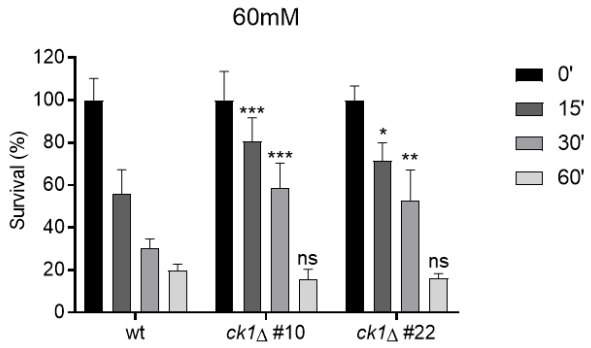


**Figure 37. *ck1*Δ displays enhance resistance to HCl-induced cell death**. Fifteen-hours germinated microconidia in PDB medium of the wild type (wt), *ck1*Δ and complemented strain. At time 0', 60 mM HCl was added to medium. Germlings were collected before (time 0) and 15, 30, 60 minutes after HCl-treatment. Germlings collected before (time 0') and 15, 30, 60 minutes after HCl-treatment were diluted 1:100 and plated on PDA plates. After two days of incubation at 28 °C, the number of colonies was quantified to determine the effect of HCl on cell survival. (*) $p$ <0.05, (**) $p$ <0.01, (***) $p$ <0.001, ns (non-significant) *versus* wt according to two-way ANOVA Bonferroni Test. Bars show mean ± s.d from at least two independent biological experiments with three technical replicates each.

## 9. Role of key regulators of Pma1 activity on $pH_c$ homeostasis in *Fusarium oxysporum*

To test the role of Ck1 and Ptk2 on cytosolic pH homeostasis, the deletion alleles were generated in the genetic background of the wild type strain expressing the fluorescent ratiometric pH sensor pHluorin (transformant #9 expressing high levels of pHluorin), by replacing the *ck1* or *ptk2* coding region with the *Phleo*$^R$ or *Neo*$^R$ resistance cassettes, respectively, using the split-marker protocol [Figure 38A]. PCR analysis identified initially the transformants carrying a homologous insertion of the *ck1* locus [Figure 38B], and Southern blot analysis identified six *ck1*Δ::pHluorin transformants in which the 4,1 Kb hybridizing *Nsi* I fragment corresponding to the wild type *ck1* allele had been replaced by the expected 2,5 Kb fragment [Figure 38C].

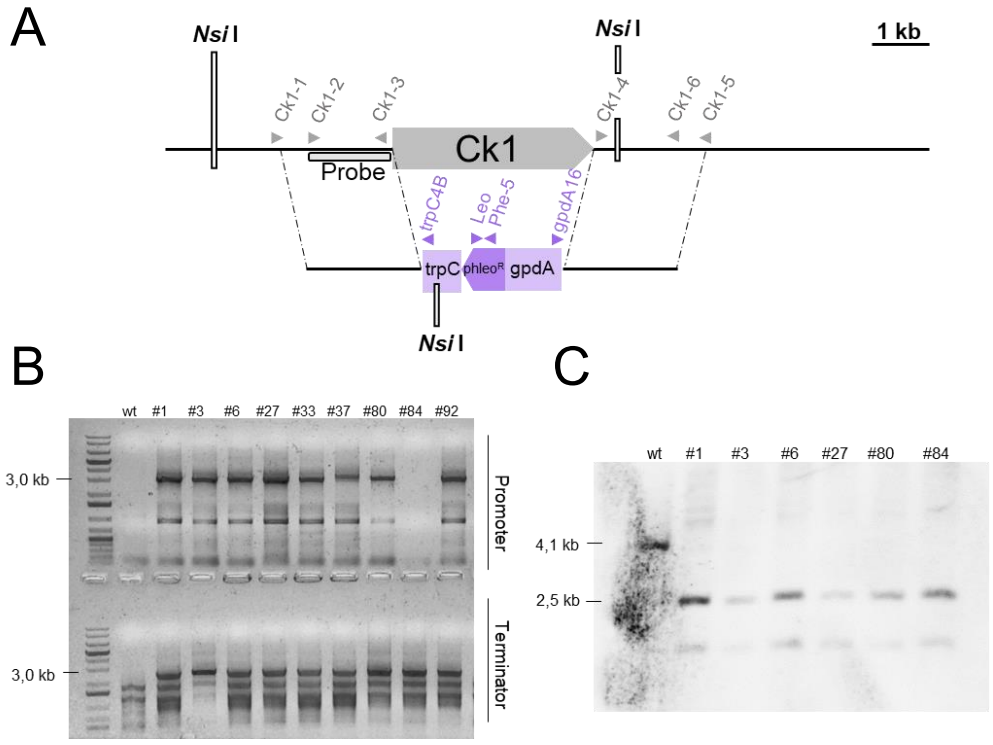


**Figure 38. Targeted disruption of the *ck1* gene in the *F. oxysporum* strain expressing pHluorin.** (**A**) Physical maps of the *ck1* locus and strategy for the replacement of the coding region with the split-marker method using the *Phleo*$^{R}$ cassete as selective marker (*ck1*Δ allele). Positions of *Nsi* I restriction sites are shown. Gray (*ck1*) and purple (*Phleo*$^{R}$) arrowheads indicate the relative positions of the primers used for generation of the gene disruption constructs and PCR analyses of the transformants; the probe used for Southern blot analysis is indicated as gray bar. Scale bar, 1kb. (**B**) PCR analysis to confirm homologous recombination of the construct into the genome of the transformants using the primers pairs: Ck1-1/Pheo-5(promotor region) and Ck1-5/Leo (terminator region). (**C**) Southern blot hybridization analysis of the wild type (wt) strain and six independent *ck1*Δ transformants. Genomic DNA treated with *Nsi* I, separated in an agarose gel, transferred to a nylon membrane and hybridized with the probe indicated in (A).

Moreover, three *ptk2*Δ transformants were identified in which the 6,9 Kb hybridizing *Xho* I corresponding to the wild type allele was replaced by a 13,9 Kb fragment, revealing homologous insertion in these transformants [Figure 39B]. Fluorescence levels in all generated mutants were comparable to those of the original strain expressing pHluorin (transformant #9; data not shown).

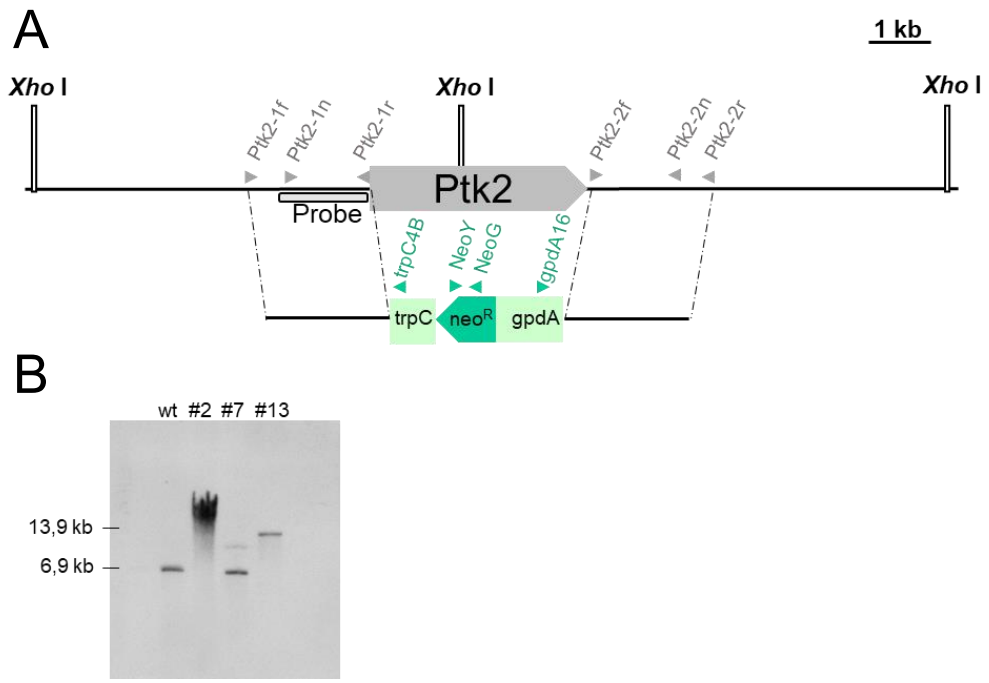


**Figure 39. Targeted disruption of the *ptk2* gene in the *F. oxysporum* strain expressing pHluorin.** (**A**) Physical maps of the *ptk2* locus and strategy for the replacement of the coding region with the split-marker method using the *Neo*$^R$ cassette as selective marker (*ptk2*Δ alllele). Positions of *Xho* I restriction sites are shown. Gray (*ptk1*) and orange (*Neo*$^R$) arrowheads indicate the relative positions of the primers used for generation of the gene disruption constructs and the probe used for Southern blot analysis is indicated as gray bar. Scale bar, 1kb. (**B**) Southern blot hybridization analysis of the wild type (wt) strain and three independents *ptk2*Δ transformants. Genomic DNA treated with *Xho* I, separated in an agarose gel, transferred to a nylon membrane and hybridized with the probe indicated in (A).

To explore the role of these key regulators of Pma1 activity in $pH_c$ homeostasis, we measured steady state $pH_c$ in the *ck1*Δ::pHluorin#80 and *ptk2*Δ::pHluorin #13 mutants. For this, cells were maintained for two hours in KSU buffer at pH 6,0. Our results revealed that $pH_c$ in the *ck1*Δ::pHluorin #80 mutant was around 6,1, which is approximately 0,7 pH units lower than original strain, while $pH_c$ in the *ptk2*Δ::pHluorin #13 strain was around 8,1, which is 1,3 units higher than in original strain [Figure 40].

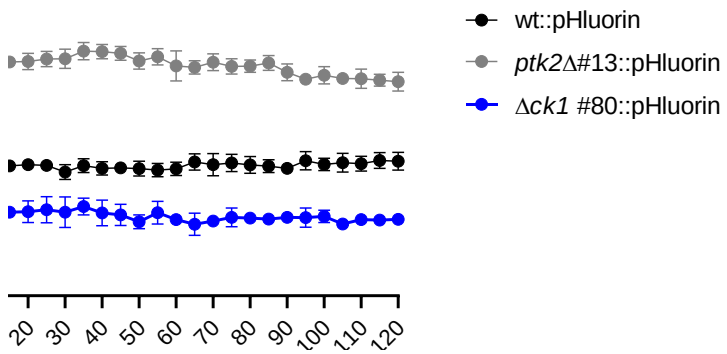


**Figure 40. The Pma1 regulators, Ck1 and Ptk2, affect $pH_c$ homeostasis.** Fifteen-hour germinated microconidia in YPD medium buffered at pH 7.4 with 20 mM HEPES of the *F. oxysporum* wild type (wt), *ck1*Δ::pHluorin #80 and *ptk2*Δ ::pHluorin #13 in strains expressing pHluorin were resuspended in KSU buffered at pH 6,0 and transferred to microwells and pre-incubated one hour at 28°C. The $pH_c$ was monitored spectrophluorometrically every 5 minutes for 2 hours. For $pH_c$ determination, the ratio between the emission intensities (collected at 510 nm) after excitation at 395 nm and 475 nm was calculated. Data show the mean ± s.d of three replicate microwells from one representative experiment. Experiments were performed at least twice times with similar results.

## 10. Ck1 is not required for regulation of vacuolar pH

Although *ck1*Δ knockout mutants show increased Pma1 activity (see Figure 28B), the $pH_c$ in these mutants was not more alkaline, as would be expected. One possible explanation is that the increased activity of Pma1 could negatively affect vacuolar ATPase (V-ATPase) activity, which could be responsible for an acidic cytosol. It has been reported that in fungal cells, the V-ATPase, a multiprotein complex that mediates acidification of the vacuole, the endosomes, or the Golgi, is also an important regulator of $pH_c$ homeostasis (Kane, 2016). Previous work in our group confirmed that Concanamycin A, a specific inhibitor of the vacuolar $H^+$-ATPase, (Huss *et al.*, 2002), induces an increase of $pH_v$ by 0,3 units (Fernandez, 2017). Here we found that addition of Concanamycin A induced a sustained drop of $pH_c$ of 0,77 units when compared with DMSO [Figure 41].

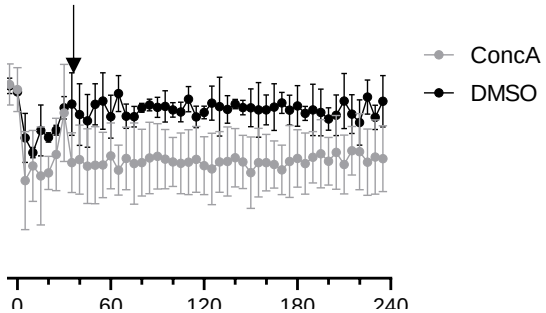


**Figure 41. Vacuolar ATPase contribute to pHc homeostasis in *F. oxysporum.*** Fifteen-hour germinated microconidia of *F. oxysporum* wild type strain were washed and resuspended in KSU buffered at pH 6,0 and incubated for one hour at 28ºC. At time 0, 25 µM of the specific V-ATPase inhibitor Concanamycin A or DMSO (solvent control) were added to the KSU buffer. The $pH_c$ was monitored every 5 minutes for 4 hours. Data show the mean ± s.d of three replicate microwells from one representative experiment. Experiments were performed twice with similar results.

For measurement of vacuolar pH ($pH_v$), fungal cells were stained with the ratiometric vacuolar dye BCECF-AM as previously described (Fernandes, 2017). To obtain a $pH_v$ calibration curve, cells were permeabilized with nigericin in the presence of buffers adjusted to different pH values, as described for $pH_c$ determination. Fluorescence was measured and ratios of emission intensities were calculated after excitation at 490 nm and 440 nm.

The steady state $pH_v$ was monitored for 90 minutes in the wild type, *ck1*Δ #10 mutant and *ck1*Δ+*ck1*#5 complemented strains. No significant differences of $pH_v$ were observed between these strains [**Figure** 42].

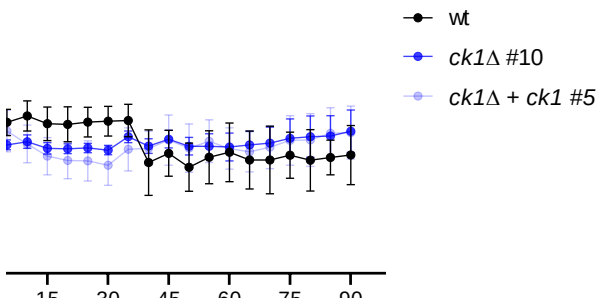


**Figure 42. Loss of Ck1 does not affect vacuolar pH in *F. oxysporum.*** Fifteen-hours germinated microconidia of *F. oxysporum* were washed and suspended in KSU buffer at pH 6,0, before being stained with 5 µM BCECF-AM for 15 minutes at 28ºC in the dark. Cells were then washed twice with KSU at pH 6,0, transferred to a microtiter wells plate and incubated for 60 min at 28 ºC at 170 rpm. Fluorescence intensities were recorded after excitation at 490 nm and 440 nm in a spectrofluorometer. For determination of $pH_v$ the ratio between the emission intensities (collected at 535 nm) was calculated and normalized to the standard curve. $pH_v$ was monitored every 5 minutes for 90 min. Data show the means ±s.d. of three replicate microwells from one representative experiment. Experiments were performed twice with similar results.

## 11. Ck1contributes to activation of the invasive growth MAPK Fmk1

Our group previously demonstrated that ambient pH governs infectious growth in the plant pathogen *F. oxysporum* by reprogramming the phosphorylation level of the IG MAPK Fmk1 (Masachis *et al.*, 2016). More recently, we showed that cytosolic acidification causes Fmk1 dephosphorylation with a concomitant increase in phosphorylation levels of the CWI MAPK Mpk1 (Fernandes *et al.*, 2022a). To understand the role of Ck1 in MAPK signaling, we followed the phosphorylation levels of Fmk1 and Mpk1 in the *ck1*Δ mutants. Both the *ck1*Δ mutant and the complemented strain exhibited lower phosphorylation levels of Fmk1 at basal conditions (pH 7) compared to the wild type strain, while phosphorylation of Mpk1 was induced similarly in all strains in response to acidification [Figure 43].

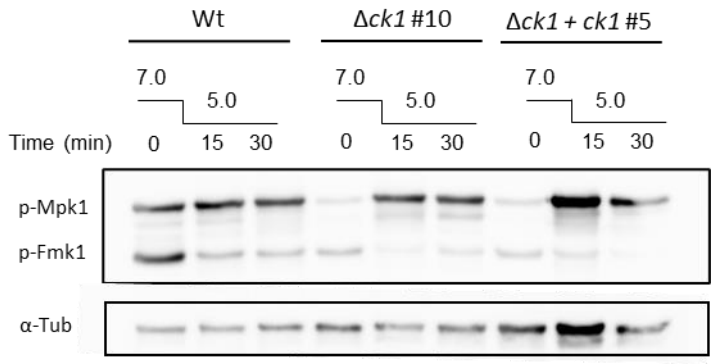


**Figure 43. Ck1 is required for activation of Mpk1.** Fifteen-hour germinated microconidia in PDB medium of the wild type (wt), *ck1*Δ and complemented strains were washed and resuspended in KSU buffered at pH 7,0 and pre-incubated for one hour at 28ºC. At time 0, diluted HCl was added to change the pH of the buffer from 7,0 to 5,0. Protein extracts collected before (time 0) and 15 or 30 minutes after acidification were subjected to immunoblot analysis with anti-phospho-p44/42 MAPK antibody to specifically detect phosphorylated p-Mpk1 and p-Fmk1, respectively. Anti-α-tubulin (α-tub) was used as a loading control.

Next, in regulation of Pma1 and $pH_c$, we monitored the phosphorylation level of the Fmk1 and Mpk1 in the wild type, *ck1*Δ mutant and complemented strains, before and after addition of diethylstilbestrol (DES), a specific inhibitor of the $H^+$-ATPase Pma1, which causes rapid acidification of $pH_c$ (Fernandes *et al.*, 2022a). In cells grown at pH 6,0, the basal level of phosphorylation of Fmk1 and Mpk1 was markedly reduced in the *ck1*Δ mutant compared to the wild type and the complemented strain [Figure 44, time 0']. Furthermore, as previously reported (Fernandes *et al.*, 2022a), addition of DES caused a rapid increase of Mpk1 phosphorylation and a decrease of Fmk1 phosphorylation levels in the wild type strain, whereas no such response was detected in the *ck1*Δ knockout mutant and the complemented strain [Figure 44, times 5' and 10'].

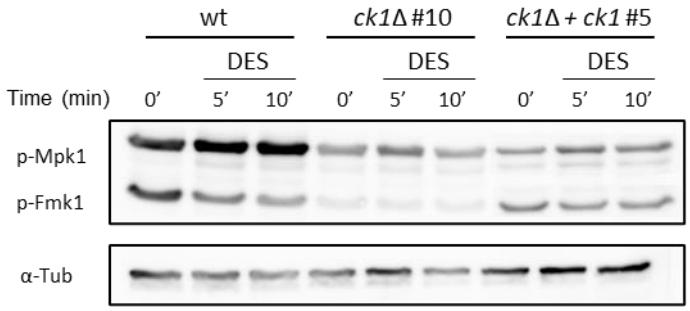


**Figure 44. Ck1 contributes to the rapid phosphorylation response after $pH_c$ acidification by DES.** Fifteen-hours germinated microconidia in PDB medium of the wild type (wt), *ck1*Δ mutant and complemented strains were washed and resuspended in KSU buffered at pH 6,0 and pre-incubated for one hour at 28ºC. At time 0, 0.5 mM DES was added to the KSU buffer. Protein extracts collected before (time 0) and 5 or 10 minutes after DES were subjected to immunoblot analysis with anti-phospho-p44/42 MAPK antibody to specifically detect phosphorylated p-Mpk1 and p-Fmk1, respectively. Anti-α-tubulin (α-tub) was used as a loading control.

We next asked whether the growth at different pH could lead to changes on phosphorylation levels of the MAPK. Therefore, we decided to test the effect of growth at pH 5 and 7 in a buffered medium. Our results showed that the phosphorylation levels of the MAPK Fmk1 remained lower than wild type independently of the pH of the medium. On the other hand, Mpk1 showed a similar phosphorylation pattern in *ck1*Δ mutant when compared with the wild type strain at pH 5. However, we detected an increase on Mpk1 phosphorylation level in *ck1*Δ mutant when compared with the wild type strain or complemented strain at pH 7 [Figure 45].

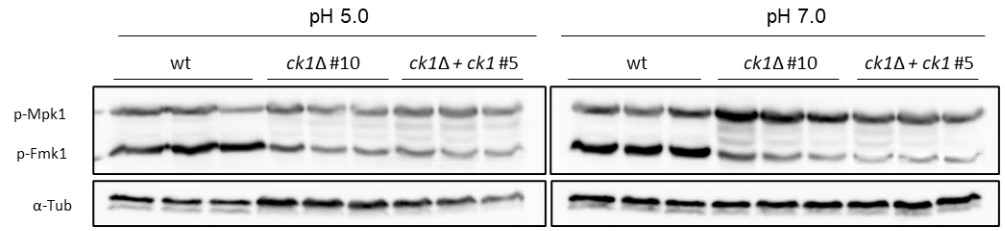


**Figure 45. Ck1 contributes to Fmk1 phosphorylation levels independent on the ambient pH.** Fifteen-hours germinated microconidia of the wild type (wt), *ck1*Δ mutant and complemented strain at 28°C in PDB buffered at pH 5,0 or 7,0 with 100 mM MES. Total protein extracts were collected and subjected to immunoblot analysis with anti-phospho-p44/42 MAPK antibody to specifically detect phosphorylated p-Mpk1 and p-Fmk1, respectively. Anti-α-tubulin (α-tub) was used as a loading control.

## 12. Ck1 is essential for invasive hyphal growth and pathogenicity in *Fusarium oxysporum*

To evaluate the role of Ck1 in invasive growth, a cellophane penetration assay was performed on MM plates that were either unbuffered or buffered at pH 5,0 or 7,0 with 100 mM MES, to analyze the capacity to penetrate through a cellulose layer (Prados Rosales & Di Pietro, 2008). As previously reported, the wild type and the complemented strain were able to penetrate the cellophane on unbuffered MM plates as well as on plates buffered at pH 7, but not on plates buffered at pH5 [Figure 46A]. However, the *ck1*Δ mutants were unable to penetrate the cellophane membrane at any pH suggesting that Ck1 promotes invasive hyphal growth of *F. oxysporum.*

A pathogenicity assay was conducted by dip-inoculating the roots of tomato plants with fresh microconidia. Plants inoculated with the *ck1*Δ mutants showed no disease symptoms 40 days after inoculation, whereas the mortality rate in plants inoculated with the wild type or the complemented strain was close to 100% [Figure 46B]. These results evidence that Ck1 is essential for pathogenicity of *F. oxysporum* on tomato plants.

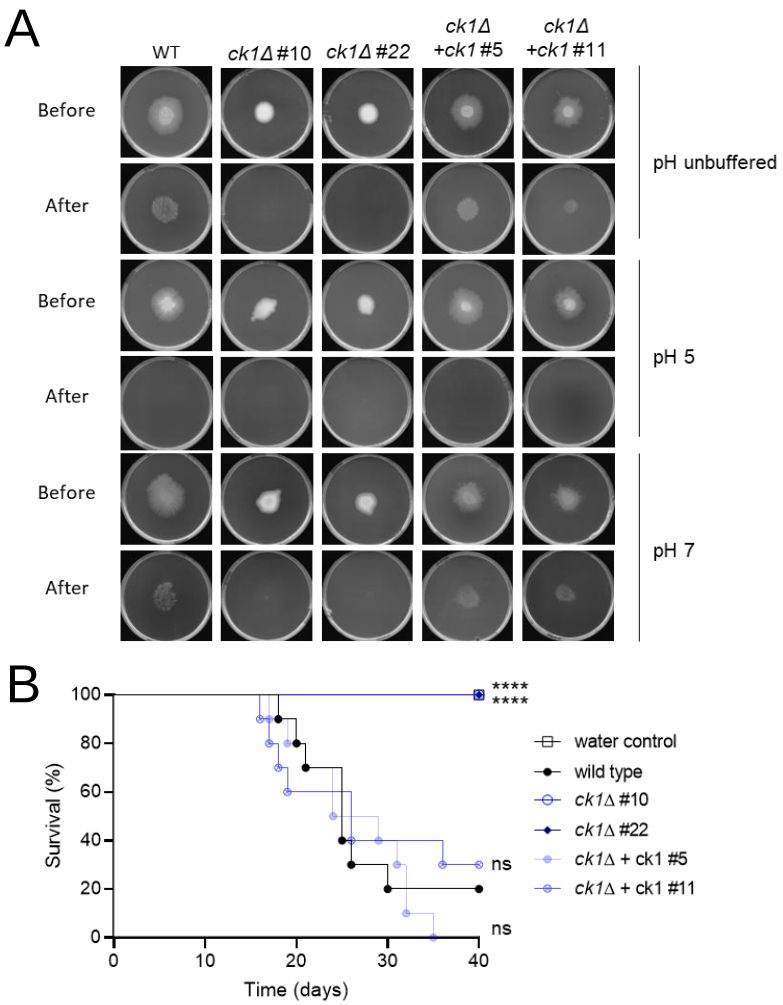


**Figure 46. Ck1 regulates infection mechanisms in *F. oxysporum*.** (**A**) Invasive growth of the *F. oxysporum* wild type (wt), *ck1*Δ and complement mutant strains was determined by growing fungal colonies on top of cellophane membranes placed on MM plates either unbuffered pH and buffered to pH 7,0 or 5,0 with 100 mM MES. After 3 days at 28ºC plates were imaged (Before), the cellophane with the fungal colony was removed and plates were incubated for an additional day to visualize the presence of mycelium, indicating penetration through the cellophane (After). Images shown are representative of three independent experiments, each with three plates per treatment. (**B**) Kaplan–Meier plots showing survival of tomato plants (cv. Monica) inoculated by dipping roots into a suspension of $5x10^6$ microconidia/mL of the indicated fungal strains. Control water-solution without fungal were also included. Control water-solution without fungal were also included. Percentage survival of tomato plants was plotted for 40 days. Data shown are from one representative experiment. (****) $p$ <0.0001, ns (non-significant) *versus* wt according to log-rank test. Data shown are from one representative experiment. Experiments were performed twice with similar results.

## 13. Ck1 controls hyphal chemotropism towards acid pH

A critical step during the infection process of *F. oxysporum* is the capacity to chemically locate plant roots in the soil. To examine the possible role of ambient pH in chemotropic growth, germlings were exposed to competing gradients of alkaline and acidic pH. The wild type and the complemented strain re-directed growth towards acidic pH, whereas the knockout mutant lacking *ck1* presented an inverted pH tropism, growing preferentially towards alkaline pH [Figure 47].

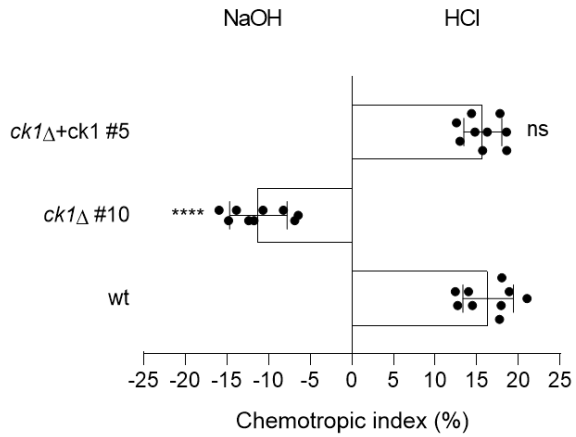


**Figure 47. Ck1 is involved in chemotropic pH sensing**. Directed growth of germ tubes of the *F. oxysporum* wild type (wt), *ck1*Δ #10 and complemented mutant strains was determined after eight hours exposure to opposing gradients of 25 mM HCl and NaOH. (****) $p$ <0.0001, ns (non-significant) *versus* wt according to Welch's t-test. Data show the mean ±s.d from at least three independent experiments with three replicates (n=500 germ tubes per experiment) each.

## Subchapter II. Role of the small Pma1-associated peptide Pmp1 in *Fusarium oxysporum*

## Results

### 1. *In silico* identification of the *pmp1* orthologue in *Fusarium oxysporum*

The Pmp1 is a 38-residue PM protein of the *S. cerevisiae* that regulates the activity of the H+-ATPase Pma1 (Navarre *et al.*, 1994). A BLASTp search of the *F. oxysporum* genome sequence with the amino acid sequence of *S. cerevisiae* Pmp1 (YCR024C-A) as a bait identified a single Pmp1 orthologue in *F. oxysporum* (FOXG_03480). This gene, located on chromosome 7, encodes a predicted protein of 64 amino acids that exhibits 45% identity with Pmp1 of *S. cerevisiae* and a similar degree of identity with filamentous fungi such as *M. oryzae* (MGG_15899; 47%), *N. crassa* (NCU11337; 49%), *C. neoformans* (CND05550; 39%) and *A. nidulans* (AN3944; 44%).

### 2. Targeted deletion of *pmp1* in *Fusarium oxysporum*

To investigate the role of Pmp1 in *F. oxysporum* we generated a *pmp1*Δ allele by replacing the complete ORF with the *Hyg*$^{R}$ resistance cassette using the "split-marker" technique [Figure 48A]. The two constructs obtained, each containing a flanking region of the gene and 75% of the *Hyg*$^{R}$ cassette, were used to transform protoplasts of the *F. oxysporum* wild type strain. Transformants carrying a homologous insertion at the *pmp1* locus were initially identified by PCR analyses using two pairs of primers that hybridize outside of the fragments used for transformation and inside of the resistance cassette [Figure 48B]. Selected candidate knockout strains were further analyzed by Southern blot to confirm the insertion of a single copy of the construct into the genome. The genomic DNA of the wild type strain and putative knockouts in *pmp1* locus were treated with the restriction enzymes *Hind* III. Hybridization with a probe located in the promotor region of the *pmp1* gene showed replacement of the 3,0 Kb hybridizing band of the wild type *pmp1* allele by a 5,5 Kb band in the *pmp1*Δ knockout mutant #$14_1$, indicating that a single homologous replacement event had occurred in this transformant [Figure 48C].

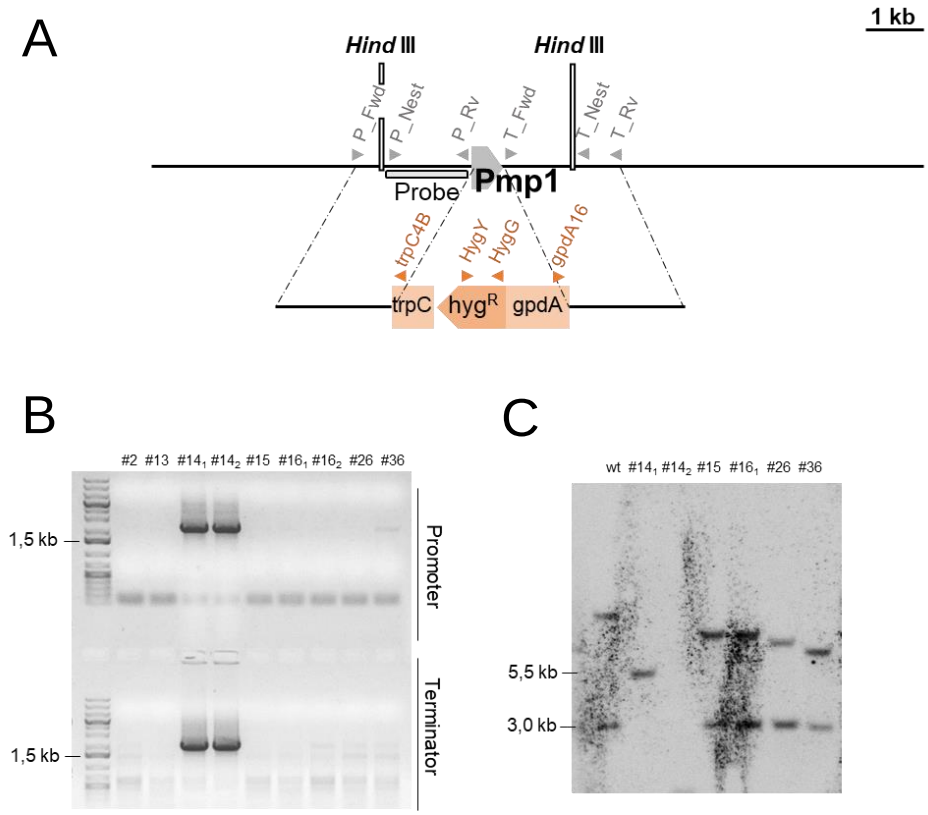


**Figure 48. Targeted deletion of the *F. oxysporum pmp1* gene.** (**A**) Physical maps of the *pmp1* locus and strategy for the replacement of the coding region with the split-marker method using the *Hyg*$^{R}$ cassete as selective marker (*pmp1*Δ allele). Positions of *Hind* III restriction sites are shown. Gray (*pmp1*) and orange (*Hyg*$^{R}$) arrowheads indicate the relative positions of the primers used for generation of the gene disruption constructs and PCR analysis of the transformants; the probe used for Southern blot analysis is indicated as gray bar. Scale bar, 1kb. (**B**) PCR analysis to confirm homologous recombination of the construct into the genome of the transformants using the primers pairs: P_Fwd/trpC4B (promotor region) and T_Rv/gpda16 (terminator region). (**C**) Southern blot hybridization analysis of the wild type strain (wt) and and six independent *pmp1*Δ transformants. Genomic DNA was treated with *Hind* III separated in an agarose gel, transferred to a nylon membrane and with hybridized with the probe indicated in (A).

## 3. Pmp1 has no role in regulation of Pma1 activity in *Fusarium oxysporum*

To explore the effect of Pmp1 on Pma1 activity, membranes were isolated from fifteen-hours germinated microconidia in PDB medium from the wild type and *pmp1*Δ mutant strains. We observed that the activity of Pma1 in the *pmp1*Δ mutant was slightly higher (17%) than in the wild type, although this difference was not statistically significant [Figure 49].

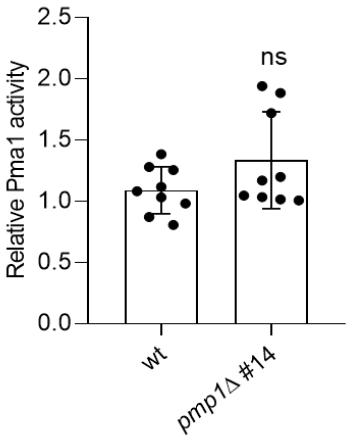


**Figure 49. Activity of Pma1 is not affected in the *pmp1*Δ knockout mutant.** Analysis of Pma1 ATPase activity was assayed in total membranes isolated from fifteen-hours germinated microconidia in PDB medium of the wild type (wt) and *pmp1*Δ #14 mutant strains. Activity was normalized to that of the wt strain. ns (non-significant) *versus* wt according to Welch's t-test. Data shown are the mean ± s.d. from three independent biological experiments with three technical replicates each.

## 4. Pmp1 regulates growth in *Fusarium oxysporum*

To evaluate the role of Pmp1 in vegetative hyphal growth, the wild type and *pmp1*Δ mutant were grown on potato-dextrose-agar (PDA) and minimal medium (MM) plates for 9 days and colony growth was monitored 3, 6 and 9 days after inoculation [Figure 50].

Interestingly, we observed a faster growth in *pmp1*Δ mutant when compared with the wild type strain, being more pronounced on PDA. In average we observed a 20% increase in colony area of the *pmp1*Δ mutant compared to the wild type strain at 9 days after inoculation [Figure 50]. Moreover, the *pmp1*Δ mutant exhibited a more uniform colony morphology [Figure 50].

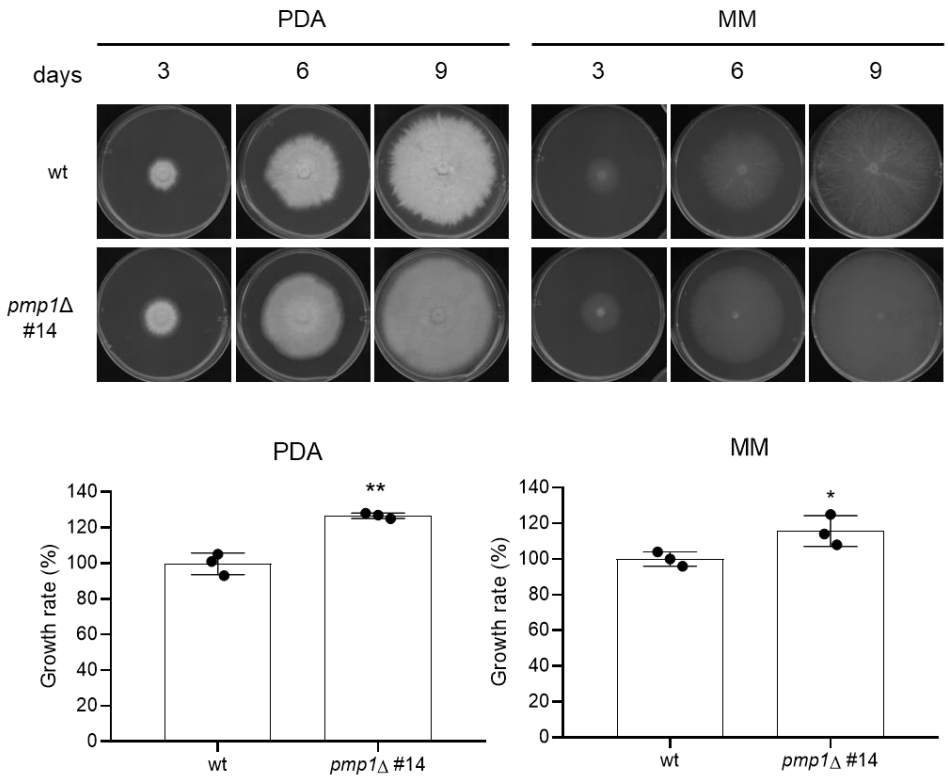


**Figure 50. Pmp1 regulates colony growth.** (**A**) Aliquots of $5x10^4$ fresh microconidia of the wild type (wt), and *pmp1*Δ #14 mutant were spot-inoculated on potato dextrose agar (PDA) and minimal medium (MM) plates and incubated at 28°C for 9 days. Colonies were scanned after 3, 6 and 9 days. (**B**) Colony area of the indicated strains on PDA and MM after 9 days was measured and normalized to that of the wild-type strain (100%). (*) $p$ <0.05 and (**) $p$ <0.01 *versus* wt, according to Welch's t-test. Data show representative means ± s.d. from three independent plates per strain and medium.

## 5. Pmp1 controls colony growth under extreme pH and cell wall stress

To further understand the role of Pmp1 in hyphal growth a growth assay was performed on YPGA plates buffered at pH 4, 6, and 8 and fungal growth was monitored for 3 days. In all pH conditions the *pmp1*Δ #14 mutant had a larger colony size with more extensive aerial hyphae compared to the wild type strain. The most dramatic differences were observed at acidic and alkaline pH conditions. Besides the faster growth, the *pmp1*Δ #14 mutant showed a different colony phenotype with more compact colonies almost without aerial hyphae at pH 8,0 [Figure 51]. Overall, these

results appear to indicate that Pmp1 can also play a role on adaptation to different pH environments.

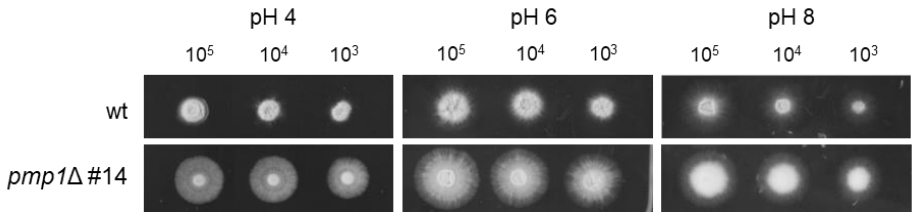


**Figure 51. Pmp1 is relevant for cell growth at extreme pH values in *F. oxysporum.*** Aliquots of $10^5$, $10^4$ and $10^3$ fresh microconidia of the indicated strains were spot-inoculated on YPDA plates adjusted at pH 4, 6 and 8. Control plates without adjustment were also included. The plates were incubated at 28 °C for 3 days and scanned. Plates shown are representative of three independent replicates for each strain and growth condition.

We next tested the role of Pmp1 in cell wall and hyperosmotic stress response by wild type and *pmp1*Δ mutant strains were grown on YPGA containing CR or CFW (cell wall stress-inducing compounds); and NaCl or sorbitol (osmotic stress inducers). In this phenotypical growth assay, we observed that the *pmp1*Δ mutant strain showed a reduced sensitivity to CR compared to the wild type strain. Nevertheless, in the presence of CFW, another known cell wall stressor, the mutant showed similar sensitivity to the wild type strain [Figure 52]. No differences were observed in sensitivity to osmotic stress inducer compound NaCl or sorbitol [Figure 52].

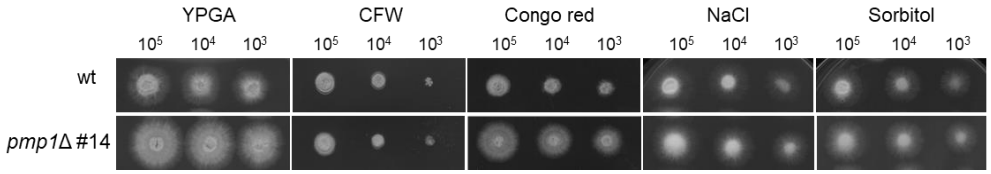


**Figure 52. Pmp1 is relevant for cell wall stress response in *F. oxysporum.*** Aliquots of $10^5$, $10^4$ and $10^3$ fresh microconidia of the indicated strains were spot-inoculated on YPDA plates complemented with CFW (50 µg/mL), CR (100 µg/mL), NaCl (1,2 M) and Sorbitol (1,25 M). Control plates without any compound were also included. The plates were incubated at 28 °C for 3 days and scanned. Plates shown are representative of three independent replicates for each strain and growth condition.

## 6. Pmp1 is not important for invasive growth and plant infection in *Fusarium oxysporum*

To evaluate the role of Pmp1 in invasive growth, a cellophane penetration assay was performed on MM plates as described above. No difference between the wild type and *pmp1*Δ mutant strains was detected in any of the conditions tested [Figure 53A].

Furthermore, we evaluated the role of Pmp1 in infecting tomato plants through a pathogenicity assay. Our results revealed that Pmp1 is not relevant for the infection process [Figure 53B].

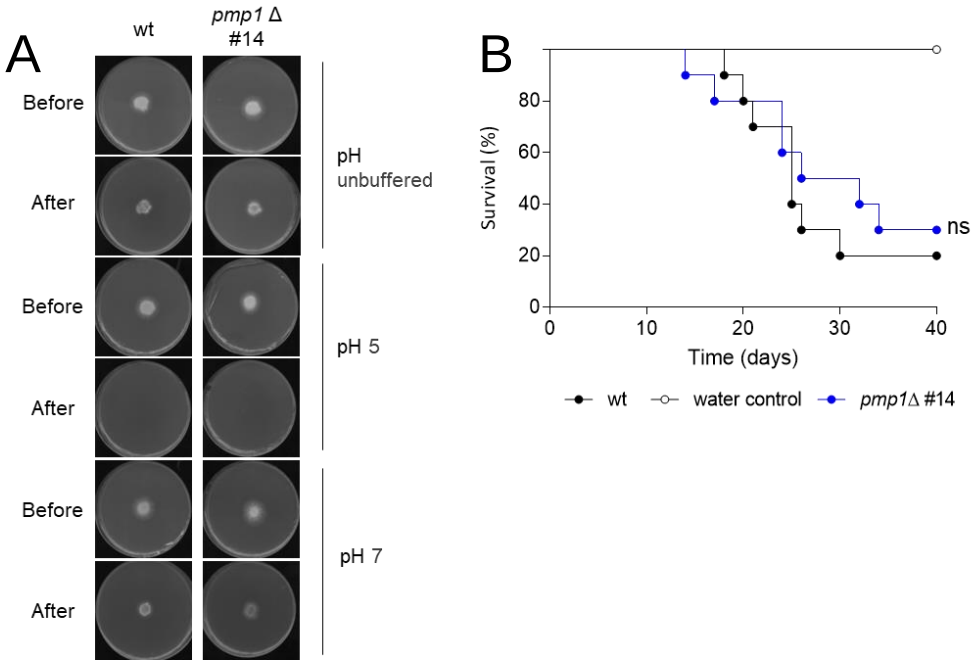


**Figure 53. Pmp1 is not relevant for important infection-related mechanisms in *F. oxysporum.*** (**A**) Invasive growth of the F. oxysporum wild type (wt), *pmp1*Δ #14 mutant strains was determined by growing fungal colonies on top of cellophane membranes placed on MM plates with either unbuffered or buffered at pH 7,0 or 5,0 with 100 mM MES. After 3 days at 28 $^{o}$C, plates were imaged (before), the cellophane with the fungal colony was removed and plates were incubated for an additional day to visualize the presence of mycelium, indicating penetration through the cellophane (after). Images shown are representative of two independent experiments, each with three plates per treatment (**B**) Kaplan–Meier plots showing survival of tomato plants (cv. Monica) inoculated by dipping roots into a suspension of 5x10$^{6}$ microconidia/mL of the indicated fungal strains. Control water-solution without fungal were also included. Percentage survival of tomato plants was plotted for 40 days. Data shown are from one representative experiment. ns (non-significant) *versus* wt according to log-rank test.

# Chapter IV

# Chapter IV. Role of Pma1 on *Fusarium oxysporum* pathogenicity

## Overview

Pma1 is a PM $H^+$-ATPase whose activity at the cell surface is essential for cell viability (Serrano *et al.*, 1986a). Pma1 is in charge of extruding $H^+$ from the cytosol, coupled with hydrolysis of ATP (Ambesi *et al.*, 2000; Lee *et al.*, 2017; Rane *et al.*, 2019). According to estimates, approximately 50% of the ATP in a fungal cell is consumed by Pma1 (Burgstaller, 1997). Pma1 plays a key role in fungal development and pathogenicity by maintaining $pH_c$ homeostasis and regulating ion and nutrient uptake (Zhgun *et al.*, 2020). In arbuscular mycorrhizal (AM) fungi, Pma1 increases the proton pumping activity and energizes nutrient uptake during fungal invasion of the plant (Requena *et al.*, 2003; Wang *et al.*, 2014). Due to its potential as an antifungal target, Pma1 has been the subject of extensive mutagenesis with the aim of analyzing structure-function relationship (Mason *et al.*, 2014; Morsomme *et al.*, 2000; Rane *et al.*, 2019). Mason *et al.* (2014) reported that truncation of different regions of Pma1 results in a variety of phenotypes. In *S. cerevisiae*, a temperature-sensitive *pma1* allele, *pma1-10*, was shown to have impaired stability at the cell surface (Gong & Chang, 2001). At the restrictive temperature (37°C), newly synthesized Pma1-10 mutant protein undergoes rapid internalization from the cell surface followed by delivery to the vacuole for degradation, thus impairing cell growth (Gong & Chang, 2001). The use of a temperature-sensitive Pma1 strain therefore represents a useful tool to investigate the role of this essential ATPase in fungal development and cell signaling, but this approach has not been explored so far in *F. oxysporum*. On the other hand, overexpression of *pma1* has been performed to understand its role in different processes and mechanisms (Lee *et al.*, 2017; Li *et al.*, 2022). In *S. cerevisiae, pma1* overexpression led to enhanced tolerance to weak acid, oxidative stress and ethanol (Lee *et al.*, 2017), as well as activation of the Hog1 MAPK pathway (Eraso *et al.*, 2011).

Growing evidence suggests that Pma1 plays a central role in fundamental developmental processes in fungal cells. However, few studies so far have explored in detail the role of this ATPase in fungal plant pathogens, due to its essential role for cell survival. In this work we tested different genetic approaches to unravel the role of Pma1 on *F. oxysporum* pathogenicity.

## Results

### 1. Generation of a *pma1* overexpressing strain

In order to overexpress the *pma1* gene, we inserted an additional copy into the genome of the wild type strain, either under the control of its native promoter or of the strong translation elongation factor 1 (*tef1*) promotor. In the first approach, a DNA fragment encompassing the open reading frame (ORF) of *pma1* (FOXG_11289) together with 1500 bp upstream (promoter) and downstream (terminator) sequences was amplified from genomic DNA. In the second approach the *tef1* promoter was amplified from *F. oxysporum* (FOXG_03515) and fused with a fragment encompassing the ORF of the *pma1* gene plus 1500 bp of the 3'-flanking region (terminator) [Figure 54A]. *F. oxysporum* protoplasts were co-transformed with the DNA fragments and with the hygromycin resistance cassette [Figure 54A]. *Hyg*$^{R}$ transformants were selected to evaluate the transcript levels of the *pma1* gene through RT-qPCR analysis. All the transformants analyzed showed higher transcript levels of the *pma1* gene than the wild type strain [Figure 54B]. Therefore, we selected the transformants with the highest expression level of *pma1*: #2, #17 and #24 (10-fold, 7-fold and 5-fold increase, respectively, relative to the wild type strain) carrying *pma1*-OE (*pma1* under control of its native promoter) and #5, #8 and #14 (13-fold, 19-fold and 11-fold increase, respectively, relative to the wild type strain) carrying the Tef1-pma1 construct [Figure 54B].

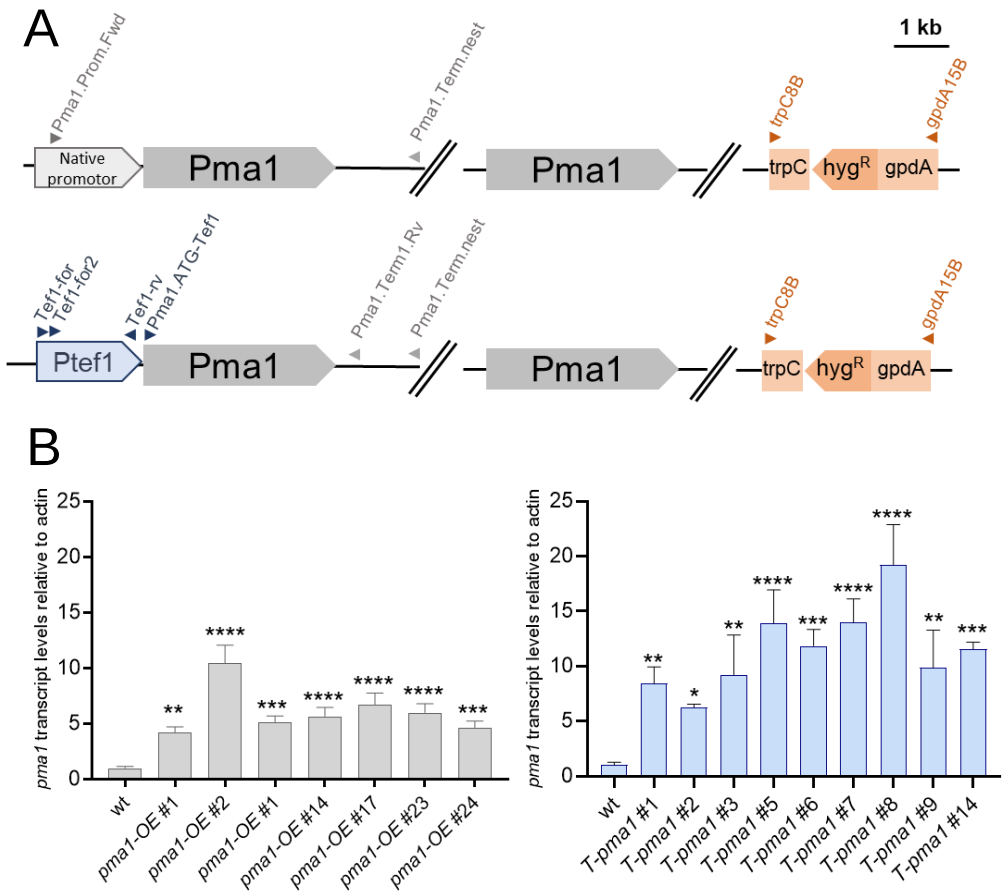


**Figure 54. Two approaches to overexpress *pma1* in *F. oxysporum*.** (**A**) Schematic representation of the strategies followed to insert an additional copy of *pma1* under the control of either its native *pma1* promotor or the strong *tef1* promotor (*Ptef1*). Protoplasts of the wild type strain were co-transformed with either of the constructs and the *Hyg*$^R$ cassette gene as a selective marker. Gray (*pma1*), blue (*Ptef1* promotor) and orange (*Hyg*$^R$) arrowheads indicate the relative positions of the primers used for generation of the gene overexpression constructs and RT-qPCR analysis of the transformants. Scale bar, 1kb. (**B**) Fifteen-hours germinated microconidia of the wild type and *Hyg*$^R$ transformants were collected and frozen for RNA isolation. RT-qPCR analysis was performed with specific primers Pma1.1/Pma1.2 and transcript levels were normalized to those of the actin gene. Data shown represent the mean and standard deviations of two biological replicates, each including three technical replicates. (*) $p$ <0.05, (**) $p$ <0.01, (***) $p$ <0.001, (****) $p$ <0.0001 *versus* wt, according to Welch's t-test. Data show representative means ± s.d. from three technical replicates.

## 2. Overexpression of *pma1* confers slightly increased acid tolerance

We tested the tolerance of the *pma1*-overexpressing transformants to different acids and to oxidative stress caused by hydrogen peroxide ($H_2O_2$) or menadione. The Tef1-*pma1* #5, Tef1-*pma1* #8, *pma1-OE* #2 and *pma1-OE* #17 transformants were

slightly more resistant to propionic acid and aminobenzoic acid than the wild type strain, whereas resistance to acetic acid was not changed in any of the tested mutants. On the other hand, these transformants did not show an increase in resistance to $H_2O_2$ or menadione [Figure 55].

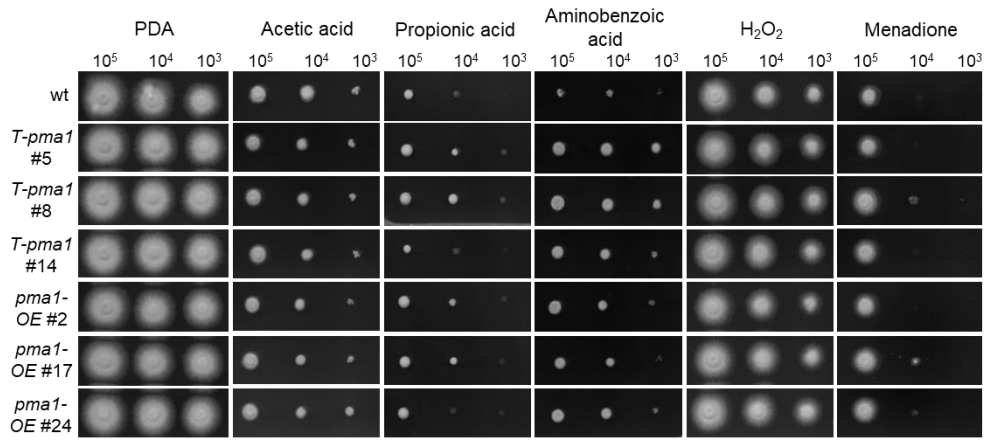


**Figure 55. Overexpression of *pma1* triggers increased acid stress tolerance.** Aliquots of $10^5$, $10^4$ and $10^3$ fresh microconidia of the indicated strains were spot-inoculated on PDA plates supplemented with acetic acid (15 mM), propionic acid (10 mM), aminobenzoic acid (10 mM), $H_2O_2$ (2 mM) or menadione (116 µM). Control plates without any compound were also included. The plates were incubated at 28 °C for 3 days and scanned. Plates shown are representative of three independent replicates for each strain and growth condition.

## 3. Overexpression of *pma1* has no effect on MAPK regulation in response to ambient pH shifts

A charge in ambient or cytosolic pH causes reprogramming of the phosphorylation levels of the MAPKs Fmk1, Mpk1 and Hog1 (Fernandes *et al.*, 2022a; Masachis *et al.*, 2016). Because Pma1 is a key player in regulation of $pH_c$ homeostasis, we used western blot analysis to monitor the phosphorylation pattern of Fmk1 and Mpk1, in response to extracellular acidification (pH change from 6,0 to 3,0) in the wild type and the *pma1* overexpressing strains. As previously reported (Fernandes *et al.*, 2022a), external acidification caused a rapid increase of Mpk1 and a decrease of Fmk1 phosphorylation levels, both in the wild type and in the *pma1* overexpressing strains [Figure 56]. This suggests that the increased expression of *pma1* does not affect the regulation of MAPKs in response to pH shifts.

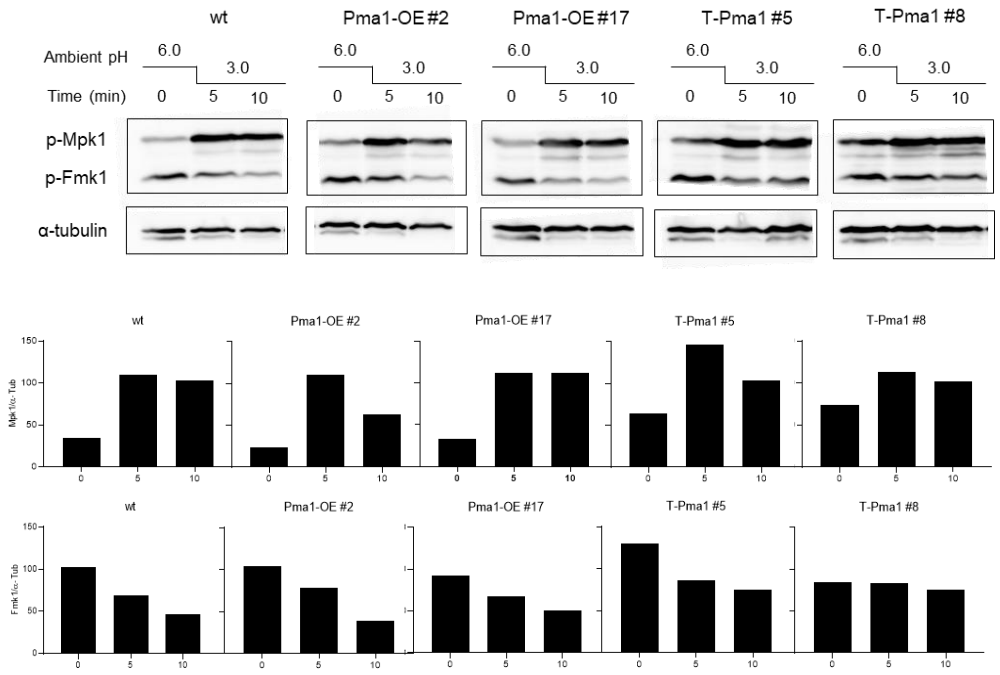


**Figure 56. Overexpression of *pma1* does not affect MAPK regulation in response to extracellular pH shifts.** Fifteen-hour germinated microconidia in PDB medium of the wild type (wt) and indicated *pma1* overexpressing strains were washed and resuspended in KSU buffer at pH 6,0 and pre-incubated for one hour at 28ºC. At time 0, diluted HCl was added to shift the pH from 6,0 to 3,0. Protein extracts collected before (time 0) or 5 or 10 minutes after acidification were subjected to immunoblot analysis with anti-phospho-p44/42 MAPK antibody to specifically detect phosphorylated p-Mpk1 and p-Fmk1, respectively. Anti-α-tubulin (α-tub) was used as a loading control. Graphs show the ratio of p-Mpk1 or p-Fmk1 band intensity normalized to α-tubulin.

## 4. Increased expression of *pma1* has no effect on infection mechanisms of *Fusarium oxysporum*

To evaluate the effect of Pma1 overexpression on invasive growth, a cellophane penetration assay was performed on MM plates either unbuffered or buffered at pH 5,0 or 7,0 with 100 mM MES to analyze the capacity to penetrate through a cellulose layer (Prados Rosales & Di Pietro, 2008). As expected, the wild type strain was able to penetrate the cellophane both in unbuffered and pH 7,0 conditions, but not at pH 5,0 (Fernandes *et al.*, 2022a). A similar phenotype was observed in the Tef1-*pma1* #5, Tef1-*pma1* #8, *pma1-OE* #2 and *pma1-OE* #17 strains, suggesting that overexpression of *pma1* has no effect on invasive growth [Figure 57A].

A pathogenicity assay was carried out by dip-inoculating the roots of tomato plants with fresh microconidia of the wild type and the different strains, confirming that *pma1* overexpression does not interfere with pathogenicity of *F. oxysporum*, since no changes in virulence were detected in the analyzed strains [Figure 57B].

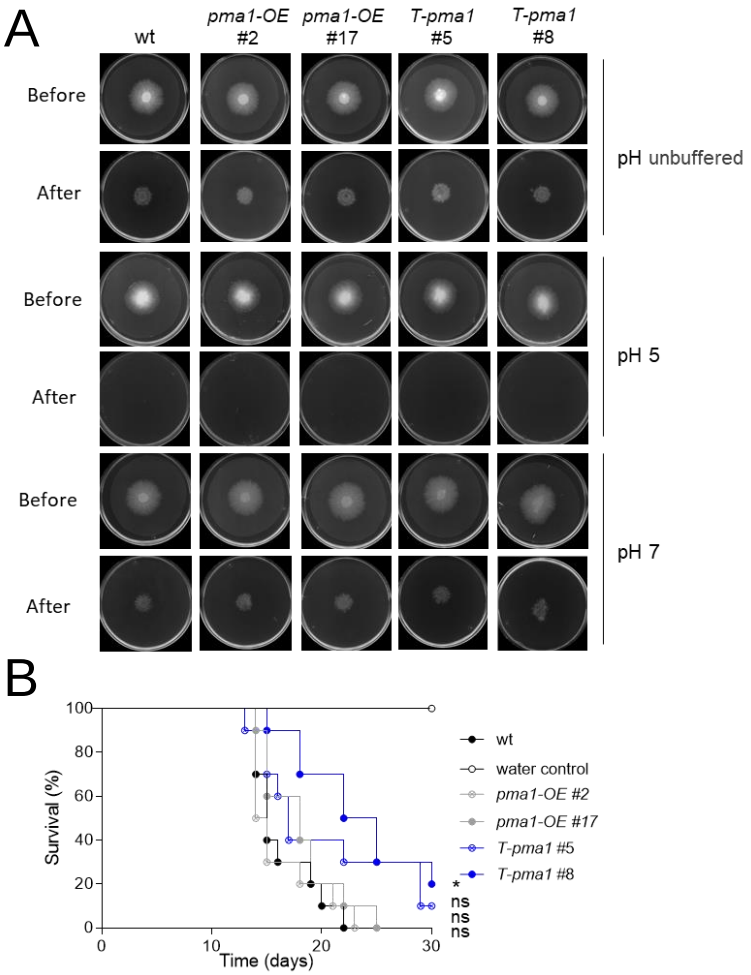


**Figure 57. Overexpression of *pma1* has no effect on infection-related processes of *F. oxysporum*.** (**A**) Invasive growth of the *F. oxysporum* wild type, *pma1-OE* and Tef1-*pma1* strains was determined by growing fungal colonies on top of cellophane membranes placed on MM plates either unbuffered or buffered to pH 7,0 or 5,0 with 100 mM MES. After 3 days at 28ºC, plates were imaged (Before), the cellophane with the fungal colony was removed and plates were incubated for an additional day to visualize the presence of mycelium, indicating penetration through the cellophane (After). Images shown are representative of three independent experiments, each with three plates per treatment. (**B**) Kaplan–Meier plots showing survival of tomato plants (cv. Monica) inoculated by dipping roots into a suspension of $5x10^6$ microconidia/mL of the indicated fungal strains. Control water-solution without fungal were also included. Percentage survival of tomato plants was plotted for 40 days. Data shown are from one representative experiment. ns (non-significant) *versus* wt according to log-rank test.

## 5. Generation of a strain carrying a temperature-sensitive *pma1$^{ts}$* allele

In yeast, a strain carrying a temperature-sensitive *pma1* allele (Pma1-10) carrying two amino acid modifications (A165G and V197I) was previously generated to elucidate the role of this essential ATPase in different cellular processes (Gong & Chang, 2001). To follow a similar approach in *F. oxysporum*, we first performed an alignment of the Pma1 proteins from *S. cerevisiae* (YGL008C) and *F. oxysporum* (FOXG_11289) which revealed a conservation of the amino acid residues mutated in Pma1-10, suggesting that an analogous approach might be viable in this filamentous fungus [Figure 58A].

To generate a *pma1* temperature-sensitive allele in *F. oxysporum*, DNA fragments from the wild type *pma1* gene were amplified with primers carrying the desired mutations (primers Pma1.3 and Pma1.4) plus 1000 bp upstream and downstream of the mutations, using primer pairs Pma1.1/Pma1.2 and Pma1.5/Pma1.6, respectively [Figure 58B]. The three amplified fragments were then fused and the resulting DNA construct was co-transformed with the hygromycin resistance cassette into *F. oxysporum* protoplasts. Hygromycin-resistant transformants were selected and grown at the standard growth temperature of *F. oxysporum* (28°C) and at a restrictive temperature (33 °C) to test temperature sensitivity. We identified one candidate transformant, *pma1$^{ts}$* #49, showing growth defects both at the restrictive and permissive temperatures while all the other transformants tested grew similar to the wild type [Figure 58C].

To confirm that the *pma1*$^{ts}$ #49 transformant carries a homologous insertion of the *pma1$^{ts}$* allele at the *pma1* locus, genomic DNA extracted from the strain was amplified using the primers Pma1_ATG/Pma1_6N, and the obtained DNA fragment was sequenced using the primers Pma1_Fwd_ts/Pma1_nested_nested [Figure 58B]. Alignment of the obtained nucleotide sequence confirmed that transformant *pma1*$^{ts}$ #49 mutant carries a single *pma1* allele with the expected mutations resulting in the amino acid changes A168G and V200I [Figure 58D].

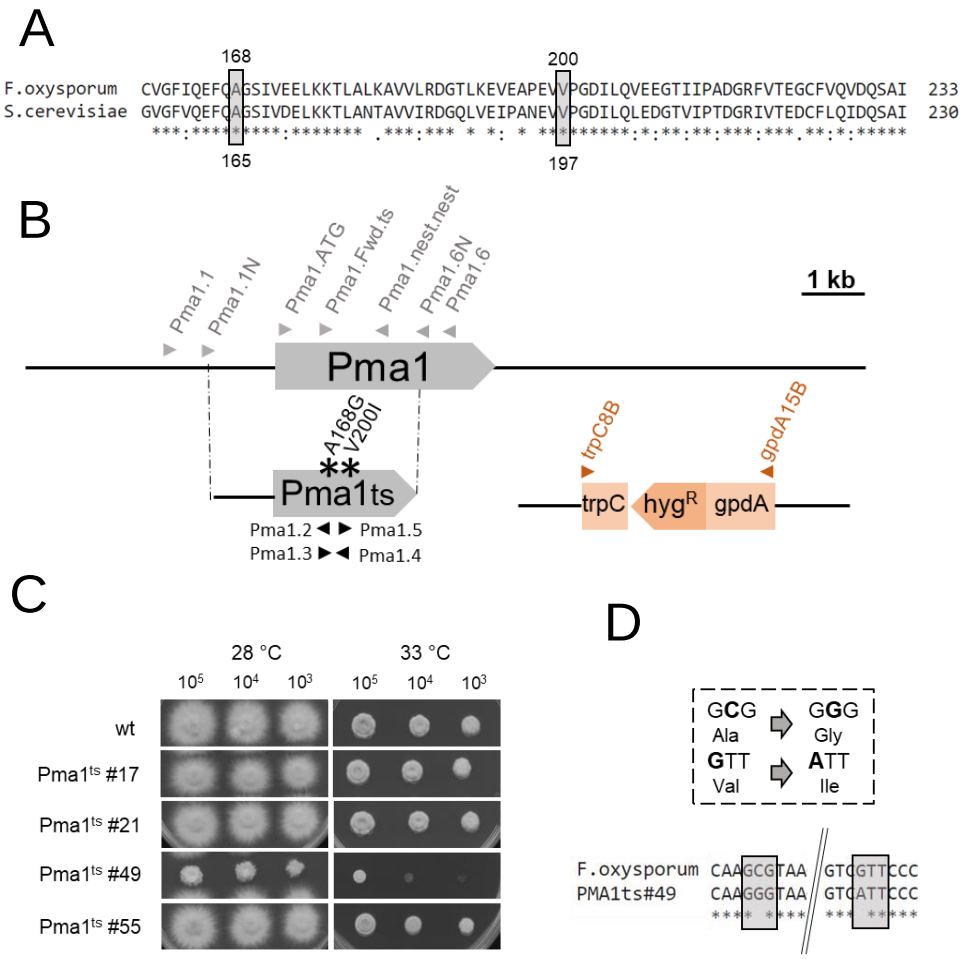


**Figure 58. Generation of a F. oxysporum strain carrying a pma1 temperature-sensitive *pma1$^{ts}$* allele.** (**A**) Alignment showing that the amino acid residues A165 and V197 (grey box) responsible for the *S. cerevisiae* temperature-sensitive *pma1$^{ts}$* allele are conserved in the *F. oxysporum* Pma1 protein Protein alignment was performed with the ClustalOmega Software. (**B**) Schematic representation of the strategy used for the replacement of the *pma1* coding region with the *pma1$^{ts}$* allele by co-transformation with the *Hyg*R cassette as selective marker. The relative position of the gray primers, black primers (carrying the mutations) and orange primers (HygR cassette) are indicated by arrowheads. Scale bar, 1kb. (**C**) Growth on PDA plates of the wild type strain and different hygromycin-resistant transformants at 28°C and 33°C. (**D**) Sequences obtained using the primers Pma1_Fwd_ts (forward) and Pma1_nested_nested (reverse) and alignment between sequences of the wild type and the *pma1$^{ts}$*#49 strains.

## 6. Effect of temperature on growth of the *pma1$^{ts}$* mutant strain

To further evaluate the temperature sensitivity of the *pma1$^{ts}$* #49 mutant strain, we analyzed colony growth on PDA plates at different temperatures ranging from 24 to 37ºC. Colony growth of the *pma1$^{ts}$* #49 mutant was progressively reduced at higher temperatures compared with that of the wild type strain, while at 24ºC only slight

differences were observed between the two strains [Figure 59]. According to these results, we defined 24°C as the permissive temperature and 34 ºC as the restrictive temperature for *pma1*$^{ts}$ #49 growth, since at 34 or 37ºC the *pma1*$^{ts}$ #49 mutant was fully unable to grow, while the wild type strain still exhibited residual growth, albeit with severe growth defects [Figure 59].

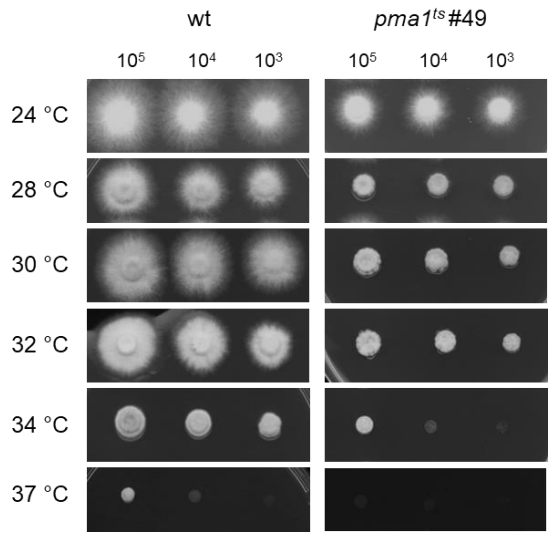


**Figure 59. Effect of temperature on colony growth of the *pma1*$^{ts}$ mutant.** Aliquots of $10^5$, $10^4$ and $10^3$ fresh microconidia of the indicated strains were spot-inoculated on PDA plates and incubated at 24°C, 28°C, 32°C, 34°C and 37°C. The plates were incubated at 28 °C for 3 days and scanned. Plates shown are representative of three independent replicates for each strain and growth condition.

To precisely determine the growth rate of the *pma1*$^{ts}$ #49 mutant at the different temperatures, we selected the temperatures 24ºC, 28ºC and 32ºC to repeat the growth assay, increasing the incubation time to 10 days [Figure 60A]. We found that the *pma1*$^{ts}$ #49 mutant presented a reduction of growth rate of approximately 67,2% at 24 ºC compared to the wild type strain. Interestingly, this reduction was increased to 82,7% at 28ºC and to 95,5% at 32ºC[Figure 60B]. However, at the latter temperature, the wild type strain presented a reduction of about 60% when compared to 28ºC.

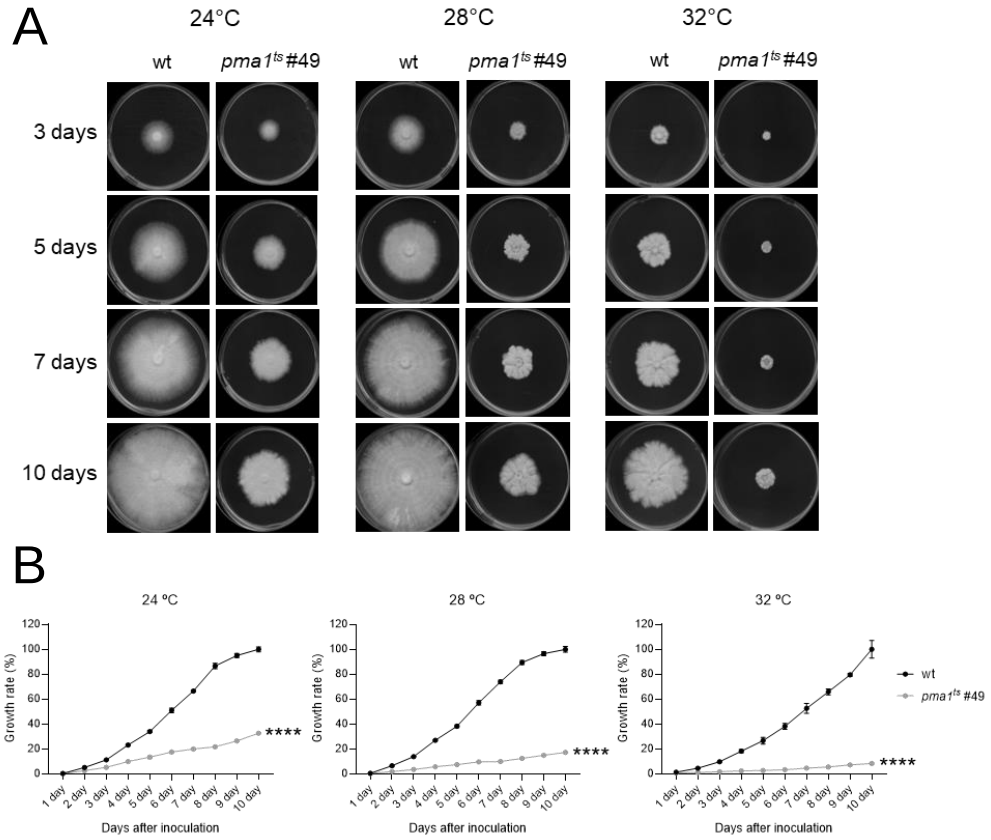


**Figure 60. The *pma1$^{ts}$* mutant is affected in its ability to grow on solid medium.** (**A**) Aliquots of 5x10$^4$ fresh microconidia of the wild type (wt), and *pma1$^{ts}$* mutant were spot-inoculated on potato dextrose agar (PDA) and incubated at 24, 28 and 32°C for 10 days. Colonies were imaged every day after inoculation. (**B**) Colony area was measured every day and normalized to that of the wild type strain (100%) at the last day of each temperature. (****) $p$ <0.0001 *versus* wt, according to Welch's t-test. Data show representative means ± s.d from three independent plates per strain and temperature analyzed.

## 7. Restrictive temperature drastically inhibits the activity of Pma1 in the *pma1$^{ts}$* mutant

According to the optimized protocol (see Materials and Methods for more detail), the evaluation of the activity of H$^+$-ATPase Pma1 requires growth of the strains in liquid medium. Therefore, we tested growth of the strains in liquid Yeast Dextrose (YD) medium at temperatures ranging from 24 to 37ºC. The growth rate of the *pma1$^{ts}$* #49 mutant at 24 ºC did not differ significantly from that of the wild type strain [Figure 61]. By contrast, growth rate of the *pma1$^{ts}$* #49 mutant at higher temperatures was significantly lower than that in the wild type and was basically halted at 37 ºC.

Therefore, we defined 24 °C as permissive growth temperature for *pma1*$^{ts}$ and 37 °C as restrictive temperature for experiments in liquid medium.

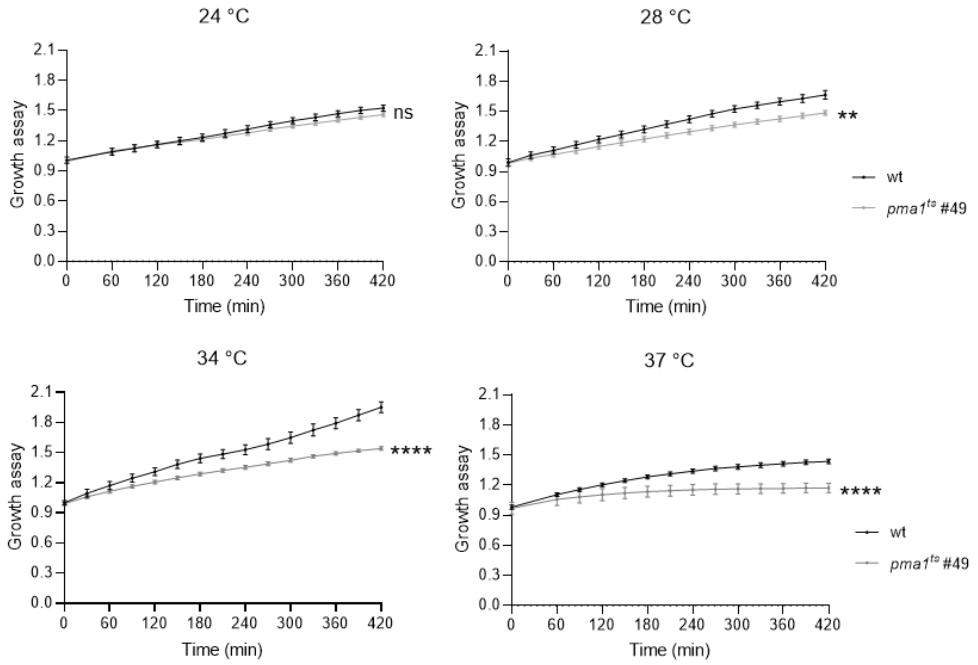


**Figure 61. Effect of temperature on growth of the *pma1*$^{ts}$ mutant in liquid medium.** Microconidia (2.5x10$^4$) of the wild type (wt) and *pma1*$^{ts}$ #49 strains were germinated in 200 µL YD medium buffered at pH 7.4 with 20 mM HEPES in 96 Microtiter™ plate wells for fifteen-hours at 24 ºC and 170 rpm. At time 0, the temperature was changed from 24 ºC to 28, 34 or 37 ºC, or kept at 24 ºC as a control. Absorbance at 600 nm was measured at the indicated times after the temperature change for 7 hours. Values were normalized to time-point 0'. Graphs show the mean± s.d. from three independent replicate microwells from one representative experiment. (**) $p$ <0.01, (****) $p$ <0.0001 and ns (non-significant) *versus* wt according to Welch's t-test.

We next tested the effect of the *pma1*$^{ts}$ mutations on Pma1 activity. Plasma membranes were isolated from the wild type and *pma1*$^{ts}$ #49 mutant germinated for fifteen-hours at 24ºC and then transferred either to 24ºC or 37ºC. Mycelia were collected at different time points after the transfer. At time-point zero, no difference in Pma1 activity was observed between the strains (0,0093 *vs* 0,0114 mmol/min/g) [Figure 62]. At later time points, there was a significant increase in $H^+$-ATPase activity in the wild type strain both at 24ºC and 37ºC, while in the *pma1*$^{ts}$ #49 strain the activity of Pma1 remained mostly constant at 24ºC whereas it dropped dramatically at the time point of 60 minutes after shifting the temperature to 37ºC [Figure 62].

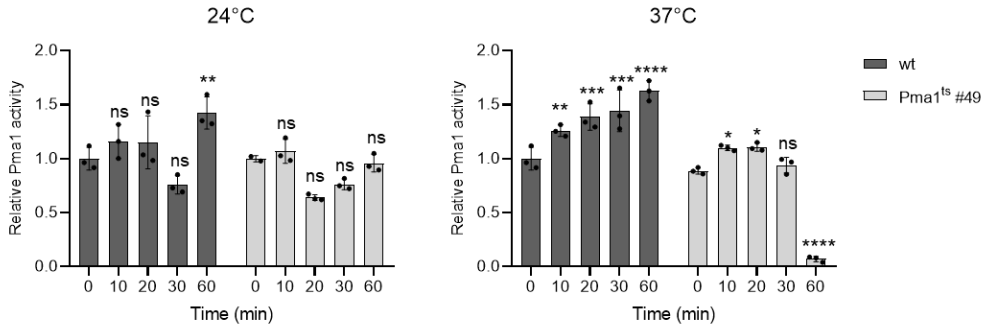


**Figure 62. The *pma1$^{ts}$* mutant shows a drastic decrease in Pma1 activity at 37ºC.** ATPase activity was assayed in total membranes isolated from fifteen-hours germinated microconidia of the *F. oxysporum* wild type (wt) and *pma1$^{ts}$* #49 mutant. At time 0, the culture was either shifted from 24ºC to 37ºC or kept at 24ºC as a control. Total membranes isolated before (time 0) or 10, 20, 30 or 60 minutes after the shift. ATPase activity was normalized to that of time 0 of the wt strain for each temperature condition. (*) $p$ <0.05, (**) $p$ <0.01, (***) $p$ <0.001, (****) $p$ <0.0001 *versus* wt according to two-way ANOVA and Bonferroni Test. Data shown are the mean ± s.d from three three technical replicates. Experiment conducted in collaboration with Maria Teresa Romero Lavirgen (Master student under my own supervision).

## 8. The *pma1$^{ts}$* mutant arrests growth at the restrictive temperature

We next evaluated the ability of the two strains to proliferate at the restrictive temperature of 37ºC. When germlings of the wild type strain were transferred to 37ºC for 24 hours, the number of colony forming units (CFU) after the incubation had increased approximately 4-fold compared to that before the incubation [Figure 63]. By contrast, in the *pma1$^{ts}$* #49 mutant the increase was only 1.4-fold compared to the time-point zero. These results suggest that cell proliferation and conidiation at the restrictive temperature was strongly reduced.

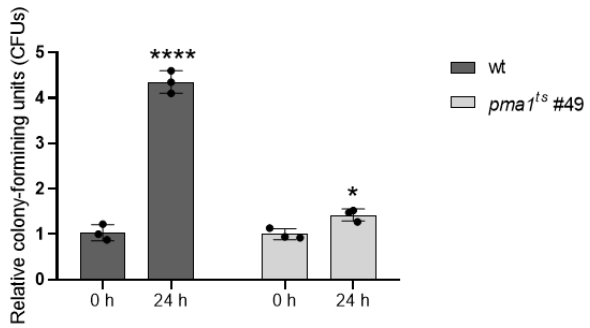


**Figure 63. The *pma1$^{ts}$* mutant halts proliferation at the restrictive temperature.** Fifteen-hours germinated microconidia in PDB medium at 24°C (time 0') were shifted to 37ºC for 24 hours. Samples collected before (time 0') and after 24h incubation at 37 °C were diluted 1:100 and plated on PDA plates. After two days of incubation at 24 °C the number of colonies was counted to determine CFU. (*) $p$ <0.05 and (****) $p$ <0.0001 *versus* time 0' for each strain according to Welch's t-test. Data shown are the mean ± s.d of three technical replicates.

Next, we assessed the ability of the strains to resume growth after 24 hours incubation at the restrictive temperature. In this assay, fungal growth was evaluated in liquid medium by measuring the absorbance at 600 nm immediately after 24 hours incubation at 37ºC (time 0') and after an additional 24h at 24 ºC. We found that *pma1*$^{ts}$ #49 was able to resume growth after the shift from restrictive to permissive temperature to the same extent as the wild type strain [Figure 64].

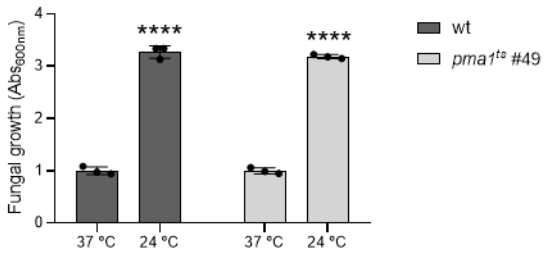


**Figure 64. The *pma1*$^{ts}$ mutant resumes growth after prolonged exposure to restrictive temperature.** Fifteen-hour germinated microconidia of the wild type (wt) and the *pma1*$^{ts}$ #49 mutant were incubated at 37ºC for 24 hours (37ºC). After shifting the temperature back to 24ºC cells were incubated for 24 hours at permissive temperature (24ºC). Growth assays were conducted in a 96 Microtiter™ plate by measuring absorbance at 600 nm at the two time points. Values were normalized to 37 ºC (time 0'). (****) $p$ <0.0001 *versus* 37ºC each strain according to Welch's t-test. Data shown are the mean ± s.d of three technical replicates.

## 9. The *pma1*$^{ts}$ mutant shows increased sensitivity to cell wall integrity stress

We next analyzed the role of Pma1 in the response to cell wall, high osmolarity and oxidative stresses. The wild type strain and *pma1*$^{ts}$ #49 mutant were grown in the presence of different stress-inducing compounds [Figure 65]. Considering the temperature-sensitivity of the mutant, the assays were performed at 24, 28 and 32ºC. Interestingly, the *pma1*$^{ts}$ #49 mutant showed a significantly higher sensitivity to CFW at all temperatures analyzed, suggesting that Pma1 plays a role in the cell wall integrity response [Figure 65]. However, the *pma1*$^{ts}$ #49 mutant did not show differential sensitivity under oxidative or hyperosmotic stress.

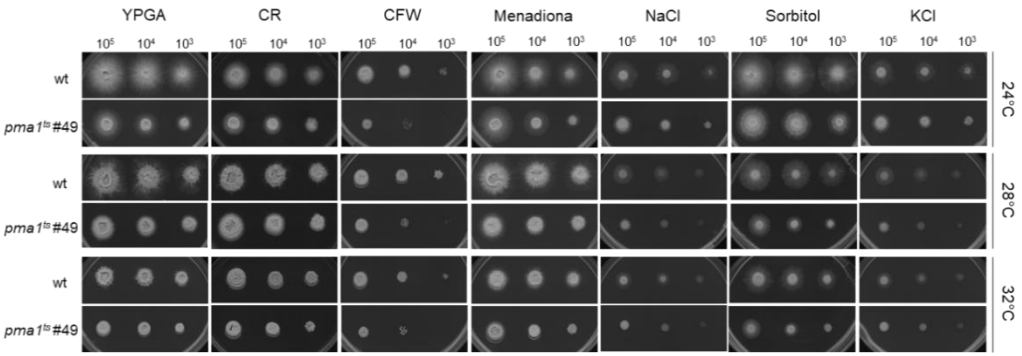


**Figure 65. Pma1 contribute to cell wall integrity response.** Aliquots of $10^5$, $10^4$ and $10^3$ fresh microconidia of the indicated strains were spot-inoculated on PDA plates supplemented with CR (100µg/ml), CFW (50µg/ml), Menadione (20 µg/mL), NaCl (1,2 M), Sorbitol (1,25 M) and KCl (1,2 M). Control plates without any compound were also included. Plates shown are representative of three independent replicates for each strain and growth condition. Experiment conducted in collaboration with Maria Teresa Romero Lavirgen (Master student under my own supervision).

## 10. The *pma1$^{ts}$* mutant shows increased sensitivity to acid pH environments

To evaluate the role of Pma1 in response to different pH environments, we tested growth on YPGA medium, either unbuffered or adjusted to pH 3, 4, 6, 8 and 9, under permissive (24ºC) and restrictive temperature conditions (32 ºC). The *pma1$^{ts}$* mutant presented severe growth defects at pH 3, 4 and 6, and grew forming very compact colonies without aerial hyphae, whereas the wild type shown a less significant growth inhibition. Conversely, at alkaline pH (pH 8 and 9) the *pma1$^{ts}$* mutant exhibited a significantly increased colony growth than in the control condition without adjusting the pH, while this effect was less marked in the wild type strain [Figure 66]. The comparative analysis between both strains was similar when tested at higher temperature (32 ºC), although the growth defects were more exacerbated, as could be expected. These results suggest that the *pma1$^{ts}$* mutant is more sensitive to variations in ambient pH and that the manipulation of the Pma1 protein could be a useful approach to study pH homeostasis [Figure 66].

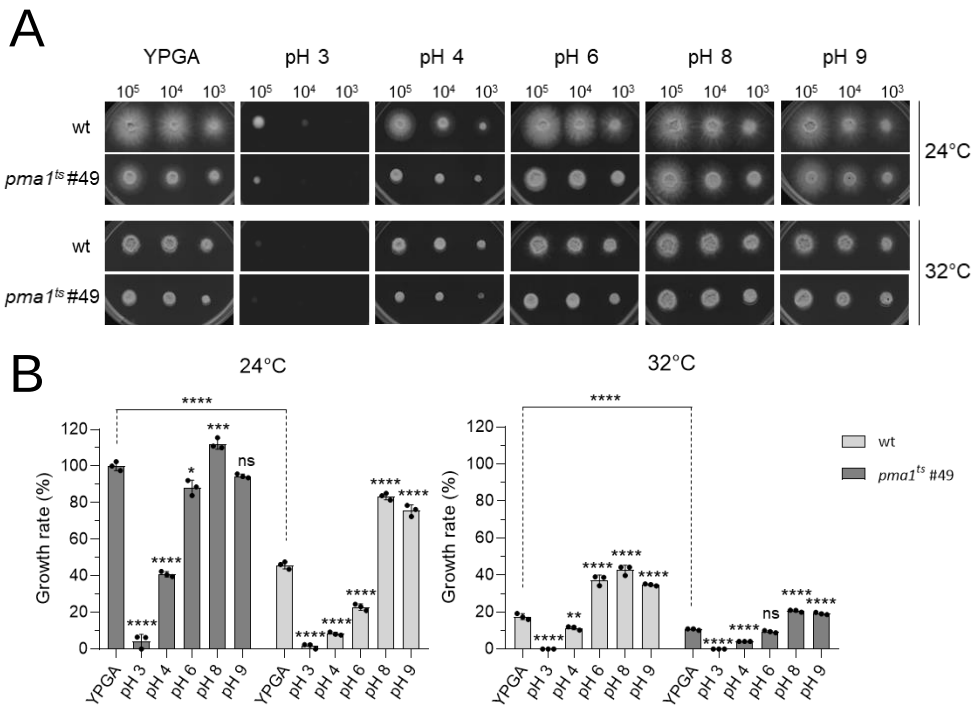


**Figure 66. The *pma1$^{ts}$* mutant shows increased sensitivity to acid pH while alkaline pH improves its growth.** (**A**) Aliquots of $10^5$, $10^4$ and $10^3$ fresh microconidia of the indicated strains were spot-inoculated on YPGA plates adjusted to the indicated pH values. Control plates without adjusting pH were also included. The plates were scanned after 3 days incubation at 24 °C or 32 °C. Experiment conducted in collaboration with Maria Teresa Romero Lavirgen (Masters student under my own supervision). (**B**) Colony area of the indicated strains at $10^5$ microconidia concentration on YPGA plates adjusted to the indicated pH was measured and normalized to that of the wild type (wt) strain at 24 °C (100%). (*) $p$ <0.05, (**) $p$ <0.01, (***) $p$ <0.001, (****) $p$ <0.0001 and ns (non-significant) *versus* YPGA at each strain, according to Welch's t-test. Data show representative means ± s.d, from three independent plates per strain.

## 11. The *pma1$^{ts}$* mutant shows attenuated virulence on tomato plants

To explore the role of Pma1 in pathogenicity, a tomato plant infection assay was performed by dip-inoculating roots with fresh microconidia of the wild type or the *pma1$^{ts}$* mutant. Plants inoculated with the *pma1$^{ts}$* #49 strain presented a significant delay in mortality compared to those infected with the wild type strain [Figure 67]. This suggests that Pma1 contributes to the infection process.

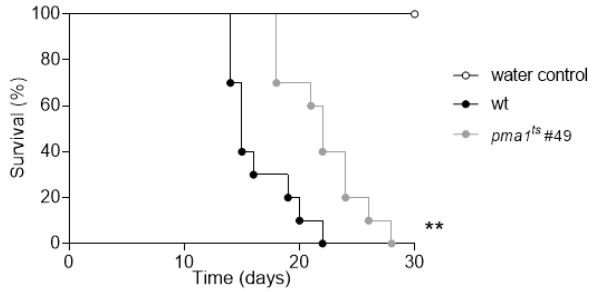


**Figure 67. The *pma1*$^{ts}$ #49 mutant shows attenuated virulence on tomato plants.** Kaplan–Meier plots showing survival of tomato plants (cv. Monica) inoculated by dipping roots into a suspension of 5x10$^6$ microconidia/mL of the indicated fungal strains. Percentage survival of tomato plants was plotted for 30 days. Data shown are from one representative experiment. (**) $p$ <0.01 *versus* wt according to log-rank test.

# Chapter V

**Part of this work was performed during a 4 month stay at the laboratory of Prof. Robert Arkowitz at University of Côte d'Azur (France).**

# Chapter V. Live cell imaging analysis of Pma1 localization in *Fusarium oxysporum* and *Candida albicans*

## Overview

It has been suggested that similar to other integral PM proteins, the $H^+$-ATPase Pma1 is synthesized and integrated into the membrane in the rough endoplasmic reticulum (ER), from where it is transported by vesicular carriers to its final destination. The protein-lipid complex formed at the ER membranes is packaged into COPII (coat protein complex II) subunits, a type of specialized transport vesicles which mediate the exit of newly synthesized Pma1 from the ER in a process dependent on the SEC genes (Roberg *et al.*, 1999; Shimoni *et al.*, 2000). Vesicles are transported from the ER to the Golgi complex and then to the PM surface by a mechanism of the secretory pathway that does not intersect with the endosomes (Gurunathan *et al.*, 2002; Harsay & Schekman, 2002). Furthermore, the synthesis and stabilization of Pma1 was independent of microtubules and cytoskeletal elements (Malinska *et al.*, 2004). Once at the PM, Pma1 is inserted into a specific region named the membrane compartment of Pma1 (MCP), which is highly stable (Benito *et al.*, 1991; Malinska *et al.*, 2004) and where Pma1 undergoes lateral diffusion (Fajardo-Somera *et al.*, 2013; Malínská *et al.*, 2003).

Several lines of evidence have suggest that Pma1 is a major protein component of glycosphingolipid- and cholesterol-enriched microdomains in the PM, also called lipid rafts (Bagnat *et al.*, 2001). Alongside, it was proposed that these microdomains contain relatively low levels of ergosterol (Grossmann *et al.*, 2007). Furthermore, shortening the C26 fatty acid of sphingolipids to a C22 fatty acid induces rapid degradation of Pma1 (Gaigg *et al.*, 2006). Although it has been proposed that entry into lipid rafts is a mechanism for regulating membrane traffic (Simons & Sampaio, 2011), the significance of lipid raft association for Pma1 trafficking, stability, and function remains unclear.

One of the main features of filamentous fungi is their apical mode of growth. During this process, cell wall expansion and exocytosis are tightly interconnected, involving the highly polarized traffic of cell wall-building secretory vesicles to the apical areas, where they deliver proteins and lipids (Bartnicki-Garcia *et al.*, 1995). Pma1 is essential for hyphal growth, although it has been shown to be absent from the hyphal

tip of the filamentous fungus *Neurospora crassa* (Fajardo-Somera *et al.*, 2013). In fungal plant pathogens, where pH plays an essential role in controlling pathogenicity (Fernandes *et al.*, 2022a), Pma1 localization has been poorly studied so far. It would be of high relevance to determine Pma1 localization during hyphal growth to understand relevant physiological processes coordinated by pH, such as chemotropic growth towards the host. Therefore, is this chapter we study the localization of fluorescently labelled Pma1 protein in *F. oxysporum* and its implication in $pH_c$. In particular, we analyzed whether in this soil-borne pathogen there is a lateral localization of Pma1 in growing hyphae, as described for the non-pathogenic fungus *N. crassa* (Fajardo-Somera *et al.*, 2013). Furthermore, we explored whether Pma1 localization could be involved in the generation of a $pH_c$ gradient along the hypha, which could be driving growth as proposed in the figure below [Figure 68].

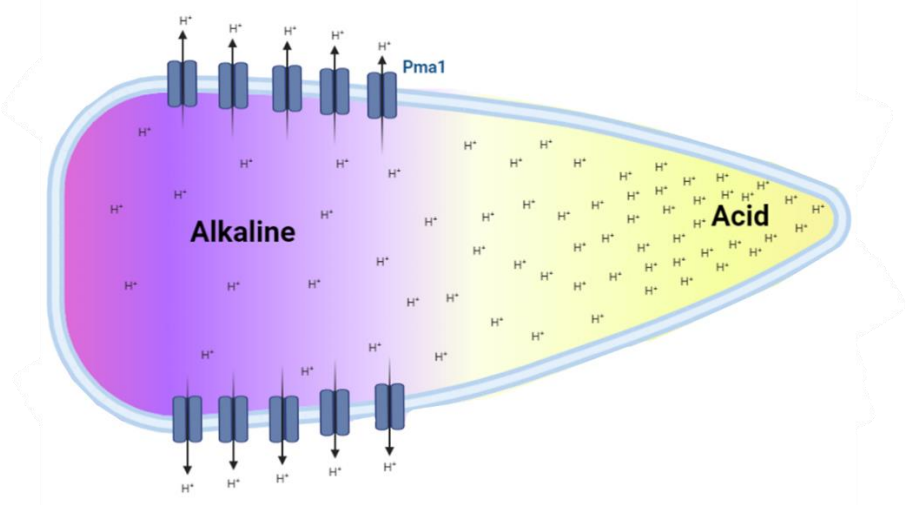


**Figure 68. Hypothetical model of a cytosolic pH gradient by asymmetric distribution of the plasma membrane $H^+$-ATPase Pma1**. The most abundant protein in the PM, the Pma1 protein has a sub-apical localization. In line with its role as key regulator of cytosolic pH homeostasis in fungi, this hypothetical model proposes the establishment of a cytosolic pH gradient along the hyphal axis as a result of the asymmetric distribution of Pma1 H+-ATPase activity.

## Results

### 1. Labelling of *Fusarium oxysporum* Pma1 with the fluorescent protein Clover

To generate a fluorescent version of the Pma1 protein in *F. oxysporum*, a *pma1* allele encompassing the entire coding region sequence was amplified from genomic DNA and fused with the GFPclover-Linker2-3xFLAG cassette amplified from the plasmid *pUC57-1XFomClover3*-3XFLAG and the *pma1* terminator region [Figure 69A]. The resulting DNA fragment and the hygromycin resistance cassette were used to co-transform *F. oxysporum* protoplasts [Figure 69A]. *Hyg*$^{R}$ transformants carrying a homologous insertion at the *pma1* locus were initially identified by PCR with two pairs of primers hybridizing outside of the fragment used for transformation [Figure 69B]. Candidate transformants showing homologous insertion of *pma1-clover* allele (#17, #54 and #57) were further validated for fluorescence intensity by wide-field fluorescence microscopy (data not shown).

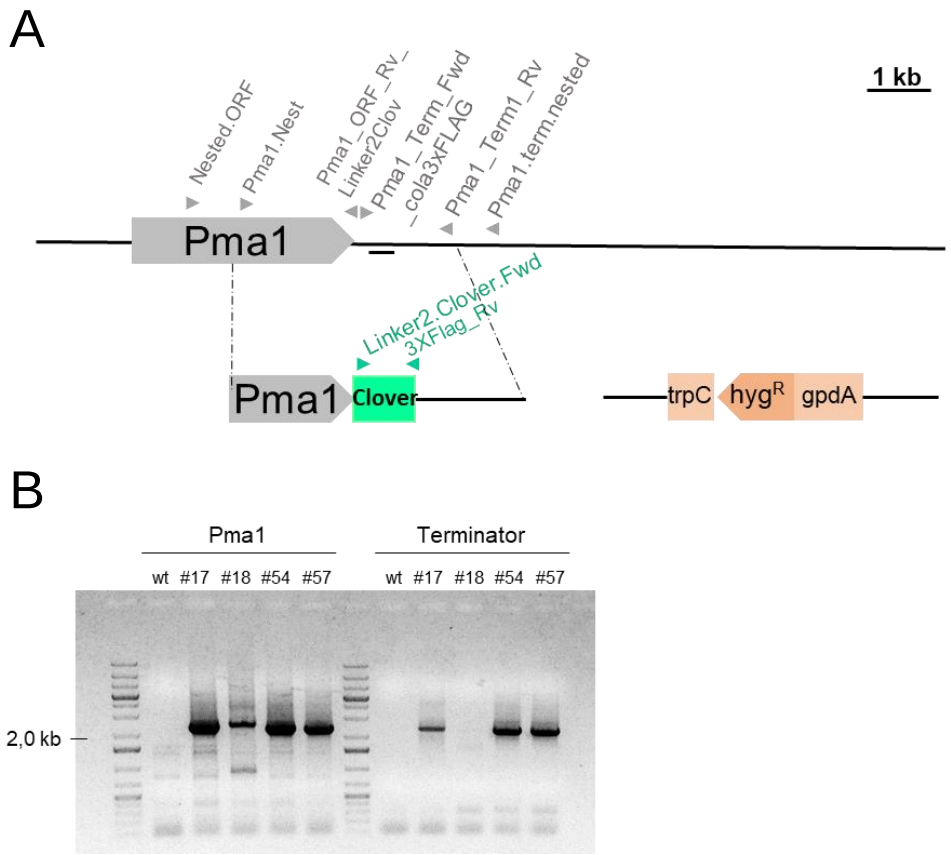


**Figure 69. Fluorescent labelling of F. oxysporum pma1 with Clover.** (**A**) Physical map of the *pma1* locus and strategy followed for labeling of the Pma1 protein with the fluorescent protein Clover, by using co-transformation with the *Hyg*$^{R}$ cassette as selective marker. Gray (*pma1*) and green (*pUC57-1XFomClover3-3XFLAG*) arrowheads indicate the relative positions of the primers used for generation of DNA fragments for transformation and PCR analysis of the transformants. Scale bar, 1kb. (**B**) PCR analysis to confirm homologous insertion of the construct into the genome of the transformants using the pairs of primers: Nested.ORF/3XFLAG_Rv (*pma1* region) and Linker2.Clover.Fwd/ Pma1.term.nested (terminator region, see A).

## 2. Localization of Pma1-clover reveals an upward gradient from the hyphal tip

Once the correct insertion of the DNA fragment of interest was confirmed, transformant #17 was selected for further studies on Pma1 localization. The distribution of Pma1-Clover along the PM was examined in young hypha after 6-12 hours of germination on MM plates, by using a confocal spinning-disk (CF) microscopy system. The fluorescence was mainly detected in the PM and strongly concentrated in the septum [Figure 70A]. Interestingly, we observed an asymmetric distribution of Pma1, with an upward gradient from the hyphal tip, where is totally absent, to the first septum of the hypha. Quantitative analysis of fluorescence intensity in the same hypha confirmed of an upward gradient from the hyphal tip and a peak of intensity corresponding to the location of septum (indicated by arrows on graph) [Figure 70B].

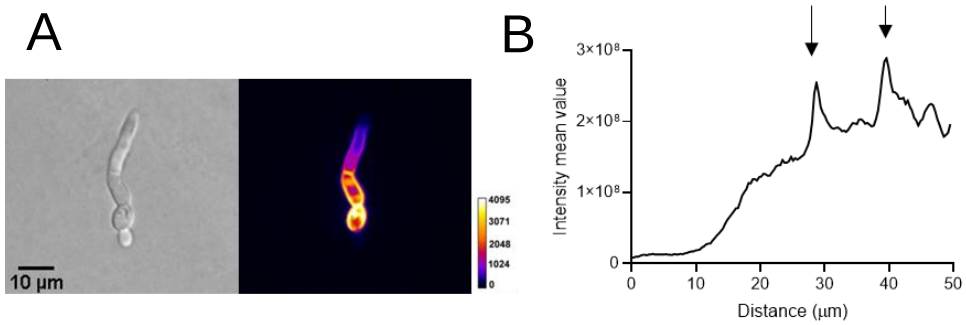


**Figure 70. Pma1 is largely absent from the tip and presents a high intensity peak in the septa of fungal hyphae.** (**A**) Microconidia of the *pma1-clover* strain germinated for 6 to 12 hours on MM plates were analyzed by spinning-disk confocal microscopy to study distribution of Pma1 along the PM of *F. oxysporum* hyphae. Figure represents a false colored sum projection of 23×0,4 µm z-sections (LUT, right panel) and DIC images (left panel) of cells expressing Pma1-clover. (**B**) A line delimiting the membrane of the hypha was drawn and fluorescence intensity was determined. Fluorescence intensity increases exponentially from the apex to the first septum (intensity peak indicated by arrows).

We next asked if the differential localization of Pma1 throughout the PM, particularly its absence from the tip, could be a conserved phenomenon in more hyphae. To this end, we analyzed the intensity of fluorescence along the PM in fifteen randomly selected hyphae showing a similar length. In all analyzed hyphae, we detected an upward gradient of Pma1-clover from the tip and a significant increase of fluorescence intensity at the first septum [Figure 71A]. To determine the percentage of PM region free of Pma1 (i.e. not showing fluorescence), we used microconidia germinated 6 to 12 hours, for which we defined a minimum mean intensity value of

$2x10^4$ absolute units (A.U.). With this analysis we observed that the percentage of Pma1 free-membrane was independent of the total size of the hypha, but remained constant throughout germination, with an area of around 27% of Pma1-free PM at the hyphal tip [Figure 71B].

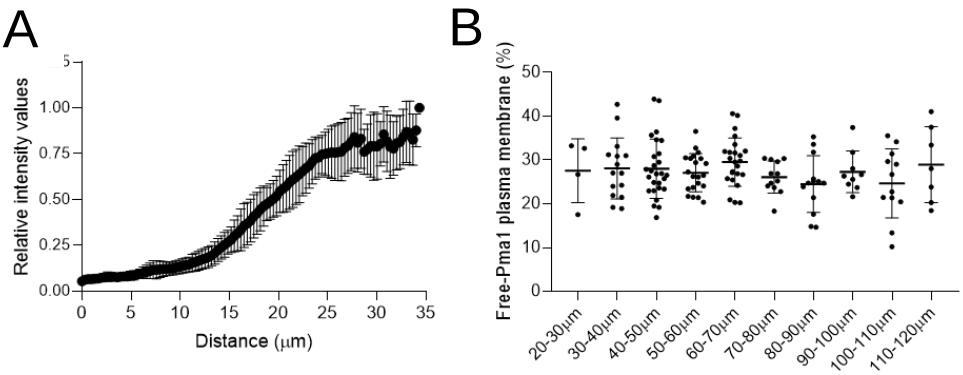


**Figure 71. Pma1display a linear upward gradient from the hyphal tip.** (**A**) Mean relative fluorescent intensity values in fifteen germinated microconidia of the Pma1-Clover strain, ranging from 30-35 µm in length. Note that Pma-1-Clover intensity increases dramatically from the tip to the first septum. (**B**) Percentage of PM where no Pma1-Clover intensity signal is detected (<20.000 A.U.) in groups of hyphae exhibiting different lengths. Note that the percentage of Pma1-free plasma membrane remains constant independent of hyphal length.

## 3. Fluorescent labelling of the *Candida albicans* Pma1 with the fluorescent protein mScarlet

To generate red fluorescent Pma1 protein in *C. albicans*, the mScarlet gene with the auxotroph marker *HIS* was amplified from the *PFa-mScarlet.CdHIS1* (CP035) plasmid using primers containing a tail with flanking regions for the *C. albicans pma1* locus (C3_00720W_A). The resulting DNA fragment was used to transform competent cells by electroporation [Figure 72A].

Prototrophic HIS+ transformants carrying a copy of the construct inserted at the *pma1* locus were initially identified in by red fluorescence in a wide-field confocal microscope [Figure 72B]. Candidates showing the highest fluorescence intensity were selected for further PCR analysis using pairs of primers hybridizing outside of the fragments used for transformation and inside of the construct [Figure 72C].

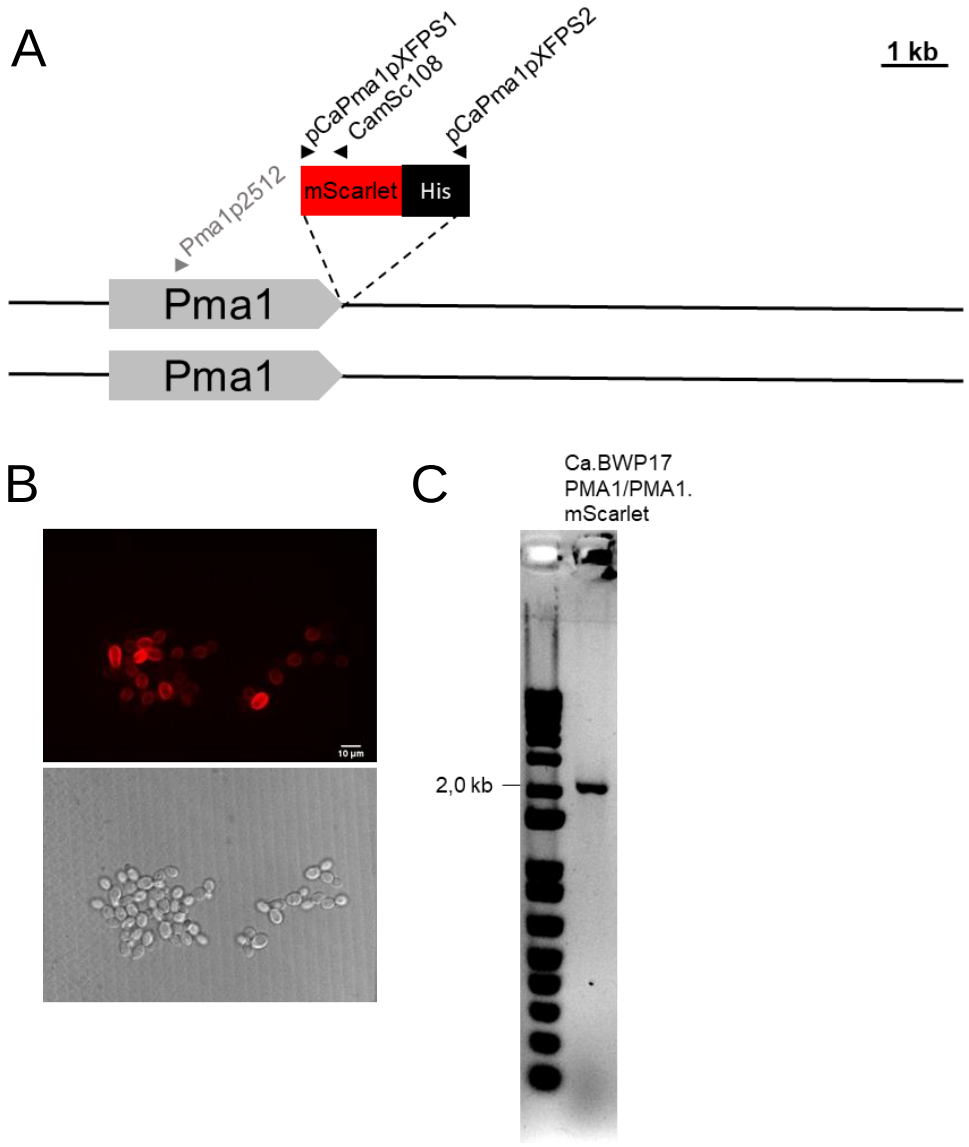


**Figure 72. Generation of a *C. albicans* strain expressing Pma1 labelled with the red fluorescence mScarlet protein.** (**A**) Physical map of the *C. albicans pma1* locus and strategy followed for labeling of the Pma1 protein using electroporation and the His cassette as selective marker (*pma1-mScarlet*). Gray (*pma1*) and black (*PFa-mScarlet.CdHIS1* plasmid (CP035)) arrowheads indicate the position primers used for generation of the fluorescence labeling construct and for PCR analysis of the transformants. (**B**) Fluorescence analysis of a transformant using a wide-field confocal microscope. (**C**) PCR analysis to confirm homologous integration of the construct into the genome of *C. albicans* using the primer pair Pma1p2512/CamSc108.

## 4. Pma1 is absent from the hyphal tips of *Candida albicans*

To study the distribution of the Pma1-mSc protein along the PM, *C. albicans* cells were grown in liquid YPD medium with 50% fetal calf serum (FCS) at 37ºC for 30 and 60 minutes, before analysis in a confocal spinning-disk (CF) microscopy system. The fluorescence distribution along the PM was similar to that observed in *F. oxysporum*, with Pma1 being largely absent from the hyphal tip [Figure 73A]. Furthermore, the upward gradient of Pma1 fluorescence showed to be conserved in ten analyzed hypha [Figure 73B].

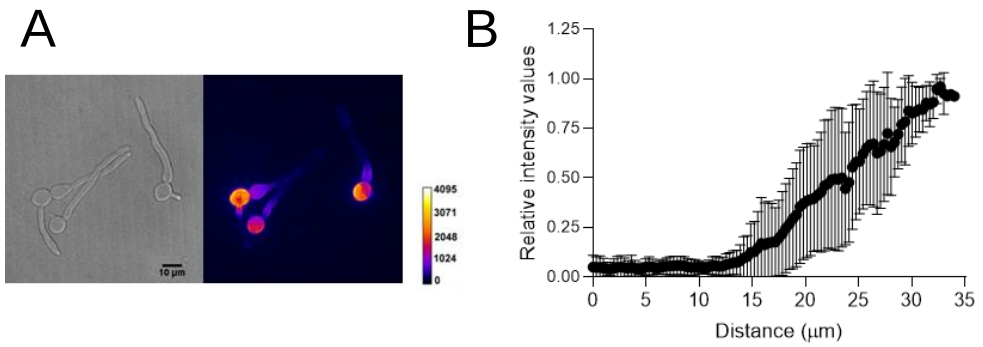


**Figure 73. Localization of fluorescently labelled Pma1 in the human pathogen *C. albicans*.** (**A**) Filamenting hyphae of *C. albicans* strain Pma1-mSc incubated 60 minutes in YPD medium with FCS at 37ºC were analyzed by fluorescence microscopy. Representative false colored sum projection of 23×0,4 µm z-sections (LUT, right panel) and DIC images (left panel) of hyphae expressing Pma1-mSc using a spinning-disk confocal microscope equipped with DPSS (561 nm). (**B**) Mean of relative fluorescence intensity throughout the PM evaluated in ten individual hyphae of the Pma1-mSc strain, ranging from 30-35 µm in length.

## 5. Cytosolic pH distribution in germ tubes of the fungal pathogens *Fusarium oxysporum* and *Candida albicans*

Because our previous results showed that Pma1 is absent from the hyphal tip of *F. oxysporum* and *C. albicans*, we hypothesized that the differential distribution along the PM could result in a pH gradient along hyphae. To test this hypothesis in the human pathogen *C. albicans*, a strain expressing the pH-sensor pHluorin 2 (PHL2) was generated in the genetic background of the Ca.BWP17PMA1/PMA1.mScarlet strain, by inserting the *pKE4-PHL2* plasmid containing PHL2. This plasmid was introduced into an ura3- recipient strain following digestion with *Nhe* I, to obtain targeted integration and reconstitution of the *URA3* locus as previously described (Tournu *et al.*, 2017) [Figure 74A]. Prototrophic *URA+* transformants carrying a *pma1-mSclarlet* allele were initially checked for pHluorin2 presence by fluorescence in a

wide-field confocal microscope [Figure 74B]. The candidate transformants #56 and #58 showing the highest fluorescence intensities were selected for further PCR analysis using the pairs of primers LUXINTDETF/LUXINTDETR, as previously described (Tournu *et al.*, 2017) [Figure 74C].

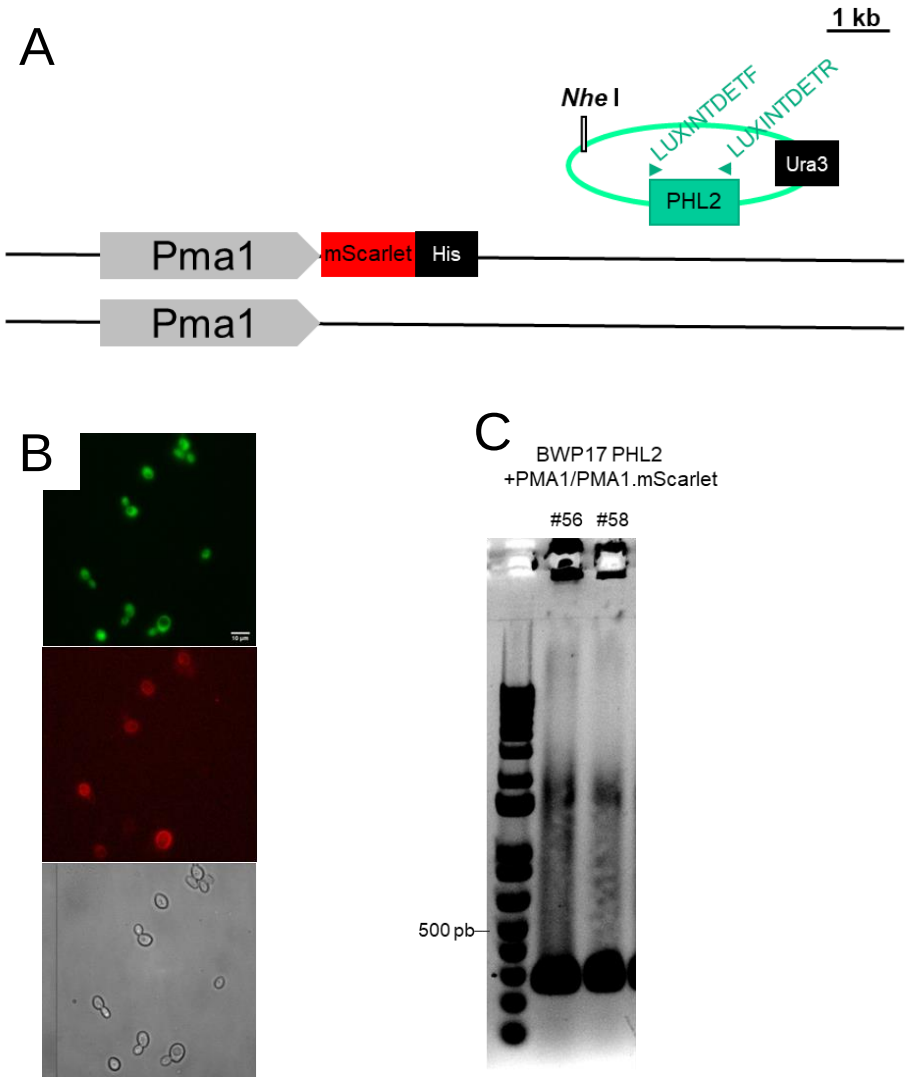


**Figure 74. Generation of a strain expressing the pH-sensor pHluorin2 in the *C. albicans* strain expressing *pma1-mScarlet*.** (**A**) Physical map of the *pma1* locus and strategy followed to insert pHluorin from the pKeI-PHL2 plasmid digested by *Nhe*I enzyme. Position of the *Nhe*I restriction site is indicated and green (pKeI-PHL2 plasmid primers) arrowheads indicate the position used for PCR analysis of the transformants. (**B**) Fluorescence intensity analysis in the transformants obtained by using a wide-field confocal microscope. (**C**) PCR analysis to confirm correct insertion of the *PHL2* gene into the genome by using the pair of primers: LUXINTDETF/LUXINTDETR.

## 6. Set-up of a method for determination of cytosolic pH

We then attempted to determine $pH_c$ distribution along the length of the hyphae both in *C. albicans* and *F. oxysporum*. To obtain a calibration curve for the determination of $pH_c$ in the wild type strain of *C. albicans* expressing the pH sensor pHluorin (PHL2), yeast cells harvested at exponential growth ($DO_{600nm}$=0.6) were germinated in 50% FCS at 37ºC for 60 minutes, washed with a buffer solution at pH 6,0 and permeabilized with nigericin for 30 minutes in the presence of buffers at different pH values ranging from 5,5 to 8,5. Similarly, a calibration curve was obtained in *F. oxysporum* by using a strain expressing the pH-sensitive GFP protein pHluorin, as previously described (Fernandes *et al.*, 2022b). Briefly, fifteen hours germinated microconidia were used to measure $pH_c$, since localization of pHluorin was shown to be not homogeneously distributed in the cytosol of germlings at an earlier stage (Fernandes, 2017). Germlings were washed with a buffer solution at pH 6,0 and permeabilized with nigericin for 30 minutes in the presence of buffers at different pH values ranging from 5,5 to 8,5, as described for *C. albicans*.

Fluorescence was measured in a Spinning-disk confocal microscope, through excitation of samples with a diode (405 nm) and Argon (488 nm) lasers and an emission wavelength of 510 nm for both excitation wavelengths, using a UMPL APO 40x dry objective. The images were set to 8 bits and the background was subtracted using the lookup table HiLo (ImageJ/Fiji) by adjusting the contrast. We subtracted the same background value for all images of an experiment, and a line was drawn to delimit the shape of the cell, measuring the intensity within the line after excitation at 405 and 488 nm [Figure 75A – 76A]. Finally, the 405/488 nm ratio was calculated for each pH value and normalized to the ratio obtained at pH 7. The obtained calibration curve displayed a linear response to pH values between 5,5 – 8,5 [Figure 75B – 76B]. Emission intensities detected after 405- and 488-nm excitation, at pH 5,5 and 8,5 were used to calculate the minimum and maximum ratios. The calculated $pK_a$ of pHluorin/PHL2 was 6.9±0.1 for both *F. oxysporum* and *C. albicans* [Figure 75C- 76C].

*In vivo* calibration with buffers at different pH values confirmed the pH sensitivity and spectral characteristics of the expressed pHluorin/PHL2, allowing the measurement of $pH_c$ in these fungal pathogens.

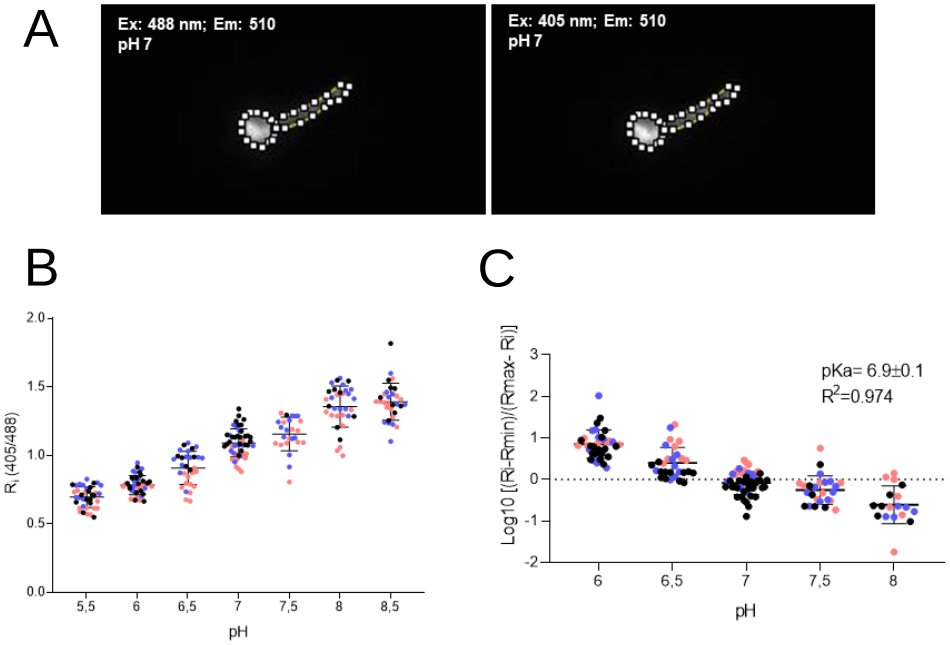


**Figure 75. Calibration curve for the measurement of cytosolic pH ($pH_c$) in *C. albicans*.** (**A**) Filamentous hyphae of *C. albicans* expressing PHL2 incubated with FCS for 60 minutes at 37ºC were washed and suspended in pH-adjusted calibration buffers ranging from 5,5 to 8,5, containing nigericin to equalize the ambient pH with $pH_c$. Microscopy images were acquired at 405 and 488 nm excitation respectively, both at 510 nm emission on a Spinning-disk confocal microscope. A line delimiting the shape of the hypha was drawn and fluorescence intensity within the line was measured at 405- and 488-nm wavelength. (**B**) Plot of fluorescence excitation ratio 405/488 ($R_i$) *versus* buffer pH. Data are shown as mean ± s.d from around thirty hyphae analyzed for each condition. (**C**) Logarithmic plot of fluorescence excitation ratio *versus* buffer pH for calculation of the pKa constant. $R_{max}$ and $R_{min}$ are the limiting values for the ratio at the extreme acidic (pH 5,5) and alkaline (pH 8,5) condition.

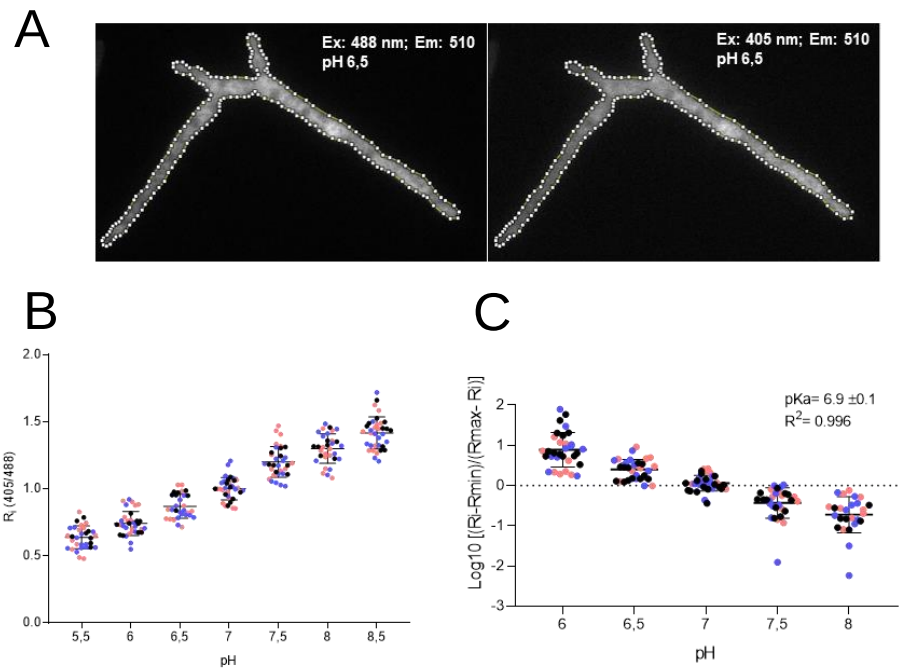


**Figure 76. Calibration curve for the measurement of cytosolic pH ($pH_c$) in *F. oxysporum*.** (**A**) Fifteen-hour germinated microconidia of *F. oxysporum* expressing pHluorin were washed and suspended in pH-adjusted calibration buffers ranging from 5,5 to 8,5, containing nigericin to equalize the ambient pH with $pH_c$. Microscopy images were acquired at 405- and 488-nm excitation respectively, both at 510 nm emission on a Spinning-disk. A line delimiting the shape of the hypha was drawn and fluorescence intensity within the line was measured at 405- and 488-nm wavelength. (**B**) Plot of fluorescence excitation ratio 405/488 ($R_i$) *versus* buffer pH. Data are shown as mean ± s.d from around thirty hyphae analyzed for each condition. (**C**) Logarithmic plot of fluorescence excitation ratio *versus* buffer pH for calculation of the pKa constant. $R_{max}$ and $R_{min}$ are the limiting values for the ratio at the extreme acidic (pH 5,5) and alkaline (pH 8,5) condition.

## 7. Measurement of $pH_c$ along the long axis of the fungal hyphae

Once we had established a method for measurement of $pH_c$ in both fungal species, we measured the $pH_c$ along the long axis of the fungal hyphae. In *C. albicans*, the wild type strain expressing the pH sensor pHluorin (PHL2) was employed. Cells in exponential growth ($DO_{600nm}$=0.6) were germinated in 50% FCS at 37ºC for 60 minutes, washed, resuspended and incubated in a buffer solution at pH 6,0 for 30 minutes. The microscopy images were acquired and treated under the same conditions used for the calibration curve using a Spinning-disk confocal microscope. A line whose thickness covers the entire cytosol of the hyphae was drawn, measuring the intensity of the line after excitation at 405- and 488-nm.

The 405/488 nm ratio was calculated for each pixel of the image, allowing to detect fluctuations in $pH_c$ from the tip to the center of the hypha, together with the previously obtained calibration line [Figure 77A]. Preliminary results of the analyzed hyphae did not show any $pH_c$ fluctuations over the long axis of fungal hyphae, but instead followed an irregular pattern [Figure 77B].

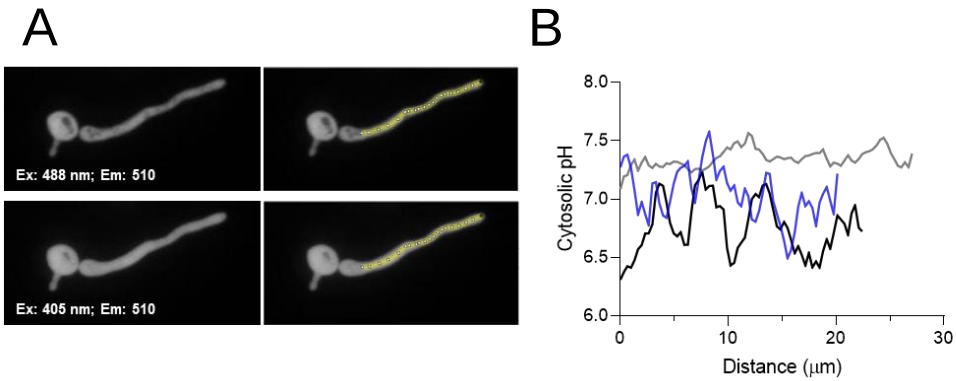


**Figure 77. Measurement of cytosolic pH along the hyphae of *C. albicans* using the ratiometric fluorescent pH probe pHluorin.** (**A**) Filamentous hyphae of *C. albicans* incubated with FCS for 60 minutes at 37ºC were subjected to $pH_c$ analysis using a Spinning-disk confocal microscope equipped with diode (405 nm) and Argon (488 nm) lasers, using a UMPL APO 40x dry. A line delimiting the cytosolic of the hypha was drawn (**B**) pH value along the cytosol of hyphae was obtained from fluorescence intensity of the line (see A) by measuring at 405 and 488 nm wavelength, and the 405/488 nm ratio was calculated for calculation of $pH_c$ following the formula obtained from the calibration curve (see Figure 75). Data show $pH_c$ value over the long axis from three hyphae analyzed in the same experimental conditions.

To test possible fluctuations of $pH_c$ along the long axis of *F. oxysporum* hyphae, fifteen-hours germinated microconidia were used. Microscopy images were acquired with the focus on the tip and treated under the same conditions used for the calibration curve using a Spinning-disk confocal microscope. A line whose thickness covers the entire cytosol of the hyphae was drawn, measuring the intensity of the line after excitation at 405- and 488-nm. The 405/488 nm ratio was calculated for each pixel of the image, allowing to detect fluctuations in $pH_c$ from the tip to the center of the hypha, together with the previously obtained calibration line [Figure 78A]. Oppositely to *C. albicans*, our preliminary results seem to indicate an upward $pH_c$ gradient from the hyphal tip to the first septum [Figure 78B].

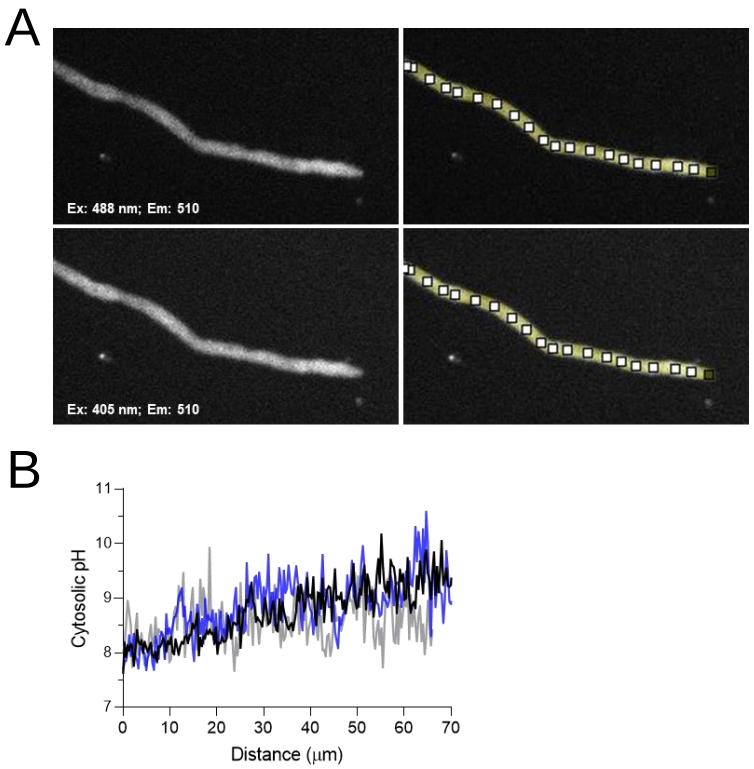


**Figure 78. Measurement of cytosolic pH along the long axis of F. oxysporum hyphae.** (**A**) Fifteen-hour germinated microconidia of *F. oxysporum* expressing pHluorin were subjected to $pH_c$ analysis using a Spinning-disk confocal microscope equipped with diode (405 nm) and Argon (488 nm) lasers, using a UMPL APO 40x dry objective. A line delimiting the cytosol of the hypha was drawn. (**B**) The $pH_c$ values along cytosolic hyphae obtained from fluorescence intensity of the line (see A) was measured at 405 and 488 nm wavelength, and the 405/488 nm ratio was used to calculate $pH_c$ values following the formula obtained from the calibration curve (see Figure 76). Data show $pH_c$ values over the long axis of three hyphae analyzed in the same experimental conditions.

# Discussion

# Discussion

## 1. pH controls chemotropic hyphal growth in *Fusarium oxysporum*

Ambient pH has long been known to play a central role in fungal growth, development and pathogenicity (Mariscal *et al.*, 2023). However, the molecular mechanisms underlying pH control of these processes has only recently started to be clarified (Fernandes *et al.*, 2022a). Results from our group demonstrated that an increase in ambient pH induces invasive growth (IG) and pathogenicity of *F. oxysporum* by triggering activation of the IG MAPK Fmk1 (Masachis *et al.*, 2016). Conversely, acidification of the rhizosphere, as observed in the presence of the bacterium *Rahnella aquatilis* through gluconic acid secretion, decreases the infectious capacity of this fungus (Palmieri *et al.*, 2020). Our research group also demonstrated that hypha of *F. oxysporum* are attracted towards tomato roots by secreted plant peroxidases which trigger activation of the MAPK Mpk1 (Nordzieke *et al.*, 2019; Turrà *et al.*, 2015).

In this study we aimed to evaluate the effect of ambient pH on hyphal chemotropism by establishing a pH gradient assay. We found that *F. oxysporum* exhibits a strong tropism towards an acid pH, which was reversed towards alkali in the *mpk1*Δ mutant. Moreover, loss of the MAPK Hog1 shown a significant reduced acid-triggered tropism.

Fungal pathogens have been known to orient hyphal growth towards chemical stimuli as nutrients, pheromones, or root exudates (Turrà *et al.*, 2015; Vitale *et al.*, 2019), but few studies have so far examined chemotropism in response to ambient pH. In the oomycete pathogen *Phytophtora palmivora*, zoospores are attracted to acidic pH (Morris *et al.*, 1995), while in human pathogenic *African trypanosomes* exogenous application of an alkaline solution (sodium hydroxide) acts as an attractant (Shaw *et al.*, 2022). Whereas in eukaryotes the mechanism governing pH chemotropism is unknown, in *Helicobacter pylori* attraction towards alkali and repulsion by acid is mainly controlled by the TlpB and TlpD chemoreceptors of acid pH belonging to the class of methyl-accepting chemotaxis proteins (MCPs), which are fundamental for colonization of the murine stomach (Croxen *et al.*, 2006; Goers Sweeney *et al.*, 2012; Huang *et al.*, 2017). Here, we found that *F. oxysporum* hypha

are attracted by acidic pH in a mechanism dependent on the CWI MAPK Mpk1. Overall, these findings suggest a role of this fungal MAPK cascade during early different stages of the infection. However, more studies are required to understand the molecular mechanisms underlying this process.

## 2. Sphingolipid acts as a chemoattractant and regulate the CWI MAPK

In order to understand the cellular components involved in $pH_c$-mediated CWI MAPK responses, a screen for loss of DES-triggered Mpk1 activation was previously performed in a subset of acid sensitive yeast mutants (Fernandes, 2017). This identified the AGC kinase Ypk1/2 as a key element upstream of the $pH_c$-triggered CWI MAPK response (Fernandes *et al.*, 2022a). Subsequently, we have made several intents to study this kinase in *F. oxysporum.* However, we found that Ypk1 is essential in this fungal plant pathogen (Fernandes *et al.*, 2022a). To further characterize the role of Ypk1, we followed alternative strategies previously described in *S. cerevisiae* (Berchtold *et al.*, 2012; Casamayor *et al.*, 1999), including the generation of a temperature sensitive or analog sensitive *ypk1* mutants, but both approaches failed to work in *F. oxysporum*.

The activity of Ypk1/2 in yeast is controlled by changes in the sphingolipid composition of the PM (García-Marqués *et al.*, 2016; Roelants *et al.*, 2011). In *F. oxysporum*, an increase in the long-base chain (LCB) sphingolipid dhSph was detected after extracellular or cytosolic acidification and this increase was also observed in the *mpk1*Δ mutant suggesting that dhSph synthesis occurs upstream of Mpk1 activation (Fernandes *et al.*, 2022a). Our results showed that the external addition of dhSph leads to a rapid phosphorylation of the MAPK Mpk1 without producing changes on $pH_c$ homeostasis. In the same way we also found that *F. oxysporum* exhibited a strong tropism towards dhSph in a dose-dependent manner, and that this response requires both the Mpk1 and Fmk1 MAPKs. Our data suggest that an increase on dhSph induced by $pH_c$ acidification acts as key signal to activate the CWI MAPK cascade, likely though the Ypk1 kinase.

pH was shown to control LCB sphingolipid levels in other fungal species. For instance, lipidomic profiling revealed an increase of the LCB sphingolipid levels in response to acetic acid in both *S. cerevisae* and *Zygosaccharomyces bailii* (Lindberg *et al.*, 2013). Interestingly, Ypk1/2 signaling was previously shown to be activated in

response to acetic acid, and its phosphorylation and activation was strictly required for acid tolerance (Guerreiro *et al.*, 2017; Mira *et al.*, 2010a). In *S. cerevisiae*, the upstream kinase Pkh1/2 was also directly activated by LCB sphingolipids, eventually leading to upregulation of Ypk1/2 (Liu *et al.*, 2005), which was shown to be required to control sphingolipid homeostasis and maintenance of cell wall integrity (Niles *et al.*, 2012; Roelants *et al.*, 2011; Roelants *et al.*, 2002). Further, TORC2 and the downstream Ypk1 kinase was shown to regulate actin polarization in *S. cerevisiae* by controlling reactive oxygen species (ROS) accumulation via Pkc1/Mpk1 MAPK cascade (Niles & Powers, 2014). Also the well-known PacC/Rim101 pathway which regulates fungal sensing of alkaline pH is activated by alterations in lipid composition of the PM (Obara & Kamura, 2021), where the C-terminal cytosolic domain of the transmembrane sensor PalH/Rim21 detects altered lipid asymmetry in the PM via interaction with the inner membrane leaflet (Nishino *et al.*, 2015; Obara & Kamura, 2021). Overall, lipids at the PM appear to be regulated by and to control several functional processes in fungal cells. Here, we discovered that dhSph plays a central role in acid signaling, controlling Mpk1 activation in response to $pH_c$ acidification. Further studies are required to elucidate mechanisms of dhSph level regulation and how it controls Mpk1 activation, because mutational studies on Ypk1 have so far failed in *F. oxysporum.*

## 3. Transcription patterns of *pma1* and *pma2* genes and plasma membrane $H^+$-ATPase activity in *Fusarium oxysporum*

*Pma1* and *pma2* encode PM $H^+$-ATPases, enzymes with critical physiological roles in fungal cells (Serrano, 1993). A possible reason for having two PM $H^+$-ATPase isoforms could be the attribution of different physiological functions, since Pma1 and Pma2 differ in their biochemical characteristics (Eraso & Portillo, 1994). Studies in *S. cerevisiae* demonstrated that *pma2* is expressed at a much lower level than the *pma1* under basal growth conditions and that *pma2* is not essential (Schlesser *et al.*, 1988; Supply *et al.*, 1993a; Viegas *et al.*, 1994). Furthermore, in yeast cells *pma2* expression is increased up to two-fold under certain stresses, such us high temperature, ethanol, octanoic acid or copper, while *pma1* expression is slightly reduced (Fernandes & Sá-Correia, 2003; Viegas *et al.*, 1995; Viegas *et al.*, 1994). In *F. oxysporum*, *pma2* expression appears to be negligible, since we found that it was 25,000 times lower than that of the *pma1* gene, suggesting it does not have a relevant role. Interestingly,

the expression and activity of Pma1 in *pma2*Δ mutants was slightly increased suggesting a potential feedback mechanism between these two ATPases as previously reported with V-ATPase, whose acute loss resulted in rapid ubiquitination and endocytosis of Pma1 from the PM (Smardon & Kane, 2014). These data indicate that in addition to being the main regulator of $pH_c$ homeostasis, Pma1 could function as a compensation mechanism for the loss of other cell ATPases.

## 4. How does loss of Pma2 influence the physiological processes of *Fusarium oxysporum*?

According to its low expression at the basal level, Pma2 showed also to be non-essential for fungal growth in *F. oxysporum.* Similarly, in the basidiomycete *Ustilago maydis* and the ascomycete *Colletotrichum higginsianum,* deletion of *pma2* had no effect on growth or basal metabolism (Korn *et al.*, 2015; Vázquez-Carrada *et al.*, 2022). However, we found that, and acid medium, the loss of *pma2* promoted growth of *F. oxysporum.* A similar effect was reported in *S. cerevisiae,* where single point mutations within the *pma2* gene allowed the yeast to grow at pH 4,0 (Morsomme *et al.*, 1998). Increased resistance to acidic conditions was due to a slight increase in Pma1 activity in the *pma2* mutants (Morsomme *et al*., 1998). Indeed, overexpression of Pma1 in *S. cerevisae* enhanced tolerance to weak acid and ethanol (Lee *et al.*, 2017). A possible explanation for this phenomenon is that increased Pma1 activity in these mutants could more rapidly correct intracellular acidification triggered by these acids, resulting in increased growth rates.

In addition, Pma2 has been shown to be important for resistance to osmotic and membrane stresses as well as for adaptation to toxic manganese concentrations. Whole genome analysis of the ascomycete black yeast *Hortaea werneckii* isolated from hypersaline water of a solar saltern show to have duplication of both *pma1* and *pma2* genes, although the transcriptional profile of these genes was dependent the salinity condition. While the *pma1* transcript levels dropped around 75% at higher salinity (3M NaCl) where growth begins to slow down, those of *pma2* were increased (Lenassi *et al.*, 2013). In contrast, in *F. oxysporum* no greater sensitivity to osmotic stress was observed in the *pma2*Δ mutant, perhaps due to the lower concentrations tested (1,2 M). In *S. cerevisiae,* a transcriptome analysis also revealed an up-regulation of *pma2* during adaptation to toxic manganese concentration. The authors

proposed a model in which the up-regulation of *pma2* is fundamental to energize the PM, a phenomenon needed to counteract manganese toxicity (Andreeva *et al.*, 2017). Some stress factors cause an increase in PM permeability, leading to a decrease in PM potential (Δψ), which might act as a primary cellular stress signal (Moskvina *et al.*, 1999). This hypothesis could explain the observed *pma2*Δ phenotype to CFW sensitivity in *F. oxysporum*. Although the activity of Pma1 is slightly increased, both ATPases differ in their biochemical characteristics and thus could respond differently to different stimuli such as ambient acidification, Mn excess or the cell wall stress.

Pma2 was also shown to be up-regulated specifically during appressorium formation and plant infection (Franck *et al.*, 2013; Korn *et al.*, 2015). A deletion mutant of *C. higginsianum* lacking *pma2* failed to induce plant defense and to penetrate the epidermis of the host plant, although the mutants formed fully melanized appressoria after inoculation and showed hyphal growth inside a cellulose membrane comparable to the wild type strain (Korn *et al.*, 2015). This suggests that Pma2 is important during the penetration stage. In *M. oryzae*, *pma2* expression was up-regulated by ammonia (Franck *et al.*, 2013), suggesting that *pma2* may be activated by pathogen-induced alkalinization. Oppositely, we found that in *F. oxysporum*, where alkalinization during infection plays a major role, the *pma2*Δ mutant is not affected in pathogenicity. However, our results suggested that Pma2 could be important at early stages of infection process as it prevents penetration at acidic pH, which could indicate a new undescribed role for this ATPase in fungal plant pathogens.

## 5. Regulators of Pma1 activity play a major role in controlling cellular functions

Pma1 activity is mainly regulated at the posttranscriptional level. Therefore, the study of proteins regulating Pma1 activity could be fundamental to understand Pma1 involvement in key cellular processes, such as growth and regulation of $pH_c$ homeostasis. In *S. cerevisiae,* loss of Ck1 increased Pma1 activity in starved cells by inducing phosphorylation of the Pma1 Ser-507 residue (Estrada *et al.*, 1996). Here we found that Pma1 proteins of filamentous fungi, including *F. oxysporum,* contain a conserved Thr residue at the analogous position, together with a casein kinase consensus phosphorylation motif (Agostinis *et al.*, 1989; Marin *et al.*, 1994). Furthermore, we discovered that Ck1 negatively regulates the $H^+$-ATPase activity in

*F. oxysporum,* suggesting that the phosphorylation of Pma1 by Ck1 is conserved in filamentous fungi. Interestingly, the *ck1*Δ mutants exhibited a strong reduction in growth rate and severe conidiation defects. These findings are in line with the compact and reduced colony growth phenotype previously reported for *ck1*Δ mutants of the human fungal pathogen *C. neoformans* and wheat scab pathogen *F. graminearum* (Wang *et al.*, 2011; Zhu *et al.*, 2022). Meanwhile, a mutant in the Ck1 homolog *yck2* in *C. albicans* was defective in hyphal growth under inducing conditions, forming chains of elongated yeast cells similar to pseudo-hyphae (Jung *et al.*, 2017). Similar conidiation defects as in *F. oxysporum ck1*Δ were observed in *ck1*Δ mutants of *M. oryzae* and *F. graminearum* (Shi *et al.*, 2019; Zhang *et al.*, 2014; Zhu *et al.*, 2022). Overall, these results suggest that Ck1 plays a largely conserved role in polar hyphal extension, particularly on solid media, as well as in conidiation.

Our result further showed that *ck1*Δ exhibited increased sensitivity to SDS and hyperosmotic stress. In line with this, a previous study in *C. neoformans* suggested that Ck1 regulates the expression and phosphorylation of the MAPKs Mpk1 and Hog1 under cell wall integrity and osmotic stress (Wang *et al.*, 2011). Besides, the *C. albicans yck2*Δ/*yck2*Δ strain was also hypersensitive to SDS, but in contrast to *F. oxysporum*, this mutant also showed increased sensitivity to CR and CFW (Jung *et al.*, 2017). This suggests an important role of Ck1 in fungal stress responses, although its contribution appears to be different between different species.

Pma1 has been described as the main regulator of $pH_c$ homeostasis, but its link with changes in ambient pH has not been addressed so far. Interestingly, we found that fungus-induced extracellular alkalinization during colony growth was lost in the *F. oxysporum ck1*Δ mutant. Furthermore, the *ck1*Δ mutant exhibited an increased resistance to acids induced cell death [Figure 79] as previously described in *S. cerevisiae* (Lee *et al.*, 2017). Different concentrations of acids added to exponentially growing *S. cerevisiae* cells shown to induce cell death exhibiting apoptosis-like features such as chromatin condensation along the nuclear envelope, exposure of PS on the outer leaflet of the PM, or DNA fragmentation (Giannattasio *et al.*, 2005; Malakar *et al.*, 2008). Importantly, we found that a *ck1*Δ mutant in *F. oxysporum* also showed an increased resistance to acetic acid (AA), which was stronger than when fungal cells were exposed to HCl. Particularly, we found that *ck1*Δ mutant cells exposed to HCl only showed increase resistance high until 30 minutes treatment in

an one hour experiment. The overactivity of Pma1 in the *ck1*Δ mutant can possibly compensate the cytosolic acidification triggered by acid compounds, which could lead to an enhanced tolerance to these conditions.

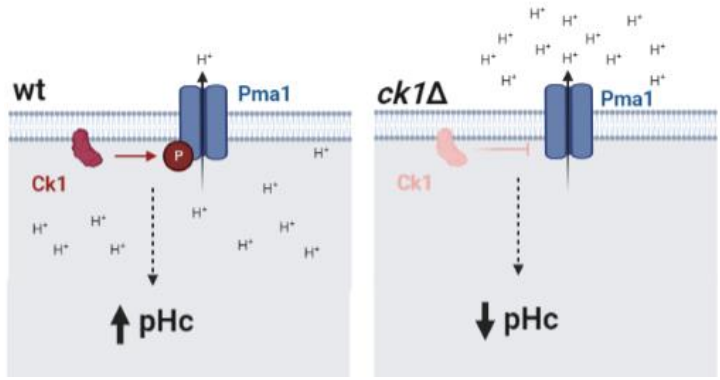


**Figure 79. Ck1 negatively regulates Pma1 H⁺-ATPase Pma1 activity in *F. oxysporum.*** Pma1 pumps protons out of the cell, establishing an electrochemical gradient across the PM by hydrolyzing ATP. The *ck1*Δ mutant exhibits higher Pma1 activity that confers increased resistant to acid-induced cell death.

*F. oxysporum,* similarly to other fungi, exhibits robust $pH_c$ homeostasis (Orij *et al.*, 2009; Valkonen *et al.*, 2014). Even upon extreme shifts in extracellular pH followed by a rapid oscillation in $pH_c$, the value returns to homeostatic levels after one hour (Fernandes *et al.*, 2022a), suggesting the presence of an efficient cellular mechanism of $pH_c$ control. This is of biological relevance as fungal pathogens are constantly exposed to oscillations in the surrounding ambient pH. Therefore, these organisms require a robust homeostatic mechanism to maintain $pH_c$ at constant levels in order to survive, proliferate and invade the host. Considering our aim of evaluating the effect of different regulators on $pH_c$ dynamics, we used the genetically encoded ratiometric pH sensor pHluorin, previously reported in *F. oxysporum* (Fernandes *et al.*, 2022b). Contrary to expectations, $pH_c$ was substantially lower in the *ck1*Δ mutant than in original *F. oxysporum* strain. Meanwhile, loss of the kinase Ptk2, described as a positive regulator of Pma1 in yeast, triggered an increase on $pH_c$ of around 1,3 units when compared with original strain. These unexpected findings could be due to a compensatory effect of other ATPases such as the vacuolar ATPase, whose activity was shown to be regulated in response to cytosolic and ambient pH in coordination with the $H^+$-ATPase Pma1 (Kane, 2016; Martínez-Muñoz & Kane, 2017). Indeed, we

found that the application of a specific inhibitor of the vacuolar $H^+$-ATPase, Concanamycin A (Huss *et al.*, 2002), induced a decrease of $pH_c$ in *F. oxysporum.* However, the *ck1*Δ mutant displayed a similar vacuolar pH to the wild type strain, indicating that the cytosolic acidification observed in the *ck1*Δ mutant is not due to a reduced V-ATPase activity as a compensatory mechanism.

In addition to the $H^+$-ATPases Pma1 and V-ATPase, a class of transporters that has been shown to play a significant role in $pH_c$ comprises the alkali cation/$H^+$ transporters. The main source of energy for these secondary transporters is provided by the proton gradients generated by the ATPases (Ariño *et al.*, 2019). Pma1 is considered to be the major generator of PM potential (Δψ) and V-ATPase in the vacuolar membrane is responsible for acidification of this organelle and generation of the Δψ over the membranes of the vacuole, Golgi and late endosomes. The $K^+$ transporters Trk1 and Trk2 functioning is highly dependent of the Δψ. These $K^+$ transporters have been implicated in $pH_c$ homeostasis (Yenush, 2016; Yenush *et al.*, 2002), but other $Na^+/H^+$ antiporters distributed across cell membranes such as Nha1 (in the PM), Kha1 (in the Golgi membrane), or Nhx1 (in late endosome) were also shown to have a smaller, but significant role in $pH_c$ regulation. The loss of Nha1 led to increased $pH_c$ (Ariño *et al.*, 2010; Sychrová *et al.*, 1999), while the *kha1*Δ mutants exhibited cytosolic acidification coincident with internal Golgi alkalinization (Ramírez *et al.*, 1998) and *nhx1* Δ mutants showed a decreased $pH_c$ as well as increased salt sensitivity (Brett *et al.*, 2005). In addition, mutants in Nhx1 were defective in trafficking linked with $pH_c$ homeostasis (Mukherjee *et al.*, 2006). Furthermore, two exchangers were also identified in the vacuolar membrane: Vnx1 was shown to exchange both $Na^{2+}$ /$K^+$ cations for $H^+$ (Cagnac *et al.*, 2020; Cagnac *et al.*, 2007) while Vcx1p functions as $Ca^{2+}$ /$K^+$ exchanger for $H^+$ (Cagnac *et al.*, 2010). Besides these, the fungal cell possess many more transporters which are pH dependent, such as the putative $Cl^-$ /$H^+$ antiporter Gef1 (Braun *et al.*, 2010) and various nutrient/$H^+$ symporters (Canadell & Ariño, 2016), but their role in $pH_c$ regulation remains to be elucidated

[Figure 80]. Alterations in the expression and activity of these transporters might also affect $pH_c$ homeostasis in the *ck1*Δ mutant.

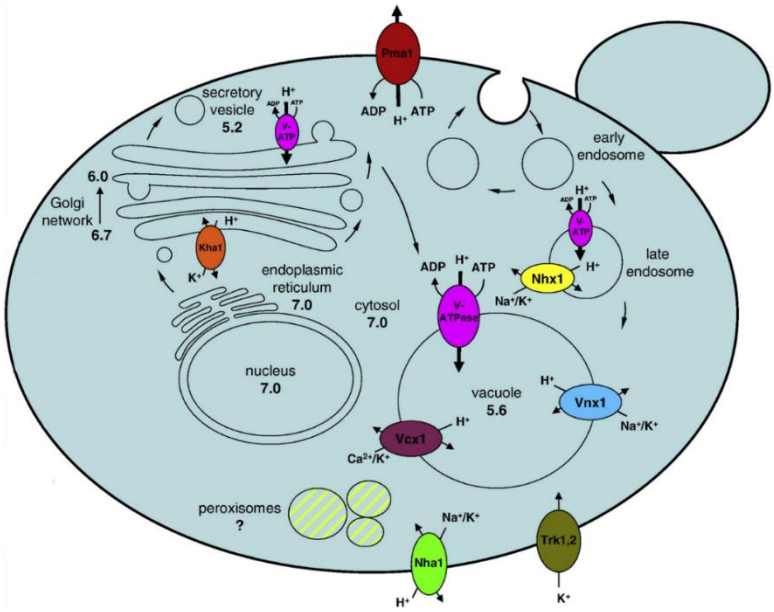


**Figure 80. Contributors to pH regulation.** The two main contributors to the building of Δψ by export of protons against the gradient at the cost of ATP are the Pma2 in the PM and V-ATPase in various organellar membranes. The alkali cation/$H^+$ exchangers in the PM (Nha1) and various organellar membranes (Vnx1, Vcx1,Nhx1, Kha1) as well as $K^+$ Trk1,2 use the energy stored in the Δψ to symport or transport ions and contribute to $pH_c$ homeostasis (Orij et al., 2011).

Despite the defect in growth ability of ck1 mutants conserved in different fungi (Jung *et al.*, 2017; Shi *et al.*, 2019; Wang *et al.*, 2011; Zhu *et al.*, 2022), no plausible explanation has been provided so far. The cytosolic acidification observed in the *F. oxysporum ck1*Δ mutant in this work sheds new light on the possible mechanisms underlying this defect in growth capacity. In yeast, a decrease in $pH_c$ triggers the release of the transcriptional repressor Opi1 which inhibits transcription of multiple phospholipid biosynthetic genes, thereby limiting membrane biosynthesis and, consequently, growth (Young *et al.*, 2010). Moreover, a decrease of $pH_c$ in *S. cerevisiae* causes inactivation of the Ras/PKA signaling pathway, which is essential for coordinating cell growth and proliferation with nutritional status (Dechant *et al.*, 2010).

The ortholog of the yeast Fus3/Kss1 MAPKs was shown to be crucial for infection of several fungal plant pathogens (Di Pietro *et al.*, 2001; Lev *et al.*, 1999;

Ruiz-Roldán *et al.*, 2001; Takano *et al.*, 2000; Zhao *et al.*, 2005). This MAPK was found to be crucial for infection-related functions such as invasive growth, vegetative hyphal fusion, root adhesion and virulence towards the tomato plant (Prados Rosales & Di Pietro, 2008; Turrà *et al.*, 2015). A critical first step in the course of *F. oxysporum* infection is the capacity to locate the plant roots in the soil, which relies on chemotropic sensing of root exudate released by the tomato root and is mediated by the conserved CWI MAPK Mpk1 (Turrà *et al.*, 2015). Here, we found that germ tubes can sense and direct growth towards a gradient of acid pH, but that the loss of Mpk1 impairs acid-triggered tropism, directing growth towards alkali. Similarly, the *ck1*Δ mutant also exhibited an inverted chemotropism in the direction of alkali rather than acidic pH. This aberrant pH tropism could be a consequence to the increased activity of Pma1 in the *ck1*Δ mutant, leading to acidification of the surrounding hyphae that could interfere with Mpk1-mediated sensing of the acid pH gradient. Further supporting this idea, we observed that Mpk1 phosphorylation after a downshift of pH was impaired in this mutant.

Recently, a link between $pH_c$ homeostasis and fungal virulence has begun to emerge, since cytosolic acidification was shown to control MAPK activity in a manner similar to extracellular acidification (i.e. inhibition of Fmk1 and activation of Mpk1 and Hog1) (Fernandes *et al.*, 2022a). In line with the lower $pH_c$ observed in *ck1*Δ mutant, we observed that phosphorylation of the IG MAPK Fmk1 was markedly inhibited, leading to a reduced capacity to cross cellophane membranes and infect tomato plants. This effect on $pH_c$ could explain the conserved role of Ck1 in pathogenicity of different fungal species such as *C. neoformans*, *M. oryzae* and *F. graminearum* (Shi *et al.*, 2019; Wang *et al.*, 2011; Zhu *et al.*, 2022).

In *S. cerevisiae,* the small peptide Pmp1 was co-purified together with Pma1 and shown to enhance Pma1 $H^+$-ATPase activity (Navarre *et al.*, 1994; Navarre *et al.*, 1992). It has been shown that Pmp1 has a positively charged cytoplasmic domain that is able to specifically interact with PS lipids (Beswick *et al.*, 2011; Coic *et al.*, 2005), suggesting a role in locating Pma1 in the PM. Studies in *S. cerevisiae* revealed that Pma1 represents a major protein component of sphingolipid-enriched microdomains in the PM, called lipid or membrane raft (Bagnat *et al.*, 2001). Recently, Van't Kooster *et al.* (2020) reported that ergosterol is depleted from the periprotein lipidome of Pma1, whereas PS is enriched relative to the bulk PM (van 't Klooster *et al.*, 2020).

Furthermore, in the fungal pathogens *C. neoformans,* Pma1 is also fractionated into the membrane raft (Farnoud *et al.*, 2015), and the absence of ceramide synthase interferes with Pma1 activity and cell growth (Munshi *et al.*, 2018). Farnaud *et al.* (2014) reported that the inability of *C. neoformans* to degrade complex sphingolipids into phytoceramide resulted in significant inhibition of Pma1 by reduced oligomerization of the pump, causing hypersensitivity to acidic pH (Farnoud *et al.*, 2014).

How the Pmp1 peptide regulates and interacts with the membrane protein Pma1 remains elusive. We observed that loss of Pmp1 in *F. oxysporum* produced a slight increase in Pma1 activity, although it was not significant, suggesting that the interaction of Pmp1 with Pma1 does not regulate Pma1 function at least under the experimental conditions tested. However, we observed that *pmp1*Δ mutants show enhanced hyphal growth even at very acidic or alkaline pH, suggesting that Pmp1 could affect Pma1 localization at the PM, rather than the activity of this ATPase. On the other hand, the Pmp1 did not appear to be relevant for penetration through cellophane membranes or pathogenicity of *F. oxysporum*. Thus, the exact role of this peptide in filamentous fungi remains to be discovered.

## 6. Pma1 regulates fungal development and pathogenicity of *Fusarium oxysporum*

Most studies had focused on regulation of Pma1 expression and activity to understand its role in different biological processes (Lee *et al.*, 2017; Li *et al.*, 2022; Mahmoud *et al.*, 2017). Some of these studies used specific inhibitors of this $H^+$-ATPase, such as DES and orthovanadate (Fernandes *et al.*, 2022a; Kahm *et al.*, 2012; Mahmoud *et al.*, 2017; Moskvina *et al.*, 1999), but these compounds irreversibly lead to death of the fungus, not allowing longer-time analysis to understand the role of Pma1 in biological processes.

Transcriptional profiling revealed that *pma1* expression increased upon exposure to AA (Lee *et al.*, 2015). Furthermore, ectopic *pma1* overexpression in *S. cerevisiae* improved tolerance not only to acetic acid or other weak acids such as benzoic-, propionic- or sorbic-acid, but also to oxidative stress and ethanol (Lee *et al.*, 2017). So far, few studies have addressed the role of Pma1 in $pH_c$ homeostasis control and pathogenicity in fungi. Therefore, we attempted to develop different

genetic approaches to study this ATPase in the plant pathogen *F. oxysporum*. As previously demonstrated, *pma1* overexpression in *F. oxysporum* caused increased tolerance to acids confirming the importance of Pma1 in regulation of acid responses. Global gene expression analysis in yeast cells overexpressing either the wild type or a dominant lethal *pma1* allele was shown to activate the Hog1 MAPK pathway (Eraso *et al.*, 2011). More recently, it was shown that ectopic *pma1* overexpression in yeast constitutively activates the Hog1 and the Stl2/Mpk1 MAPK cascades (Lee *et al.*, 2017). However, in our experiments we did not observe any difference in the acid-triggered Mpk1 activation in the *pma1* overexpressing strain when compared to the wild type strain. This could be a consequence of the high abundance of Pma1 in the PM and to its relatively long half-life (Benito *et al.*, 1991). For instance, increased total ATPase activity induced by glucose was shown to be caused by an increase in Pma1 catalytic activity rather than in the amount Pma1 protein itself (Eraso & Portillo, 1994). Changes in expression of Pma1 could not significantly affect its activity, which is mainly regulated at posttranslational level (Kane, 2016). Therefore, processes regulated by pH, such as MAPK signaling, invasive growth or virulence towards tomato plants, were not significantly altered in the overexpressing strain.

We further generated a temperature-sensitive *pma1* allele to attempt partial and/or reversible inhibition of this essential protein in *F. oxysporum*, as previously described in *S. cerevisiae* (Gong & Chang, 2001). In the yeast, the temperature-sensitive mutant Pma1-10, Pma1 was destroyed in a ubiquitin-dependent manner and delivered to vacuolar degradation after 30 minutes at the restrictive temperature (Gong & Chang, 2001; Liu & Chang, 2006). Oppositely, at the permissive temperature, Pma1-10 followed the secretory pathway and had sufficient catalytic activity to support growth when properly directed and stabilized at PM (Liu & Chang, 2006). In *F. oxysporum*, generation of a *pma1*-temperature sensitive strain by introducing the mutations A168G and V200I into Pma1, led to a delay on the colony growth even at permissive temperature, although this effect was more accentuated at restrictive temperature. Importantly, the growth rate at permissive temperature in liquid culture was not affected and the analysis of the $H^+$-ATPase activity showed no differences between the *pma1*$^{ts}$ mutant and Pma1 wild type, whereas after one hour at the restrictive temperature we observed an almost total block in $H^+$-ATPase activity in the *pma1*$^{ts}$ mutant. Interestingly, after 24 hours at the restrictive temperature, the *pma1*$^{ts}$

mutant recovered growth capacity in liquid medium similar to the wild type, suggesting that this allele provides a powerful tool to study the role of Pma1 in fungal developmental processes or in $pH_c$ homeostasis without causing irreversible cell death. We noted that the $H^+$-ATPase activity in the *F. oxysporum* wild type strain increased after a temperature rise to 37ºC, indicating that heat activates the catalytic Pma1 activity although the underlying mechanism remains unknown.

Our results also showed that the *pma1$^{ts}$* mutant exhibits increased sensitivity to the cell wall perturbing agent Calcofluor White (CFW) at permissive- and restrictive-temperature. In line with our results, silencing of *pma1* though RNA interference in *Penicillium digitatum* reduced the cell wall content of chitin and glucan and to increase the activity of some chitinases and glucanases (Li *et al.*, 2022). Chitin and glucan are the main components of the fungal cell wall and maintaining its stability an integrity (Sun *et al.*, 2019). Therefore, our results suggest that loss of Pma1 at the PM in the *pma1$^{ts}$* mutant can signal for changes at the CW, which could lead to increased sensitivity to cell wall disrupting agents in this mutant.

Our results of colony growth at different pH indicate that mutations in Pma1 might confer higher sensitivity to pH changes. Acidic pH induces cytosolic acidification and activates Pma1 activity (Fernandes *et al.*, 2022a; Zhao *et al.*, 2021). The two changes in Pma1-10, A165G and V197I, are predicted to reside in the transmembrane segments 2 and the coding region of the A-domain of the Pma1 protein [Figure 4C] (Zhao *et al.*, 2021). Although the activity of the PM hexamer Pma1 is determined by interaction between the R- and P-domain, the mutations in *pma1$^{ts}$* might interfere with the activation mechanism of Pma1 in response to acid pH.

Several studies suggest that Pma1 plays an important role in fungal growth and pathogenicity (Li *et al.*, 2022; Serrano *et al.*, 1986b; Wu *et al.*, 2022). For instance, Pma1 deletion in *F. graminearum* impaired fungal growth, pathogenicity and sexual and asexual development (Wu *et al.*, 2022). Silencing of the *pma1* gene in *P. digitatum* affected vegetative growth and pathogenicity (Li *et al.*, 2022). Our results show that partial loss of Pma1 function also inhibited growth and pathogenicity in *F. oxysporum.* Regarding pathogenicity, our results are in line with studies in the phytopathogenic fungus *Leptosphaeria maculans,* where reduction of Pma1 activity interferes with the electrochemical transmembrane gradient and leads to defective turgor pressure in

conidia at the host plant surface (Remy *et al.*, 2008). However, the function and regulation of this PM $H^+$-ATPase during infection is not completely clear. In *P. digitatum*, *pma1* silencing significantly decreased the activity of cell wall-degrading enzymes during infection of citrus fruits (Li *et al.*, 2022). On the other hand, loss of Pma1 in *F. graminearum* decreased the production of mycotoxins, impairing mycelial invasion and pathogenicity (Wu *et al.*, 2022).

Our hypothesis is that a reduction in Pma1 activity could lead to an accumulation of protons in the cytosol, thereby triggering cytosolic acidification. As demonstrated previously (Fernandes *et al.*, 2022a), a decrease in $pH_c$ inhibits the activation of the IG MAPK Fmk1, which could explain the decreased virulence of the *pma1$^{ts}$* mutant. Besides this hypothesis, it is important to note that the infection assay was performed at 28°C, which could partially affect growth of the *pma1$^{ts}$* mutant leading to decreased capability to infect tomato roots.

Membrane proteins have been implicated key cellular processes such as transport, cell signaling, energy transduction or cell adhesion. These proteins are embedded within a large complex environment essentially composed of a high variety of lipids and proteins. Lipids can strongly influence the structure, assembly, and function of membrane proteins through interactions especially at the interface with the membrane (Bogdanov *et al.*, 2014; Ernst *et al.*, 2010; Overduin & Esmaili, 2019). The coordination of the multiple cellular processes that occur at the PM requires a tight spatial organization into specialized domains, characterized by different size, stability and protein/lipid composition (Athanasopoulos *et al.*, 2019). Compartmentalization of the PM has been studied in detail in *S. cerevisiae*, including the membrane compartment containing the $H^+$-ATPase Pma1 (MCP), which is enriched in sphingolipids (van 't Klooster *et al.*, 2020). The transport and stabilization of Pma1 at the PM was independent of microtubules and cytoskeletal elements (Malinska *et al.*, 2004). More recently, loss of the primary PS flippase Drs2, which is localized to the transmembrane Golgi network (TGN), was shown to cause missorting of around 25% of Pma1 to the vacuole, as well as mislocalization of the membrane compartments containing Pma1 (MCP) and the arginine permease Can1 (MCC), due to a defect in sorting at the TGN (Hankins *et al.*, 2015).

The Pma1 protein is stable at the PM and shows lateral diffusion (Fajardo-Somera *et al.*, 2013; Malínská *et al.*, 2003; Rane *et al.*, 2019). In the ascomycete *N. crassa,* Pma1 is evenly distributed throughout the PM in conidia, while in mature hyphae it is localized in sub-apical regions and in completed septa (Fajardo-Somera *et al.*, 2013). Similarly, we observed differential distribution of Pma1 in the fungal pathogens *F. oxysporum* and *C. albicans* with Pma1 being largely absent from the tip of the hyphae and following an upward gradient with increasing distance from the hyphal tip to the septum. Importantly, the gradient was conserved in all hyphae analyzed and the percentage of Pma1 coverage was independent of the total length of the hypha.

The mechanism by which Pma1 adopts a sub-apical arrangement in the PM is unknown. Fajardo-Somera *et al.* (2013) proposed that exocytosis occurs in distal regions of the hypha, following a kiss-and-run (K&R) mechanism which does not involve expansion of the PM. During K&R, proteins are released but the vesicles do not completely collapse, that is, the vesicle membrane does not fully fuse with the PM and does not supply to membrane expansion (Keighron *et al.*, 2012; Wen *et al.*, 2017). However, the mechanisms of K&R have not been identified in fungi.

The activity of Pma1 has been related to many physiological processes, such as growth and pathogenicity, but its location at the PM has not been linked to the regulation of these processes. In the human pathogen *C. albicans*, it was demonstrated that Pma1 plays a central role in the establishment of cell polarity and filamentation, showing also sub-apical distribution in mature hyphae (Rane *et al.*, 2019). In accordance with Pma1 localization and activity the protons would be pumped out mainly in the distal regions of the hypha, thus creating a pH gradient along the cytosol from the tip to the septum. Therefore, we decided to study whether the sub-apical localization of Pma1 in *F. oxysporum* could contribute to the establishment of a $pH_c$ gradient along the hyphal axis. To measure $pH_c$ we used strains expressing pHluorin previously reported for *F. oxysporum* (Fernandes *et al.*, 2022b) and *C. albicans* (Tournu *et al.*, 2017). Even though the $pH_c$ measured in the germlings treated with nigericin for the calculation of the calibration curve was homogeneous, the $pH_c$ in growing germ tubes calculated from confocal microscopy was quite uneven in the preliminary experiments. Interestingly, the $pH_c$ values obtained in these measurements are somewhat higher than those previously reported

in *F. oxysporum* and which were acquired by spectrofluorometry (Fernandes *et al.*, 2022a). This discrepancy may be a consequence of pHluorin not being uniformly distributed throughout the germ tube or of a photobleaching phenomenon in the acquired images. Nonetheless, preliminary results in *F. oxysporum* hyphae seem to indicate an ascending $pH_c$ gradient from the tip to the center of the hyphae. This is in line with an early study of cytosolic pH in *N. crassa* using the pH indicator bromocresol green, where apical zones had an acid pH, while the sub-apical regions presented a more alkaline pH (McGillviray & Gow, 1987). Further studies are required to fully characterize the role of sub-apical localization of the essential protein Pma1 and to determine whether its activity is able to generate a gradient along the PM of growing hyphae.

# Conclusions

# Conclusiones

## Conclusions

1. *Fusarium oxysporum* re-directs hyphal growth towards an acidic pH gradient in a Mpk1-dependent manner.
2. The sphingolipid dihydrosphingosine acts as a signal to activate the CWI MAPK cascade and as a dose-dependent chemoattractant.
3. Loss of the Pma2 $H^+$-ATPase isoform leads to a slight increase of transcript levels and activity of Pma1 which improves growth at acidic pH.
4. Pma2 contributes to membrane stress resistance and to adaptation to toxic manganese concentrations.
5. Loss of the casein kinase Ck1 leads to a 3-fold increase in Pma1 activity, accompanied by extracellular acidification and increased resistance to acid-triggered cell death.
6. Loss of Ck1 causes a decrease of $pH_c$, which correlates with impaired Fmk1 phosphorylation, invasive growth and capacity of infect tomato plants.
7. The peptide Pmp1 regulates fungal growth at highly acidic- and alkaline-pH but is not relevant for pathogenicity.
8. Overexpression of *pma1* causes increased acid tolerance but has no detectable effect on the regulation of MAPKs.
9. Expression of a *pma1*$^{ts}$ allele leads to a delay on growth and almost complete inhibition of $H^+$-ATPase activity at the restrictive temperature.
10. The partial loss of Pma1 activity in the *pma1*$^{ts}$ mutant causes a delay in plant infection.
11. Distribution of Pma1 along the plasma membrane shows an upward gradient with increasing distance from the hyphal tip in the fungal pathogens *F. oxysporum* and *C. albicans.*

## Conclusiones

1. *Fusarium oxysporum* redireccionan el crecimiento de la hifa hacia un pH ácido de manera dependiente de la vía de señalización Mpk1.
2. El esfingolípido dihidroesfingosina actúa como señal en la activación de la cascada MAPK Mpk1 y como quimioatrayente dependiente de la dosis.
3. La pérdida de la isoforma $H^+$-ATPasa Pma2 conduce a un ligero aumento de los niveles de transcripción y actividad de Pma1, lo cual mejora el crecimiento en pH ácido.
4. Pma2 contribuye a la resistencia al estrés de la membrana y a la adaptación a la concentración tóxica de manganeso.
5. La pérdida de la caseína quinasa Ck1 aumentó 3 veces la actividad de Pma1, acompañada de una acidificación extracelular y aumento de la resistencia a la muerte celular provocada por ácido.
6. La pérdida de Ck1 provocó una disminución en la homeostasis de $pH_c$ que se correlaciona con un defecto en la fosforilación de Fmk1, crecimiento invasivo y capacidad de infectar la planta de tomate.
7. El péptido Pmp1 regula el crecimiento fúngico incluso a pH altamente ácido y alcalino, pero no es relevante para la patogenicidad.
8. La sobreexpresión de *pma1* causa una mayor tolerancia a compuestos ácidos, pero no tiene ningún efecto detectable en la regulación de las MAPKs.
9. La expresión de un alelo *pma1*$^{ts}$ conduce un retraso en el crecimiento y casi la completa inhibición de la actividad de la $H^+$-ATPasa a temperatura restrictiva.
10. La pérdida parcial de actividad Pma1, en el mutante *pma1*$^{ts}$, conduce un retraso en la infición de la planta.
11. La distribución de Pma1 a lo largo de la membrana plasmática muestra un gradiente ascendente desde el extremo de la hifa en los patógenos fúngicos *F. oxysporum* y *C. albicans.*

# References

## References


Agostinis, P., Pinna, L. A., Meggio, F., Marin, O., Goris, J., Vandenheede, J. R., & Merlevede, W. (1989). A synthetic peptide substrate specific for casein kinase I. *FEBS Lett*, *259*(1), 75-78. https://doi.org/10.1016/0014-5793(89)81498-x

Alkan, N., Espeso, E. A., & Prusky, D. (2013). Virulence regulation of phytopathogenic fungi by pH. *Antioxid Redox Signal*, *19*(9), 1012-1025. https://doi.org/10.1089/ars.2012.5062

Ambesi, A., Miranda, M., Petrov, V. V., & Slayman, C. W. (2000). Biogenesis and function of the yeast plasma-membrane H(+)-ATPase. *J Exp Biol*, *203*(Pt 1), 155-160. https://doi.org/10.1242/jeb.203.1.155

Andreeva, N., Kulakovskaya, E., Zvonarev, A., Penin, A., Eliseeva, I., Teterina, A., Lando, A., Kulakovskiy, I. V., & Kulakovskaya, T. (2017). Transcriptome profile of yeast reveals the essential role of PMA2 and uncharacterized gene YBR056W-A (MNC1) in adaptation to toxic manganese concentration. *Metallomics*, *9*(2), 175-182. https://doi.org/10.1039/c6mt00210b

Ariño, J., Ramos, J., & Sychrova, H. (2019). Monovalent cation transporters at the plasma membrane in yeasts. *Yeast*, *36*(4), 177-193. https://doi.org/10.1002/yea.3355

Ariño, J., Ramos, J., & Sychrová, H. (2010). Alkali metal cation transport and homeostasis in yeasts. *Microbiol Mol Biol Rev*, *74*(1), 95-120. https://doi.org/10.1128/mmbr.00042-09

Arneborg, N., Jespersen, L., & Jakobsen, M. (2000). Individual cells of *Saccharomyces cerevisiae* and *Zygosaccharomyces bailii* exhibit different short-term intracellular pH responses to acetic acid. *Arch Microbiol*, *174*(1-2), 125-128. https://doi.org/10.1007/s002030000185

Athanasopoulos, A., Andre, B., Sophianopoulou, V., & Gournas, C. (2019). Fungal plasma membrane domains. *FEMS Microbiol Rev*, *43*(6), 642-673. https://doi.org/10.1093/femsre/fuz022

Bagar, T., Altenbach, K., Read, N. D., & Bencina, M. (2009). Live-Cell imaging and measurement of intracellular pH in filamentous fungi using a genetically encoded ratiometric probe. *Eukaryot Cell*, *8*(5), 703-712. https://doi.org/10.1128/ec.00333-08

Bagnat, M., Chang, A., & Simons, K. (2001). Plasma membrane proton ATPase Pma1p requires raft association for surface delivery in yeast. *Mol Biol Cell*, *12*(12), 4129-4138. https://doi.org/10.1091/mbc.12.12.4129

Bagnat, M., Keränen, S., Shevchenko, A., Shevchenko, A., & Simons, K. (2000). Lipid rafts function in biosynthetic delivery of proteins to the cell surface in yeast. *Proc Natl Acad Sci U S A*, *97*(7), 3254-3259. https://doi.org/10.1073/pnas.97.7.3254

Baron, J. A., Chen, J. S., & Culotta, V. C. (2015). Cu/Zn superoxide dismutase and the proton ATPase Pma1p of *Saccharomyces cerevisiae*. *Biochem Biophys Res Commun*, *462*(3), 251-256. https://doi.org/10.1016/j.bbrc.2015.04.127

Bartnicki-Garcia, S., Bartnicki, D. D., Gierz, G., López-Franco, R., & Bracker, C. E. (1995). Evidence that Spitzenkörper behavior determines the shape of a fungal hypha: a test of the hyphoid model. *Exp Mycol*, *19*(2), 153-159. https://doi.org/10.1006/emyc.1995.1017

Benito, B., Moreno, E., & Lagunas, R. (1991). Half-life of the plasma membrane ATPase and its activating system in resting yeast cells. *Biochim Biophys Acta*, *1063*(2), 265-268. https://doi.org/10.1016/0005-2736(91)90381-h

Berchtold, D., Piccolis, M., Chiaruttini, N., Riezman, I., Riezman, H., Roux, A., Walther, T. C., & Loewith, R. (2012). Plasma membrane stress induces relocalization of Slm proteins and activation of TORC2 to promote sphingolipid synthesis. *Nat Cell Biol*, *14*(5), 542-547. https://doi.org/10.1038/ncb2480

Bertuzzi, M., Schrettl, M., Alcazar-Fuoli, L., Cairns, T. C., Muñoz, A., Walker, L. A., Herbst, S., Safari, M., Cheverton, A. M., Chen, D., Liu, H., Saijo, S., Fedorova, N. D., Armstrong-James, D., Munro, C. A., Read, N. D., Filler, S. G., Espeso, E. A., Nierman, W. C., . . . Bignell, E. M. (2014). The pH-responsive PacC transcription factor of *Aspergillus fumigatus* governs epithelial entry and tissue invasion during pulmonary aspergillosis. *PLoS Pathog*, *10*(10), e1004413. https://doi.org/10.1371/journal.ppat.1004413

Beswick, V., Isvoran, A., Nedellec, P., Sanson, A., & Jamin, N. (2011). Membrane interface composition drives the structure and the tilt of the single transmembrane helix protein PMP1: MD studies. *Biophys J*, *100*(7), 1660-1667. https://doi.org/10.1016/j.bpj.2011.02.002

Bi, F., Barad, S., Ment, D., Luria, N., Dubey, A., Casado, V., Glam, N., Mínguez, J. D., Espeso, E. A., Fluhr, R., & Prusky, D. (2016). Carbon regulation of environmental pH by secreted small molecules that modulate pathogenicity in phytopathogenic fungi. *Mol Plant Pathol*, *17*(8), 1178-1195. https://doi.org/10.1111/mpp.12355

Bianchi, F., Syga, Ł., Moiset, G., Spakman, D., Schavemaker, P. E., Punter, C. M., Seinen, A. B., van Oijen, A. M., Robinson, A., & Poolman, B. (2018). Steric exclusion and protein conformation determine the localization of plasma membrane transporters. *Nat Commun*, *9*(1), 501. https://doi.org/10.1038/s41467-018-02864-2

Biju, V. C., Fokkens, L., Houterman, P. M., Rep, M., & Cornelissen, B. J. C. (2017). Multiple evolutionary trajectories have led to the emergence of races in *Fusarium oxysporum* f. sp. *lycopersici*. *Appl Environ Microbiol*, *83*(4). https://doi.org/10.1128/aem.02548-16

Blackburn, M. R., Haruta, M., & Moura, D. S. (2020). Twenty Years of Progress in Physiological and Biochemical Investigation of RALF Peptides. *Plant Physiol*, *182*(4), 1657-1666. https://doi.org/10.1104/pp.19.01310

Bogdanov, M., Dowhan, W., & Vitrac, H. (2014). Lipids and topological rules governing membrane protein assembly. *Biochim Biophys Acta*, *1843*(8), 1475-1488. https://doi.org/10.1016/j.bbamcr.2013.12.007

Both, M., Eckert, S. E., Csukai, M., Müller, E., Dimopoulos, G., & Spanu, P. D. (2005). Transcript profiles of *Blumeria graminis* development during infection reveal a cluster of genes that are potential virulence determinants. *Mol Plant Microbe Interact*, *18*(2), 125-133. https://doi.org/10.1094/mpmi-18-0125

Bouillet, L. E., Cardoso, A. S., Perovano, E., Pereira, R. R., Ribeiro, E. M., Trópia, M. J., Fietto, L. G., Tisi, R., Martegani, E., Castro, I. M., & Brandão, R. L. (2012). The involvement of calcium carriers and of the vacuole in the glucose-induced calcium signaling and activation of the plasma membrane H(+)-ATPase in *Saccharomyces cerevisiae* cells. *Cell Calcium*, *51*(1), 72-81. https://doi.org/10.1016/j.ceca.2011.10.008

Braun, N. A., Morgan, B., Dick, T. P., & Schwappach, B. (2010). The yeast CLC protein counteracts vesicular acidification during iron starvation. *J Cell Sci*, *123*(Pt 13), 2342-2350. https://doi.org/10.1242/jcs.068403

Brett, C. L., Tukaye, D. N., Mukherjee, S., & Rao, R. (2005). The yeast endosomal Na+K+/H+ exchanger Nhx1 regulates cellular pH to control vesicle trafficking. *Mol Biol Cell*, *16*(3), 1396-1405. https://doi.org/10.1091/mbc.e04-11-0999

Burgstaller, W. (1997). Transport of small lons and molecules through the plasma membrane of filamentous fungi. *Crit Rev Microbiol*, *23*(1), 1-46. https://doi.org/10.3109/10408419709115129

Cagnac, O., Aranda-Sicilia, M. N., Leterrier, M., Rodriguez-Rosales, M. P., & Venema, K. (2010). Vacuolar cation/H+ antiporters of *Saccharomyces cerevisiae*. *J Biol Chem*, *285*(44), 33914-33922. https://doi.org/10.1074/jbc.M110.116590

Cagnac, O., Baghour, M., Jaime-Pérez, N., Aranda-Sicilia, M. N., Sánchez-Romero, M. E., Rodríguez-Rosales, M. P., & Venema, K. (2020). Deletion of the N-terminal domain of the yeast vacuolar (Na(+) ,K(+) )/H(+) antiporter Vnx1p improves salt tolerance in yeast and transgenic *Arabidopsis*. *Yeast*, *37*(1), 173-185. https://doi.org/10.1002/yea.3450

Cagnac, O., Leterrier, M., Yeager, M., & Blumwald, E. (2007). Identification and characterization of Vnx1p, a novel type of vacuolar monovalent cation/H+ antiporter of *Saccharomyces cerevisiae*. *J Biol Chem*, *282*(33), 24284-24293. https://doi.org/10.1074/jbc.M703116200

Calcagno-Pizarelli, A. M., Negrete-Urtasun, S., Denison, S. H., Rudnicka, J. D., Bussink, H. J., Múnera-Huertas, T., Stanton, L., Hervás-Aguilar, A., Espeso, E. A., Tilburn, J., Arst, H. N., Jr., & Peñalva, M. A. (2007). Establishment of the ambient pH signaling complex in *Aspergillus nidulans*: PalI assists plasma membrane localization of PalH. *Eukaryot Cell*, *6*(12), 2365-2375. https://doi.org/10.1128/ec.00275-07

Canadell, D., & Ariño, J. (2016). Interactions Between Monovalent Cations and Nutrient Homeostasis. *Adv Exp Med Biol*, *892*, 271-289. https://doi.org/10.1007/978-3-319-25304-6_11

Cantrell, S. A., Dianese, J. C., Fell, J., Gunde-Cimerman, N., & Zalar, P. (2011). Unusual fungal niches. *Mycologia*, *103*(6), 1161-1174. https://doi.org/10.3852/11-108

Carmelo, V., Santos, H., & Sá-Correia, I. (1997). Effect of extracellular acidification on the activity of plasma membrane ATPase and on the cytosolic and vacuolar pH of Saccharomyces cerevisiae. *Biochim Biophys Acta*, *1325*(1), 63-70. https://doi.org/10.1016/s0005-2736(96)00245-3

Casamayor, A., Torrance, P. D., Kobayashi, T., Thorner, J., & Alessi, D. R. (1999). Functional counterparts of mammalian protein kinases PDK1 and SGK in budding yeast. *Curr Biol*, *9*(4), 186-197. https://doi.org/10.1016/s0960-9822(99)80088-8

Catlett, N. L., Lee, B.-N., Yoder, O. C., & Turgeon, B. G. (2003). Split-Marker Recombination for Efficient Targeted Deletion of Fungal Genes. *Fungal Genetics Reports*, *50*(1), 9-11. https://doi.org/10.4148/1941-4765.1150

Causton, H. C., Ren, B., Koh, S. S., Harbison, C. T., Kanin, E., Jennings, E. G., Lee, T. I., True, H. L., Lander, E. S., & Young, R. A. (2001). Remodeling of yeast genome expression in response to environmental changes. *Mol Biol Cell*, *12*(2), 323-337. https://doi.org/10.1091/mbc.12.2.323

Cervantes-Chávez, J. A., Ortiz-Castellanos, L., Tejeda-Sartorius, M., Gold, S., & Ruiz-Herrera, J. (2010). Functional analysis of the pH responsive pathway Pal/Rim in the phytopathogenic basidiomycete Ustilago maydis. *Fungal Genet Biol*, *47*(5), 446-457. https://doi.org/10.1016/j.fgb.2010.02.004

Chen, G., Liu, X., Zhang, L., Cao, H., Lu, J., & Lin, F. (2013). Involvement of MoVMA11, a Putative Vacuolar ATPase c' Subunit, in Vacuolar Acidification and Infection-Related Morphogenesis of *Magnaporthe oryzae*. *PLoS One*, *8*(6), e67804. https://doi.org/10.1371/journal.pone.0067804

Chen, R. E., & Thorner, J. (2007). Function and regulation in MAPK signaling pathways: lessons learned from the yeast *Saccharomyces cerevisiae*. *Biochim Biophys Acta*, *1773*(8), 1311-1340. https://doi.org/10.1016/j.bbamcr.2007.05.003

Chen, Y., Li, B., Xu, X., Zhang, Z., & Tian, S. (2018). The pH-responsive PacC transcription factor plays pivotal roles in virulence and patulin biosynthesis in *Penicillium expansum*. *Environ Microbiol*, *20*(11), 4063-4078. https://doi.org/10.1111/1462-2920.14453

Coic, Y. M., Vincent, M., Gallay, J., Baleux, F., Mousson, F., Beswick, V., Neumann, J. M., & de Foresta, B. (2005). Single-spanning membrane protein insertion in membrane mimetic systems: role and localization of aromatic residues. *Eur Biophys J*, *35*(1), 27-39. https://doi.org/10.1007/s00249-005-0002-1

Couteaudier, Y., & Alabouvette, C. (1990). Survival and inoculum potential of conidia and chlamydospores of *Fusarium oxysporum* f.sp. *lini* in soil. *Can J Microbiol*, *36*(8), 551-556. https://doi.org/10.1139/m90-096

Croxen, M. A., Sisson, G., Melano, R., & Hoffman, P. S. (2006). The *Helicobacter pylori* chemotaxis receptor TlpB (HP0103) is required for pH taxis and for colonization of the gastric mucosa. *J Bacteriol*, *188*(7), 2656-2665. https://doi.org/10.1128/jb.188.7.2656-2665.2006

Danhof, H. A., & Lorenz, M. C. (2015). The *Candida albicans* ATO gene family promotes neutralization of the macrophage phagolysosome. *Infect Immun*, *83*(11), 4416-4426. https://doi.org/10.1128/iai.00984-15

Davidzon, M., Alkan, N., Kobiler, I., & Prusky, D. (2010). Acidification by gluconic acid of mango fruit tissue during colonization via stem end infection by Phomopsis mangiferae. *Postharvest Biology and Technology*, *55*(2), 71-77. https://doi.org/https://doi.org/10.1016/j.postharvbio.2009.08.009

Davis, D. A. (2009). How human pathogenic fungi sense and adapt to pH: the link to virulence. *Curr Opin Microbiol*, *12*(4), 365-370. https://doi.org/10.1016/j.mib.2009.05.006

Day, A. M., Herrero-de-Dios, C. M., MacCallum, D. M., Brown, A. J. P., & Quinn, J. (2017). Stress-induced nuclear accumulation is dispensable for Hog1-dependent gene expression and virulence in a fungal pathogen. *Sci Rep*, *7*(1), 14340. https://doi.org/10.1038/s41598-017-14756-4

Day, A. M., McNiff, M. M., da Silva Dantas, A., Gow, N. A. R., & Quinn, J. (2018). Hog1 regulates stress tolerance and virulence in the emerging fungal pathogen *Candida auris*. *mSphere*, *3*(5). https://doi.org/10.1128/mSphere.00506-18

Dean, R., Van Kan, J. A., Pretorius, Z. A., Hammond-Kosack, K. E., Di Pietro, A., Spanu, P. D., Rudd, J. J., Dickman, M., Kahmann, R., Ellis, J., & Foster, G. D. (2012). The Top 10 fungal pathogens in molecular plant pathology. *Mol Plant Pathol*, *13*(4), 414-430. https://doi.org/10.1111/j.1364-3703.2011.00783.x

Dechant, R., Binda, M., Lee, S. S., Pelet, S., Winderickx, J., & Peter, M. (2010). Cytosolic pH is a second messenger for glucose and regulates the PKA pathway through V-ATPase. *Embo j*, *29*(15), 2515-2526. https://doi.org/10.1038/emboj.2010.138

Dechant, R., Saad, S., Ibáñez, A. J., & Peter, M. (2014). Cytosolic pH regulates cell growth through distinct GTPases, Arf1 and Gtr1, to promote Ras/PKA and TORC1 activity. *Mol Cell*, *55*(3), 409-421. https://doi.org/10.1016/j.molcel.2014.06.002

deHart, A. K., Schnell, J. D., Allen, D. A., & Hicke, L. (2002). The conserved Pkh-Ypk kinase cascade is required for endocytosis in yeast. *J Cell Biol*, *156*(2), 241-248. https://doi.org/10.1083/jcb.200107135

Deprez, M. A., Eskes, E., Wilms, T., Ludovico, P., & Winderickx, J. (2018). pH homeostasis links the nutrient sensing PKA/TORC1/Sch9 ménage-à-trois to stress tolerance and longevity. *Microb Cell*, *5*(3), 119-136. https://doi.org/10.15698/mic2018.03.618

Devare, M. N., Kim, Y. H., Jung, J., Kang, W. K., Kwon, K. S., & Kim, J. Y. (2020). TORC1 signaling regulates cytoplasmic pH through Sir2 in yeast. *Aging Cell*, *19*(6), e13151. https://doi.org/10.1111/acel.13151

Di Pietro, A., García-MacEira, F. I., Méglecz, E., & Roncero, M. I. (2001). A MAP kinase of the vascular wilt fungus *Fusarium oxysporum* is essential for root penetration and pathogenesis. *Mol Microbiol*, *39*(5), 1140-1152.

Di Pietro, A., & Roncero, M. I. (1998). Cloning, expression, and role in pathogenicity of pg1 encoding the major extracellular endopolygalacturonase of the vascular wilt pathogen *Fusarium oxysporum*. *Mol Plant Microbe Interact*, *11*(2), 91-98. https://doi.org/10.1094/mpmi.1998.11.2.91

Diakov, T. T., & Kane, P. M. (2010). Regulation of vacuolar proton-translocating ATPase activity and assembly by extracellular pH. *J Biol Chem*, *285*(31), 23771-23778. https://doi.org/10.1074/jbc.M110.110122

Dolz-Edo, L., van der Deen, M., Brul, S., & Smits, G. J. (2019). Caloric restriction controls stationary phase survival through Protein Kinase A (PKA) and cytosolic pH. *Aging Cell*, *18*(3), e12921. https://doi.org/10.1111/acel.12921

Edel-Hermann, V., & Lecomte, C. (2019). Current status of *Fusarium oxysporum* formaespeciales and races. *Phytopathology*, *109*(4), 512-530. https://doi.org/10.1094/phyto-08-18-0320-rvw

Eraso, P., Mazón, M. J., & Portillo, F. (2006). Yeast protein kinase Ptk2 localizes at the plasma membrane and phosphorylates in vitro the C-terminal peptide of the H+-ATPase. *Biochim Biophys Acta*, *1758*(2), 164-170. https://doi.org/10.1016/j.bbamem.2006.01.010

Eraso, P., Mazón, M. J., Posas, F., & Portillo, F. (2011). Gene expression profiling of yeasts overexpressing wild type or misfolded Pma1 variants reveals activation of the Hog1 MAPK pathway. *Mol Microbiol*, *79*(5), 1339-1352. https://doi.org/10.1111/j.1365-2958.2010.07528.x

Eraso, P., & Portillo, F. (1994). Molecular mechanism of regulation of yeast plasma membrane H(+)-ATPase by glucose. Interaction between domains and identification of new regulatory sites. *J Biol Chem*, *269*(14), 10393-10399. https://www.ncbi.nlm.nih.gov/pubmed/8144622

Ernst, A. M., Contreras, F. X., Brügger, B., & Wieland, F. (2010). Determinants of specificity at the protein-lipid interface in membranes. *FEBS Lett*, *584*(9), 1713-1720. https://doi.org/10.1016/j.febslet.2009.12.060

Estrada, E., Agostinis, P., Vandenheede, J. R., Goris, J., Merlevede, W., François, J., Goffeau, A., & Ghislain, M. (1996). Phosphorylation of yeast plasma membrane H+-ATPase by casein kinase I. *J Biol Chem*, *271*(50), 32064-32072. https://doi.org/10.1074/jbc.271.50.32064

Fajardo-Somera, R. A., Bowman, B., & Riquelme, M. (2013). The plasma membrane proton pump PMA-1 is incorporated into distal parts of the hyphae independently of the Spitzenkorper in *Neurospora crassa*. *Eukaryot Cell*, *12*(8), 1097-1105. https://doi.org/10.1128/EC.00328-12

Farnoud, A. M., Mor, V., Singh, A., & Del Poeta, M. (2014). Inositol phosphosphingolipid phospholipase C1 regulates plasma membrane ATPase (Pma1) stability in *Cryptococcus neoformans*. *FEBS Lett*, *588*(21), 3932-3938. https://doi.org/10.1016/j.febslet.2014.09.005

Farnoud, A. M., Toledo, A. M., Konopka, J. B., Del Poeta, M., & London, E. (2015). Raft-like membrane domains in pathogenic microorganisms. *Curr Top Membr*, *75*, 233-268. https://doi.org/10.1016/bs.ctm.2015.03.005

Fernandes, A. R., & Sá-Correia, I. (2003). Transcription patterns of PMA1 and PMA2 genes and activity of plasma membrane H+-ATPase in *Saccharomyces cerevisiae* during diauxic growth and stationary phase. *Yeast*, *20*(3), 207-219. https://doi.org/10.1002/yea.957

Fernandes, T. R., Mariscal, M., Serrano, A., Segorbe, D., Fernández-Acero, T., Martín, H., Turrà, D., & Di Pietro, A. (2022a). Cytosolic pH controls fungal MAPK signaling and pathogenicity. *bioRxiv*, 2022.2010.2023.513408. https://doi.org/10.1101/2022.10.23.513408

Fernandes, T. R., Segorbe, D., Prusky, D., & Di Pietro, A. (2017). How alkalinization drives fungal pathogenicity. *PLoS Pathog*, *13*(11), e1006621. https://doi.org/10.1371/journal.ppat.1006621

Fernandes, T. R., Serrano, A., & Di Pietro, A. (2022b). In vivo monitoring of cytosolic pH using the ratiometric pH sensor pHluorin. *Methods Mol Biol*, *2391*, 99-107. https://doi.org/10.1007/978-1-0716-1795-3_9

Franck, W. L., Gokce, E., Oh, Y., Muddiman, D. C., & Dean, R. A. (2013). Temporal analysis of the *Magnaporthe oryzae* proteome during conidial germination and cyclic AMP (cAMP)-mediated appressorium formation. *Mol Cell Proteomics*, *12*(8), 2249-22465. https://doi.org/10.1074/mcp.M112.025874

Gaigg, B., Toulmay, A., & Schneiter, R. (2006). Very long-chain fatty acid-containing lipids rather than sphingolipids per se are required for raft association and stable surface transport of newly synthesized plasma membrane ATPase in yeast. *J Biol Chem*, *281*(45), 34135-34145. https://doi.org/10.1074/jbc.M603791200

Gandía, M., Garrigues, S., Hernanz-Koers, M., Manzanares, P., & Marcos, J. F. (2019). Differential roles, crosstalk and response to the antifungal protein AfpB in the three Mitogen-Activated Protein Kinases (MAPK) pathways of the citrus postharvest pathogen *Penicillium digitatum*. *Fungal Genet Biol*, *124*, 17-28. https://doi.org/10.1016/j.fgb.2018.12.006

García-Marqués, S., Randez-Gil, F., Dupont, S., Garre, E., & Prieto, J. A. (2016). Sng1 associates with Nce102 to regulate the yeast Pkh-Ypk signalling module in response to sphingolipid status. *Biochim Biophys Acta*, *1863*(6 Pt A), 1319-1333. https://doi.org/10.1016/j.bbamcr.2016.03.025

Garnaud, C., García-Oliver, E., Wang, Y., Maubon, D., Bailly, S., Despinasse, Q., Champleboux, M., Govin, J., & Cornet, M. (2018). The Rim pathway mediates antifungal tolerance in *Candida albicans* through newly identified Rim101 transcriptional targets, including Hsp90 and Ipt1. *Antimicrob Agents Chemother*, *62*(3). https://doi.org/10.1128/aac.01785-17

Gasch, A. P., Spellman, P. T., Kao, C. M., Carmel-Harel, O., Eisen, M. B., Storz, G., Botstein, D., & Brown, P. O. (2000). Genomic expression programs in the response of yeast cells to environmental changes. *Mol Biol Cell*, *11*(12), 4241-4257. https://doi.org/10.1091/mbc.11.12.4241

Giannattasio, S., Guaragnella, N., Corte-Real, M., Passarella, S., & Marra, E. (2005). Acid stress adaptation protects *Saccharomyces cerevisiae* from acetic acid-

induced programmed cell death. *Gene*, *354*, 93-98. https://doi.org/10.1016/j.gene.2005.03.030

Goers Sweeney, E., Henderson, J. N., Goers, J., Wreden, C., Hicks, K. G., Foster, J. K., Parthasarathy, R., Remington, S. J., & Guillemin, K. (2012). Structure and proposed mechanism for the pH-sensing *Helicobacter pylori* chemoreceptor TlpB. *Structure*, *20*(7), 1177-1188. https://doi.org/10.1016/j.str.2012.04.021

Gong, X., & Chang, A. (2001). A mutant plasma membrane ATPase, Pma1-10, is defective in stability at the yeast cell surface. *Proc Natl Acad Sci U S A*, *98*(16), 9104-9109. https://doi.org/10.1073/pnas.161282998

Goossens, A., de La Fuente, N., Forment, J., Serrano, R., & Portillo, F. (2000). Regulation of yeast H(+)-ATPase by protein kinases belonging to a family dedicated to activation of plasma membrane transporters. *Mol Cell Biol*, *20*(20), 7654-7661. https://doi.org/10.1128/mcb.20.20.7654-7661.2000

Grossmann, G., Opekarová, M., Malinsky, J., Weig-Meckl, I., & Tanner, W. (2007). Membrane potential governs lateral segregation of plasma membrane proteins and lipids in yeast. *Embo j*, *26*(1), 1-8. https://doi.org/10.1038/sj.emboj.7601466

Guaragnella, N., Antonacci, L., Passarella, S., Marra, E., & Giannattasio, S. (2011). Achievements and perspectives in yeast acetic acid-induced programmed cell death pathways. *Biochem Soc Trans*, *39*(5), 1538-1543. https://doi.org/10.1042/bst0391538

Guerreiro, J. F., Mira, N. P., Santos, A. X. S., Riezman, H., & Sa-Correia, I. (2017). Membrane phosphoproteomics of yeast early response to acetic acid: Role of Hrk1 kinase and lipid biosynthetic pathways, in particular sphingolipids. *Front Microbiol*, *8*, 1302. https://doi.org/10.3389/fmicb.2017.01302

Gurunathan, S., David, D., & Gerst, J. E. (2002). Dynamin and clathrin are required for the biogenesis of a distinct class of secretory vesicles in yeast. *Embo j*, *21*(4), 602-614. https://doi.org/10.1093/emboj/21.4.602

Hankins, H. M., Sere, Y. Y., Diab, N. S., Menon, A. K., & Graham, T. R. (2015). Phosphatidylserine translocation at the yeast trans-Golgi network regulates protein sorting into exocytic vesicles. *Mol Biol Cell*, *26*(25), 4674-4685. https://doi.org/10.1091/mbc.E15-07-0487

Harsay, E., & Schekman, R. (2002). A subset of yeast vacuolar protein sorting mutants is blocked in one branch of the exocytic pathway. *J Cell Biol*, *156*(2), 271-285. https://doi.org/10.1083/jcb.200109077

Haruta, M., Sabat, G., Stecker, K., Minkoff, B. B., & Sussman, M. R. (2014). A peptide hormone and its receptor protein kinase regulate plant cell expansion. *Science*, *343*(6169), 408-411. https://doi.org/10.1126/science.1244454

Heit, S., Geurts, M. M. G., Murphy, B. J., Corey, R. A., Mills, D. J., Kühlbrandt, W., & Bublitz, M. (2021). Structure of the hexameric fungal plasma membrane proton pump in its autoinhibited state. *Sci Adv*, *7*(46), eabj5255. https://doi.org/10.1126/sciadv.abj5255

Henne, W. M., Buchkovich, N. J., Zhao, Y., & Emr, S. D. (2012). The endosomal sorting complex ESCRT-II mediates the assembly and architecture of ESCRT-III helices. *Cell*, *151*(2), 356-371. https://doi.org/10.1016/j.cell.2012.08.039

Herrador, A., Livas, D., Soletto, L., Becuwe, M., Léon, S., & Vincent, O. (2015). Casein kinase 1 controls the activation threshold of an $\alpha$-arrestin by multisite phosphorylation of the interdomain hinge. *Mol Biol Cell*, *26*(11), 2128-2138. https://doi.org/10.1091/mbc.E14-11-1552

Herranz, S., Rodríguez, J. M., Bussink, H. J., Sánchez-Ferrero, J. C., Arst, H. N., Jr., Peñalva, M. A., & Vincent, O. (2005). Arrestin-related proteins mediate pH signaling in fungi. *Proc Natl Acad Sci U S A*, *102*(34), 12141-12146. https://doi.org/10.1073/pnas.0504776102

Hilty, J., Smulian, A. G., & Newman, S. L. (2008). The *Histoplasma capsulatum* vacuolar ATPase is required for iron homeostasis, intracellular replication in macrophages and virulence in a murine model of histoplasmosis. *Mol Microbiol*, *70*(1), 127-139. https://doi.org/10.1111/j.1365-2958.2008.06395.x

Hu, G., Bakkeren, E., Caza, M., Horianopoulos, L., Sánchez-León, E., Sorensen, M., Jung, W., & Kronstad, J. W. (2021). Vam6/Vps39/TRAP1-domain proteins influence vacuolar morphology, iron acquisition and virulence in *Cryptococcus neoformans*. *Cell Microbiol*, *23*(12), e13400. https://doi.org/10.1111/cmi.13400

Huang, J. Y., Goers Sweeney, E., Guillemin, K., & Amieva, M. R. (2017). Multiple acid sensors control *Helicobacter pylori* colonization of the stomach. *PLoS Pathog*, *13*(1), e1006118. https://doi.org/10.1371/journal.ppat.1006118

Huss, M., Ingenhorst, G., König, S., Gassel, M., Dröse, S., Zeeck, A., Altendorf, K., & Wieczorek, H. (2002). Concanamycin A, the specific inhibitor of V-ATPases, binds to the V(o) subunit c. *J Biol Chem*, *277*(43), 40544-40548. https://doi.org/10.1074/jbc.M207345200

Igbaria, A., Lev, S., Rose, M. S., Lee, B. N., Hadar, R., Degani, O., & Horwitz, B. A. (2008). Distinct and combined roles of the MAP kinases of *Cochliobolus heterostrophus* in virulence and stress responses. *Mol Plant Microbe Interact*, *21*(6), 769-780. https://doi.org/10.1094/mpmi-21-6-0769

Jangir, P., Mehra, N., Sharma, K., Singh, N., Rani, M., & Kapoor, R. (2021). Secreted in xylem genes: Drivers of host adaptation in *Fusarium oxysporum*. *Front Plant Sci*, *12*, 628611. https://doi.org/10.3389/fpls.2021.628611

Jaramillo, V. D., Sukno, S. A., & Thon, M. R. (2015). Identification of horizontally transferred genes in the genus *Colletotrichum* reveals a steady tempo of bacterial to fungal gene transfer. *BMC Genomics*, *16*(1), 2. https://doi.org/10.1186/1471-2164-16-2

Jiao, W., Liu, X., Li, Y., Li, B., Du, Y., Zhang, Z., Chen, Q., & Fu, M. (2022). Organic acid, a virulence factor for pathogenic fungi, causing postharvest decay in fruits. *Mol Plant Pathol*, *23*(2), 304-312. https://doi.org/10.1111/mpp.13159

Jung, S. I., Rodriguez, N., Irrizary, J., Liboro, K., Bogarin, T., Macias, M., Eivers, E., Porter, E., Filler, S. G., & Park, H. (2017). Yeast casein kinase 2 governs morphology, biofilm formation, cell wall integrity, and host cell damage of *Candida albicans*. *PLoS One*, *12*(11), e0187721. https://doi.org/10.1371/journal.pone.0187721

Kahm, M., Navarrete, C., Llopis-Torregrosa, V., Herrera, R., Barreto, L., Yenush, L., Ariño, J., Ramos, J., & Kschischo, M. (2012). Potassium starvation in yeast: mechanisms of homeostasis revealed by mathematical modeling. *PLoS Comput Biol*, *8*(6), e1002548. https://doi.org/10.1371/journal.pcbi.1002548

Kamoun, S., & Zipfel, C. (2016). Fungal pathogenesis: Host modulation every which way. *Nat Microbiol*, *1*(6), 16075. https://doi.org/10.1038/nmicrobiol.2016.75

Kane, P. M. (2016). Proton transport and pH control in fungi. *Adv Exp Med Biol*, *892*, 33-68. https://doi.org/10.1007/978-3-319-25304-6_3

Kang, W. K., Kim, Y. H., Kang, H. A., Kwon, K. S., & Kim, J. Y. (2015). Sir2 phosphorylation through cAMP-PKA and CK2 signaling inhibits the lifespan extension activity of Sir2 in yeast. *Elife*, *4*. https://doi.org/10.7554/eLife.09709

Keighron, J. D., Ewing, A. G., & Cans, A. S. (2012). Analytical tools to monitor exocytosis: a focus on new fluorescent probes and methods. *Analyst*, *137*(8), 1755-1763. https://doi.org/10.1039/c2an15901e

Kim, J. Y. (2016). Human fungal pathogens: Why should we learn? *J Microbiol*, *54*(3), 145-148. https://doi.org/10.1007/s12275-016-0647-8

Kim, S. W., Park, Y. K., Joo, Y. J., Chun, Y. J., Hwang, J. Y., Baek, J. H., & Kim, J. (2019). Subunits of the vacuolar H+-ATPase complex, Vma4 and Vma10, are essential for virulence and represent potential drug targets in *Candida albicans*. *Fungal Biol*, *123*(10), 709-722. https://doi.org/10.1016/j.funbio.2019.06.002

Korn, M., Schmidpeter, J., Dahl, M., Muller, S., Voll, L. M., & Koch, C. (2015). A genetic screen for pathogenicity genes in the hemibiotrophic fungus *Colletotrichum higginsianum* identifies the plasma membrane proton pump Pma2 required for host penetration. *PLoS One*, *10*(5), e0125960. https://doi.org/10.1371/journal.pone.0125960

Kühlbrandt, W., Zeelen, J., & Dietrich, J. (2002). Structure, mechanism, and regulation of the *Neurospora* plasma membrane H+-ATPase. *Science*, *297*(5587), 1692-1696. https://doi.org/10.1126/science.1072574

Landraud, P., Chuzeville, S., Billon-Grande, G., Poussereau, N., & Bruel, C. (2013). Adaptation to pH and role of PacC in the rice blast fungus *Magnaporthe oryzae*. *PLoS One*, *8*(7), e69236. https://doi.org/10.1371/journal.pone.0069236

Lecchi, S., Nelson, C. J., Allen, K. E., Swaney, D. L., Thompson, K. L., Coon, J. J., Sussman, M. R., & Slayman, C. W. (2007). Tandem phosphorylation of Ser-911 and Thr-912 at the C terminus of yeast plasma membrane H+-ATPase

leads to glucose-dependent activation. *J Biol Chem*, *282*(49), 35471-35481. https://doi.org/10.1074/jbc.M706094200

Lee, Y., Nasution, O., Choi, E., Choi, I. G., Kim, W., & Choi, W. (2015). Transcriptome analysis of acetic-acid-treated yeast cells identifies a large set of genes whose overexpression or deletion enhances acetic acid tolerance. *Appl Microbiol Biotechnol*, *99*(15), 6391-6403. https://doi.org/10.1007/s00253-015-6706-y

Lee, Y., Nasution, O., Lee, Y. M., Kim, E., Choi, W., & Kim, W. (2017). Overexpression of PMA1 enhances tolerance to various types of stress and constitutively activates the SAPK pathways in *Saccharomyces cerevisiae*. *Appl Microbiol Biotechnol*, *101*(1), 229-239. https://doi.org/10.1007/s00253-016-7898-5

Lenassi, M., Gostinčar, C., Jackman, S., Turk, M., Sadowski, I., Nislow, C., Jones, S., Birol, I., Cimerman, N. G., & Plemenitaš, A. (2013). Whole genome duplication and enrichment of metal cation transporters revealed by de novo genome sequencing of extremely halotolerant black yeast *Hortaea werneckii*. *PLoS One*, *8*(8), e71328. https://doi.org/10.1371/journal.pone.0071328

Lengeler, K. B., Davidson, R. C., D'Souza, C., Harashima, T., Shen, W. C., Wang, P., Pan, X., Waugh, M., & Heitman, J. (2000). Signal transduction cascades regulating fungal development and virulence. *Microbiol Mol Biol Rev*, *64*(4), 746-785. https://doi.org/10.1128/mmbr.64.4.746-785.2000

Lev, S., Sharon, A., Hadar, R., Ma, H., & Horwitz, B. A. (1999). A mitogen-activated protein kinase of the corn leaf pathogen *Cochliobolus heterostrophus* is involved in conidiation, appressorium formation, and pathogenicity: diverse roles for mitogen-activated protein kinase homologs in foliar pathogens. *Proc Natl Acad Sci U S A*, *96*(23), 13542-13547. https://doi.org/10.1073/pnas.96.23.13542

Li, J., Yang, S., Li, D., Peng, L., Fan, G., & Pan, S. (2022). The plasma membrane H(+)-ATPase is critical for cell growth and pathogenicity in *Penicillium digitatum*. *Appl Microbiol Biotechnol*, *106*(13-16), 5123-5136. https://doi.org/10.1007/s00253-022-12036-4

Lindberg, L., Santos, A. X., Riezman, H., Olsson, L., & Bettiga, M. (2013). Lipidomic profiling of *Saccharomyces cerevisiae* and *Zygosaccharomyces bailii* reveals critical changes in lipid composition in response to acetic acid stress. *PLoS One*, *8*(9), e73936. https://doi.org/10.1371/journal.pone.0073936

Liu, K., Zhang, X., Lester, R. L., & Dickson, R. C. (2005). The sphingoid long chain base phytosphingosine activates AGC-type protein kinases in *Saccharomyces cerevisiae* including Ypk1, Ypk2, and Sch9. *J Biol Chem*, *280*(24), 22679-22687. https://doi.org/10.1074/jbc.M502972200

Liu, Y., & Chang, A. (2006). Quality control of a mutant plasma membrane ATPase: ubiquitylation prevents cell-surface stability. *J Cell Sci*, *119*(Pt 2), 360-369. https://doi.org/10.1242/jcs.02749

Livak, K. J., & Schmittgen, T. D. (2001). Analysis of relative gene expression data using real-time quantitative PCR and the 2(-Delta Delta C(T)) Method. *Methods*, *25*(4), 402-408. https://doi.org/10.1006/meth.2001.1262

López-Berges, M. S., Rispail, N., Prados-Rosales, R. C., & Di Pietro, A. (2010). A nitrogen response pathway regulates virulence functions in *Fusarium oxysporum* via the protein kinase TOR and the bZIP protein MeaB. *Plant Cell*, *22*(7), 2459-2475. https://doi.org/10.1105/tpc.110.075937

Lucena-Agell, D., Hervás-Aguilar, A., Múnera-Huertas, T., Pougovkina, O., Rudnicka, J., Galindo, A., Tilburn, J., Arst, H. N., Jr., & Peñalva, M. A. (2016). Mutational analysis of the *Aspergillus* ambient pH receptor PalH underscores its potential as a target for antifungal compounds. *Mol Microbiol*, *101*(6), 982-1002. https://doi.org/10.1111/mmi.13438

Luo, G., Gruhler, A., Liu, Y., Jensen, O. N., & Dickson, R. C. (2008). The sphingolipid long-chain base-Pkh1/2-Ypk1/2 signaling pathway regulates eisosome assembly and turnover. *J Biol Chem*, *283*(16), 10433-10444. https://doi.org/10.1074/jbc.M709972200

Ma, L. J., Geiser, D. M., Proctor, R. H., Rooney, A. P., O'Donnell, K., Trail, F., Gardiner, D. M., Manners, J. M., & Kazan, K. (2013). *Fusarium* pathogenomics. *Annu Rev Microbiol*, *67*, 399-416. https://doi.org/10.1146/annurev-micro-092412-155650

Ma, L. J., van der Does, H. C., Borkovich, K. A., Coleman, J. J., Daboussi, M. J., Di Pietro, A., Dufresne, M., Freitag, M., Grabherr, M., Henrissat, B., Houterman, P. M., Kang, S., Shim, W. B., Woloshuk, C., Xie, X., Xu, J. R., Antoniw, J., Baker, S. E., Bluhm, B. H., . . . Rep, M. (2010). Comparative genomics reveals mobile pathogenicity chromosomes in *Fusarium*. *Nature*, *464*(7287), 367-373. https://doi.org/10.1038/nature08850

Mahmoud, S., Planes, M. D., Cabedo, M., Trujillo, C., Rienzo, A., Caballero-Molada, M., Sharma, S. C., Montesinos, C., Mulet, J. M., & Serrano, R. (2017). TOR complex 1 regulates the yeast plasma membrane proton pump and pH and potassium homeostasis. *FEBS Lett*, *591*(13), 1993-2002. https://doi.org/10.1002/1873-3468.12673

Malakar, D., Dey, A., Basu, A., & Ghosh, A. K. (2008). Antiapoptotic role of S-adenosyl-l-methionine against hydrochloric acid induced cell death in *Saccharomyces cerevisiae*. *Biochim Biophys Acta*, *1780*(7-8), 937-947. https://doi.org/10.1016/j.bbagen.2008.03.014

Malardier, L., Daboussi, M. J., Julien, J., Roussel, F., Scazzocchio, C., & Brygoo, Y. (1989). Cloning of the nitrate reductase gene (niaD) of *Aspergillus nidulans* and its use for transformation of *Fusarium oxysporum*. *Gene*, *78*(1), 147-156. https://doi.org/10.1016/0378-1119(89)90322-3

Malinska, K., Malinsky, J., Opekarova, M., & Tanner, W. (2004). Distribution of Can1p into stable domains reflects lateral protein segregation within the plasma membrane of living *S. cerevisiae* cells. *J Cell Sci*, *117*(Pt 25), 6031-6041. https://doi.org/10.1242/jcs.01493

Malínská, K., Malínský, J., Opekarová, M., & Tanner, W. (2003). Visualization of protein compartmentation within the plasma membrane of living yeast cells. *Mol Biol Cell*, *14*(11), 4427-4436. https://doi.org/10.1091/mbc.e03-04-0221

Manteau, S., Abouna, S., Lambert, B., & Legendre, L. (2003). Differential regulation by ambient pH of putative virulence factor secretion by the phytopathogenic fungus *Botrytis cinerea*. *FEMS Microbiol Ecol*, *43*(3), 359-366. https://doi.org/10.1111/j.1574-6941.2003.tb01076.x

Marin, O., Meggio, F., Sarno, S., Andretta, M., & Pinna, L. A. (1994). Phosphorylation of synthetic fragments of inhibitor-2 of protein phosphatase-1 by casein kinase-1 and -2. Evidence that phosphorylated residues are not strictly required for efficient targeting by casein kinase-1. *Eur J Biochem*, *223*(2), 647-653. https://doi.org/10.1111/j.1432-1033.1994.tb19037.x

Mariscal, M., Fernandes, T. R., & Di Pietro, A. (2023). Role of pH in the control of fungal MAPK signalling and pathogenicity. In B. Scott & C. Mesarich (Eds.), *Plant Relationships: Fungal-Plant Interactions* (pp. 227-238). Springer International Publishing. https://doi.org/10.1007/978-3-031-16503-0_9

Mariscal, M., Miguel-Rojas, C., Hera, C., Fernandes, T. R., & Di Pietro, A. (2022). *Fusarium oxysporum* casein kinase 1, a negative regulator of the plasma membrane H+-ATPase Pma1, is required for development and pathogenicity. *Journal of Fungi*, *8*(12), 1300. https://doi.org/10.3390/jof8121300

Martínez-Muñoz, G. A., & Kane, P. (2017). Vacuolar and plasma membrane proton pumps collaborate to achieve cytosolic pH homeostasis in yeast. *J Biol Chem*, *292*(19), 7743. https://doi.org/10.1074/jbc.A117.710470

Masachis, S., Segorbe, D., Turrà, D., Leon-Ruiz, M., Fürst, U., El Ghalid, M., Leonard, G., López-Berges, M. S., Richards, T. A., Felix, G., & Di Pietro, A. (2016). A fungal pathogen secretes plant alkalinizing peptides to increase infection. *Nat Microbiol*, *1*(6), 16043. https://doi.org/10.1038/nmicrobiol.2016.43

Mason, A. B., Allen, K. E., & Slayman, C. W. (2014). C-terminal truncations of the *Saccharomyces cerevisiae* PMA1 H+-ATPase have major impacts on protein conformation, trafficking, quality control, and function. *Eukaryot Cell*, *13*(1), 43-52. https://doi.org/10.1128/ec.00201-13

Mattern, I. E., Punt, P. J., & Hondel, C. A. M. J. J. V. d. (1988). A vector for *Aspergillus* transformation conferring phleomycin resistance. *Fungal Genetics Reports*, *35*. https://doi.org/10.4148/1941-4765.1533

Merhej, J., Richard-Forget, F., & Barreau, C. (2011). The pH regulatory factor Pac1 regulates Tri gene expression and trichothecene production in *Fusarium graminearum*. *Fungal Genet Biol*, *48*(3), 275-284. https://doi.org/10.1016/j.fgb.2010.11.008

Minematsu, A., Miyazaki, T., Shimamura, S., Nishikawa, H., Nakayama, H., Takazono, T., Saijo, T., Yamamoto, K., Imamura, Y., Yanagihara, K., Kohno, S., Mukae, H., & Izumikawa, K. (2019). Vacuolar proton-translocating ATPase is required

for antifungal resistance and virulence of *Candida glabrata*. *PLoS One*, *14*(1), e0210883. https://doi.org/10.1371/journal.pone.0210883

Mira, N. P., Becker, J. D., & Sá-Correia, I. (2010a). Genomic expression program involving the Haa1p-regulon in *Saccharomyces cerevisiae* response to acetic acid. *Omics*, *14*(5), 587-601. https://doi.org/10.1089/omi.2010.0048

Mira, N. P., Teixeira, M. C., & Sá-Correia, I. (2010b). Adaptive response and tolerance to weak acids in *Saccharomyces cerevisiae*: a genome-wide view. *Omics*, *14*(5), 525-540. https://doi.org/10.1089/omi.2010.0072

Miyara, I., Shafran, H., Davidzon, M., Sherman, A., & Prusky, D. (2010). pH Regulation of ammonia secretion by *Colletotrichum gloeosporioides* and its effect on appressorium formation and pathogenicity. *Mol Plant Microbe Interact*, *23*(3), 304-316. https://doi.org/10.1094/mpmi-23-3-0304

Miyara, I., Shnaiderman, C., Meng, X., Vargas, W. A., Diaz-Minguez, J. M., Sherman, A., Thon, M., & Prusky, D. (2012). Role of nitrogen-metabolism genes expressed during pathogenicity of the alkalinizing *Colletotrichum gloeosporioides* and their differential expression in acidifying pathogens. *Mol Plant Microbe Interact*, *25*(9), 1251-1263. https://doi.org/10.1094/mpmi-01-12-0017-r

Mollapour, M., Fong, D., Balakrishnan, K., Harris, N., Thompson, S., Schüller, C., Kuchler, K., & Piper, P. W. (2004). Screening the yeast deletant mutant collection for hypersensitivity and hyper-resistance to sorbate, a weak organic acid food preservative. *Yeast*, *21*(11), 927-946. https://doi.org/10.1002/yea.1141

Morris, B. M., Reid, B., & Gow, N. A. R. (1995). Tactic response of zoospores of the fungus *Phytophthora palmivora* to solutions of different pH in relation to plant infection. *Microbiology (Reading)*, *141*(5), 1231-1237. https://doi.org/10.1099/13500872-141-5-1231

Morsomme, P., & Boutry, M. (2000). The plant plasma membrane H(+)-ATPase: structure, function and regulation. *Biochim Biophys Acta*, *1465*(1-2), 1-16. https://doi.org/10.1016/s0005-2736(00)00128-0

Morsomme, P., Dambly, S., Maudoux, O., & Boutry, M. (1998). Single point mutations distributed in 10 soluble and membrane regions of the *Nicotiana plumbaginifolia* plasma membrane PMA2 H+-ATPase activate the enzyme and modify the structure of the C-terminal region. *J Biol Chem*, *273*(52), 34837-34842. https://doi.org/10.1074/jbc.273.52.34837

Morsomme, P., Slayman, C. W., & Goffeau, A. (2000). Mutagenic study of the structure, function and biogenesis of the yeast plasma membrane H(+)-ATPase. *Biochim Biophys Acta*, *1469*(3), 133-157. https://doi.org/10.1016/s0304-4157(00)00015-0

Moskvina, E., Imre, E. M., & Ruis, H. (1999). Stress factors acting at the level of the plasma membrane induce transcription via the stress response element (STRE) of the yeast *Saccharomyces cerevisiae*. *Mol Microbiol*, *32*(6), 1263-1272. https://doi.org/10.1046/j.1365-2958.1999.01438.x

Mousson, F., Coïc, Y. M., Baleux, F., Beswick, V., Sanson, A., & Neumann, J. M. (2002). Deciphering the role of individual acyl chains in the interaction network between phosphatidylserines and a single-spanning membrane protein. *Biochemistry*, *41*(46), 13611-13616. https://doi.org/10.1021/bi026274b

Mukherjee, S., Kallay, L., Brett, C. L., & Rao, R. (2006). Mutational analysis of the intramembranous H10 loop of yeast Nhx1 reveals a critical role in ion homoeostasis and vesicle trafficking. *Biochem J*, *398*(1), 97-105. https://doi.org/10.1042/bj20060388

Munshi, M. A., Gardin, J. M., Singh, A., Luberto, C., Rieger, R., Bouklas, T., Fries, B. C., & Del Poeta, M. (2018). The role of ceramide synthases in the pathogenicity of *Cryptococcus neoformans*. *Cell Rep*, *22*(6), 1392-1400. https://doi.org/10.1016/j.celrep.2018.01.035

Murray, M. G., & Thompson, W. F. (1980). Rapid isolation of high molecular weight plant DNA. *Nucleic Acids Res*, *8*(19), 4321-4325. https://doi.org/10.1093/nar/8.19.4321

Naranjo-Ortiz, M. A., & Gabaldón, T. (2019). Fungal evolution: major ecological adaptations and evolutionary transitions. *Biol Rev Camb Philos Soc*, *94*(4), 1443-1476. https://doi.org/10.1111/brv.12510

Navarre, C., Catty, P., Leterme, S., Dietrich, F., & Goffeau, A. (1994). Two distinct genes encode small isoproteolipids affecting plasma membrane H(+)-ATPase activity of *Saccharomyces cerevisiae*. *J Biol Chem*, *269*(33), 21262-21268.

Navarre, C., Ghislain, M., Leterme, S., Ferroud, C., Dufour, J. P., & Goffeau, A. (1992). Purification and complete sequence of a small proteolipid associated with the plasma membrane H(+)-ATPase of *Saccharomyces cerevisiae*. *J Biol Chem*, *267*(9), 6425-6428.

Niles, B. J., Mogri, H., Hill, A., Vlahakis, A., & Powers, T. (2012). Plasma membrane recruitment and activation of the AGC kinase Ypk1 is mediated by target of rapamycin complex 2 (TORC2) and its effector proteins Slm1 and Slm2. *Proc Natl Acad Sci U S A*, *109*(5), 1536-1541. https://doi.org/10.1073/pnas.1117563109

Niles, B. J., & Powers, T. (2012). Plasma membrane proteins Slm1 and Slm2 mediate activation of the AGC kinase Ypk1 by TORC2 and sphingolipids in *S. cerevisiae*. *Cell Cycle*, *11*(20), 3745-3749. https://doi.org/10.4161/cc.21752

Niles, B. J., & Powers, T. (2014). TOR complex 2-Ypk1 signaling regulates actin polarization via reactive oxygen species. *Mol Biol Cell*, *25*(24), 3962-3972. https://doi.org/10.1091/mbc.E14-06-1122

Nishino, K., Obara, K., & Kihara, A. (2015). The C-terminal Cytosolic Region of Rim21 Senses Alterations in Plasma Membrane Lipid Composition: Insights into sensing mechanisms for plasma membrane lipid asymmetry. *J Biol Chem*, *290*(52), 30797-30805. https://doi.org/10.1074/jbc.M115.674382

Nobile, C. J., Solis, N., Myers, C. L., Fay, A. J., Deneault, J. S., Nantel, A., Mitchell, A. P., & Filler, S. G. (2008). *Candida albicans* transcription factor Rim101

mediates pathogenic interactions through cell wall functions. *Cell Microbiol*, *10*(11), 2180-2196. https://doi.org/10.1111/j.1462-5822.2008.01198.x

Nordzieke, D. E., Fernandes, T. R., El Ghalid, M., Turrà, D., & Di Pietro, A. (2019). NADPH oxidase regulates chemotropic growth of the fungal pathogen *Fusarium oxysporum* towards the host plant. *New Phytol*, *224*(4), 1600-1612. https://doi.org/10.1111/nph.16085

Novarina, D., Guerra, P., & Milias-Argeitis, A. (2021). Vacuolar localization via the N-terminal domain of Sch9 is required for TORC1-dependent phosphorylation and downstream signal transduction. *J Mol Biol*, *433*(24), 167326. https://doi.org/10.1016/j.jmb.2021.167326

Obara, K., & Kamura, T. (2021). The Rim101 pathway mediates adaptation to external alkalization and altered lipid asymmetry: hypothesis describing the detection of distinct stresses by the Rim21 sensor protein. *Curr Genet*, *67*(2), 213-218. https://doi.org/10.1007/s00294-020-01129-0

Orij, R., Brul, S., & Smits, G. J. (2011). Intracellular pH is a tightly controlled signal in yeast. *Biochim Biophys Acta*, *1810*(10), 933-944. https://doi.org/10.1016/j.bbagen.2011.03.011

Orij, R., Postmus, J., Ter Beek, A., Brul, S., & Smits, G. J. (2009). In vivo measurement of cytosolic and mitochondrial pH using a pH-sensitive GFP derivative in *Saccharomyces cerevisiae* reveals a relation between intracellular pH and growth. *Microbiology (Reading)*, *155*(Pt 1), 268-278. https://doi.org/10.1099/mic.0.022038-0

Orij, R., Urbanus, M. L., Vizeacoumar, F. J., Giaever, G., Boone, C., Nislow, C., Brul, S., & Smits, G. J. (2012). Genome-wide analysis of intracellular pH reveals quantitative control of cell division rate by pH(c) in *Saccharomyces cerevisiae*. *Genome Biol*, *13*(9), R80. https://doi.org/10.1186/gb-2012-13-9-r80

Ost, K. S., O'Meara, T. R., Huda, N., Esher, S. K., & Alspaugh, J. A. (2015). The *Cryptococcus neoformans* alkaline response pathway: identification of a novel rim pathway activator. *PLoS Genet*, *11*(4), e1005159. https://doi.org/10.1371/journal.pgen.1005159

Overduin, M., & Esmaili, M. (2019). Memtein: The fundamental unit of membrane-protein structure and function. *Chem Phys Lipids*, *218*, 73-84. https://doi.org/10.1016/j.chemphyslip.2018.11.008

Palmgren, M., & Morsomme, P. (2019). The plasma membrane H(+) -ATPase, a simple polypeptide with a long history. *Yeast*, *36*(4), 201-210. https://doi.org/10.1002/yea.3365

Palmieri, D., Vitale, S., Lima, G., Di Pietro, A., & Turrà, D. (2020). A bacterial endophyte exploits chemotropism of a fungal pathogen for plant colonization. *Nat Commun*, *11*(1), 5264. https://doi.org/10.1038/s41467-020-18994-5

Park, H. S., Jun, S. C., Han, K. H., Hong, S. B., & Yu, J. H. (2017). Diversity, application, and synthetic biology of industrially important *Aspergillus Fungi*. *Adv Appl Microbiol*, *100*, 161-202. https://doi.org/10.1016/bs.aambs.2017.03.001

Pearce, G., Moura, D. S., Stratmann, J., & Ryan, C. A., Jr. (2001). RALF, a 5-kDa ubiquitous polypeptide in plants, arrests root growth and development. *Proc Natl Acad Sci U S A*, *98*(22), 12843-12847. https://doi.org/10.1073/pnas.201416998

Peñalva, M. A., Lucena-Agell, D., & Arst, H. N., Jr. (2014). Liaison alcaline: Pals entice non-endosomal ESCRTs to the plasma membrane for pH signaling. *Curr Opin Microbiol*, *22*, 49-59. https://doi.org/10.1016/j.mib.2014.09.005

Peñalva, M. A., Tilburn, J., Bignell, E., & Arst, H. N., Jr. (2008). Ambient pH gene regulation in fungi: making connections. *Trends Microbiol*, *16*(6), 291-300. https://doi.org/10.1016/j.tim.2008.03.006

Pereira, M. B., Tisi, R., Fietto, L. G., Cardoso, A. S., França, M. M., Carvalho, F. M., Trópia, M. J., Martegani, E., Castro, I. M., & Brandão, R. L. (2008). Carbonyl cyanide m-chlorophenylhydrazone induced calcium signaling and activation of plasma membrane H(+)-ATPase in the yeast *Saccharomyces cerevisiae*. *FEMS Yeast Res*, *8*(4), 622-630. https://doi.org/10.1111/j.1567-1364.2008.00380.x

Pereira, R. R., Castanheira, D., Teixeira, J. A., Bouillet, L. E., Ribeiro, E. M., Trópia, M. M., Alvarez, F., Correa, L. F., Mota, B. E., Conceição, L. E., Castro, I. M., & Brandão, R. L. (2015). Detailed search for protein kinase(s) involved in plasma membrane H+-ATPase activity regulation of yeast cells. *FEMS Yeast Res*, *15*(2). https://doi.org/10.1093/femsyr/fov003

Pérez-Nadales, E., Alastruey-Izquierdo, A., Linares-Sicilia, M. J., Soto-Debrán, J. C., Abdala, E., García-Rodríguez, J., Montejo, M., Muñoz, P., Lletí, M. S., Rezusta, A., de Pipaón, M. R. P., Yáñez, L., Merino, E., Campos-Herrero, M. I., Costa-Mateo, J. M., Fortún, J., García-Lozano, T., Garcia-Vidal, C., Fernández-Ruiz, M., . . . Nucci, M. (2021). Invasive fusariosis in nonneutropenic Patients, Spain, 2000-2015. *Emerg Infect Dis*, *27*(1), 26-35. https://doi.org/10.3201/eid2701.190782

Pérez-Nadales, E., & Di Pietro, A. (2011). The membrane mucin Msb2 regulates invasive growth and plant infection in *Fusarium oxysporum*. *Plant Cell*, *23*(3), 1171-1185. https://doi.org/10.1105/tpc.110.075093

Pfaffl, M. W. (2001). A new mathematical model for relative quantification in real-time RT-PCR. *Nucleic Acids Res*, *29*(9), e45. https://doi.org/10.1093/nar/29.9.e45

Portillo, F. (2000). Regulation of plasma membrane H(+)-ATPase in fungi and plants. *Biochim Biophys Acta*, *1469*(1), 31-42. https://doi.org/10.1016/s0304-4157(99)00011-8

Powell, W. A., & Kistler, H. C. (1990). In vivo rearrangement of foreign DNA by *Fusarium oxysporum* produces linear self-replicating plasmids. *J Bacteriol*, *172*(6), 3163-3171. https://doi.org/10.1128/jb.172.6.3163-3171.1990

Prados Rosales, R. C., & Di Pietro, A. (2008). Vegetative hyphal fusion is not essential for plant infection by *Fusarium oxysporum*. *Eukaryot Cell*, *7*(1), 162-171. https://doi.org/10.1128/ec.00258-07

Prusky, D., McEvoy, J. L., Saftner, R., Conway, W. S., & Jones, R. (2004). Relationship between host acidification and virulence of *Penicillium* spp. on apple and citrus fruit. *Phytopathology*, *94*(1), 44-51. https://doi.org/10.1094/phyto.2004.94.1.44

Punt, P. J., Oliver, R. P., Dingemanse, M. A., Pouwels, P. H., & van den Hondel, C. A. (1987). Transformation of *Aspergillus* based on the hygromycin B resistance marker from *Escherichia coli*. *Gene*, *56*(1), 117-124. https://doi.org/10.1016/0378-1119(87)90164-8

Qu, L., Wang, L., Ji, H., Fang, Y., Lei, P., Zhang, X., Jin, L., Sun, D., & Dong, H. (2022). Toxic mechanism and biological detoxification of fumonisins. *Toxins (Basel)*, *14*(3). https://doi.org/10.3390/toxins14030182

Rajarammohan, S. (2021). Redefining plant-necrotroph interactions: The thin line between hemibiotrophs and necrotrophs. *Front Microbiol*, *12*, 673518. https://doi.org/10.3389/fmicb.2021.673518

Ramírez, J., Ramírez, O., Saldaña, C., Coria, R., & Peña, A. (1998). A *Saccharomyces cerevisiae* mutant lacking a K+/H+ exchanger. *J Bacteriol*, *180*(22), 5860-5865. https://doi.org/10.1128/jb.180.22.5860-5865.1998

Rana, A., Sahgal, M., & Johri, B. N. (2017). *Fusarium oxysporum*: Genomics, diversity and plant–host interaction. In T. Satyanarayana, S. K. Deshmukh, & B. N. Johri (Eds.), *Developments in Fungal Biology and Applied Mycology* (pp. 159-199). Springer Singapore. https://doi.org/10.1007/978-981-10-4768-8_10

Rane, H. S., Hayek, S. R., Frye, J. E., Abeyta, E. L., Bernardo, S. M., Parra, K. J., & Lee, S. A. (2019). *Candida albicans* Pma1p contributes to growth, pH homeostasis, and hyphal formation. *Front Microbiol*, *10*, 1012. https://doi.org/10.3389/fmicb.2019.01012

Rascle, C., Dieryckx, C., Dupuy, J. W., Muszkieta, L., Souibgui, E., Droux, M., Bruel, C., Girard, V., & Poussereau, N. (2018). The pH regulator PacC: a host-dependent virulence factor in *Botrytis cinerea*. *Environ Microbiol Rep*, *10*(5), 555-568. https://doi.org/10.1111/1758-2229.12663

Redkar, A., Gimenez Ibanez, S., Sabale, M., Zechmann, B., Solano, R., & Di Pietro, A. (2022a). *Marchantia polymorpha* model reveals conserved infection mechanisms in the vascular wilt fungal pathogen *Fusarium oxysporum*. *New Phytol*, *234*(1), 227-241. https://doi.org/10.1111/nph.17909

Redkar, A., Sabale, M., Zuccaro, A., & Di Pietro, A. (2022b). Determinants of endophytic and pathogenic lifestyle in root colonizing fungi. *Curr Opin Plant Biol*, *67*, 102226. https://doi.org/10.1016/j.pbi.2022.102226

Remy, E., Meyer, M., Blaise, F., Chabirand, M., Wolff, N., Balesdent, M. H., & Rouxel, T. (2008). The Lmpma1 gene of *Leptosphaeria maculans* encodes a plasma membrane H+-ATPase isoform essential for pathogenicity towards oilseed

rape. *Fungal Genet Biol*, *45*(7), 1122-1134. https://doi.org/10.1016/j.fgb.2008.04.008

Rep, M. (2005). Small proteins of plant-pathogenic fungi secreted during host colonization. *FEMS Microbiol Lett*, *253*(1), 19-27. https://doi.org/10.1016/j.femsle.2005.09.014

Rep, M., Meijer, M., Houterman, P. M., van der Does, H. C., & Cornelissen, B. J. (2005). *Fusarium oxysporum* evades I-3-mediated resistance without altering the matching avirulence gene. *Mol Plant Microbe Interact*, *18*(1), 15-23. https://doi.org/10.1094/mpmi-18-0015

Requena, N., Breuninger, M., Franken, P., & Ocón, A. (2003). Symbiotic status, phosphate, and sucrose regulate the expression of two plasma membrane H+-ATPase genes from the mycorrhizal fungus Glomus mosseae. *Plant Physiol*, *132*(3), 1540-1549. https://doi.org/10.1104/pp.102.019042

Rhee, K. H., Scarborough, G. A., & Henderson, R. (2002). Domain movements of plasma membrane H(+)-ATPase: 3D structures of two states by electron cryo-microscopy. *Embo j*, *21*(14), 3582-3589. https://doi.org/10.1093/emboj/cdf385

Rispail, N., Soanes, D. M., Ant, C., Czajkowski, R., Grünler, A., Huguet, R., Perez-Nadales, E., Poli, A., Sartorel, E., Valiante, V., Yang, M., Beffa, R., Brakhage, A. A., Gow, N. A., Kahmann, R., Lebrun, M. H., Lenasi, H., Perez-Martin, J., Talbot, N. J., . . . Di Pietro, A. (2009). Comparative genomics of MAP kinase and calcium-calcineurin signalling components in plant and human pathogenic fungi. *Fungal Genet Biol*, *46*(4), 287-298. https://doi.org/10.1016/j.fgb.2009.01.002

Roberg, K. J., Crotwell, M., Espenshade, P., Gimeno, R., & Kaiser, C. A. (1999). LST1 is a SEC24 homologue used for selective export of the plasma membrane ATPase from the endoplasmic reticulum. *J Cell Biol*, *145*(4), 659-672. https://doi.org/10.1083/jcb.145.4.659

Roelants, F. M., Breslow, D. K., Muir, A., Weissman, J. S., & Thorner, J. (2011). Protein kinase Ypk1 phosphorylates regulatory proteins Orm1 and Orm2 to control sphingolipid homeostasis in *Saccharomyces cerevisiae*. *Proc Natl Acad Sci U S A*, *108*(48), 19222-19227. https://doi.org/10.1073/pnas.1116948108

Roelants, F. M., Torrance, P. D., Bezman, N., & Thorner, J. (2002). Pkh1 and Pkh2 differentially phosphorylate and activate Ypk1 and Ykr2 and define protein kinase modules required for maintenance of cell wall integrity. *Mol Biol Cell*, *13*(9), 3005-3028. https://doi.org/10.1091/mbc.e02-04-0201

Rollins, J. A., & Dickman, M. B. (2001). pH signaling in *Sclerotinia sclerotiorum*: identification of a pacC/RIM1 homolog. *Appl Environ Microbiol*, *67*(1), 75-81. https://doi.org/10.1128/aem.67.1.75-81.2001

Ruijter, G. J. G., van de Vondervoort, P. J. I., & Visser, J. (1999). Oxalic acid production by *Aspergillus niger*: an oxalate-non-producing mutant produces citric acid at pH 5 and in the presence of manganese. *Microbiology (Reading)*, *145 ( Pt 9)*, 2569-2576. https://doi.org/10.1099/00221287-145-9-2569

Ruiz-Roldán, M. C., Maier, F. J., & Schäfer, W. (2001). PTK1, a mitogen-activated-protein kinase gene, is required for conidiation, appressorium formation, and pathogenicity of *Pyrenophora teres* on barley. *Mol Plant Microbe Interact*, *14*(2), 116-125. https://doi.org/10.1094/mpmi.2001.14.2.116

Schindelin, J., Arganda-Carreras, I., Frise, E., Kaynig, V., Longair, M., Pietzsch, T., Preibisch, S., Rueden, C., Saalfeld, S., Schmid, B., Tinevez, J. Y., White, D. J., Hartenstein, V., Eliceiri, K., Tomancak, P., & Cardona, A. (2012). Fiji: an open-source platform for biological-image analysis. *Nat Methods*, *9*(7), 676-682. https://doi.org/10.1038/nmeth.2019

Schlesser, A., Ulaszewski, S., Ghislain, M., & Goffeau, A. (1988). A second transport ATPase gene in *Saccharomyces cerevisiae*. *J Biol Chem*, *263*(36), 19480-19487.

Schüller, C., Mamnun, Y. M., Mollapour, M., Krapf, G., Schuster, M., Bauer, B. E., Piper, P. W., & Kuchler, K. (2004). Global phenotypic analysis and transcriptional profiling defines the weak acid stress response regulon in *Saccharomyces cerevisiae*. *Mol Biol Cell*, *15*(2), 706-720. https://doi.org/10.1091/mbc.e03-05-0322

Segorbe, D., Di Pietro, A., Pérez-Nadales, E., & Turrà, D. (2017). Three *Fusarium oxysporum* mitogen-activated protein kinases (MAPKs) have distinct and complementary roles in stress adaptation and cross-kingdom pathogenicity. *Mol Plant Pathol*, *18*(7), 912-924. https://doi.org/10.1111/mpp.12446

Selvig, K., & Alspaugh, J. A. (2011). pH response pathways in fungi: Adapting to host-derived and environmental signals. *Mycobiology*, *39*(4), 249-256. https://doi.org/10.5941/myco.2011.39.4.249

Serra-Cardona, A., Petrezsélyová, S., Canadell, D., Ramos, J., & Ariño, J. (2014). Coregulated expression of the Na+/phosphate Pho89 transporter and Ena1 Na+-ATPase allows their functional coupling under high-pH stress. *Mol Cell Biol*, *34*(24), 4420-4435. https://doi.org/10.1128/mcb.01089-14

Serrano, R. (1993). Structure, function and regulation of plasma membrane H(+)-ATPase. *FEBS Lett*, *325*(1-2), 108-111. https://doi.org/10.1016/0014-5793(93)81424-x

Serrano, R., Kielland-Brandt, M. C., & Fink, G. R. (1986a). Yeast plasma membrane ATPase is essential for growth and has homology with (Na+ + K+), K+- and Ca2+-ATPases. *Nature*, *319*(6055), 689-693. https://doi.org/10.1038/319689a0

Serrano, R., Kielland-Brandt, M. C., & Fink, G. R. (1986b). Yeast plasma membrane ATPase is essential for growth and has homology with (Na+ + K+), K+- and Ca2+-ATPases. *Nature*, *319*(6055), 689-693. https://doi.org/10.1038/319689a0

Shaw, S., Knüsel, S., Abbühl, D., Naguleswaran, A., Etzensperger, R., Benninger, M., & Roditi, I. (2022). Cyclic AMP signalling and glucose metabolism mediate pH taxis by *African trypanosomes*. *Nat Commun*, *13*(1), 603. https://doi.org/10.1038/s41467-022-28293-w

Shi, H. B., Chen, N., Zhu, X. M., Su, Z. Z., Wang, J. Y., Lu, J. P., Liu, X. H., & Lin, F. C. (2019). The casein kinase MoYck1 regulates development, autophagy, and virulence in the rice blast fungus. *Virulence*, *10*(1), 719-733. https://doi.org/10.1080/21505594.2019.1649588

Shimoni, Y., Kurihara, T., Ravazzola, M., Amherdt, M., Orci, L., & Schekman, R. (2000). Lst1p and Sec24p cooperate in sorting of the plasma membrane ATPase into COPII vesicles in *Saccharomyces cerevisiae*. *J Cell Biol*, *151*(5), 973-984. https://doi.org/10.1083/jcb.151.5.973

Shnaiderman, C., Miyara, I., Kobiler, I., Sherman, A., & Prusky, D. (2013). Differential activation of ammonium transporters during the accumulation of ammonia by *Colletotrichum gloeosporioides* and its effect on appressoria formation and pathogenicity. *Mol Plant Microbe Interact*, *26*(3), 345-355. https://doi.org/10.1094/mpmi-07-12-0170-r

Simons, K., & Sampaio, J. L. (2011). Membrane organization and lipid rafts. *Cold Spring Harb Perspect Biol*, *3*(10), a004697. https://doi.org/10.1101/cshperspect.a004697

Smardon, A. M., & Kane, P. M. (2014). Loss of vacuolar H+-ATPase activity in organelles signals ubiquitination and endocytosis of the yeast plasma membrane proton pump Pma1p. *J Biol Chem*, *289*(46), 32316-32326. https://doi.org/10.1074/jbc.M114.574442

Srinivas, C., Nirmala Devi, D., Narasimha Murthy, K., Mohan, C. D., Lakshmeesha, T. R., Singh, B., Kalagatur, N. K., Niranjana, S. R., Hashem, A., Alqarawi, A. A., Tabassum, B., Abd Allah, E. F., & Chandra Nayaka, S. (2019). *Fusarium oxysporum* f. sp. *lycopersici* causal agent of vascular wilt disease of tomato: Biology to diversity- A review. *Saudi J Biol Sci*, *26*(7), 1315-1324. https://doi.org/10.1016/j.sjbs.2019.06.002

Steindorff AS, Persinoti GF, Monteiro VN, & RN, S. (2015). Fungal metabolic diversity. In Gupta VK, Mach RL, & S. S (Eds.), *Fungal biomolecules: sources, applications and recent developments* (pp. 239-262). Wiley, Chichester.

Stratford, M., Nebe-von-Caron, G., Steels, H., Novodvorska, M., Ueckert, J., & Archer, D. B. (2013). Weak-acid preservatives: pH and proton movements in the yeast Saccharomyces cerevisiae. *Int J Food Microbiol*, *161*(3), 164-171. https://doi.org/10.1016/j.ijfoodmicro.2012.12.013

Stratford, M., Plumridge, A., Nebe-von-Caron, G., & Archer, D. B. (2009). Inhibition of spoilage mould conidia by acetic acid and sorbic acid involves different modes of action, requiring modification of the classical weak-acid theory. *Int J Food Microbiol*, *136*(1), 37-43. https://doi.org/10.1016/j.ijfoodmicro.2009.09.025

Struck, C., Siebels, C., Rommel, O., Wernitz, M., & Hahn, M. (1998). The plasma membrane H(+)-ATPase from the biotrophic rust fungus *Uromyces fabae*: molecular characterization of the gene (PMA1) and functional expression of the enzyme in yeast. *Mol Plant Microbe Interact*, *11*(6), 458-465. https://doi.org/10.1094/mpmi.1998.11.6.458

Sun, C., Jin, L., Cai, Y., Zheng, X., & Yu, T. (2019). (1→3)- $\beta$ -D-glucan from yeast cell wall: Characteristic and potential application in controlling postharvest disease of pear. *Postharvest Biology and Technology*, *154*, 105-114. https://doi.org/https://doi.org/10.1016/j.postharvbio.2019.04.021

Sun, S., Hoy, M. J., & Heitman, J. (2020). Fungal pathogens. *Curr Biol*, *30*(19), R1163-r1169. https://doi.org/10.1016/j.cub.2020.07.032

Sun, Y., Cao, C., Jia, W., Tao, L., Guan, G., & Huang, G. (2015). pH regulates white-opaque switching and sexual mating in *Candida albicans*. *Eukaryot Cell*, *14*(11), 1127-1134. https://doi.org/10.1128/ec.00123-15

Supply, P., Wach, A., & Goffeau, A. (1993a). Enzymatic properties of the PMA2 plasma membrane-bound H(+)-ATPase of *Saccharomyces cerevisiae*. *J Biol Chem*, *268*(26), 19753-19759.

Supply, P., Wach, A., Thinès-Sempoux, D., & Goffeau, A. (1993b). Proliferation of intracellular structures upon overexpression of the PMA2 ATPase in *Saccharomyces cerevisiae*. *J Biol Chem*, *268*(26), 19744-19752.

Sychrová, H., Ramírez, J., & Peña, A. (1999). Involvement of Nha1 antiporter in regulation of intracellular pH in *Saccharomyces cerevisiae*. *FEMS Microbiol Lett*, *171*(2), 167-172. https://doi.org/10.1111/j.1574-6968.1999.tb13428.x

Takano, Y., Kikuchi, T., Kubo, Y., Hamer, J. E., Mise, K., & Furusawa, I. (2000). The *Colletotrichum lagenarium* MAP kinase gene CMK1 regulates diverse aspects of fungal pathogenesis. *Mol Plant Microbe Interact*, *13*(4), 374-383. https://doi.org/10.1094/mpmi.2000.13.4.374

Torres, A. M., Weeden, N. F., & Martín, A. (1993). Linkage among isozyme, RFLP and RAPD markers in *Vicia faba*. *Theor Appl Genet*, *85*(8), 937-945. https://doi.org/10.1007/bf00215032

Tournu, H., Luna-Tapia, A., Peters, B. M., & Palmer, G. E. (2017). In vivo indicators of cytoplasmic, vacuolar, and extracellular pH using pHluorin2 in *Candida albicans*. *mSphere*, *2*(4). https://doi.org/10.1128/mSphere.00276-17

Trópia, M. J., Cardoso, A. S., Tisi, R., Fietto, L. G., Fietto, J. L., Martegani, E., Castro, I. M., & Brandão, R. L. (2006). Calcium signaling and sugar-induced activation of plasma membrane H(+)-ATPase in *Saccharomyces cerevisiae* cells. *Biochem Biophys Res Commun*, *343*(4), 1234-1243. https://doi.org/10.1016/j.bbrc.2006.03.078

Turra, D., & Di Pietro, A. (2015). Chemotropic sensing in fungus-plant interactions. *Curr Opin Plant Biol*, *26*, 135-140. https://doi.org/10.1016/j.pbi.2015.07.004

Turrà, D., El Ghalid, M., Rossi, F., & Di Pietro, A. (2015). Fungal pathogen uses sex pheromone receptor for chemotropic sensing of host plant signals. *Nature*, *527*(7579), 521-524. https://doi.org/10.1038/nature15516

Turrà, D., Segorbe, D., & Di Pietro, A. (2014). Protein kinases in plant-pathogenic fungi: conserved regulators of infection. *Annu Rev Phytopathol*, *52*, 267-288. https://doi.org/10.1146/annurev-phyto-102313-050143

Valkonen, M., Penttilä, M., & Benčina, M. (2014). Intracellular pH responses in the industrially important fungus *Trichoderma reesei*. *Fungal Genet Biol*, *70*, 86-93. https://doi.org/10.1016/j.fgb.2014.07.004

van 't Klooster, J. S., Cheng, T. Y., Sikkema, H. R., Jeucken, A., Moody, B., & Poolman, B. (2020). Periprotein lipidomes of *Saccharomyces cerevisiae* provide a flexible environment for conformational changes of membrane proteins. *Elife*, *9*. https://doi.org/10.7554/eLife.57003

van Dam, P., Fokkens, L., Schmidt, S. M., Linmans, J. H., Kistler, H. C., Ma, L. J., & Rep, M. (2016). Effector profiles distinguish formae speciales of *Fusarium oxysporum*. *Environ Microbiol*, *18*(11), 4087-4102. https://doi.org/10.1111/1462-2920.13445

Vázquez-Carrada, M., Feldbrügge, M., Olicón-Hernández, D. R., Guerra-Sánchez, G., & Pardo, J. P. (2022). Functional analysis of the plasma membrane H(+)-ATPases of *Ustilago maydis*. *J Fungi (Basel)*, *8*(6). https://doi.org/10.3390/jof8060550

Vecchiarelli, A., Pericolini, E., Gabrielli, E., Kenno, S., Perito, S., Cenci, E., & Monari, C. (2013). Elucidating the immunological function of the *Cryptococcus neoformans* capsule. *Future Microbiol*, *8*(9), 1107-1116. https://doi.org/10.2217/fmb.13.84

Viegas, C. A., Sebastião, P. B., Nunes, A. G., & Sá-Correia, I. (1995). Activation of plasma membrane H(+)-ATPase and expression of PMA1 and PMA2 genes in *Saccharomyces cerevisiae* cells grown at supraoptimal temperatures. *Appl Environ Microbiol*, *61*(5), 1904-1909. https://doi.org/10.1128/aem.61.5.1904-1909.1995

Viegas, C. A., Supply, P., Capieaux, E., Van Dyck, L., Goffeau, A., & Sá-Correia, I. (1994). Regulation of the expression of the H(+)-ATPase genes PMA1 and PMA2 during growth and effects of octanoic acid in *Saccharomyces cerevisiae*. *Biochim Biophys Acta*, *1217*(1), 74-80.

Vitale, S., Di Pietro, A., & Turra, D. (2019). Autocrine pheromone signalling regulates community behaviour in the fungal pathogen *Fusarium oxysporum*. *Nat Microbiol*, *4*(9), 1443-1449. https://doi.org/10.1038/s41564-019-0456-z

Vylkova, S. (2017). Environmental pH modulation by pathogenic fungi as a strategy to conquer the host. *PLoS Pathog*, *13*(2), e1006149. https://doi.org/10.1371/journal.ppat.1006149

Vylkova, S., Carman, A. J., Danhof, H. A., Collette, J. R., Zhou, H., & Lorenz, M. C. (2011). The fungal pathogen *Candida albicans* autoinduces hyphal morphogenesis by raising extracellular pH. *mBio*, *2*(3), e00055-00011. https://doi.org/10.1128/mBio.00055-11

Wang, B., Han, Z., Gong, D., Xu, X., Li, Y., Sionov, E., Prusky, D., Bi, Y., & Zong, Y. (2022). The pH signalling transcription factor PacC modulate growth, development, stress response and pathogenicity of *Trichothecium roseum*. *Environ Microbiol*, *24*(3), 1608-1621. https://doi.org/10.1111/1462-2920.15943

Wang, E., Yu, N., Bano, S. A., Liu, C., Miller, A. J., Cousins, D., Zhang, X., Ratet, P., Tadege, M., Mysore, K. S., Downie, J. A., Murray, J. D., Oldroyd, G. E., & Schultze, M. (2014). A H+-ATPase that energizes nutrient uptake during mycorrhizal symbioses in rice and *Medicago truncatula*. *Plant Cell*, *26*(4), 1818-1830. https://doi.org/10.1105/tpc.113.120527

Wang, Y., Liu, T. B., Patel, S., Jiang, L., & Xue, C. (2011). The casein kinase I protein Cck1 regulates multiple signaling pathways and is essential for cell integrity and fungal virulence in *Cryptococcus neoformans*. *Eukaryot Cell*, *10*(11), 1455-1464. https://doi.org/10.1128/ec.05207-11

Wasserstrom, L., & Wendland, J. (2021). Role of RIM101 for sporulation at alkaline pH in *Ashbya gossypii*. *J Fungi (Basel)*, *7*(7). https://doi.org/10.3390/jof7070527

Wen, X., Saltzgaber, G. W., & Thoreson, W. B. (2017). Kiss-and-Run is a significant contributor to synaptic exocytosis and endocytosis in photoreceptors. *Front Cell Neurosci*, *11*, 286. https://doi.org/10.3389/fncel.2017.00286

Wilms, T., Swinnen, E., Eskes, E., Dolz-Edo, L., Uwineza, A., Van Essche, R., Rosseels, J., Zabrocki, P., Cameroni, E., Franssens, V., De Virgilio, C., Smits, G. J., & Winderickx, J. (2017). The yeast protein kinase Sch9 adjusts V-ATPase assembly/disassembly to control pH homeostasis and longevity in response to glucose availability. *PLoS Genet*, *13*(6), e1006835. https://doi.org/10.1371/journal.pgen.1006835

Wilson, R. B., Davis, D., & Mitchell, A. P. (1999). Rapid hypothesis testing with *Candida albicans* through gene disruption with short homology regions. *J Bacteriol*, *181*(6), 1868-1874. https://doi.org/10.1128/jb.181.6.1868-1874.1999

Wood, A. K. M., Walker, C., Lee, W. S., Urban, M., & Hammond-Kosack, K. E. (2020). Functional evaluation of a homologue of plant rapid alkalinisation factor (RALF) peptides in *Fusarium graminearum*. *Fungal Biol*, *124*(9), 753-765. https://doi.org/10.1016/j.funbio.2020.05.001

Wu, L., Yuan, Z., Wang, P., Mao, X., Zhou, M., & Hou, Y. (2022). The plasma membrane H(+) -ATPase FgPMA1 regulates the development, pathogenicity, and phenamacril sensitivity of *Fusarium graminearum* by interacting with FgMyo-5 and FgBmh2. *Mol Plant Pathol*, *23*(4), 489-502. https://doi.org/10.1111/mpp.13173

Xu, J. R., & Hamer, J. E. (1996). MAP kinase and cAMP signaling regulate infection structure formation and pathogenic growth in the rice blast fungus *Magnaporthe grisea*. *Genes Dev*, *10*(21), 2696-2706. https://doi.org/10.1101/gad.10.21.2696

Yadeta, K. A., & BP, J. T. (2013). The xylem as battleground for plant hosts and vascular wilt pathogens. *Front Plant Sci*, *4*, 97. https://doi.org/10.3389/fpls.2013.00097

Yang, L., Ukil, L., Osmani, A., Nahm, F., Davies, J., De Souza, C. P., Dou, X., Perez-Balaguer, A., & Osmani, S. A. (2004). Rapid production of gene replacement

constructs and generation of a green fluorescent protein-tagged centromeric marker in *Aspergillus nidulans*. *Eukaryot Cell*, *3*(5), 1359-1362. https://doi.org/10.1128/ec.3.5.1359-1362.2004

Yenush, L. (2016). Potassium and sodium transport in yeast. *Adv Exp Med Biol*, *892*, 187-228. https://doi.org/10.1007/978-3-319-25304-6_8

Yenush, L., Mulet, J. M., Ariño, J., & Serrano, R. (2002). The Ppz protein phosphatases are key regulators of K+ and pH homeostasis: implications for salt tolerance, cell wall integrity and cell cycle progression. *Embo j*, *21*(5), 920-929. https://doi.org/10.1093/emboj/21.5.920

Young, B. P., Shin, J. J., Orij, R., Chao, J. T., Li, S. C., Guan, X. L., Khong, A., Jan, E., Wenk, M. R., Prinz, W. A., Smits, G. J., & Loewen, C. J. (2010). Phosphatidic acid is a pH biosensor that links membrane biogenesis to metabolism. *Science*, *329*(5995), 1085-1088. https://doi.org/10.1126/science.1191026

Zhang, F., Meng, Y., Wang, Y., Zhu, S., Liu, R., Li, J., Xu, L., & Huang, L. (2022). VmPma1 contributes to virulence via regulation of the acidification process during host infection in *Valsa mali*. *Int J Biol Macromol*, *228*, 123-137. https://doi.org/10.1016/j.ijbiomac.2022.12.178

Zhang, H., Wu, Z., Wang, C., Li, Y., & Xu, J. R. (2014). Germination and infectivity of microconidia in the rice blast fungus *Magnaporthe oryzae*. *Nat Commun*, *5*, 4518. https://doi.org/10.1038/ncomms5518

Zhang, L., Lv, R., Dou, X., Qi, Z., Hua, C., Zhang, H., Wang, Z., Zheng, X., & Zhang, Z. (2011). The function of MoGlk1 in integration of glucose and ammonium utilization in *Magnaporthe oryzae*. *PLoS One*, *6*(7), e22809. https://doi.org/10.1371/journal.pone.0022809

Zhang, X., Liu, W., Li, Y., Li, G., & Xu, J. R. (2017). Expression of HopAI interferes with MAP kinase signalling in *Magnaporthe oryzae*. *Environ Microbiol*, *19*(10), 4190-4204. https://doi.org/10.1111/1462-2920.13884

Zhang, X., Yang, Z., Wu, D., & Yu, F. (2020). RALF-FERONIA signaling: linking plant immune response with cell growth. *Plant Commun*, *1*(4), 100084. https://doi.org/10.1016/j.xplc.2020.100084

Zhao, P., Zhao, C., Chen, D., Yun, C., Li, H., & Bai, L. (2021). Structure and activation mechanism of the hexameric plasma membrane H(+)-ATPase. *Nat Commun*, *12*(1), 6439. https://doi.org/10.1038/s41467-021-26782-y

Zhao, X., Kim, Y., Park, G., & Xu, J. R. (2005). A mitogen-activated protein kinase cascade regulating infection-related morphogenesis in *Magnaporthe grisea*. *Plant Cell*, *17*(4), 1317-1329. https://doi.org/10.1105/tpc.104.029116

Zhgun, A., Dumina, M., Valiakhmetov, A., & Eldarov, M. (2020). The critical role of plasma membrane H+-ATPase activity in cephalosporin C biosynthesis of Acremonium chrysogenum. *PLoS One*, *15*(8), e0238452. https://doi.org/10.1371/journal.pone.0238452

Zhou, J. Y., Hao, D. L., & Yang, G. Z. (2021). Regulation of cytosolic pH: The contributions of plant plasma membrane H(+)-ATPases and multiple transporters. *Int J Mol Sci*, *22*(23). https://doi.org/10.3390/ijms222312998

Zhu, J., Hu, D., Liu, Q., Hou, R., Xu, J. R., & Wang, G. (2022). Stage-Specific Genetic Interaction between FgYCK1 and FgBNI4 during Vegetative Growth and Conidiation in *Fusarium graminearum*. *Int J Mol Sci*, *23*(16). https://doi.org/10.3390/ijms23169106